MOVING PLATFORM FOPEN RADAR PROTOTYPE DEVELOPMENT

William L. Emeny

Syracuse University

Prepared for:

Army Land Warfare Laboratory

June 1974

UNCLASSIFIED

SECURITY CLASSIFICATION OF THIS PAGE (When Data Entered)

REPORT DOCUMENTATION PAGE		READ INSTRUCTIONS BEFORE COMPLETING FORM
1 REPORT NUMBER TECHNICAL REPORT #LWL-CR-07P72	2 GOVT ACCESSION NO	3 RECIPIENT'S CATALOG NUMBER
4 TITLE (and Subtitle) MOVING PLATFORM FOPEN RADAR (New Techniques In Airborne Foliage Penetration Radar)		5 TYPE OF REPORT & PERIOD COVERED Final Report 6 PERFORMING ORG REPORT NUMBER
7 AUTHOR(s) William L. Emeny		8 CONTRACT OR GRANT NUMBER(s) DAAD05-72-C-0299
9 PERFORMING ORGANIZATION NAME AND ADDRESS Syracuse University Research Corporation Merrill Lane, University Heights Syracuse, NY 13210		10 PROGRAM ELEMENT, PROJECT, TASK AREA & WORK UNIT NUMBERS LWL Task 07-P-72
11 CONTROLLING OFFICE NAME AND ADDRESS US Army Land Warfare Laboratory Aberdeen Proving Ground, MD 21005		12 REPORT DATE June 1974 13 NUMBER OF PAGES 254
14 MONITORING AGENCY NAME & ADDRESS(if different from Controlling Office)		15 SECURITY CLASS (of this report) UNCLASSIFIED 15a DECLASSIFICATION DOWNGRADING SCHEDULE

16 DISTRIBUTION STATEMENT (of this Report)

APPROVED FOR PUBLIC RELEASE; DISTRIBUTION UNLIMITED

17 DISTRIBUTION STATEMENT (of the abstract entered in Block 20, if different from Report)

N/A

18 SUPPLEMENTARY NOTES

None

19 KEY WORDS (Continue on reverse side if necessary and identify by block number)

Airborne Radar
VHF Radar
Foliage Penetration Radar
Digital Processing
Interactive Graphics Displays

20 ABSTRACT (Continue on reverse side if necessary and identify by block number)

This report describes work done by Syracuse University Research Corporation (SURC) under Contract No. DAAD05-72-C-0299 for the US Army Land Warfare Laboratory to develop a flying prototype airborne foliage penetration (FOPEN) Radar. A 140 MHz base station FOPEN radar was mounted in a DC-3 aircraft with the antenna mounted perpendicular to the flight path. Data was gathered which enabled the radar cross section of different types of foliage to be determined. A target of known radar cross section, a corner reflector, was

DD FORM 1 JAN 73 1473 EDITION OF 1 NOV 65 IS OBSOLETE

UNCLASSIFIED

SECURITY CLASSIFICATION OF THIS PAGE (When Data Entered)

fabricated and used to calibrate the system.

Measurements were then made on different types of targets located in the open and concealed by foliage. The targets included the corner reflector, small to large trucks, two artillery pieces, and a UH-1D helicopter both with and without rotor blade movement.

It was determined that the radar cross section of the foliage was too large to permit reliable detections of concealed targets for the resolution of the measurement system, and a decision was made to reduce the operating frequency to 50 MHz. Modifications were made to the data recording system, radar, and antenna, after which additional clutter and calibrated target (dipole) measurements were made. The results showed a dramatic reduction in clutter cross section and indicate that a simple static target detection system is feasible.

In parallel with the data gathering program, a primary signal processor/display system was developed based on the Fast Fourier Transform (FFT), a reliable off-the-shelf minicomputer, and an operators display with interactive graphics. The system was completed and used to process, analyze and display the 140 and 50 MHz data.

Although close to producing the first practical airborne foliage penetration radar, this program was terminated prematurely due to the closing of the US Army Land Warfare Laboratory.

PREFACE

This program was based on two prior contracts with the Syracuse University Research Corporation (SURC). The first developed and fielded several prototype 140 MHz FOPEN radars for Vietnam use; the second flew the base station 140 MHz FOPEN to determine the feasibility of an airborne FOPEN system. Mr. Louis Surgent of the United States Army Land Warfare Laboratory was the Army Program Manager for this and previous efforts.

ACKNOWLEDGEMENTS

The successful completion of any program is not possible without the efforts of dedicated people and organizations. All of the work represented by this document was supported by contractual agreements with the United States Army Land Warfare Laboratory.

Our special thanks are extended to members of that organization and to Mr. L. Surgent for his patience, perseverance, optimism and technical guidance.

Special credit is due to Dr. T. Tamir, Dr. G. Naditch, and George M. Foster, for their invaluable efforts in carrying out theoretical studies and analysis.

Further credit is extended to Mr. J. Rodems for his foresight and guiding influence throughout the entire program.

A large measure of credit should go to the many technical personnel at SURC who contributed their efforts, in most cases, without recognition under varied and often difficult circumstances.

ABSTRACT

This report describes work done by Syracuse University Research Corporation (SURC) under Contract No. DAAD05-72-C-0299 for the United States Army Land Warfare Laboratory to develop a flying prototype airborne foliage penetration (FOPEN) Radar. A 140 MHz base station FOPEN radar was mounted in a DC-3 aircraft with the antenna mounted perpendicular to the flight path. Data was gathered which enabled the radar cross section of different types of foliage to be determined. A target of known radar cross section, a corner reflector, was fabricated and used to calibrate the system.

Measurements were then made on different types of targets located in the open and concealed by foliage. The targets included the corner reflector, small to large trucks, two artillery pieces, and a UH-1D helicopter both with and without rotor blade movement.

It was determined that the radar cross section of the foliage was too large to permit reliable detections of concealed targets for the resolution of the measurement system, and a decision was made to reduce the operating frequency to 50 MHz. Modifications were made to the data recording system, radar, and antenna after which additional clutter and calibrated target (a dipole) measurements were made. The results showed a dramatic reduction in clutter cross section and indicate that a simple static target detection system is feasible.

In parallel with the data gathering program, a primary signal processor/display system was developed based on the Fast Fourier Transform (FFT), a reliable off-the-shelf minicomputer, and an operators display with interactive graphics. The system was completed and used to process, analyze and display the 140 and 50 MHz data.

Although close to producing the first practical airborne foliage penetration radar, this program was terminated prematurely due to the closing of the United States Army Land Warfare Laboratory.

SUMMARY

This report describes work done by Syracuse University Research Corporation (SURC) under Contract No. DAAD05-72-C-0299 for the United States Army Land Warfare Laboratory to develop a flying prototype airborne foliage penetration (FOPEN) Radar. A 140 MHz base station FOPEN radar was mounted in a DC-3 aircraft with the antenna mounted perpendicular to the flight path. Data was gathered which enabled the radar cross section of different types of foliage to be determined. A target of known radar cross section, a corner reflector, was fabricated and used to calibrate the system.

Measurements were then made of different types of targets located in the open and concealed by foliage. The targets included the corner reflector, small to large trucks, two artillery pieces and a UH-1D helicopter both with and without rotor blade movement.

It was determined that the radar cross section of the foliage was too large to permit reliable detections of concealed targets for the resolution of the measurement system, and a decision was made to reduce the operating frequency to 50 MHz. Modifications were made to the data recording system, radar, and antenna, after which additional clutter and calibrated target (a dipole) measurements were made. The results showed a dramatic reduction in clutter cross section and indicate that a simple static target detection system is feasible.

In parallel with the data gathering program, a primary signal processor/display system was developed based on the Fast Fourier Transform (FFT) on a reliable off-the-shelf minicomputer, and on an operator's display with interactive graphics. The system was completed and used to process, analyze and display the 140 and 50 MHz data.

The significant results and conclusions are summarized below:

a. The data gathered at both 140 and 50 MHz was sufficiently reliable and repeatable to enable the measurement of the radar cross sections of both point targets and distributed targets.

b. Within the parameters of the simple 140 MHz system, sufficient resolution was not available to detect targets concealed by foliage without false alarms.

c. The detection of static targets concealed by foliage has been demonstrated at 140 MHz and sufficient data is available to show the practicality of such a system if the resolution cell were reduced from 100' x 100' to 15' x 15'.

d. Reducing the radar frequency from 140 MHz to 50 MHz effectively reduced the energy received from the clutter by 15 dB.

e. A simple, unfocused, side-looking radar is feasible and could be demonstrated with nominal changes to the existing 50 MHz radar. The existing computer, signal processor, and display could be flown to demonstrate this radar with only a small program change.

TABLE OF CONTENTS

LIST OF ILLUSTRATIONS

LIST OF TABLES

1.0 INTRODUCTION

The purpose of this report is to present the practical and theoretical investigations into Moving Platform Foliage Penetration Radars (FOPEN) completed by SURC under Contract DAAD05-72-C-0299.

The overall objective of this program was to develop a prototype moving platform FOPEN radar system which could make real time reliable detections of targets which may or may not be embedded in foliage. The developed system was to be delivered as a fieldable system with its primary signal processor based on a Fast Fourier Transform (FFT). An additional objective was the establishment of a statistical model to form the basis of comparison for the experimental data. At the conclusion of this program the equipment was to be delivered to the U.S. Army Land Warfare Laboratory (LWL).

The program was the culmination of two prior contracts successfully completed by SURC for LWL. The first (Contract number DAAD05-68-C-0430) witnessed the development of the ORCRIST FOPEN radar, a VHF radar with foliage penetration ability, which was utilized as an airborne instrument to gather data on the problems involved in developing an airborne FOPEN radar.

With its feasibility proven and operational usefulness decided, a second program was initiated (Contract number DAAD05-71-C-0156). This program required the instrumentation of a radar and data collection system. It called for the collection of large amounts of pertinent data and the performance of a computer aided analysis of the data. The instrumented radar is shown in Figure 1.0. This radar is described fully in the final report of that program[1] and is utilized (in varying form) in the present program. The computer aided data analysis was to determine the distinguishing characteristics of the target and clutter doppler from the data collected. As a result of the analysis, a signal processing technique was devised that provided detection of targets from an airborne platform. The feasibility of detecting man-made objects such as cars, trucks, and buildings from this platform was also demonstrated.

One of the primary and most significant results of the program was the determination of a process that eliminated, to a large extent, the doppler return due to the platform motion. Based on the premise that the clutter exhibited short-term stationarity (and this was shown to be generally true) a frequency filter was determined based on past clutter history. This filter, which continually adapted to the clutter environment, greatly reduced the doppler response due to the platform motion. In addition it was found

---

[1] SURC TR-71-249 "Moving Platform Investigation for FOPEN Radar", November 1971.

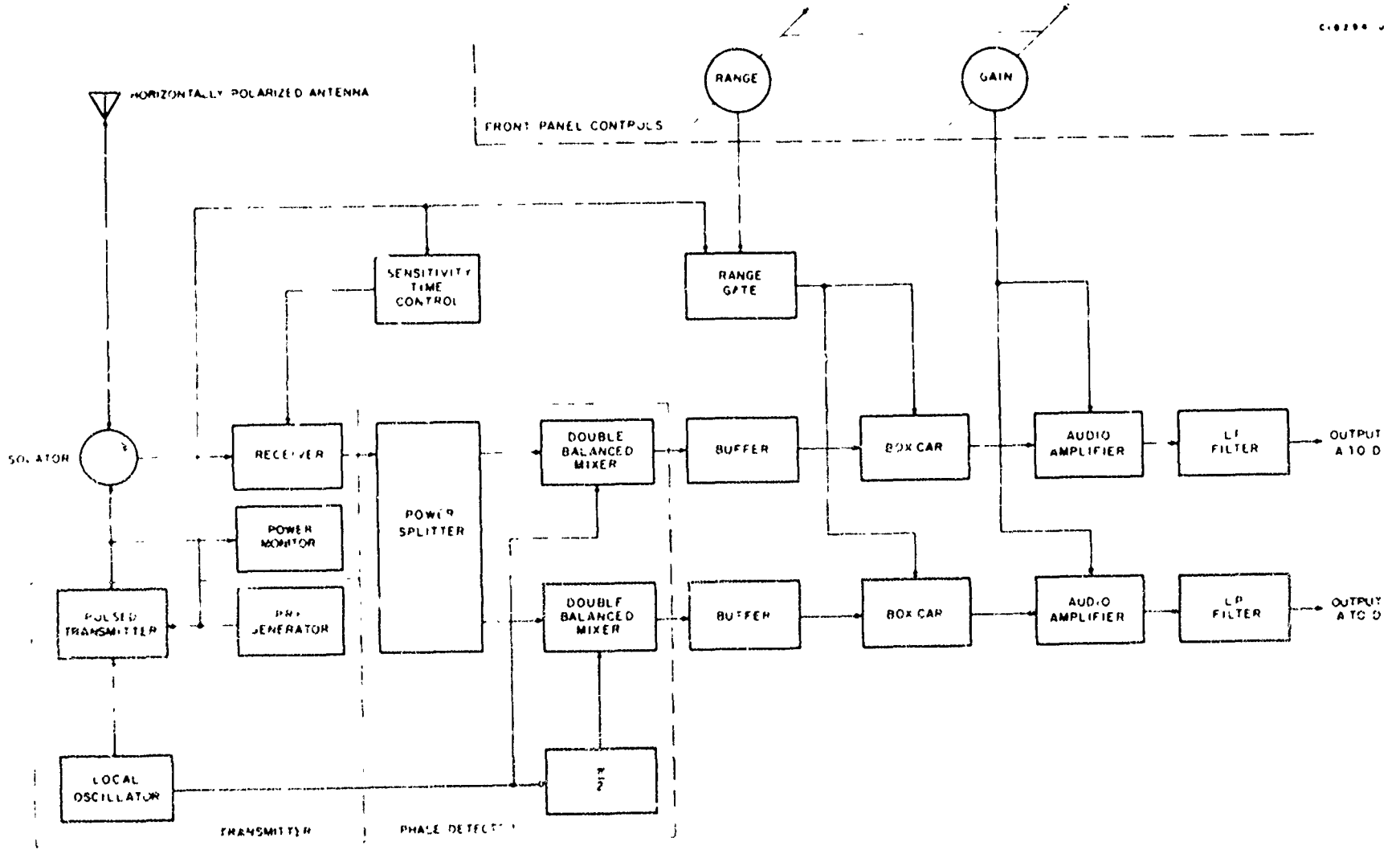

Figure 1.0. Instrumentation FOPEN Radar

that fixed targets as well as moving targets could be identified in some situations through the use of doppler frequency descrimination techniques.

Some general observations made during the analysis of the data are as follows:

1. Effects of the stabilization of the platform are minimal because:

   a. small platform motions are manifest as a contribution to the Doppler spread of the main-beam clutter (due to the ground speed of the aircraft)

   b. relatively long wavelen of carrier

   c. platform jitter is smoothed out in the spectral averaging procedure used in the processing programs.

2. When crossing the boundary between two distinct clutter environments the probability of false alarms is greatly increased. However, the types of processing in use adapts to the clutter characteristics very rapidly, and little change should be noted in the detection probabilities.

3. When flying over relatively homogeneous clutter the results have indicated some degree of "short-term stationarity". Little change is noted in the clutter spectrum as the time base of the spectrum is shifted.

4. The highest peak in the frequency domain corresponds to the Doppler frequency of the main-beam boresight relative velocity (proportional to the ground speed of the aircraft).

5. Large azimuthal beamwidths result in many spectral contributions at frequencies below the peak (tapering off as a function of cos θ and according to the antenna pattern).

6. Relatively few contributions above the peak are due to clutter (unless it is moving clutter) and hence, targets approaching the aircraft stand out above the noise more readily than receding targets which compete with non-moving clutter off the aircraft center line.

1.1 Program Objectives

The overall objective of the program was to develop and deliver a fieldable prototype airborne FOPEN radar system which can make real time reliable detection of targets that may or may not be embedded in foliage. This fieldable system was to have a primary signal processor based on the Fast Fourier Transform (FFT), a reliable minicomputer, an operators position with display, an instrumented radar, and an unfocused aperature.

The data collected utilizing this system was to be included in the data base accumulated during previous programs. The establishment of a statistical model was required to form the basis of comparison for the experimental data.

1.1.1 Additional Frequency Utilized for System Improvement

During the course of the program it became apparent that a reduction in carrier frequency would result in a reduction in clutter return of 15 to 20 dB. This means[2] of improving the target to clutter ratio was implemented and tested with expected results later in the program.

1.2 General Procedures

The conceptual radar and processor required the digitization of a doppler signal derived from a base banded pulse doppler radar with minicomputer controlled digital doppler beam sharpening as the prime processing technique. The pulse doppler radar was expected to be a Multi Purpose FOPEN radar[3] furnished by the government.

A fieldable prototype processor was to be developed and utilized in conjunction with the basic radar. The processor would include a minicomputer, a CRT display and a hardwired FFT. The FFT provides the doppler beam sharpening function which is displayed in a map format on the CRT.

Additionally, a statistical model was to be established to form the basis of comparison for the experimental data. It was recognized at the outset that a major portion of the program would need to be devoted to instrumentation, data collection, and analysis of data to establish the validity of the model, as well as, the validity of measured cross-sections of various types of clutter, of targets, and of combinations of clutter and targets.

To accomplish the program objectives the effort was divided into four major sections which were:

1) Hardware Development
2) Analytical Studies
3) Data Collection
4) Testing

---

[2] "Methods for Improving Target to Clutter Ratio For FOPEN Radar". SURC proposal 1-2U134A, 24 September 1973.

[3] "Foliage Penetration Radar: History and Developed Technology" by L.V. Surgent, Jr. LWL Report 7474, May 1974.

1.2.1 Hardware Development

The hardware development effort included the development of the hard-wired Fast Fourier Transform, the development of a display, its refresh memory and computer interfaces and the development of the hardware processor. Section 2 describes in detail the data analysis system fabricated for the program.

1.2.2 Analytical Studies

The analytical studies were concerned with the development of the processing algoritnms to be used by the radar processor, and with the theoretical investigation of the statistical aspects of clutter and the effect of clutter on moving platform radars. These studies also provided theoretical backup in the form of detection probability for targets of given cross section in various types of clutter and provided a basis for establishing a clutter model and clutter cross section models.

The theoretical investigation into the effect of clutter on moving platform radars was devoted to vegetation clutter and the statistical aspects of that clutter. More specifically, the case studied was that of homogeneous forest clutter. This case represented a simple ideal case that should be understood prior to studying other cases of interest. Section 3 describes the analytic studies concerning the development of processing algorithms. Section 7 presents the results of the clutter statistics study.

1.2.3 Data Collection

Data collection formed a large portion of the program. Included in this effort was the instrumentation of a side looking radar fixed to the test aircraft. Data was collected in various forms at various locations and added to the data bank.

Section 4 describes the data collection system utilized in the program.

1.2.4 Testing

The testing program was extensive. The requirement for correlation between the statistical model and collected data is described in Sections 5, 6, 7, and 8.

1.3 Summary of Results

The objective of fabricating a deliverable prototype moving platform FOPEN radar system has been achieved. The data analysis and display portion is shown in Figure 1.1.

A21720-U

1.3.1 Brief Description

A brief description of this system is included here, however, for more complete details refer to Sections 2 and 4.

The digital processing section of the FOPEN radar system consists of an analog to digital interface, a Varian 620/L-100 minicomputer, a hardware Fast Fourier Transform, a Digital TV display, and a keyset. This section inputs time domain radar data, converts it to doppler data, processes it and generates a display on the CRT. The keyset is used by the operator to control this part of the system and to input data required by the system.

Figure 1.2 shows a block diagram of the system described in the following paragraphs. The analog radar data is input into the computer memory by the radar interface. The software processor converts this data to doppler information using the hardware Fast Fourier Transform, then filters this data further. The software display generator converts this information into a meaningful pattern on the Digital TV display. The keyset is used by the operator to control or modify the processing and the display format.

1.3.1.1 Display (Figure 1.3)

The display consists of two presentations super-imposed on the same screen. The graphics display can generate 8 levels of gray-scale and may be removed down the screen as new data is displayed. In this way a sequence of the most recent data can be presented on the screen. The overlay display has neither gray scale nor mobility. This display is used for alphanumeric displays and for fixed overlays on the graphic data.

1.3.1.2 Keyboard (Figure 1.4)

The keyboard consists of a standard keyboard with an array of function keys on each side of it. Figure 1.4 shows the arrangement of the keyboard and the organization of the function keys. The group of function keys on the left are used to control the operation of the system. The central keyboard and the typesetting function keys are used to enter data into the system. The group of functions at the right allow the operator to display and modify data used by the systems.

1.3.1.3 Data Input

The Digital processing equipment is interfaced to the radar system via the analog to digital converter. This device translates up to 8 channels of analog signals to digital equivalents.

1.3.1.4 Processors

The digital radar processing system can have 8 different processor types available for use. These processors are organized into two banks of four

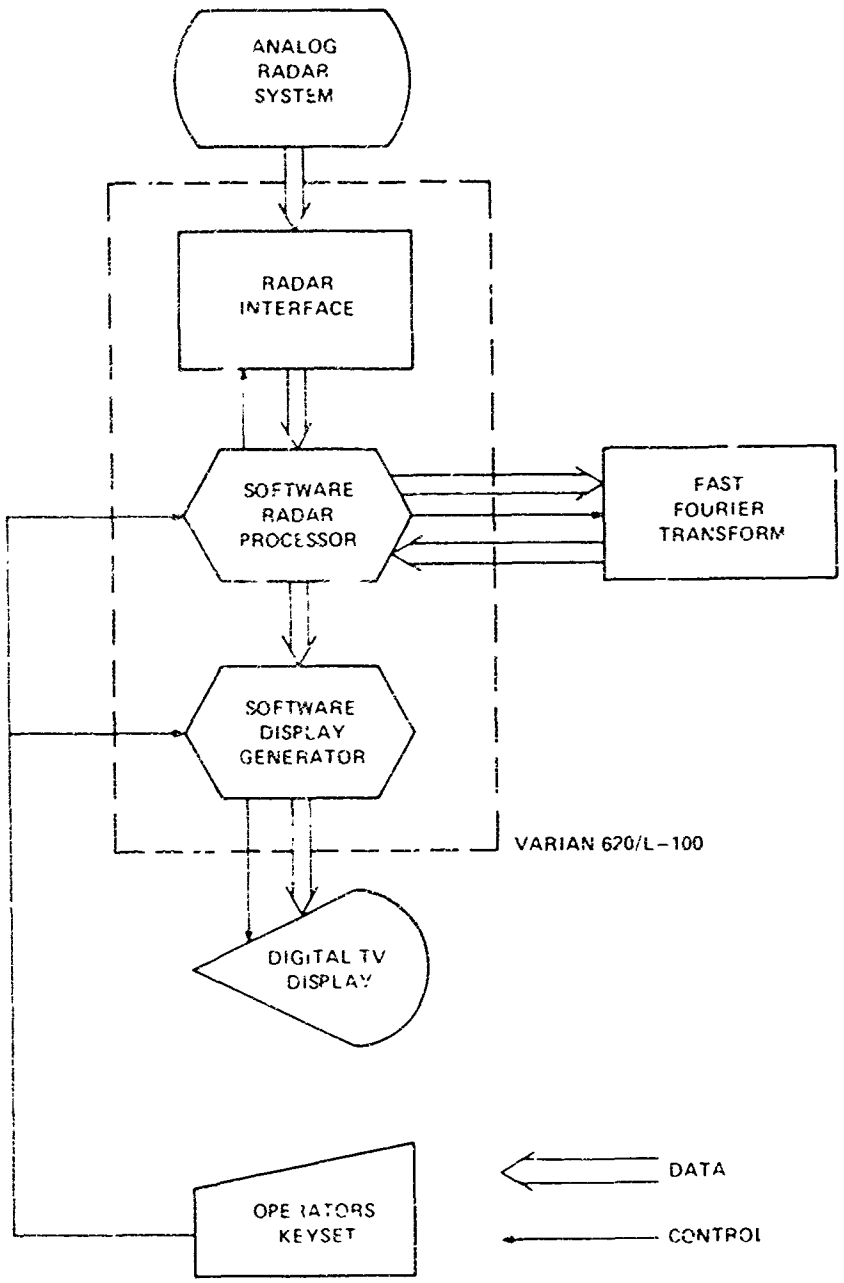

Figure 1.2 System Block Diagram

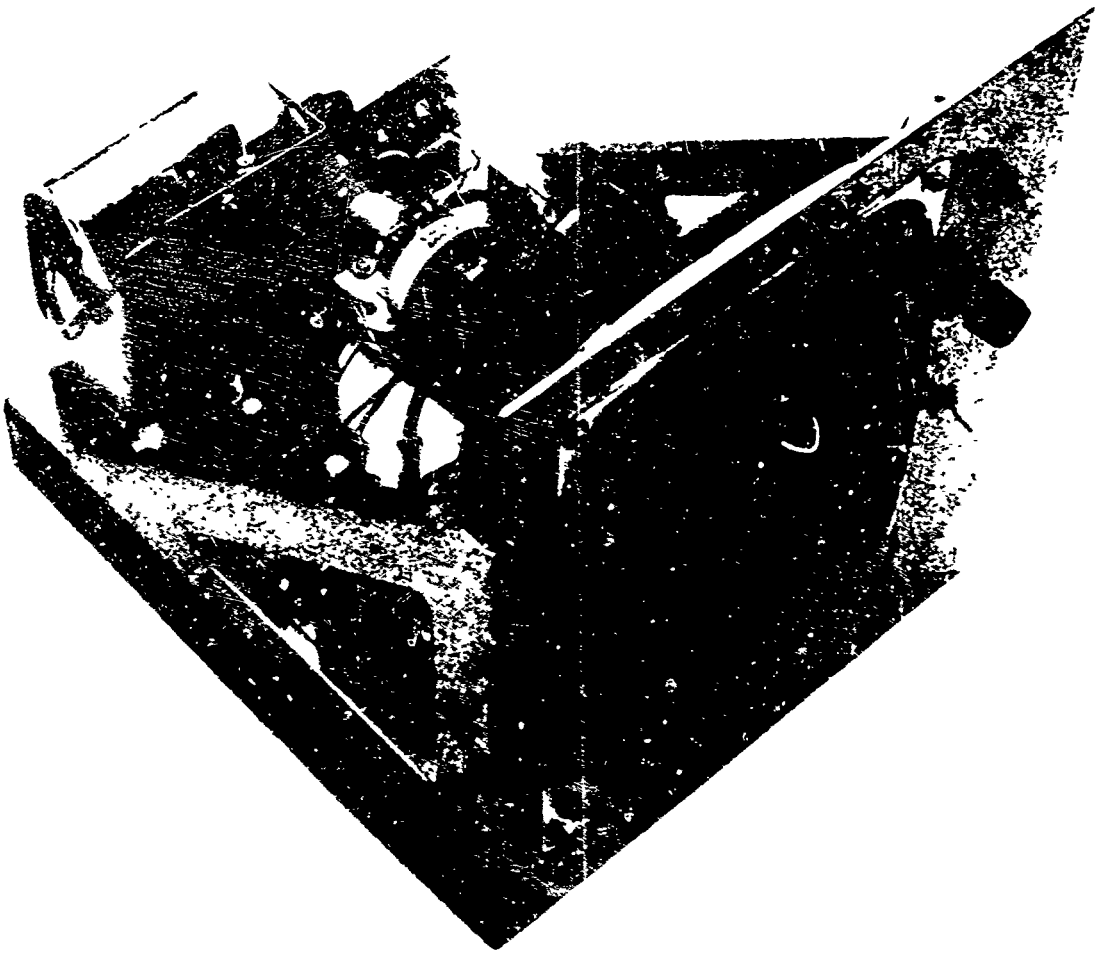

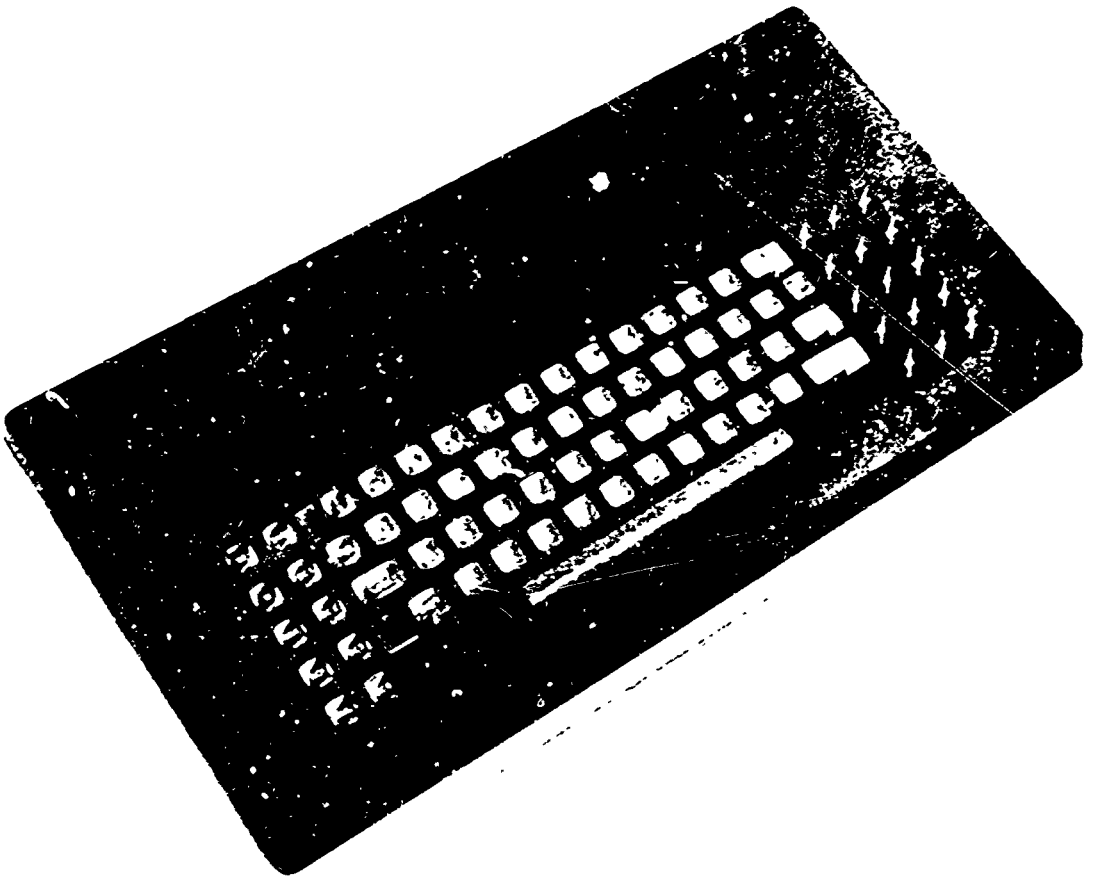

processors. The operator can select any one of these processors for use by proper use of the mode keys and processor select keys.

1.3.1.5 FFT Processor (Figure 1.5)

The Fast Fourier Transform (FFT) processing unit efficiently computes the discrete Fourier Transform of a time series of discrete data samples to produce its discrete frequency spectrum. The FFT unit operates as a peripheral processor to the LWL 620/L-100 Varian minicomputer. Series of digitized radar data samples are collected by the minicomputer and then transferred to the FFT unit to be transformed into their frequency spectrum. The resultant spectrum data are then returned to the minicomputer for further processing.

The FFT unit operates on the digitized radar data in near real time since the transform is performed in approximately eight milliseconds. This includes the time necessary to load the FFT unit with the digitized radar data and also the time to unload the frequency spectrum data into the minicomputer. Thus, approximately 125 DFT's may be performed each second by the FFT unit.

The size of the FFT unit is 256 complex words. Each radar data input word has a real and imaginary part, each consisting of 16 bits. The spectrum resulting from the transform process is also complex, producing spectra, each having a 16-bit real part, and a 16-bit imaginary part.

1.3.1.6 Power Supply

The power required for the processing and display system are either integral parts of purchased equipment or selected regulated power supplies that are mounted in the fabricated drawers.

1.3.1.7 System Software

The system software is designed to process large volumes of data with a fast turn around time. Concurrently, other tasks are required to provide the operator with the capability to modify this processing and to monitor its progress. Because of the large volume of data and the time restrictions on its processing, a two-priority system is used in the software. This system gives the processing complete priority over any other tasks being done by the program.

1.3.1.8 Executive Program

The executive program determines which program is to be executed at any given time. This is done by scanning two control tables. These control tables contain all the information required to link to any active program in the system. The executive program scans the control table in a circular fashion. Control is transferred to active programs as they are encountered during the scan.

1.3.2 Signal Processing

The output of the radar, when flying over vegetated terrain, is always a rapidly fluctuating, noise-like signal. These fluctuations are of two kinds. First, a rapid fluctuation which is due to the random interference of waves scattered from different trees. Secondly, a slower modulation of the rapid fluctuations by an envelope which is due to the actual variation of vegetation density.

It is shown theoretically that the clutter voltage signal from a uniform, random forest should be Gaussian White noise over a passband of doppler frequencies corresponding to the center of the antenna pattern (for a side-looking antenna). The signal at the output of the radar (after absolute squaring) should therefore have an exponential distribution of amplitudes.

This conclusion was tested against SURC radar data. The data was found to fit the expected distributions to within the expected standard deviation for all valid cases studied. This fact allows one to find the expected target detection probability and false alarm rate for any given threshold setting and target-to-mean-clutter ratio, simply by using the graphs published in most radar handbooks.[4] In this way it can be seen that acceptable radar performance demands that the target signal be about 13 dB above the mean clutter signal in order that the large upward random fluctuations of the clutter do not cause excessive false alarms.

1.3.3 An Economical Airborne FOPEN Radar System

The concept of an economical airborne foliage penetration radar system has been demonstrated during this program. The use of the unfocused synthetic aperture with beam sharpening provided by the FFT unit combines to form a small real time data collection system costing far less than other current systems. The small size is useful in that the system can be mounted in a smaller aircraft to be utilized for a moving platform.

A. Instrumentation Radar Results

A prototype radar was assembled, tested and utilized for the required data collection. The feasibility of detecting man-made objects such as a standard target (corner reflector), cars, trucks, and buildings using this radar was demonstrated. However, the tests indicated that the use of 140 MHz does not seem appropriate for this type radar without more sophisticated techniques of beam focusing to reduce the resolution cell to 15 feet by 15 feet. When operating at 140 MHz the clutter return

---

[4] "A Study of Clutter in Moving Platform FOPEN Radar Systems", SURC TD-73-190, April 1973, George M. Foster, Consultant, Author.

and the standard target return were inseparable. The need for an additional 10 dB of target resolution was indicated. The radar frequency was reduced to 50 MHz and additional tests performed.

B. Data Analysis System Results

A complete prototype data anlysis system was devised, fabricated and tested for use as the processing portion of the airborne foliage penetration radar. In doing so, the concept of a real time reliable detection and analysis system was demonstrated.

An operator position complete with display and keyboard was developed for use in real time detection of targets. A useful, although not necessarily complete for all situations, set of processing routines was developed for the data analysis system and display system.

1.3.4 The Use of 140 MHz in Measurement of Clutter Returns

The use of 140 MHz in measurement of clutter returns was accomplished. Cross sections of lakes, pastures, and woods have been determined. The results of these tests briefly stated are:

A. Lake Data

The lake data reinforces the data from other programs which indicates that the cross section of water is a function of wind velocity and the direction from which the measurement is taken, since the returns are a function of the wave fronts and crests.

B. Pasture Data

Pasture data indicates that returns from fences, occasional trees and perhaps a slight roll to the land provide the majority of clutter cross section of this environment.

C. Forest Data

Of more significance is the forest cross section data, since it is not obtainable from currently available literature. Included in the data base is a substantial amount of data on the cross sections of northern forests both coniferous and deciduous.

1.3.5 The Use of 50 MHz in Measurement of Clutter Returns

The initial airborne measurements utilizing the lower frequency were very encouraging. The target to clutter ratio is considerably enhanced as was predicted in references (2) and (4) and as indicated by previous reports from AFCRL.

The interested reader is referred to Sections 5, 6, 7, and 8 for complete

details of the clutter measurement and cross section measurement efforts.

1.3.6 Airborne Data Collection

During the contract period significant portions of the collected data were included into the data base. Especially noteworthy are cross section measurements of forest environments that are not currently found in the available literatures (σ_o, at 140 MHz, for northern forests is on the order of 0.1 and 0.2).

Also of significance is the close correlation between actual environment and recorded data. As shown in Figure 1.6 the radar map presented on the display closely approximates the aerial photo of the same area.

The results of the airborne data collection effort can be summarized as follows: (Further details are given in Sections 6 and 8.).

1) A close correlation between the known terrain and the collected data.

2) The collected data were sufficiently reliable to include in the data base.

3) The operation of the radar at 50 MH enhances the clutter-to-target ratio.

4) At 140 MHz certain background environments result in poor target resolution.

5) The ability to experimentally determine radar cross sections of both joint targets and distributed clutter.

The Vincent Corners Tests yielded the most significant results, they were:

1) Fence lines and large stands of woods can give returns as strong as the standard target.

2) The use of a simple threshold detector in this environment is not practical.

3) Man-made objects and natural objects with sharp changes in cross sections cannot be separated from other corner reflector-like objects such as trucks.

4) The standard target return is discernible and measurable (although tests were conducted with the target in open areas and not shaded by trees).

A22061-U

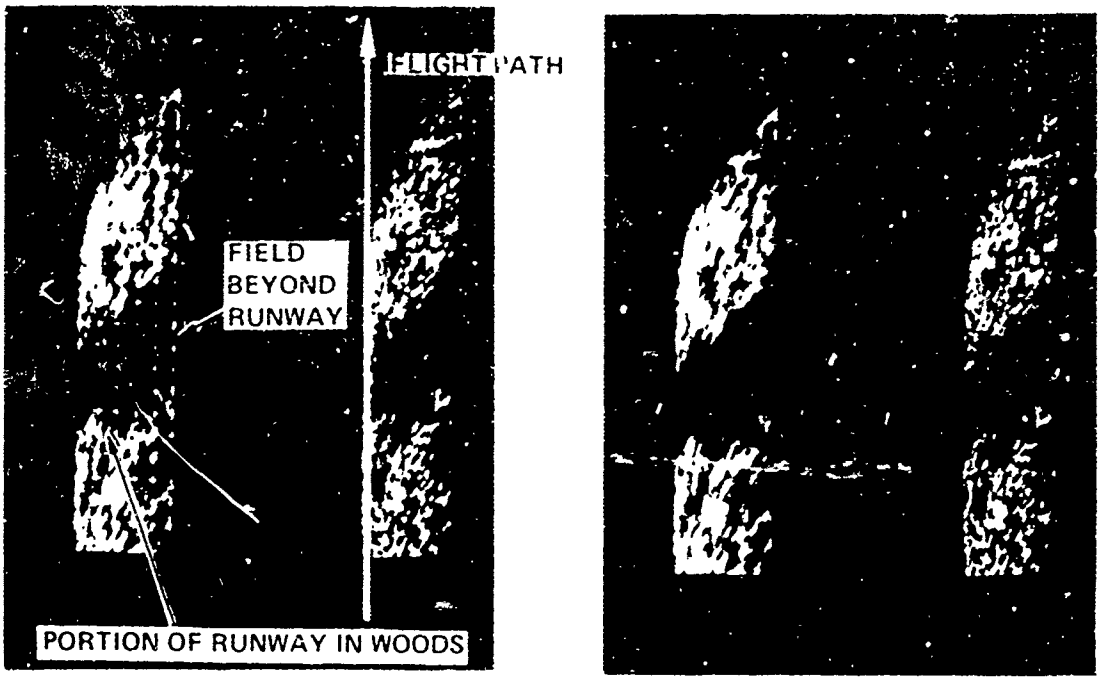

(a) RADAR MAP OF RUNWAY AREA (WITH 200 ft REFERENCE GRID)

(b) RADAR MAP OF RUNWAY AREA

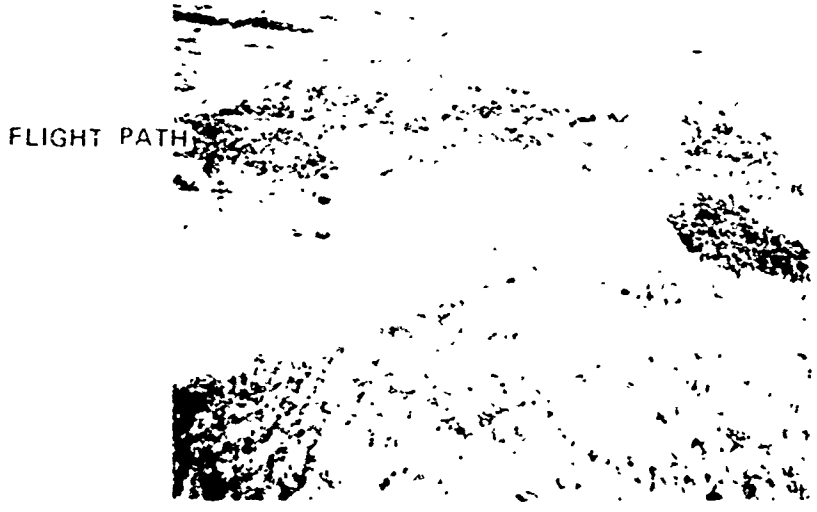

Figure 1.6 Correlation of Aerial Photogram with [illegible] Map

5) The calculated spectra and observed terrain are closely correlated.

In addition the other tests provided results which included:

The close correlation of the calculated and measured glint radar cross section of a helicopter was very encouraging. It is noted that the tactical usefulness of glint radar cross sections is probably minimal since it is highly dependent angle of arrival (the broadside illumination of a vehicle). Other attempts to correlate the recorded returns with expected returns were less successful than at the Aberdeen Proving Ground due to test conditions.

While experimentally unsuccessful during the test period, it should be emphasized that the magnitude of the glint cross section of a panel truck or armored personnel carrier should be sufficient to discern from the background clutter of the environments tested.

1.3.7 Polarization Study

The data used for this analysis was collected during the Moving Platform Study Contract (DAAD05-71-C-0156).

For this experiment a cross-polarized antenna was mounted on the front of a DC-3 aircraft in which the LWL-SURC FOPEN Radar, operating at 140 MCS was mounted. The transmitter was connected to the horizontal element via the usual duplexer system. The backscattered signal was received on both the vertical and the horizontal antenna elements and recorded on separate channels of the digital tape recorder. On the ground the data from each channel is fast Fourier transformed and the amplitude found in the usual way.

The experiments analyzed are numbers 299 and 300 taken at Camp Drum in Northern New York State and numbers 180 and 181 taken at Pompey Center Road near Syracuse, New York. The terrain at Camp Drum was flat and fairly heavily wooded with northern pine. These pines are a small pine with trunk diameter 6 - 12 inches and very thin branches. The region around Pompey Center Road is unevenly wooded, mostly with deciduous type trees. This region is not a forest, but contains steep hills, pasture land, houses and fences as well as trees. This region has not been checked in detail from the ground, hence it is not known exactly what is within the measuring cell at a given time. It is probable that most of the backscattering comes from trees of the deciduous type.

There does not appear to be any significant correlation in the fine structure of the variation of the signals from the vertical and horizontal receive channels. When a horizontal wave is transmitted and the target is deciduous forest, the horizontally received and vertically received signals are of the same average amplitude. When the target is a conifer forest, the vertically polarized received signal is about 20 dB weaker. This means

that certain types of targets which depolarize a radar wave strongly, such as missile launchers, field guns, etc., could be detected in a conifer forest by the use of polarization ratios. The detection of personnel does seem feasible from this platform by using polarization ratios.

1.3.8 Statistical Model

A statistical model (presented in Section 7.0) was theoretically derived which adequately describes the statistical data collected. Additionally, the reader may consult reference 4 for concise supplemental information. Comparison of data collected with the LWL-SURC airborne radar system and the statistical model indicate that the collected data points are within, or very close, to a standard deviation from the theoretical line.

1.4 Summary of Recommendations

Based upon the work accomplished during this program, the following recommendations are considered pertinent.

1.4.1 Addition of Focusing

A demonstration of additional focusing may be feasible. Other programs accomplished by AFCRL for the Air Force could form the basis for this effort. Adding this function to the present system may still allow its use in the smaller aircraft and the combined cost of this program and prior programs may still prove to be less expensive than highly focused systems.

1.4.2 Continuation of Glint Cross Section Measurements

The Glint Cross Section Measurement could be a useful technique. Further work in this area may provide information leading to a method of monitoring road traffic, monitoring stretches of coast line or other areas where personnel or vehicles may be moving parallel to the flight path.

1.4.3 Continuation of 50 MHz Effort

Tests completed late in the program and the associated data analyses provide the basis for serious consideration of additional effort in this area.

Benefits accrued in continuing this effort would be less expensive since SURC presently (1) has the equipment, in working condition, (2) has supplemental computer facilities all primed to accomplish this effort and (3) has the working knowledge of the system necessary for immediate continuation of the effort.

Additionally, the data collected could fill a void in current literature. Comparative data obtained from the initial 50 MHz flight test and previous 140 MHz effort are shown in Table 1.1.

Table 1.1

Comparison of Radar σ_o

Environment	140 MHz	50 MHz
Heavy Woods - Swamp	.84	.30
Northern Forest	.15	.02

2.0 DATA ANALYSIS SYSTEM DEVELOPMENT

A real time data analysis system was developed by SURC for utilization in the study of foliage penetration by radar for the United States Army under Contract DAAD05-72-C-0299. This system is shown in Figure 2.1.

The digital processing section of the FOPEN radar system consists of an analog to digital interface, a Varian 620/L-100 minicomputer, a hardware Fast Fourier Transform, a Digital TV display and a keyset. This section inputs time domain doppler radar data, converts it to digital data, processes it and generates a display on the CRT.

2.1 System Equipment

2.1.1 Minicomputer

The Varian 620-L is a small general purpose computer which uses a 16-bit word with a memory cycle time of 900 nanoseconds. The Varian 620-L in the SURC system is provided with 12K words of core memory, hardware multiply and divide, real time clock, priority interrupt module, and power failure/restart.

Hardware developed by SURC includes the digital TV display, the FFT processor and a number of interfaces to the Varian 620-L. These interfaces were for the display, FFT processor, A/D converters, and paper tape reader. Additionally an interface was developed to connect the Varian 620-L to a larger computer system in SURC's hybrid simulation laboratory. This allowed the software development phase of the program to take advantage of the many peripherals and existing software of the larger computer system.

The keyset is used by the operator to control or modify the processing and the display format.

Figure 2.1 also indicates the data flow through the digital processor. The analog radar data is input into the computer memory by the radar interface. The software processor converts this data to doppler information using the hardware Fast Fourier Transform, then filters this data further. The software display generator converts this information into a meaningful pattern on the Digital TV display.

2.1.2 Display

The display selected for this system is a Ball Brothers Research Corporation CRT monitor which measures 9 inches diagonally and utilizes P4 phosphor. The circuits are transistorized and printed circuit board construction is used throughout the monitor.

Modifications to this monitor include rotating the CRT 90 degrees so that the long dimension is in the vertical plane and ruggedization of its construction to meet the airborne application requirements.

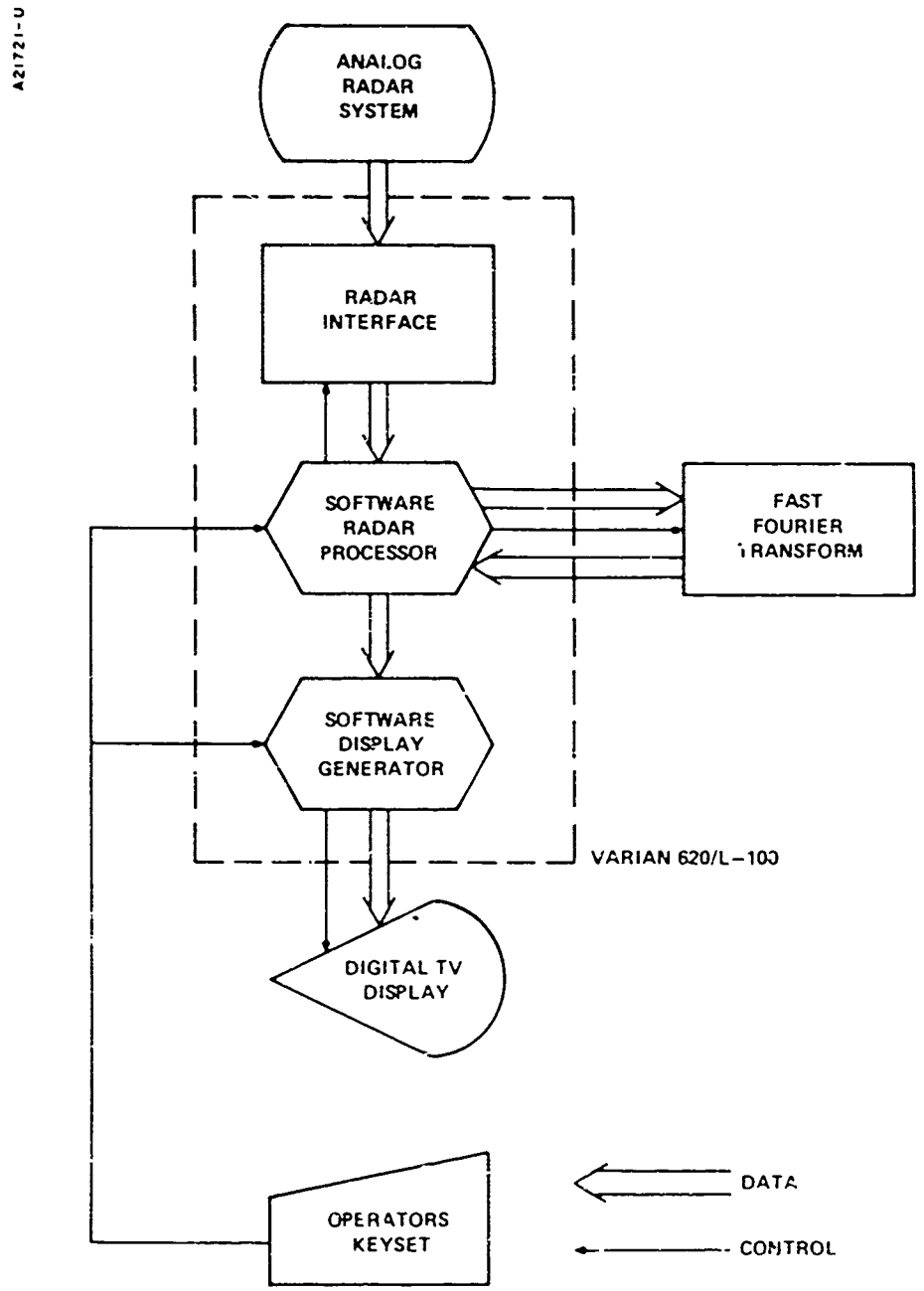

Figure 2.1 System Block Diagram

The display picture is produced using digital TV techniques. A non-interlaced frame is formed by vertical raster lines. The unbalanced or viewable portion of each frame provides a display grid of 256 by 256 picture elements. The frames are presented at a rate of approximately 53 Hz which produces a non-flickering display. Updating a display frame requires a period of one frame cycle or approximately 19 milliseconds.

The display can present both graphics and characters on two independent frames overlaid on the screen. One frame, a black and white display with no gray scale, is used primarily for alphanumeric information. The second frame providing eight levels of gray scale, is used to display graphic data, and is capable of being shifted to produce a moving map type of display. When shifted, new picture elements are entered at the top of the display frame and the oldest picture elements at the bottom of the display frame are discarded. Fixed data may be presented overlaid on a moving map type of display when both types of presentations are used simultaneously. Existing data in either frame may be modified by adding, subtracting, averaging or replacing it with data from the minicomputer. This capability allows at least a limited amount of data manipulation to be done on the display itself.

2.1.2.1 Radar Data Display

Radar data may be displayed as plots of signal strength as a function of doppler frequency using either the y-coordinate or the gray scale as the signal strength axis. An alternative display may be produced through a relatively simple coordinate transform that results in a strip map of the terrain with gray scale indications of signal strength at each area of ground.

2.1.2.2 Frequency Data Plots

Frequency data may be displayed as a family of horizontal lines which vary in brightness. In this presentation the x-coordinate represents doppler frequency plotted linearly with zero doppler frequency occupying the center of the line. The brightness of each spot on the line indicates the strength of the return at that particular doppler frequency. As new data is entered the lines move down the screen creating a time-sequenced frequency data plot.

2.1.2.3 Map

Mapping data is displayed in strips shaped in the form of an arc, that is, the map displays are a strip map of the ground with a curved upper margin. Each strip represents the area on the ground covered by the range gate at that time. Each strip is a linear map and as with other displays the map moves down the screen as new data is entered. The x,y coordinate of the display represent cross range and down range, respectively, and brightness represents the strength of the return signal from each area of ground. Further information on map display geometry is included as Appendix B.

Graphics data is created in two different modes. In one mode, vectors

are created by joining vertical line segments of variable lengths end to end. This mode is especially useful in forming graph plots or histograms. The second graphics mode produces vector segments of one to seven elements in length which may be placed on successive vertical raster lines in an overlap or non-overlap fashion to produce a band of map data. Dominant features of the data may be emphasized by varying the intensity or gray scale.

Characters are generated for presentation on the display. A set of 128 characters may be presented at any location in a display frame. Each character is produced on a five by seven picture element matrix. Two elements between successive characters are left blank for separation.

2.1.3 Display Generator

The display generator performs the vector, map, and character generation functions. To accomplish this the generator, developed at SURC, translates the minicomputer's digital word commands and data into a picture for presentation on the monitor. The display pictures which are stored in shift register memories located in the display generator are made available to the CRT monitor in video signal form at the frame rate of 53 Hz. In addition to video signals the display generator produces the horizontal and vertical synchronization signals to drive the display sweep circuits. Also the display generator contains the facilities for performing analog to digital conversions for eight analog signals.

At the beginning of each display frame the display generator issues an interrupt to the minicomputer (frame rate 53 Hz). If the display is to be updated, the minicomputer outputs to the display generator digital word commands (1) to establish the mode of operation of the display generation and (2) to establish the starting address of a block of display data words located in its core memory.

For one of the display modes, each picture element may have one of eight possible gray scale levels. Three bits of data for each picture element are stored in the refresh memories to define this gray scale level. In a second display mode, only a single intensity level is available. A separate refresh memory is used for this display mode. For both display modes, a total of four refresh memories each 256 by 256 bits in length are used.

The updated display picture is stored in the serial shift register memories whose starting address has been given to the display generator. Updating may consist of adding, subtracting, averaging or replacing, the data contained in the refresh memories. During the display frame, the data words are successively accessed by the display generator. The accessing of these data words is done by a direct memory access mode of operation, requiring no action by the minicomputer program other than the initial commands at the start of the display frame. The outputs of the serial shift register memories are digital to analog signals converted to video signals. The display generator performs its vector, map, and character generation functions in

updating the display picture.

As indicated, the display generator has the facilities to perform analog to digital conversions on a total of eight analog signals. An Analog Devices, Inc. 12 bit A/D converter is used for this purpose. The device can convert analog signals to digital numbers in 15 microseconds. The minicomputer controls the A/D operation via the display generator by selecting the analog signals to be converted, the rate of conversion, and the number of samples to be taken. Data samples are entered into the minicomputer memory by the display generator using the direct memory access feature of the minicomputer.

2.1.4 FFT Processor

The Fast Fourier Transform (FFT) processing unit efficiently computes the discrete Fourier transform (DFT) of a time series of discrete data samples to produce its discrete frequency spectrum. The FFT unit operates as a peripheral processor to the LWL 620/L-100 Varian minicomputer. Series of digitized radar data samples are collected by the minicomputer and then transferred to the FFT unit to be transformed into their frequency spectrum. The resultant spectrum data are then returned to the minicomputer for further processing.

The FFT unit operates on the digitized radar data in near real time since the transform is performed in approximately eight milliseconds. This includes the time necessary to load the FFT unit with the digitized radar data and also the time to unload the frequency spectrum data into the minicomputer. Thus approximately 125 DFT's may be performed each second by the FFT unit.

The size of the FFT unit is 256 complex words. Each radar data input word has a real and imaginary part, each consisting of 16-bits. The spectrum resulting from the transformation process is also complex, producing spectra, each having a 16-bit real part, and a 16-bit imaginary part.

2.1 4.1 FFT Computations

A signal flow diagram of the LWL FFT algorithm is shown in Figure 2.2. For purposes of simplification, the diagram illustrates an 8-point discrete Fourier transform (DFT) instead of the actual 256-point DFT used in the LWL processor. Each node in the signal flow diagram represents a variable, and the arrows that terminate at that node originate at the nodes whose variables contribute to the value of the variable at that node. The contributions are additive, and the weight of each contribution, if other than unity, is indicated by the constant close to the arrowhead. The quantity $e^{j2\pi/N)k}$ is denoted by W^k in the diagram. The expression for the DFT of the algoritm is:

$$F_k = \sum_{n=0}^{N-1} f_n W^{nk}, \quad \text{for } 0 \leq k \leq N-1$$

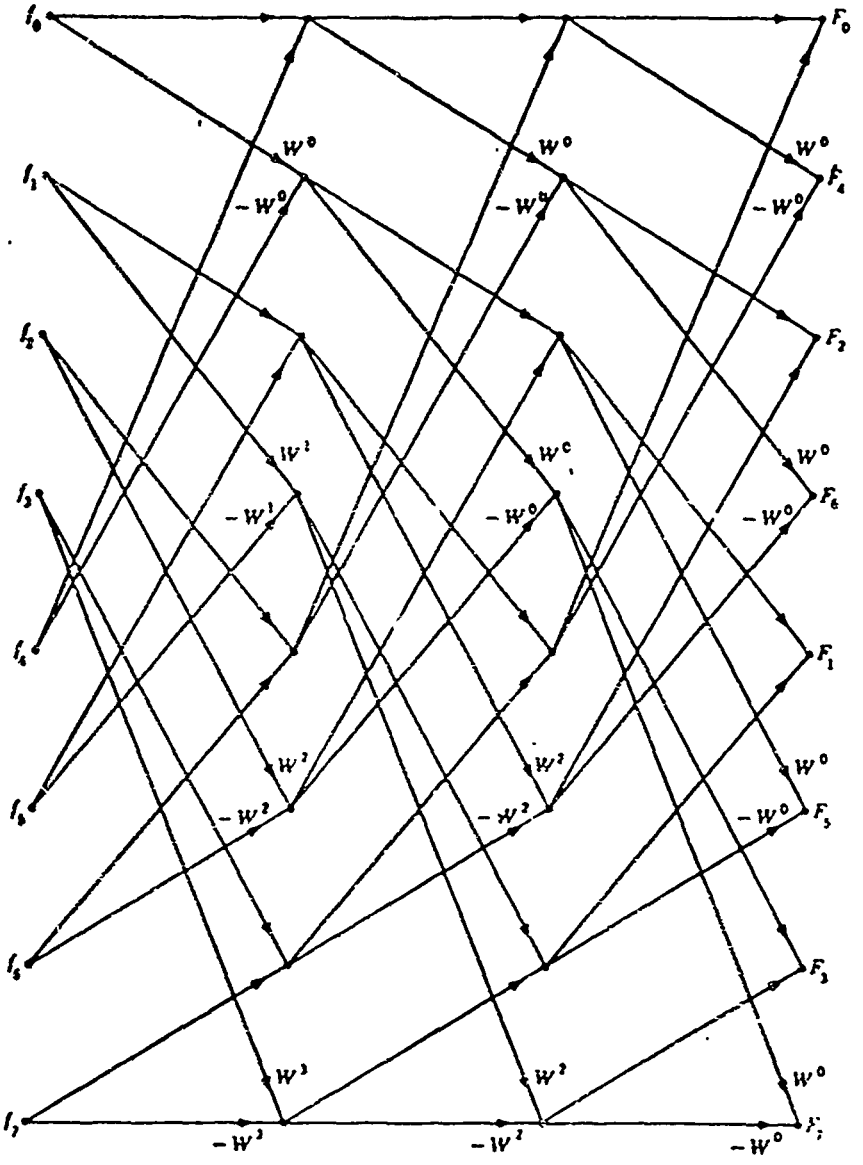

Figure 2.2. Signal Flow Diagram

The signal flow diagram illustrates the computations necessary for evaluating an 8-point DFT. If the diagram is examined closely, it can be seen that there are three sets or stages of calculations, and the calculations necessary from one stage to the next stage are identical in each case. The number of stages required for the DFT is equal to $\log_2 N$, so that for the 256-point DFT eight stages are necessary.

In each stage, the calculation required to determine the value of the even numbered nodes is simply $f_n + f_n + N/2$, for $0 \leq n \leq N/2-1$. The values of the odd numbered nodes are determined by multiplying the constants W^k by $(f_n - f_n + N/2)$, for $0 \leq n \leq N/2-1$ The constants W^k are obtained from a read only memory (ROM) located in the FFT processor. The ROM contains the values for $W = e^{-j(2\pi/N)}$, and since the $\sin \theta = \cos (\pi/2 - \theta)$, the number of constants stored in the ROM pertain to only a single quadrant. Thus, it is only necessary to store 64 constants for the evaluation of the 256-point DFT for LWL. Appropriate addressing logic and complementing circuitry to obtain negative values provide the sine and cosine values for the complete 2π radians.

The block diagram (Figure 2.3) of the LWL 256 complex word FFT illustrates the manner in which these computations are performed. The values for f_n and $f_n + N/2$ are simultaneously read from the shift register memories for both the real and imaginary parts. Parallel additions and subtractions are performed on these numbers. The sum of each part is directed to its memory input multiplexer to be written in memory at the next memory write cycle. The difference of each part is directed to the multiplier input selector to be used as one of the factors in the complex multiplication of W^k times $(f_n - f_n + N/2)$. A single 16-bit high speed 2's complement multiplier performs the multiplication. Since a complex multiplication requires four partial products, the single multiplier is time-shared to produce each partial product. The partial products are stores in latch circuits in the "cross-product summer" logic. Upon completion of the multiplication process, the appropriate partial products are summed by the cross-product summer and the results are presented to the memory input multiplexers to be written into memory on the next memory write cycle. For each shift register memory read operation, there are two write operations.

2.1.4.2 Shift Register Memories

The memories used in the FFT processor are constructed about the Signetics 2521V dual 128-bit MOS static shift register. The memories are contained on printed circuit (PC) cards and each PC card has the capacity to store 256 16-bit digital words. A total of four PC memory cards (SURC No. 2980) are used by the FFT processor.

Each of the PC memory cards are organized into two sections of 128 words each, an A section and a B section. In processing one stage of the FFT, the input data words are read from the A section and processing results are written in the B section. During the next stage the situation is reversed; the input data words are read from section B and the results are

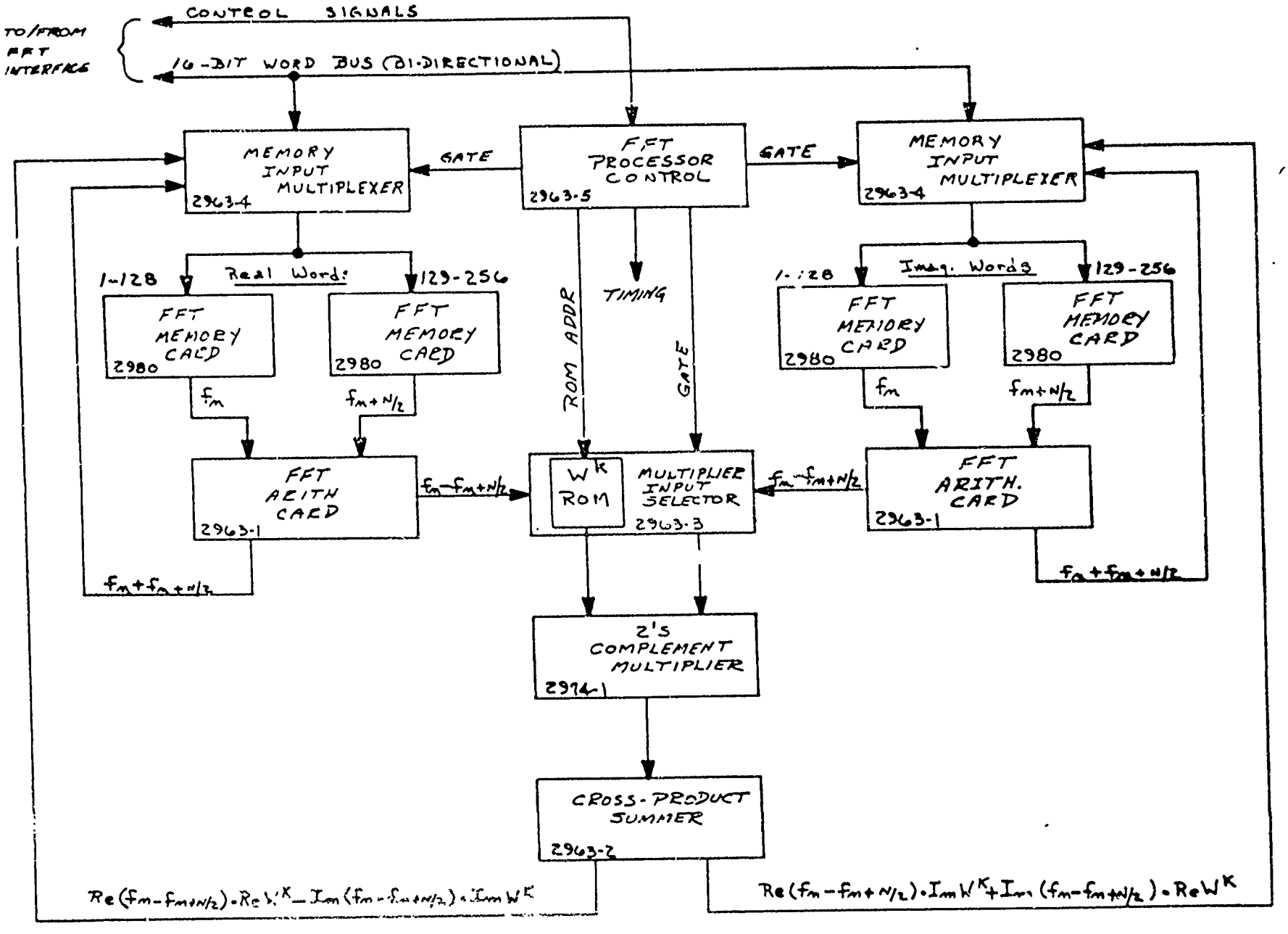

Figure 2.3. Block Diagram - 256-Complex Word FFT

written into the A section. This alternation between the A and B sections of the memory continues for each stage of the FFT process. The "raw" input data words are initially loaded into the FFT unit via the A sections of the PC memory cards. If we designate the PC memory cards as numbers 1 through 4, then following the initial loading, the 16-bit words of the real and imaginary arrays are stored as follows:

Card 1: contains real words 1 through 128
Card 2: contains real words 129 through 256
Card 3: contains imaginary words 1 through 128
Card 4: contains imaginary words 129 through 256

2.1.4.3 Read/Write Sequence

Each stage of the FFT process contains 128 computation cycles. For each cycle the shift register memories are accessed for the input data words used in the FFT computations and then the results of the computations are written in the other sections of the shift register memories, whereby they will be the source of input data words in the following stage. The nature of the FFT algorithm requires that the words resulting from the computations be reordered relative to the sequence of the input data words. The read/write sequence of the memories for a stage of the FFT process is shown in the following table. Only the set of real data words is shown, since the sequence of the imaginary set is identical. It can be seen that for each read operation, there are two memory write operations.

	Read		Write	
Cycle	Card 1	Card 2	Card 1	Card 2
1	1	129	1,2	Recirc.
2	2	130	3,4	Recirc.
3	3	131	5,6	Recirc.
+	+	+	+	+
+	+	+	+	+
63	63	191	125,126	Recirc.
64	64	192	127,128	Recirc.
65	65	193	Recirc.	129,130
66	66	194	Recirc.	131,132
-	-	-	-	-
-	-	-	-	-
126	126	254	-	251,252
127	127	255	-	253,254
128	128	256	-	255,256

2.1.4.4 Scaling

The scaling function in the FFT processor insures that during any of the arithmetic operations an overflow cannot occur. This is accomplished after examining the magnitude of the absolute value of each factor as it is entered into the FFT's shift register memory. Both parts of each factor, real and imaginary, are examined to note if the magnitude of its absolute value is greater than or equal to one-half, or greater than or equal to one fourth. If so, the fact is stored and during the following stage all factors of the FFT arrays are appropriately shifted. This examination of the magnitude of the factors is done initially as the arrays are loaded into the FFT from the minicomputer and also during each stage as the results of computations are entered into the memories. If it is observed that the absolute value of any factor's magnitude is greater than or equal to one fourth, but not one-half, then all factors are shifted right one binary position, dividing all factors by two. On a stage basis, a report of the number of shifts done on the FFT factors, is made to the FFT interface logic by the FFT processor control logic. A tally is maintained by the interface logic in a status register which will be queried by the minicomputer program.

2.1.4.5 Read Only Memories

The Read Only Memories (ROM's), located on the multiplier input selector circuit card, produce the W^k constants used in the FFT computations. There are four ROM modules and each module contains 32 8-bit digital words. The words are programmed into the modules by a fusing process and thus are premanently stored. The modules are organized to produce 64 16-bit W^k constants, where $W^k = e^{-(2\pi k/N)}$. The values stored in the ROM modules represent the cosine values for the interval from 0 to $\pi/2$ radians (Table 2.1.).

For the 256-point DFT there are 128 W^k constants necessary for the evaluation. From the signal flow diagram of Figure 2.2, which is an 8-point DFT having only 3-stages, it is shown that all of the constants are used during the first stage. In the second stage only every other one is used, and in the third stage, every fourth one. In the larger 256-point, 8-stage DFT of LWL a similar situation exists; all 128 constants are used in the first stage, 64 constants in the second stage. The selection of the proper constant for each computation in the FFT process is determined by the ROM addressing. The lower order address bits to the ROM's are masked on a stage basis to achieve the proper selection. During the first stage none of the address bits are masked and all constants are selected. In the second stage, the lower order address bit is masked and thus only every other constant is selected. In successive stages, additional address bits are masked, until the last stage is reached where all address bits are masked giving an effective address of all 0's, which is the address of the first location in the ROM's.

The evaluation of the DFT requires sine and cosine values for the

Table 2.1 ROM CONSTANTS TABLE

ADDR	VALUE	ADDR	VALUE
0	77777	32	55202
1	77766	33	54103
2	77731	34	52766
3	77647	35	51633
4	77542	36	50464
5	77412	37	47300
6	77235	38	46100
7	77036	39	44664
8	76612	40	43435
9	76344	41	42173
10	76052	42	40716
11	75535	43	37427
12	75175	44	36127
13	74612	45	34615
14	74205	46	33272
15	73554	47	31737
16	73102	48	30374
17	72405	49	27021
18	71666	50	25437
19	71125	51	24047
20	70343	52	22450
21	67537	53	21044
22	66712	54	17432
23	66044	55	16014
24	65156	56	14371
25	64247	57	12742
26	63320	58	11310
27	62351	59	07653
28	61362	60	06214
29	60354	61	04553
30	57327	62	03110
31	56264	63	01444

NOTE: Values are expressed as octal numbers and defined cosine function over interval of 0 to Pi/2 radians.

REAR

#					#
				FFT PROC CONTROL 2963-5	5
				FFT MULT INPUT SEL 2963-3	6
				FFT MULT 2974-1	7
				CROSS PROD SUMMER 2963-2	8
				(REAL) FFT ARITH 2963-1	9
1	FFT MEM (REAL 0-127)	2980		(IMAG) FFT ARITH 2963-1	10
2	FFT MEM (REAL 128-255)	2980		(REAL) FFT MEM INPUT MUX 2963-4	11
3	FFT MEM (IMAG 0-127)	2980			
4	FFT MEM (IMAG 128-255)	2980		(IMAG) FFT MEM INPUT MUX 2963-4	12

FRONT

LWL FFT CHASSIS LAYOUT

interval of 0 to π radians. Since only the cosine values for the interval of 0 to $\pi/2$ radians are stored in the ROM, interpolation is necessary to obtain the other values. The identities, $\sin\theta = \cos(\pi/2 - \theta)$ and $\cos\theta = -\cos(180 - \theta)$ are used for this purpose. Negative values are obtained by forming the 1's complement of the constant desired. The IMAG and REAL gating signals are applied to the addressing logic to select the sine or cosine function. The IMAG gating signal produces $-\sin\theta$ and the REAL gating signal produces $\cos\theta$ for the interval of 0 to π radians.

2.1.4.6 Multiplier

The multiplier used in the FFT is a high speed 2's complement multiplier constructed of 4 x 2 multiplier modules (Advanced Micro-Devices Am 2505). The multiplier is constructed on a single printed circuit card (SUR No. 2974), and is capable of multiplying two 16-bit 2's complement binary numbers to form a truncated product of 16-bits. The multiplier in the FFT is operated somewhat conservatively and it performs a multiplication in less than 750 nanoseconds. Each complex multiplication in the FFT process requires four multiplications to produce the cross products of the two complex binary numbers. The cross products are formed and stored in the cross product summer until the multiplication cycle is complete. The following multiplications are performed for each complex multiplication in the order given:

1) $R_e (f_n - f_n + N/2) \times R_e W^k$

2) $R_e (f_n - f_n + N/2) \times I_m W^k$

3) $I_m (f_n - f_n + N/2) \times R_e W^k$

4) $I_m (f_n - f_n + N/2) \times I_m W^k$

2.1.5 Keyboard

The keyboard consists of a standard keyboard with an array of function keys on each side of it. Figure 2.4a shows the arrangement of the keyboard and the organization of the function keys. The group of function keys on the left are used to control the operation of the system (Figure 2.4b). The central keyboard and the typesetting function keys are used to enter data into the system. The group of functions at the right allow the operator to display and modify data used by the system (Figure 2.4b.).

During system initialization and when displaying data values, the operator can enter new values using the central keyboard in conjunction with the typesetting functions. The quantities which can be changed are displayed on the screen along with a keyboard pointer character. This character is used to indicate the position into which the next character typed will be entered. The keyboard pointer can be moved using the typesetting functions as described in Table 2.3. After the values are entered, the keyboard pointer is removed from the screen. The alphanumeric keyboard and the

(a) KEYBOARD LAYOUT

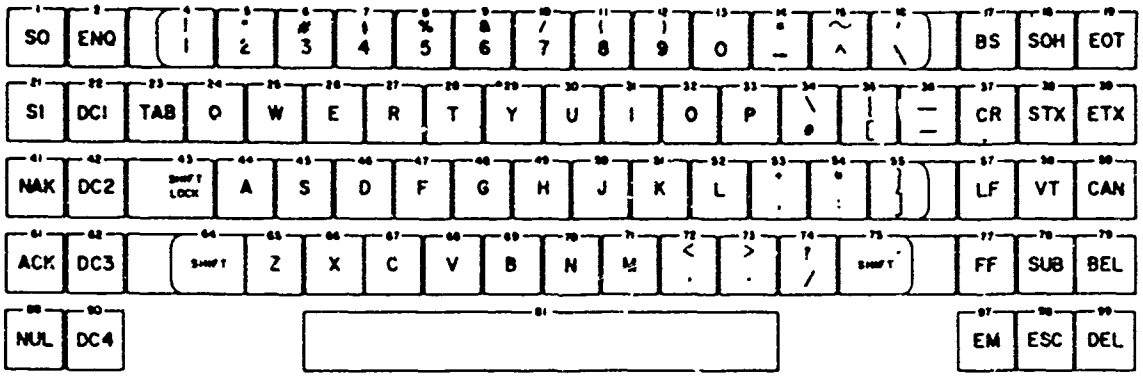

(b) FUNCTION KEY GROUPS

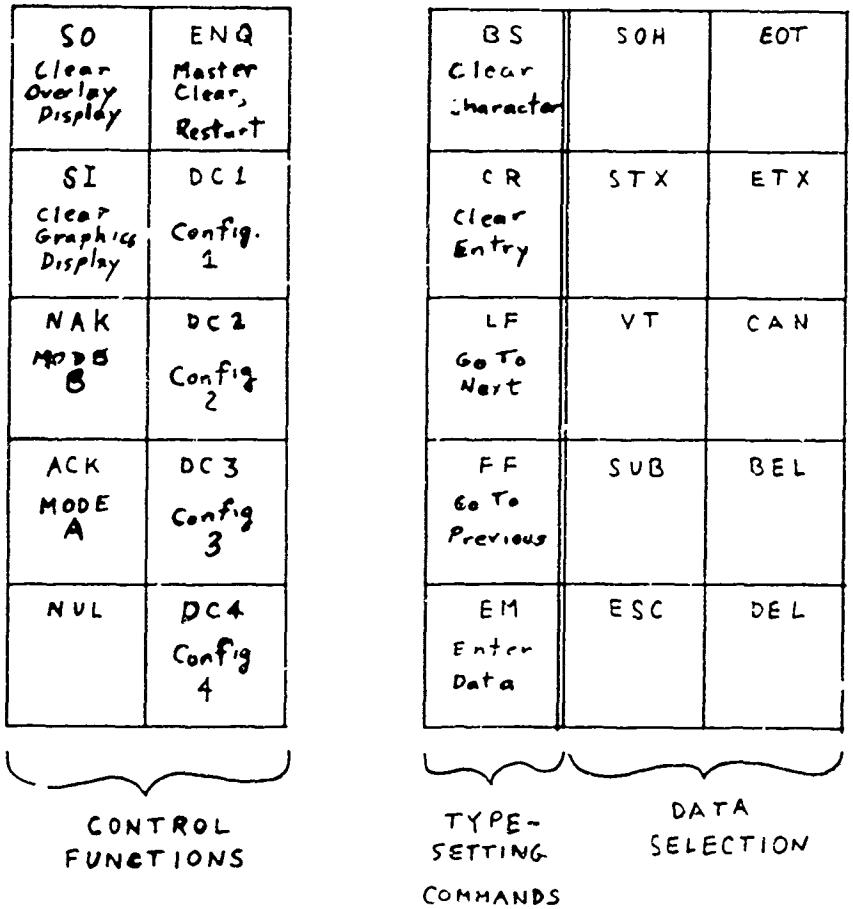

Figure 2.4. Keyboard Layout

Trble 2.2 Key Functions

Key Label	Function	Key Label	Function
	CONTROL KEY DEFINITION		
SO	Clear Overlay Display	ENG	ABORT
SI	Clear Graphics Display	DC1	Use Processor #1
NAK	Select Processor Bank A	DC2	Use Processor #2
ACK	Select Processor Bank B	DC3	Use Processor #3
NUL		DC4	Use Processor #4
	DATA SELECT DEFINITION		
SOH	Altitude	EOT	Frequency Plot Size
STX	Grid Spacing	ETX	Threshold Control 1
VT	Sample Rate	CAN	Gain Control 1
SUB	Shift Count	BEL	Threshold Control 2
ESC	Number of Averages	DEL	Gain Control 2

TYPESETTING FUNCTIONS

Key Label	Operation
BS	Erase last character. Move Pointer left one character.
CR	Erase entire entry. Move Pointer to start of entry.
LF	Move Pointer down to next line (if any).
FF	Move Pointer up to previous line (if any).
EM	Enter values, remove Pointer, disable keyboard input.

Table 2.3 Typesetting Function Definitions

Key Label	Function
BS	Move Pointer left one character, erasing the character that was there previously.
CR	Move Pointer to 1st character in data field, erasing the entire value.
LF	Move Pointer down to next line (if any). This does not modify any characters.
FF	Move Pointer up to previous line (if any). This does not modify any characters.
EM	Enter data and remove pointer. This disables all alpha-numeric and typesetting keys unless an error condition exists.

typesetting function keys will no longer have any effect on the system.

Individual values, used by the system, are selected for display and modification by the data select function keys. These keys are located in the last two columns at the right side of the keyboard. Pressing one of these keys causes the selected value to be displayed on the screen along with the keyboard pointer. The alphanumeric keyboard and function keys are then activated to allow the operator to change that value if he desires. The Data Select keys can be used at any time after System initialization.

The control keys at the left side of the keyboard perform a variety of functions in the system. The operator can clear the display, reconfigure the system or abort the run entirely using these keys. The display clear keys allow the operator to erase either the gray scale or overlay displays independently. The mode keys select banks of processors and the data control keys cause the system to switch over to a specific processor in the selected bank. (Note that the mode keys do not change the processor being used in the system.). The abort key master clears the entire system. This key terminates all processing, clears both display presentations and returns to the System initialization state.

2.1.6 Analog to Digital Interface

The Digital processing equipment is interfaced to the radar system via the analog to digital (A/D) converter. This device translates up to 8 channels of analog signals to digital equivalents. The selection of analog channels and the sampling rate is controlled by the minicomputer software. Any combination of the 8 channels can be used. The sampling rate is specified by the time delay between successive scans of the selected channels. This parameter ranges from 50 μsec to 12.8 msec in steps of 50 μsec.

2.1.7 Processors

The digital radar processing system can have 8 different processor types available for use. These processors are organized into two banks of four processors. The operator can select any one of these processors for use by hitting one of the mode keys followed by one of the processor select keys.

The processors can vary in the amount and type of filtering done on the radar data as well as the manner in which the results are presented on the display. In general, however, the processors will perform the following steps: input data, shift data, FFT, Hann, magnitude squared, logarithm, scale and display. Additional filters can be inserted into the sequence at will but the steps outlined above will be present in most of the processors.

Radar data is input from the A/D directly into memory without program intervention. The program does have to specify the number of samples and how fast to input the data. The sampling rate is defined as the time delay between successive samples of a given analog signal. This is given in

milliseconds with a resolution of .05 msec.

The number of samples input at one time is defined by the shift count. The data is processed by the Varian in blocks of 256 samples. These samples are allowed to overlap, which results in a sampling window which slides along the data. The displacement between adjacent windows is given by the shift count. The A/D interface performs one part of this process. The program shifts the old data to match with the data being input.

The next step is to translate the time domain data into the frequency domain data using the hardware FFT to produce the spectrum of the doppler components of the radar return. This data is filtered with a Hanning filter to remove distortions of the spectrum which can be caused by the FFT process.

At this point the data consists of both real and imaginary data. The next step is to compute the magnitude squared of these two sets of data by squaring each and adding the corresponding points. This produces a power spectrum of the doppler return.

The logarithm of this power spectrum is taken in order to improve the dynamic range of the data displayed allowing the smaller signals as well as the strong ones to be seen in the data.

The data is scaled as the final step before being displayed. Scaling is done in two steps and performs two functions. First, an offset is added to the data and then the result is multiplied by a scale factor. These two values determine the range of values which will be displayed as well as the upper and lower cutoff values. Any value above the upper cutoff point is limited to the cutoff value and any value below the lower threshold is set to zero.

The data is now ready to be displayed. The exact display format depends upon the processor in use but will be one of those described in the display section.

2.1.8 Paper Tape Reader

A high speed paper tape reader provides the data analysis system a relatively rapid and reliable means of loading programs or entering data into the minicomputer's core memory. The paper tape reader is a Digitronics Model 2030 Perforated Tape Reader, and is designed to read 5, 6, 7 or 8-channel perforated tape in the forward direction at speeds up to 400 characters per second.

The interface between the Model 2030 reader and the minicomputer was developed at SURC. The interface accepts digital data words from the minicomputer and translates these words into RUN and HALT commands which are directed to the reader. The channel data lines from the reader are formatted, by the interface, into digital data words and entered into the minicomputer.

2.2 Processing Software

The system is required to operate on a large amount of data in a very short time. Not only does the A/D converter input a lot of data, but due to the sampling algorithm, the effective data rate is several times that of the A/D sampling rate. Since the required processing algorithms are also fairly complicated, a number of advanced techniques are used to speed the operation. Perhaps the most important of these techniques is the hardware FFT. This device calculates a 256-complex point frequency spectrum in under 10 milliseconds of elapsed time and only uses about 2 milliseconds of computer time. In comparison, a software FFT would use on the order of 50 milliseconds to perform the same operation.

To further reduce the minicomputer load, all peripherals which transfer large quantities of data use the Direct Memory Access (DMA) option of the Varian 620/L-100. This option allows data to be input or output with a minimum of program intervention and uses a minimum of computer time to perform the actual transfer.

The software of the system is designed to minimize wasted time while retaining flexibility. Processing is performed in stages which can overlap in time. In this way, a delay in one stage can be used in another stage. Buffers used by the processors are taken from a common pool. This allows data to pile up somewhat at bottlenecks without slowing down previous steps in the process. The use of a buffer pool also facilitates the use of a number of different processing algorithms within the same system.

2.2.1 System Initialization

The system is initialized whenever one of three events occur: (1) the program is loaded from paper tape, (2) the program is manually restarted, or (3) the operator hits the abort key. The initialization program clears all I/O devices and control tables. It then enables the keyboard and display, and accepts run parameters typed by the operator. When this data has been entered, the program performs a number of preliminary calculations of constants and tables to be used later. The program then initializes control tables and flags for the run mode and starts the data flow through the system.

The system initialize routine immediately disables all interrupts and stops any I/O which may be active. All peripheral controllers are then master cleared. The keyboard and display are both initialized and the displays are cleared. The initialization then calls PCIN which initializes the processors.

The subroutine PCIN performs two functions. It must input any constants which must be supplied by the operator and then it calculates any fixed tables and constants which will remain constant during the run. These will include the FFT bin index table and the y-coordinate table used when generating map displays. Doing these calculations at this time reduces the load later

when time is at a premium.

When PCIN has finished, the initialization routine enables all interrupts and peripherals which will be used during run. Processor #1 of mode A is automatically selected. To start the flow of data through the system, one buffer of 256 samples is input to initially fill the input buffer. At this point the initialization routine can link to the executive (SCAN) and the system will be in the run mode.

2.2.2 Partial Initialization

The operator is able to change various parameters during the run. Some of these parameters affect the constants generated by PCIN, and some can affect the input constants for the A/D converter. In the first case, an abbreviated version of PCIN, called PIN1, is used to update processor constants. In the second case, the A/D is reinitialized, including the input of one full buffer. This may be noticed as a hesitation in the data flow as the one larger buffer is collected.

2.2.3 Executive Routines

The executive routines provide the linkage between the various sections of the program and assign buffers to the various programs as needed. The program linkage is done by a pair of scan loops which monitor the status of the various programs. Two scan loops are used to prevent low priority tasks from interferring with the flow of data through the system.

2.2.4 High Priority Scan Loop

The high priority scan loop performs the linkage between the various radar data processing programs and any other high priority programs. This program scans a list of functions, linking to any active ones. All processing programs are required to link back to the executive program whenever a delay is encountered as well as when they are finished. The processing programs can link back in one of three ways:

1) If the program has completed all tasks it must jump directly to SCAN. This completely removes the program from the scan table.

2) If the program encounters a delay it must call the subroutine HOLD. This subroutine stores all registers and sets the scan link to the subroutine return address. When this happens the scan is continued from the next entry. Control is returned to the program on "hold" during the next scan with all registers restored.

3) If a program finds that it is still in a wait condition after returning from a call to HOLD, the program jumps directly to

NRDY. This link preserves the hold already in the scan table but does not register the program as being "active". This is important since the low priority scan can only be accessed if the programs in the high priority scan loop are all "not ready".

In addition to the routines listed above, there is a subroutine called PHLD which allows one stage of the processor to activate the next stage. PHLD does not directly execute the next stage, and it does not return control to the executive routine. All it does is store the registers address and the proper link address in the scan table entry for the next processor stage. PHIL then immediately returns to the calling program. (Note that this may be done more than once if identical operations must be done on different data sets during one iteration. Any distinguishing characteristics must be carried to the next stage via the register contents when PHLD is called.)

2.2.5 Low Priority Scan Loop

When the high priority scan loop is able to complete an entire scan without finding any active programs, the low priority scan loop is executed. The low priority scan is advanced only one step each time it is entered. The only return allowed for a program called from this loop is to BNRD. BNRD preserves the entry in the table then returns to the high priority scan loop.

The low priority scan loop links to programs like the error report program and keyboard processor. Any functions which can tolerate a slow response should be put into the low priority scan loop.

2.2.6 Buffer Allocation

Buffers are assigned to the programs, as needed, from a common pool. Three sizes are used for the three basic types of data. A program can get a buffer assigned to it by calling the appropriate GET_ subroutine. Input buffers are 512*N words long, where N is the maximum number of range gates used. Calling GETB assigns one of these buffers. Double buffers (GETD) are 512 words long for use as complex or double precision data arrays. Scratch buffers (GETS) are 256 words long and are used for all buffers 256 or less words long.

The buffers are assigned to a program by storing that program's usage code to the reference table. When the program is done with the buffers, it can release all buffers assigned to it by calling FREC with the appropriate usage code in the A-register. FREC clears all reference table entries equal to the given code for all three types of buffer.

If a buffer will be used by the next stage in the processing the corresponding usage code must be incremented before calling FREC. Any buffer which will be used by the display must be assigned a code of 8 to prevent it from being destroyed prematurely.

2.3 Keyboard Software

The keyboard characters are input to the computer by the keyboard interrupt routine. Each time a key is struck, an interrupt is generated which causes this routine to be executed. The interrupt routine then inputs the code for the character or function key and stores it into the keyboard character stack.

The keyboard processor is a low priority program which takes the characters from the stack and acts on them. Each time this program is entered from the executive routine, it processes all characters in the stack. If the character is a function, the corresponding function routine is executed. If it is an alphanumeric character, the keyboard processor first checks to see if the keyboard is active. When the keyboard is active, the keyboard data table specifies a character store routine which is used to process the alphanumeric characters. Otherwise, the alphanumeric characters are ignored.

Keyboard processing of data entires is controlled by a keyboard data table. This table is set up by the program which requests the input. The data table consists of an arbitrary number of elements the last of which consists of all zeros. Each element specifies the display coordinates of the entry, the storage buffer address, and the character store routine to be used. Each element of the table is associated with one line on the display and one data entry.

To facilitate the use of the keyboard, two subroutines, ITAB and FILL, can be used for handling a list of parameters. ITAB displays the current value of each parameter and its label. It then activates the keyboard to allow the operator to make changes. When the operator pushes the enter key (EM), ITAB will return with all character buffers updated. The FILL subroutine can then be used to convert these buffers to a list of binary values. These routines will work for decimal numbers only but will scale each entry independently when converting them to binary. This system is used primarily during system initialization.

Function keys are processed via two function tables. The first table contains the address of the function routine to be used for each function key. The second table contains a single constant for each key which is used as an entry condition to the function routine. This second table allows one function routine to handle an entire class of functions.

2.4 Display Software

The digital TV display can only perform one operation during each raster scan. This means that each buffer, regardless of length, and each command will require 20 milliseconds to be processed and may have to wait up to 20 milliseconds before it can even be started. For this reason, it is imperative to be able to stack a number of display operations at any one time.

The display stack consists of a number of four-word entries which are referenced, circularly, via two stack pointers. This stack is controlled by three subroutines. The display interrupt subroutine, DPIN, removes entries from the stack as they are displayed. The check routine, $DCK, tests to see if the stack is full. The store routine, $DPØ, stores a new entry into the stack.

Each entry in the stack consists of four words: the display buffer address, the initial condition word, the EXC command to be used, and the buffer switch address. When the entry is processed, the first two words are output directly to the display: the initial condition word specifies the initial y-coordinate, the display mode, and selects the display buffer. (See the section on the display interface.) The third word in the stack entry is the external command instruction which is executed to start the display process. The fourth word is stored in DPIN and is used, on the next interrupt, to clear the buffer busy switch. This can be an entry in one of the buffer reference tables. In this way, the program generating the display buffer does not have to worry about calling FREC to free the buffer. A usage code of 8 is reserved for display buffers to prevent unintentional use of a display buffer before it has been processed. Note that the display stack entry is freed 20 milliseconds before the buffer can be used again.

Higher level routines are also available which will generate various types of display buffers and store them into the display stack. The general graphics routines DPLT (vector plot) and DMAP (non-linear gray scale plots) as well as the more specialized PLD2 (x,y) and PLD3 (gray-scale) are available which will handle normal data buffers. Packed character buffers are handled by DCAR and display shifts are performed easily using DSFT. The more straightforward functions such as the screen clears can be handled easily using $DCK and $DPØ. Refer to the program specification sheets for more details on the use of these programs.

2.5 A/D Software

The A/D converter is handled by two routines, ADIN and $ADI. ADIN is called during the system initialization. This routine computes the proper rate, mask, buffer size and offset values which will be used in processing A/D interrupts. ADIN also starts the initial input buffer which is always a full 256 samples. $ADI is the A/D interrupt routine. This routine tests to see if the last word of the buffer was filled then initiates the next buffer and sets the iteration mark to start the processing sequence.

For any given number of channels, n_c, and shift count, n_s, the buffer address is offset by n_c $(256 - n_s)$. Using this starting address fills only the last part of the buffer. The processor can then fill in the first part of the active buffer with old data from the previous buffer at any time during the sample iteration.

2.6 FFT Software

The FFT is normally handled by the subroutine FFT$. This subroutine assumes that the imaginary buffer immediately follows the real buffer in memory. The transformed data may be stored into the same buffer that the original data came from or it can be stored in a different buffer. This subroutine does not return until the entire transform is complete. It does, however, call HOLD which will allow other programs to operate.

FFT$ tests for three types of errors which can occur. The first is a test of the status word to check for hard errors in the FFT processor. The second test verifies that the FFT is complete when the interrupt occurs. The third test checks for loss of the interrupt. The last two errors will not normally affect the validity of the data.

2.7 Data Processors

The data processors are the heart of the system. These routines do the actual processing and filtering required to produce a meaningful display for the operator. The data processors are organized as a set of up to five processing stages. This is done to allow them to make full use of the time sharing and buffer features of the system. In addition, breaking up the processor into stages allows some of the stages to be used by other processors as well.

To give the system flexibility, a library of up to 8 different processors can be available for use. This library is organized as two banks of 4 processors. The operator can change processors at any time without interrupting the data flow through the system. Selecting different processors can modify the display format, change the degree and type of filtering done, or even change to a completely different processing philosophy. A general description of the control and data flow through a processor follows. For details on specific processors, see the program specifications. (Section 3.1.2.)

The processing sequence begins in the A/D interrupt routine. This routine sets the iteration mark to indicate that new data is ready for processing. The executive monitors this iteration mark, starting the first stage of the processor when it is set. This first stage performs any raw data shifting required and sorts the data into separate buffers. This first stage can also perform an FFT on the data. It then calls FHLD to transfer the data to the second processor stage. The first processor is still in control and can continue sorting if more than one range gate is being used or it can clean up its operations and deactivate itself by calling SCAN. When the first processor links to SCAN it will not be executed again until the next iteration mark.

The second processor has now been activated and will be executed the next time the high priority scan encounters it. The contents of the three minicomputer registers, upon execution of the second processor, will be the

same as when PHLD was called by the first processor. The three computer registers are used to pass all necessary information between the two stages including the address of the data buffer. The second processor can now operate on the data, usually reducing it in size to a single scratch buffer or less. This stage normally performs a number of steps in a single loop for efficiency. These steps will include Hanning, computing the magnitude squared, and sometimes taking the log of the data. The higher frequencies can usually be dropped in this stage to reduce the amount of data to be processed. In addition, the data is no longer in a complex form, which can cut the amount of data in half.

When the second stage is complete, the data is passed to the third stage which is activated by a call to PHLD. The second stage can then be terminated with a jump to SCAN. This completely deactivates the second stage until it is activated again by the first stage. Control is passed, in similar fashion, through all the stages of the selected processor. When the final stage (not necessarily the fifth) is reached, the process is terminated by linking to SCAN without a call to PHLD. This terminates the last stage without activating any further stage.

All stages of the processor must follow a few rules. They must link to SCAN when done. HOLD must be called when a delay occurs and NRDY must be used if the delay is still true after the first HOLD. Fixed memory tables should not be used to transfer data from stage to stage since the execution of the various stages can overlap. All buffers used during a given stage must be freed or transferred to the next stage by incrementing its usage code.

2.8 Examples of Data Processing Routines Developed for this Program

During the course of the program necessary routines were devised for operation of the Varian data processing system. A listing of these routines is included in this report for informational purposes only. A complete set of routines is included in the operation and maintenance manual.

SURC HYBRID SIMULATION LABORATORY SYSTEM

LWL SYSTEM ROUTINES

ALPHABETICAL LIST

$ADI	INT	ANALOG TO DIGITAL INTERRUPT
$DCK	DISP	CHECK DISPL STACK
$DPO	DISP	LOAD DISPL STACK
$LWL	INIT	SET UP SYSTEM
ADIN	INIT	INITIALIZE ANALOG TO DIGITAL INPUT
BKGR	EXEC	BACKGROUND SCAN
BNRD	EXEC	RETURN NOT READY FROM BACKGROUND
BS	KBD	BACK SPACE
CBDA	UTIL	CONVERT BINARY TO KBD MIXED
CIT2	INIT	COMPUTE INDEX TABLE
CKMX	UTIL	CONVERT KEYBOARD MIXED TO BINARY
CRTC	UTIL	CONVERT RTC TO MILLISECONDS
CLPT	INIT	CONVERT MAP LOCUS TO DISPLAY BUFFER
DCAR	DISP	DISPLAY CHARACTER BUFFER (PACKED)
DMAP	DISP	DISPLAY MAP
DBUG	TEST	BACKGROUND PROC. TO ACCEPT TTY AS KEYBOARD
DPIN	INT	DISPLAY INTERRUPT
DPLT	DISP	DISPLAY PLOT
DSFT	DISP	DISPLAY SHIFT
EL	KBD	ERASE LINE
EOT	KBD	TERMINATE KBD MODE
ERC	KBD	ERASE FUNCTION
EREP	BGP	REPORT ERRORS
ERROR	UTIL	FLAG ERROR
FAVE	FSUB	SUBTRACT LONG AVE, UPDATE LONG AVE
FDIF	FSUB	CALCULATE SLOPE
FF	KBD	UP LINE FEED
FFT$	UTIL	FAST FOURIER TRANSFORM
FILL	UTIL	FILL DATA TABLE FROM KBD MIXED
FLG1	FSUB	LOG OF DBL PREC. BUFFER
FLT3	FSUB	SWAP, HANN, SQUARE, AVERAGE
FLT4	FSUB	SWAP, HANN, SQUARE, LOG
FLT5	FSUB	SWAP, HANN, SQUARE, LOG, AVERAGE
FOFF	FSUB	OFFSET DATA FOR DISPLAY
FREC	UTIL	FREE ALL BUFFERS ASSIGNED
FWT1	FSUB	PREWHITEN (FLATTEN FREQUENCY RESPONSE)
GETB	UTIL	FETCH INPUT BUFFER
GETD	UTIL	FETCH DOUBLE BUFFER
GETS	UTIL	FETCH SCRATCH BUFFER
GPLT	KBD	DISPLAY GRID (LEFT SIDE ONLY)
GRID	KBDS	DISPLAY GRID OVERLAY
HOLD	EXEC	FORE GROUND HOLD
IFA1	INIT	INIT TABLES AND COMPUTE CONSTANTS
IFFT	INT	FFT INTERRUPT
IKBD	INT	KEYBOARD INTERRPUT

57	ITAB	INIT	START KBD ENTRY OF LIST
58	KBDP	KBD	DISPLAY KEYBOARD BUFFER
59	KBIN	BGP	KEYBOARD PROCESSOR
60	KERR	KBD	RESTART KBD MODE WITH ERROR MESSAGE
61	KHLD	KBD	KEYBOARD INTERNAL HOLD
62	KINT	INIT	INITIALIZE KEYBOARD PACKAGE
63	KSAL	KBD	STORE ALPHA-NUMERIC
64	KSB2	KBD	INIT KBD MODE (WITH OLD VALUES)
65	KSBR	KBD	INIT KBD MODE (FORCE NEW ENTRIES)
66	KSDC	KBD	STORE DECIMAL
67	LF	KBD	DOWN LINE FEED
68	LOG3	UTIL	COMPUTE LOG(N)
69	MOVE	UTIL	MOVE BLOCK OF CORE
70	NRDY	EXEC	RETURN !NOT READY! FROM FOREGROUND PROCESSOR
71	PC00	FGP	INITIATE PROCESSING SEQUENCE
72	PC14	FGP	PROC. STAGE ONE -- UNSCRAMBLE, SHIFT, FFT, PASS TO TWO
73	PC15	FGP	NO-OP PROCESSOR, FIRST STAGE
74	PC17	TEST	TEST PROC. STAGE ONE -- CONT INPUT, DUM, SORT, PASS TO TWO
75	PC18	TEST	TEST PROC. STAGE ONE -- TRIG INPUT, DUM, SORT, PASS TO TWO
76	PC21	FGP	PROC. STAGE TWO -- FILTER #3, COUNT AVERAGE THEN PASS TO THREE
77	PC22	FGP	NO-OP PROCESSOR, SECOND STAGE
78	PC23	FGP	PROC. STAGE TWO -- FILTER #4, PASS TO THREE
79	PC24	FGP	PROC. STAGE TWO -- FILTER #5, COUNT AVERAGE THEN PASS TO THREE
80	PC26	TEST	TEST PROC. STAGE TWO -- FFT, FILTER #3, PASS TO THREE
81	PC27	TEST	TEST PROC. STAGE TWO -- PLOT RAW DATA
82	PC31	FGP	PROC. STAGE THREE -- LOG, AVE., DISPL MAP, PLOT
83	PC32	FGP	PROC. STAGE THREE -- LOG, OFFSET, WHITEN, DISPL MAP, PLOT
84	PC33	FGP	PROC. STAGE THREE -- OFFSET, WHITEN, DISPL MAP, PLOT (HALF BUFFER)
85	PC34	FGP	PROC. STAGE THREE -- LOG, AVE., DISPL MAP, PLOT (LOW ARC OFFSET)
86	PC35	FGP	PROC. STAGE THREE -- OFFSET WHITEN, DISPL MAP, PLOT
87	PC36	TEST	TEST PROC. STAGE THREE -- LOG, AVE., DISPLAY PLOT
88	PC41	FGP	PROC. STAGE FOUR -- CLEAN UP AVERAGE
89	PC42	FGP	PROC. STAGE FOUR -- SUBT LONG AVE., DISPL MAP, CLEAN UP
90	PC43	FGP	PROC. STAGE FOUR -- SUBT LONG AVE., DISPL MAP (OFFSET), CLEAN UP
91	PCIN	INIT	INITIALIZE PROCESSOR, INPUT FLIGHT PARAM.
92	PHLD	EXEC	PLANT HOLD (FOREGROUND) -- NO LINK TO EXEC
93	PIN1	INIT	INITIALIZE PROCESSOR, NO INPUT
94	PLD2	DISP	X-Y PLOT
95	PLD3	DISP	GREY PLOT
96	POFF	INT	POWER FAILURE INTERRUPT
97	PON	INT	POWER RESTART INTERRUPT
98	RTCI	INT	RTC OVERFLOW INTERRUPT
99	SCAN	EXEC	EXECUTIVE SCAN LOOP
100	SCOM	KBD	PROCESSOR SELECT
101	SPI	KBD	INIT KBD MODE FOR SINGLE PARAM.
102	SPIS	KBD	TERM. KBD MODE AFTER SINGLE PARAM. ENTRY
103	STAT	UTIL	UPDATE STATISTICS
104	STIN	UTIL	INIT STATISTICS
105	STRP	UTIL	REPORT STATISTICS
106	SWAP	KBD	PROC. BANK SELECT FUNCTION
107	SWP3	UTIL	SWAP HALVES OF TWO BUFFERS
108	TRG	KBD	MANUAL TRIGGER FUNCTION
109	UBIN	TEST	UNIVAC BUFFER INPUT (BACKGROUND)
110	UIN1	TEST	UNIVAC INTERRUPT
111	UINL	TEST	UNIVAC INTERRUPT (DUMMY)
112	XSQT	UTIL	SQUARE ROOT

3.0 ANALYTICAL STUDIES

3.1 Theoretical Modeling

The successful translation of the frequency-domain data obtained via the FFT into a terrain map requires an understanding of the geometry of the radar-target configuration as well as the meaning of a power spectrum estimate over a finite time T using in-phase and quadrature phase doppler signals. In this section, both of these points are briefly discussed in order to help in the interpretation of the graphs that are presented throughout this report. The problem of estimating the radar cross section of a target from the power spectrum estimate is also considered.

3.1.1 Geometry of the Radar-Target Configuration

Consider an airplane travelling along a straight line at a constant altitude above ground. The plane carries a radar with an antenna mounted at right angles to the fuselage, i.e., 90° to the flight vector. As in the actual experimental configuration, the antenna is mounted on the port side (left) of the aircraft. Without significant loss of accuracy, a flat earth approximation is used.

Let the radar have slant range R_s (measured from the leading edge of the transmitted pulse to the leading edge of the range gate) and a range-gate width of ΔR_s. The altitude of the aircraft is denoted by h. A rectangular coordinate system is centered on the aircraft as shown in Figure 3.1. Note that the velocity vector is in the +y direction, and the antenna is mounted along the positive x-axis. The azimuth angle ϕ is measured from the antenna boresight, with positive angles having a positive y-coordinate and negative angles, a negative y-coordinate.

The ground range R_g is given by

$$R_g^2 = R_s^2 - h^2 = x^2 + y^2 ,$$

and the angle between the velocity vector and the range vector, denoted by ψ, is given by

$$\psi = \cos^{-1} (y/R_s) .$$

The depression angle θ is specified by the relation

$$\sin \theta = h/R_s \qquad \text{or} \qquad \cos \theta = R_g/R_s .$$

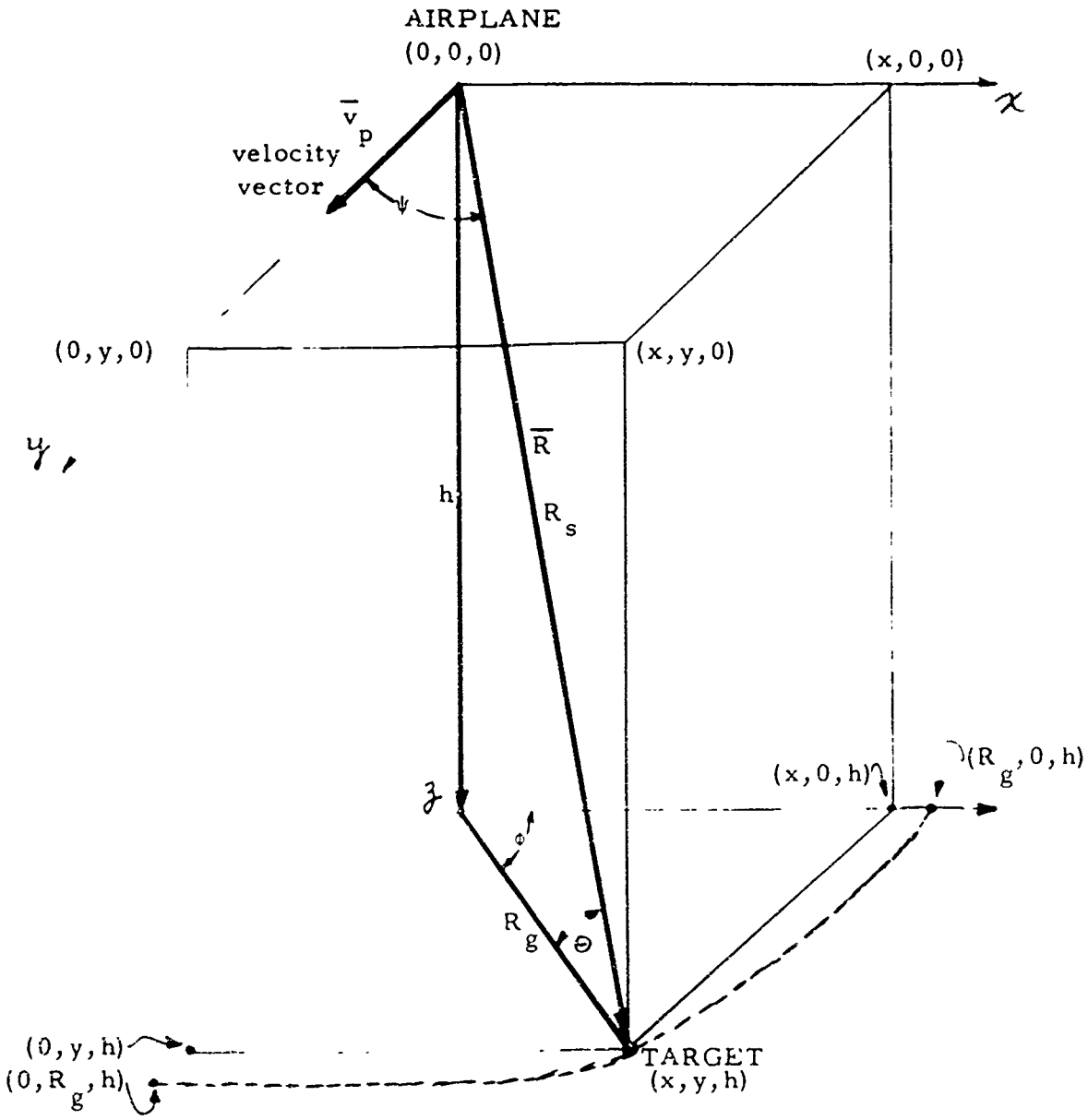

h = altitude

φ = azimuth angle

R_s = slant range = $|\bar{R}|$

R_g = ground range

ψ = angle between the vectors $\bar{v}_p$ and $\bar{R}$

$$x = R_g \cos \phi$$

$$y = R_g \sin \phi$$

$$R_s^2 = R_g^2 + h^2$$

$$= x^2 + y^2 + h^2$$

Fig. 3.1. Radar Geometry.

At this time,

$$t = t_o = \frac{R_g + \Delta R_g - y_o}{v_g} \quad . \tag{3.4}$$

The target leaves the range gate at time

$$t = t_i = \frac{R_g + \Delta R_g - y_i}{v_g} \quad , \tag{3.5}$$

where y_i, also shown in Figure 3-2, is given by

$$y_i = \sqrt{R_g^2 - x_o^2} \quad . \tag{3.6}$$

The time-on-target is thus given by $t_i - t_o$. At a negative azimuth angle the target reenters the range gate at time

$$t = t_i' = \frac{R_g + \Delta R_g + y_i}{v_g} \tag{3.7}$$

and leaves at time

$$t = t_o' = \frac{R_g + \Delta R_g + y_o}{v_g} \quad . \tag{3.8}$$

Thus, for an arbitrary time, t, a doppler return is obtained from the target only if $t_o \leq t \leq t_i$ or $t_i' \leq t \leq t_o'$. The y-coordinate of the target is given by

$$y = R_g + \Delta R_g - v_g t, \tag{3.9}$$

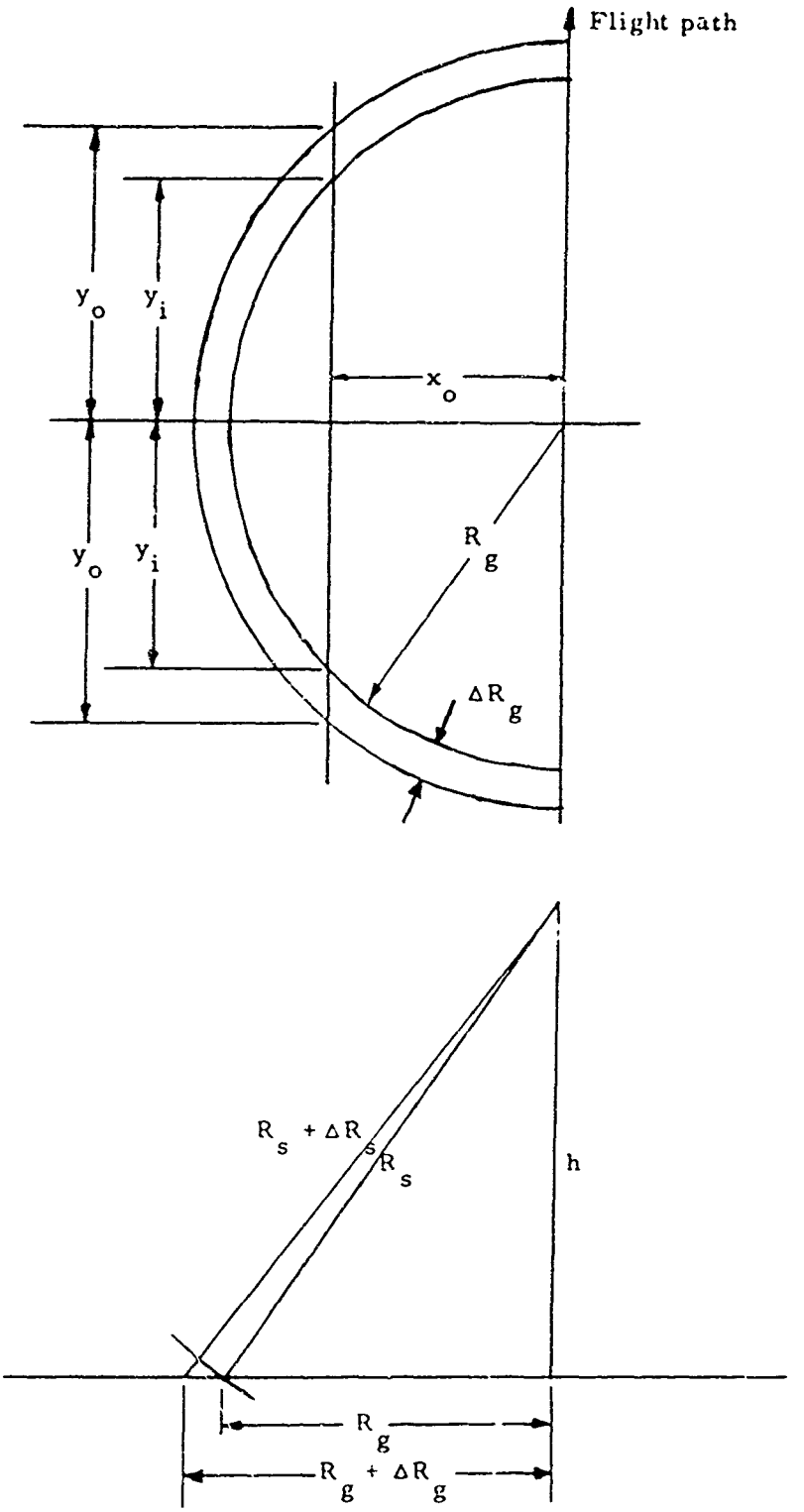

Fig. 3.2. Projections of Radar Geometry.

The range gate illuminates a semi-annulus on the ground, as illustrated in Figure 3-2. Note that the trailing edge of the range gate pulse is specified by $R_s + \Delta R_s$. The corresponding width of the annulus (the projection of the range gate on the ground) is given by

$$\Delta R_g = \sqrt{(R_s + \Delta R_s)^2 - h^2} - \sqrt{R_s^2 - h^2} \ .$$

Note that ΔR_g is independent of azimuth angle, so that $R_g + \Delta R_g$ is known as soon as h and R_s are fixed.

Let the airplane have a velocity of $\bar{v}_p$; the ground speed of the plane is given by $v_g = |\bar{v}_p|$, and the radial velocity of the target with respect to the plane, by

$$\bar{v}_r = v_g \cos \psi \, \bar{r} \ ,$$

where $\bar{r}$ is a unit vector in the radial direction. Referring to Figure 3-1, it is easily shown that

$$v_r = |\bar{v}_r| = v_g \frac{y}{R_s} = v_g \left(y / \sqrt{x^2 + y^2 + h^2}\right) \qquad (3.2)$$

$$= v_g \sin \phi \cos \theta \ .$$

Assume that a point target on the ground has a fixed position. If the airplane flies at a constant altitude h in a straight line, the x-coordinate of the target will be constant; denote it by x_o. Two distinct cases are considered below: (1) $x_o < R_g$, and (2) $R_g < x_o < R_g + \Delta R_g$.

Case 1

Let $t = 0$ be chosen as the time when a hypothetical point target along the flight path ($x = 0$) is first illuminated:

The coordinates of this point are $(0, R_g + \Delta R_g, h)$, and the coordinates of the actual target being considered are $(x_o, R_g + \Delta R_g, h)$, as can be seen by referring to Figure 3-2. The target at $x = x_o$ is first illuminated when the plane has traveled a distance $R_g + \Delta R_g - y_o$, shown in Figure 3-2, is given by

$$y_o = \sqrt{(R_g + \Delta R_g)^2 - x_o^2} \ . \qquad (3.3)$$

and the instantaneous doppler frequency by

$$f_d = 2v_r/\lambda = (2v_g/\lambda)\,(y/R_s), \tag{3.10}$$

where

$$R_s^2 = x_o^2 + y^2 + h^2 \quad .$$

Case 2

For Case 2, $R_g < x_o < (R_g + \Delta R_g)$, as illustrated in Figure 3-3. The target enters and leaves the range gate only one time; however, the time-on-target is significantly longer than for Case 1. Since the inner edge of the range gate is not intersected, Equations (3.3), (3.4) and (3.8) hold for Case 2, with the time-on-target given by $t_o' - t_o$. This situation provides some interesting possibilities for signal processing, where the doppler frequency shift of the target return is taken into account in computing the average power spectrum estimate.

3.1.2 Interpretation of the Power Spectrum Estimates

To interpret the power spectrum estimates, the relation between the finite, discrete FFT and the terrain illuminated by the range gate must be considered. Furthermore, the effect of using both in-phase and quadrature phase doppler data to form a complex-valued input to the FFT should be well understood. This problem is discussed in a separate appendix. This section concentrates on the discrete nature of the FFT, defines the term "frequency bin," and shows that the azimuth sectors corresponding to a particular bin vary in size as the azimuth angle varies.

Consider a 256-point FFT with complex-valued outputs denoted by X(n), n = 0,1,2,...,255. Since the FFT produces a cyclic output, it is sufficient to equivalently consider the set of values

$$X(k),\ k = -127, -126, \ldots, -1, 0, 1, 2, \ldots, 127, 128,$$

where the relation X(-m) = X(256-m) defines X(k) for k negative. This particular numbering system is used to represent the double-sided graphs throughout this report.

Let the sampling rate for the input data be denoted by $f_s = 1/\Delta t$, and for simplicity, let N = 256. The index k on the FFT values represents a frequency value of

$$f_k = k\, f_s/N = k/(N\Delta t) \quad .$$

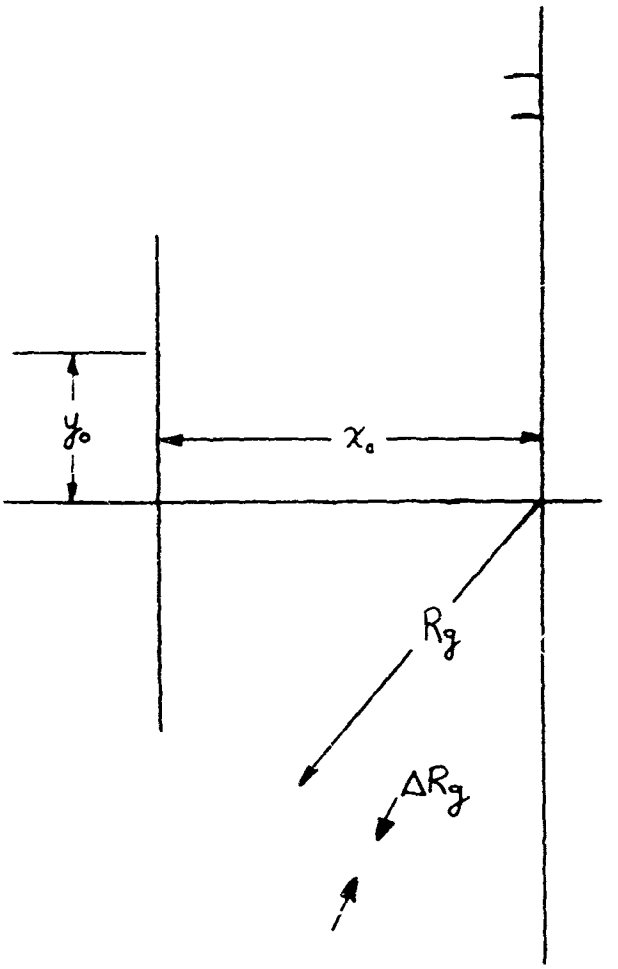

Fig. 3.3. Path of target illuminated by the range gate at $\phi = 0$.

Only these frequencies can be represented exactly by the FFT. Frequencies f such that $f_{k-1} < f < f_k$ contribute to all of the FFT coefficients, with the primary contributions going to the neighboring points. With this consideration in mind, "frequency bins," indexed by the integer k, having center frequency f_k, and a bandwidth f_s/N, are defined as a band of frequencies extending $\frac{1}{2}f_s/N$ on each side of the center frequency f_k. When applied to the doppler return signals from the radar, the bins are often referred to as "doppler frequency bins." In the FFT output, there are N frequency bins, and the maximum center frequency is $\pm\frac{1}{2}f_s$.

With reference to Figure 3.1 and the analysis of Section 3.1.1, the doppler frequency f_d due to a stationary point target is given by (3.2) and (3.10) as

$$f_d = \frac{2v_g}{\lambda} \sin\phi \cos\theta \ . \qquad (3.11)$$

Since the depression angle, θ, is determined solely by the slant range and the altitude of the aircraft, f_d can be viewed as a function of azimuth angle, ϕ. Holding all other parameters constant, a target at azimuth angle, ϕ, falls into frequency bin k if

$$f_k - \tfrac{1}{2}(f_s/N) < f_d < f_k + \tfrac{1}{2}(f_s/N) \ ,$$

where $\frac{1}{2}(f_s/N)$ is the bandwidth of the bin.

From (3.11), note that although the bandwidth of the bins are constant, the azimuthal sector included by a particular bin is a function of ϕ. An approximate relation is given by

$$\Delta\phi \cong \frac{\lambda \Delta f_d}{2v_g \cos\phi \cos\theta} \ ,$$

from which it is seen that the azimuthal segments are larger for small azimuth angles.

From the above discussion, it should not be assumed that a target will appear in a single frequency bin This would be impossible for two fundamental reasons: (1) The target's doppler frequency changes with time, especially at small azimuth angles, and (2) The inherent resolution of the finite, discrete FFT is limited to approximately the inverse of the total FFT time.

3.1.3 Improving the Target-to-Clutter Ratio

A significant improvement in the target-to-clutter ratio is realized with FFT processing due to the partitioning of the terrain covered by the range gate into doppler resolution cells. For targets positioned such that

the time-on-target is relatively long, the doppler frequency changes during the time-on-target interval. For the situation shown in Figure 3.4, the doppler frequency variation is approximately linear with time, and the target moves through several doppler frequency bins. One scheme that can capitalize on this phenomenon to improve the target-to-clutter ratio is described below.

Let the total time-on-target be denoted by T_t, as shown in Figure 3.4. The complex doppler signal (in-phase and quadrature) is sampled at a rate, f_s, during this interval, resulting in a sequence of data with $f_s T_t$ points. If a FFT were calculated using the complete interval, the energy due to the target would be spread over several frequency bins. However, if the FFT's are calculated over shorter intervals, they may be shifted in frequency to account for the doppler frequency change in the target return in such a way as to put the target in the same frequency bin each time. An average of these adjusted FFT's (on a noncoherent basis using the power spectral estimates) should result in an improvement in the target-to-clutter ratio if the clutter contributions in the doppler cells are independent. Equivalently, the spectral estimates can be averaged along a diagonal whose slope takes the radar-target geometry into account.

It is also possible to use overlapping segments for the FFT calculations. An important parameter in this situation is the number of sample points successive FFT's (i.e., the number of new data points). This parameter is denoted by ISHIFT. One criteria for choosing ISHIFT is to require the target to move exactly from one frequency bin to an adjacent bin for successive FFT's. This optimization of ISHIFT is discussed in the next section.

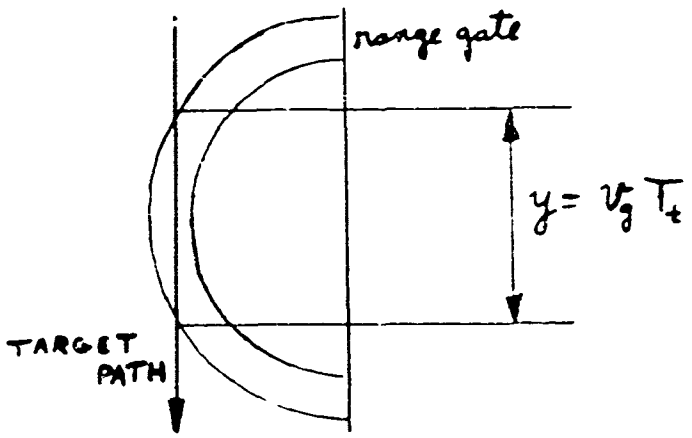

Figure 3.4 Range Gate Projection on the Ground

3.1.4 Optimizing the Parameter ISHIFT

The objective of this analysis is to find an expression that relates the parameter "ISHIFT" to the radar geometry in order that a target passing tangentially through the range gate, as shown in Figure 3.4, appears in successive, adjacent frequency bins of the discrete Fourier transform (DFT). The resulting equation, derived below, is given by

$$\text{ISHIFT} = \frac{\Delta\phi \, R_g \, N}{T \, v_g} \quad ,$$

where $\Delta\phi$ = sector angle in radians

R_g = ground range

v_g = ground speed

N = number of sample points used for one DFT

and $T = N\Delta t$ = total time required to sample data (at a sampling rate of $f_s = 1/\Delta t$).

$\Delta\phi$ is the sector angle in radians corresponding to the zero-th frequency bin of the DFT, assumed centered around zero with width $\Delta f = f_s/N = 1/T$. At ground range, R_g, the sector dimension along the ground track (y-coordinate) is approximately given by

$$d = R_g \, \Delta\phi \quad . \tag{3.12}$$

If we desire the target to move exactly one doppler frequency bin in time T_i, we must have

$$d = v_g \, T_i \quad . \tag{3.13}$$

ISHIFT is defined as the number of sample points unique to each subsequent DFT calculation, as illustrated in Figure 3.5. For an N point DFT,

$$\text{ISHIFT} = \frac{T_i}{T} \, N \quad , \tag{3.14}$$

so that the next DFT starts T_i seconds after the previous one.

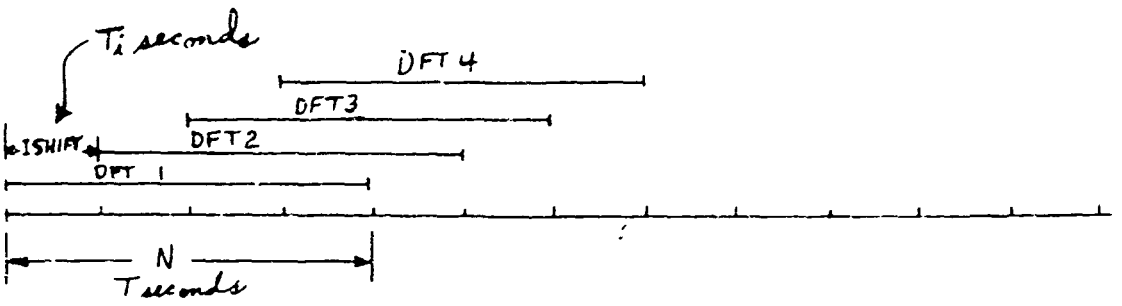

Figure 3.5. Representation of Time Data Intervals

Equations (3.12), (3.13) and (3.14) can now be combined to yield

$$\text{ISHIFT} = \frac{\Delta\phi \; R_g \; N}{v_g \; T} \tag{3.15}$$

which is the desired result. We now consider $\Delta\phi$ in more detail. The doppler frequency f_d from a point target at a depression angle θ and azimuth angle is given by (3.11) as

$$f_d = \frac{2 v_g}{\lambda} \cos\theta \sin\phi.$$

Holding θ constant,

$$\Delta f_d = \frac{2 v_g}{\lambda} \cos\theta \cos\phi \; \Delta\phi,$$

which, for small azimuth angles, is approximately given by

$$\Delta f_d = \frac{2 v_g}{\lambda} \cos\theta \; \Delta\phi . \tag{3.16}$$

Furthermore, the slant range R_s and ground range R_g are related by the equation

$$R_g = R_s \cos\theta \tag{3.17}$$

Thus, solving (3.16) and (3.17) for $\Delta\phi$,

$$\Delta\phi = \frac{\lambda \Delta f_d R_s}{2 v_g R_g} = \frac{\lambda R_s}{2 v_g T R_g} , \qquad (3.18)$$

where we have used $f_d = 1/T$.

Substituting (3.18) into (3.15),

$$\text{ISHIFT} = \frac{\lambda R_s N}{2 (v_g T)^2}$$

$$= \frac{\lambda R_s (f_s)^2}{2 v_g^2 N} , \qquad (3.19)$$

where the relation $T = N \Delta t = N/f_s$ has been used.

3.1.5 Radar Cross Section

The radar cross section of a target is a quantitative measure of the ratio of power density in the vector signal scattered in the direction of the receiver to the power density of the radar wave incident upon the target. Targets may be classified as point targets and distributed targets. One of the required objectives of this program is the reliable detection of point targets in a distributed clutter environment (i.e., detection of a standard target in a clutter-background that may be varied). Inherent in this study is the measurement of the clutter echo from environments chosen for backgrounds at the frequencies, aspect angle and polarization used. Although it is common to refer to the radar cross section of an object, it is reasonable to point out that radar cross section depends upon the target shape and material, the angle at which the target is viewed, and the frequency and polarization of the radar antennas.

3.1.5.1 Standard Target

The point target most prominently used during this program was a square corner reflector. Its cross section is given by:

The cross section (σ) of a square corner reflector[1] is:

$$\sigma_{max} = \frac{12 \pi a^4}{\lambda^2} \qquad (3.20)$$

---

[1] Barton, David K., Radar System Analysis, Prentice-Hall, Inc., Englewood Cliffs, New Jersey, 1964.

For a seven-foot corner reflector at 140 MHz where λ = 7 ft= a

$$\sigma = \frac{12 \pi a^4}{a^2}$$

$$\sigma = (12)\ (\pi)\ (49)$$

$$\sigma = 1849\ ft^2 = 171.77\ meters^2$$

The same seven-foot corner reflector at 50MHz where λ = 19.7 ft

$$\sigma = \frac{12 \pi a^4}{\lambda^2}$$

$$\sigma = \frac{(12)\ (\pi)\ (2401)}{388}$$

$$\sigma = 233\ ft^2 = 21.66\ meters^2$$

3.1.5.2 Monostatic Cross Section

A monostatic cross section of the square corner reflector was determined through an expression using direction cosines. To find the symmetry angle all three direction cosines must be equal. Thereby, all the angles are $54^\circ\ 44'$. Therefore, the depression angle of the reflector (when seated on one side) is $35^\circ\ 16'$. Further investigation of the reflected energy indicated that the locus of half power points lie in a loop which makes an angle of $11^\circ\ 9'$ about the boresight line (see Figure 3.6). This data was used to determine flight parameters for data gathering.

3.1.6 Comparison of Theoretical Cross Section to Received Data Cross Section

Initial attempts to correlate the received data and target cross section indicated that the peak received target power in one bin is only a portion of the total received power needed to calculate the target cross section. The portion of the received target power contained in the elemental filters on either side of the peak power bin must be included, therefore, the power in several bins is added to obtain the total received target power. Figure 3.7 represents the power envelope that contains the total received power necessary for cross section resolution. Computations of target cross sections require the inclusion of a single side band test signal as part of the measurement procedure.

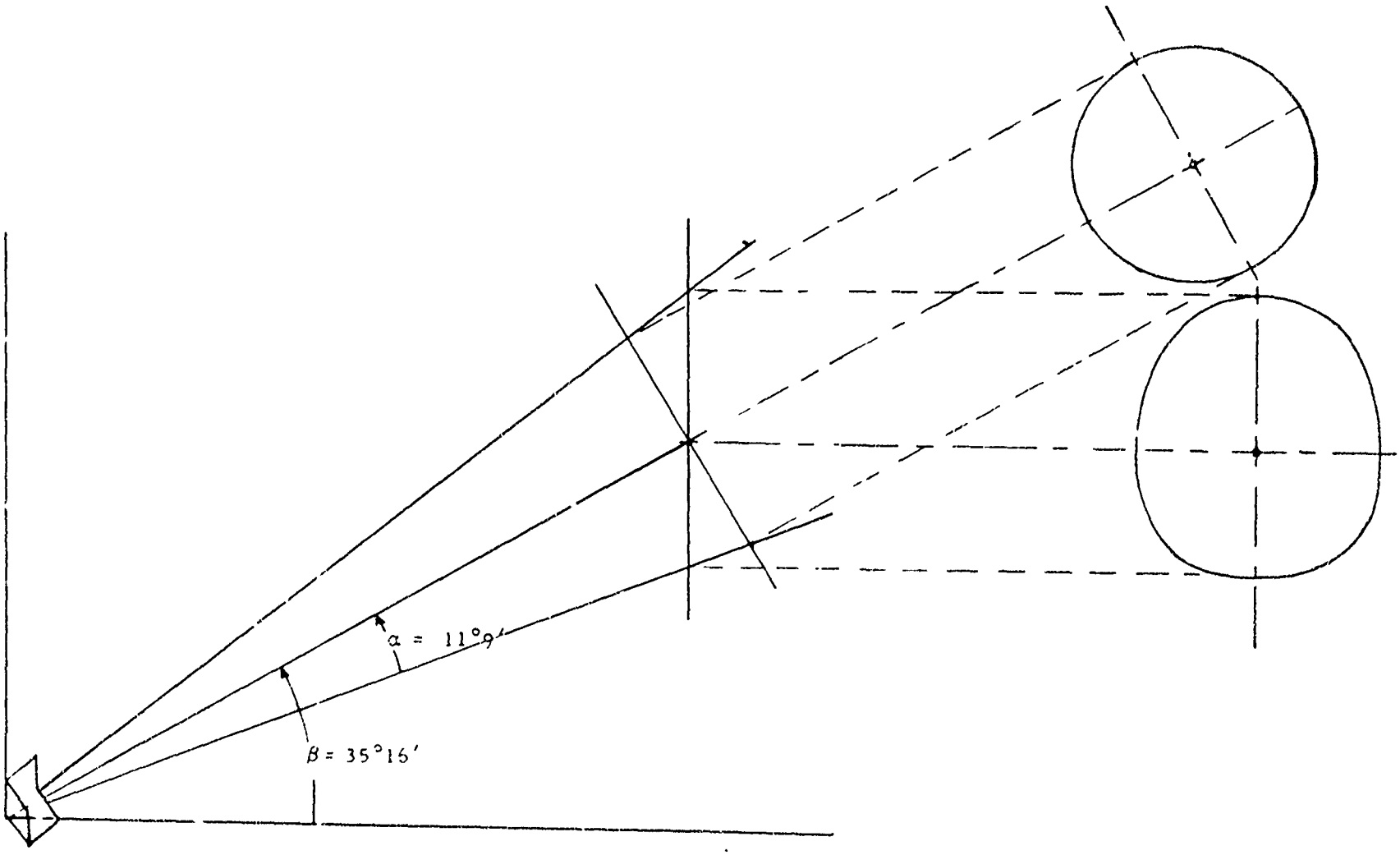

Figure 3.6. Corner Reflector Cross Section Geometry

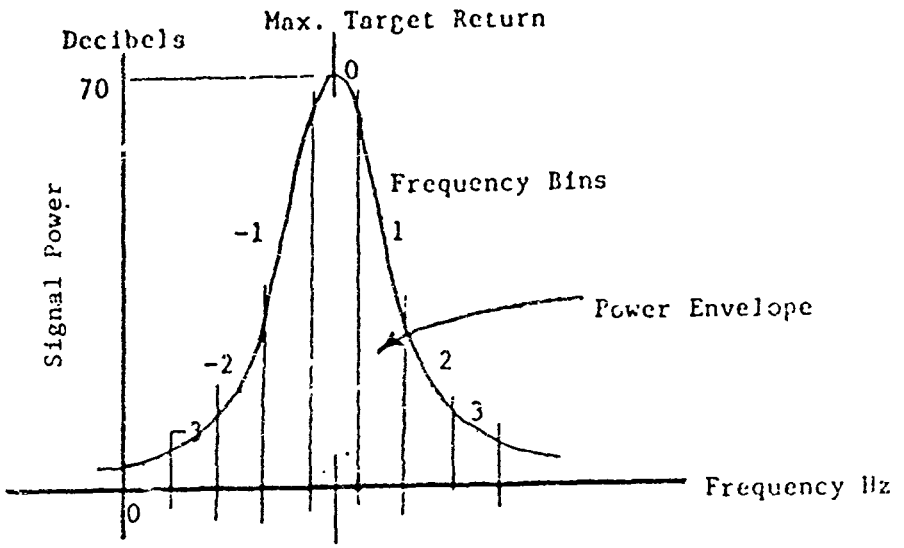

Figure 3.7 Power vs. Target Doppler Frequency

To calculate the target radar cross section (RCS) by utilizing collected data:

The received energy can be determined from the radar equation;

$$P_r = \frac{P_T G^2 \lambda^2 \sigma}{R^4 (4\pi)^3}$$

Solving for the cross section, and adding the power ratio, we have

$$\sigma = \frac{P_R R^4 (4\pi)^3}{P_T G^2 \lambda^2 (\text{Power Ratio})} \qquad (3.21)$$

To calculate the cross section, the target range (R) and the power received (P_R) must be derived for each target.

θ = depression angle

ψ = azimuth angle

λ = wavelength (ft)

v = aircraft velocity (ft/s)

f_D = doppler frequency (Hz)

In order to calculate the target's true range, we must first find the depression angle (θ), as shown in Figure 3.8.

$$\theta = \text{arc sin (Altitude/Slant Range)} \tag{3-22}$$

If the target is off boresight, then there is a ..o doppler frequency which must be used to determine the target's range. ..e following is the moving target equation:

$$f_D = \frac{2v}{\lambda} \cos\theta \sin\psi$$

Solving for sin ψ, we have

$$\sin\psi = \frac{f_D \lambda}{2v \cos\theta}$$

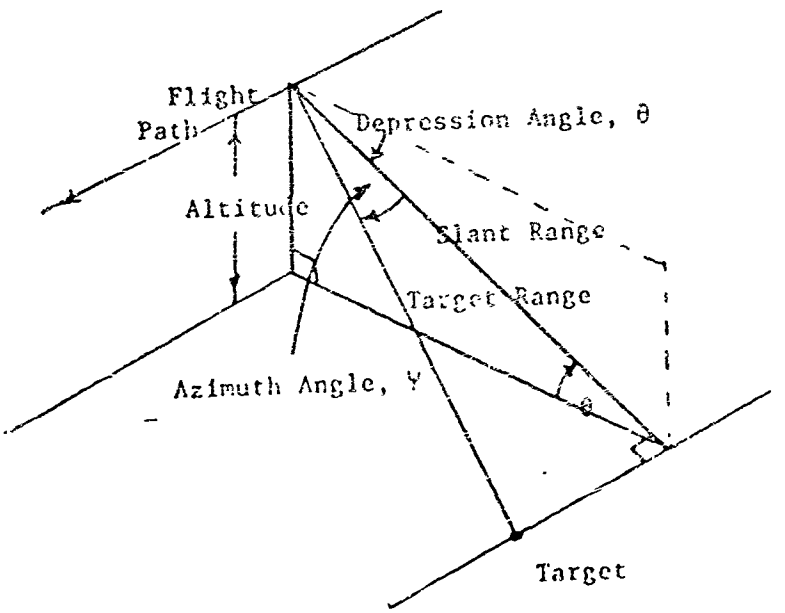

Figure 3.8 Flight Geometry

Substituting (3.22) for θ, and solving for the azimuth angle, we have,

$$\psi = \arcsin \left\{ \frac{f_D}{2v \cos (\arcsin \text{ altitude/slant range})} \right\} \qquad (3.23)$$

If $\cos \psi$ = slant range/target range,

then Target Range = $\frac{\text{Slant Range}}{\cos \psi}$

Substituting (3.23) for ψ, we have:

$$\text{Target Range} = \frac{\text{Slant Range}}{\cos \{\arcsin (f\lambda/2v \cos [\arcsin (\text{altitude/slant range})])\}} \qquad (3.24)$$

This value can now be used directly in the RCS equation (3.21).

3.1.6.1 Target Cross Section from Run 622

A test run was made to determine the cross section of a target from real data. The following is a computation of the square corner reflector radar cross section from live data.

SR = Slant Range

DS = Range Gate Dial Setting = 1.26

SR = 410 + DS (1542)

Therefore,

SR = 2353 feet

A = Altitude = 1150 feet

θ = Depression Angle = arc sin (A/SR) = 29.3°

f_D = Doppler Frequency of Target = 6.4 Hz

λ = Wavelength of Carrier Frequency = 7.03 feet

v = Velocity of the Aircraft = 199.5 feet/second

ψ = Azimuth Angle to the Target

$\psi = \arcsin (\lambda f_D/2v \cos \theta) = 7.4^\circ$

TR = Target Range

TR = SR sec ψ = 2373 feet

SSBP = SSB Generator Power = -12 dBm (Reference Signal)

ATT = SSBP Attenuation before the receiver = 40 dB

ΔP = Difference in Spectral Power between the SSB and the Target as obtained from the computer printout = -7.77 dB

RP = Receiver Power Input in dB

= SSBP - ATT + ΔP + 3 dB

= -56.8 dB or $2.104 \cdot 10^{-6}$ mW

The cross section can now be calculated.

P_T = Transmitted Power = $3 \cdot 10^6$ milliwatts

G = Antenna Gain = 3.931

L = Power Ratio = .069

$$= \frac{(RP)\ (\pi R)^4\ (4\pi)^3}{P_T\ G^2\ \lambda^2\ L} = 840 \text{ feet}^2$$

For a depression angle of 29.3° and an azimuth angle of 7.4°, the square corner reflector gives a cross section of 840 feet squared.

At this location, for this test run, the corner reflector should have produced a cross section of 1050 + 50 feet squared. Comparing the theoretical cross section to the live data cross section, we find that there is only a 20% difference.

3.1.7 Associated Programming Effort

Two programs have been written to aid in cross section evaluation:

1. The first program* automatically calculates target cross section as a function of azimuth angle.

The program takes previously generated spectra which was stored on magnetic tape and allows the operator to look at any number of these spectra for a target indication. Once a target indication is noted the operator has the option of automatically or manually processing the data to get the target

*Algorithms and constants are presented in the Letter Report for February 1973.

cross section. Pertinent data concerning the live and SSB experiment is entered via the keyset. Two parameters entered are the scanning and averaging intervals. The scanning interval determines the region in which a maxima will be located. The averaging interval dictates how many elemental filter outputs each side of the maxima will be summed together. Another parameter dictates the number of spectra to be utilized for the calculation. Once this number is reached a plot of cross section versus azimuth angle is displayed. A sample plot is shown in Figure 3.9 as compared to a theoretical plot shown in Figure 3.10. Figure 3.9 indicates no cross section around 0 Hz. This is due to the way the spectra are calculated; that is, the Hanning window and the "zeroing" of the "zeroith" elemental filter.

2. The second program increases the target-to-clutter ratio of the airborne FOPEN radar. The importance of this scheme is that it keeps a point target in one frequency bin for many seconds. Consequently, a longer interval can be used to gather data for one FFT. It is also noted that the doubling of the length of the FFT increases the signal-to-clutter ratio by a factor of two. This increased sample interval leads to smaller spacing between individual elemental filters in the frequency domain and to smaller azimuthal sectors.

The derivation of this technique follows:

Let v = aircraft velocity (feet/seconds)

λ = wavelength (feet),

R_S = slant range (feet),

t = time (seconds),

and f_s = sampling frequency = 468.75 Hz

Define the index, k, by the relation

$$t = k\,\Delta t = k/f_s. \tag{3.25}$$

The return signal from a point target, after homodyning, can be represented by

$$x(k) = I(k) + jQ(k) = \exp\{-jBt^2\}, \tag{3.26}$$

where $B = (2\pi/\lambda)\,(v^2/R_S)$.

Using (3.25) and (3.26), and defining $C = B/(f_s)^2$, we have

$$x(k) = \exp\{-jCk^2\}.$$

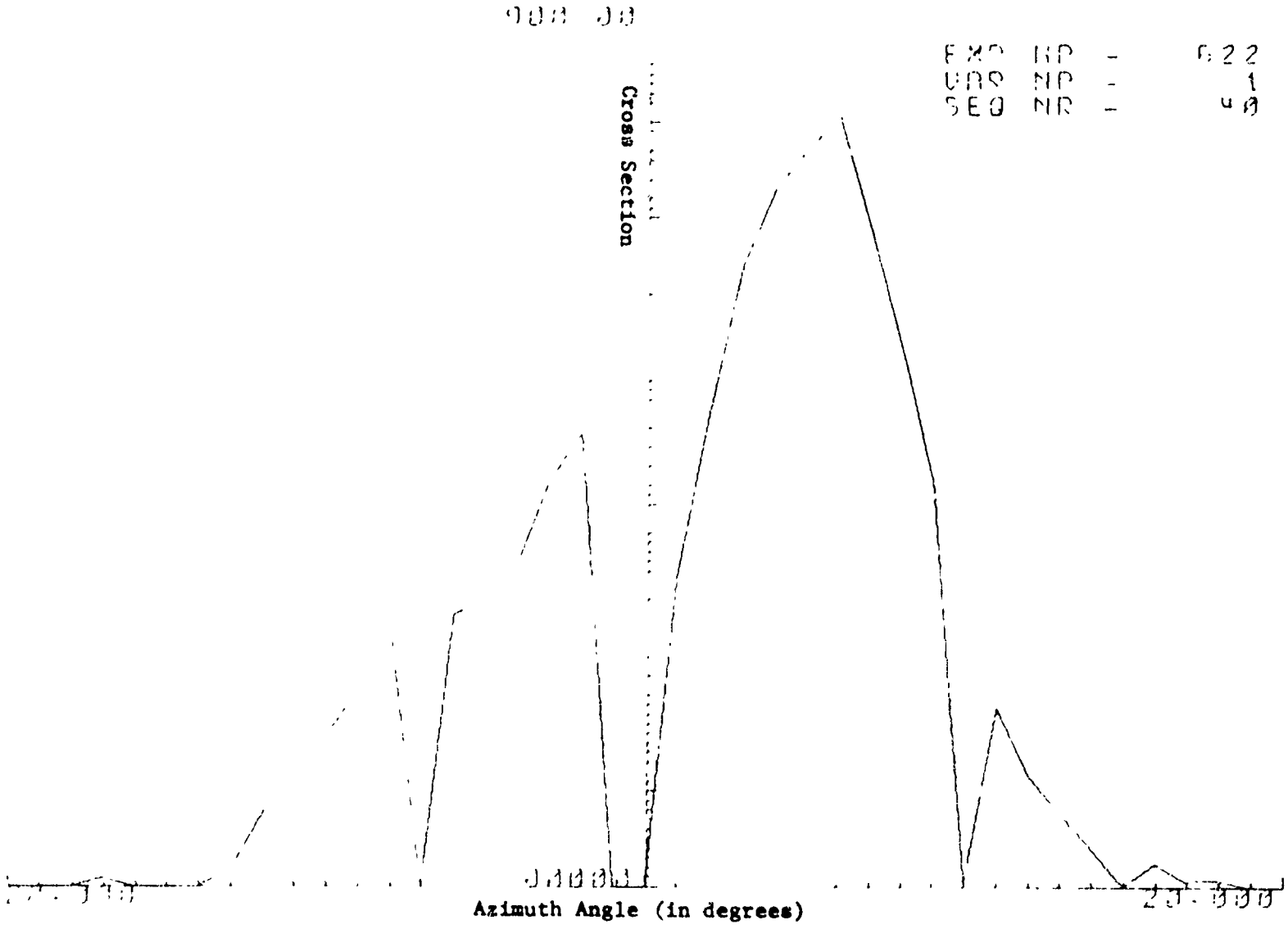

Figure 3.9. Cross Section of Square Corner Reflector from Raw Data

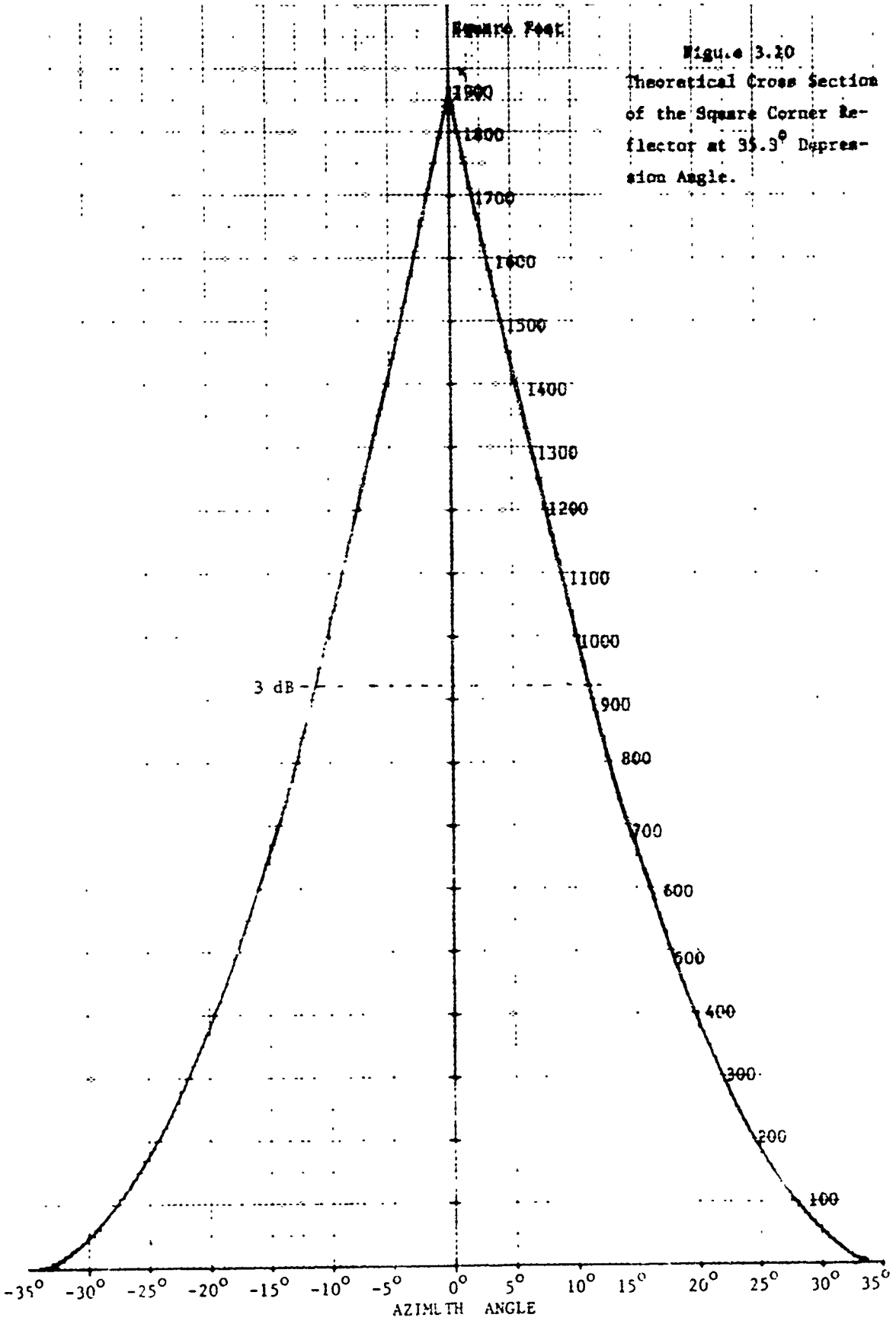

Figure 3.20
Theoretical Cross Section of the Square Corner Reflector at 35.3° Depression Angle.

We now define the modulation frequency function, $m(\ell)$, as

$$m(\ell) = \exp\{+jC\ell^2\}$$

Performing a complex multiplication of the two functions, $m(\ell)$, and the return signal, $x(k)$, yields

$$Z(k) = m(\ell)\, x(k)$$

where $\ell = n + k$, and n is a constant.

$$\begin{aligned} Z(k) &= \exp(jC\ell^2) \cdot \exp(-jCk^2) \\ &= \exp\{jC(\ell^2 - k^2)\} \\ &= \exp\{jC(n^2 + 2nk + k^2 - k^2)\} \\ &= \exp\{jC(n^2)\} \cdot \exp\{j2Cnk\} \end{aligned} \tag{3.27}$$

The first exponent on the right-hand side of (3.27) is a constant phase term. The second exponent can be written as $\exp\{j(2Cn)k\}$, where 2CN is constant and k is the time index; hence this term represents a constant frequency. Taking the discrete Fourier transform of Z(k), we will obtain a single peak in the frequency domain, indicating the presence of the point target.

Figures 3.11 and 3.12 are representative outputs of this program with and without the scheme being utilized. Both spectra are computed with 1024 sample points over the same time period. No averaging has been done which explains the amount of variance noticeable in the spectra. As expected, the target signal is now a narrow peak (Figure 3.11) due to the modulation scheme. One also notices that the signal-to-clutter ratio in Figure 3.11 is 3 to 4 dB better than in Figure 3.12, as predicted.

3.1.8 Theoretical Investigations

A number of theoretical investigations were undertaken to determine the limitations imposed upon the prototype system by the natural and operational environments. Three of these investigations are included as appendices to this report. The limitations encountered in this program as in other programs of a similar nature were ground clutter, aspect angle and glint reflections.

It is obvious from these investigations and a literature search that the results of the program could be affected drastically by experimental conditions.

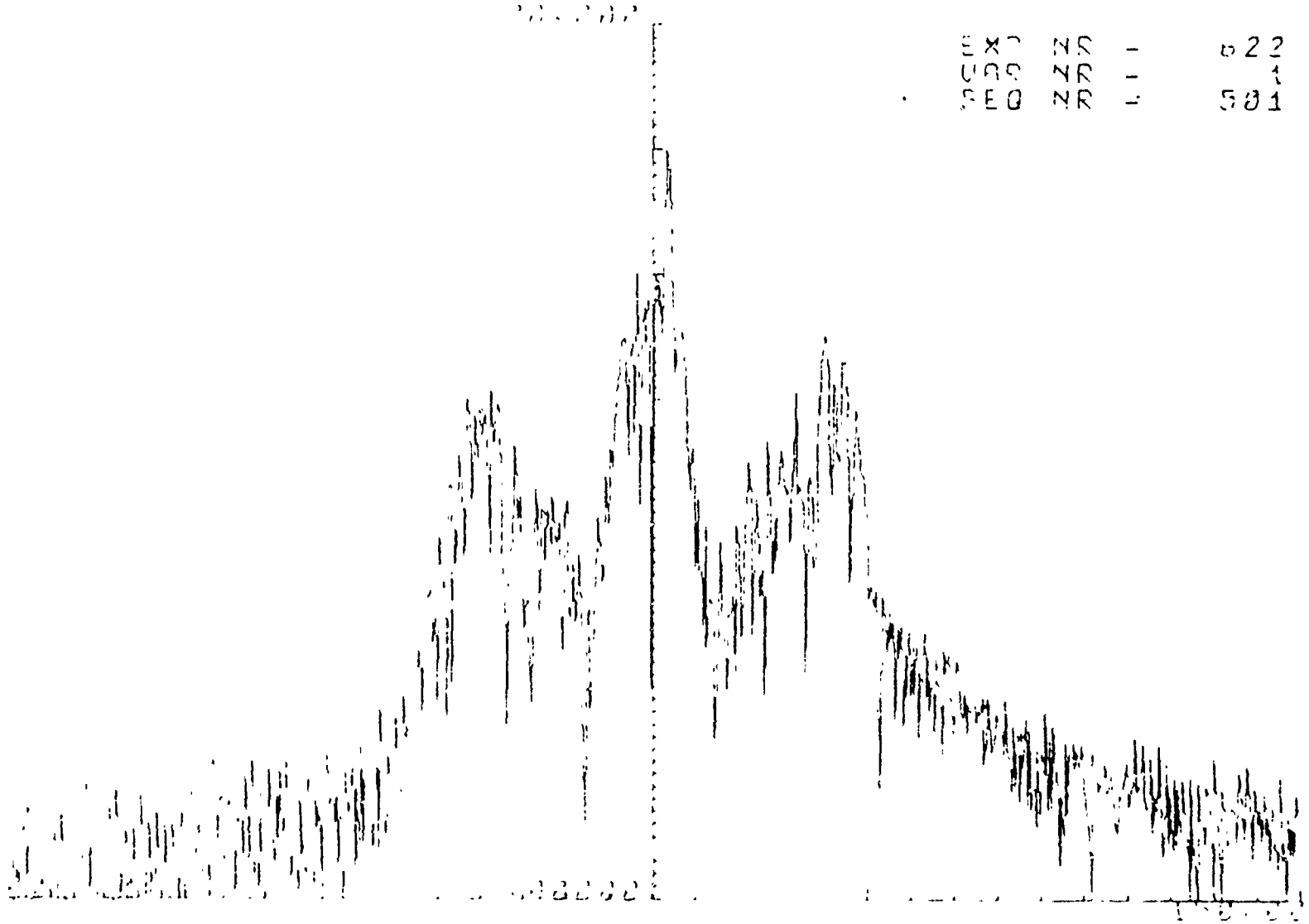

Figure 3.11. Clutter Depressed Spectra

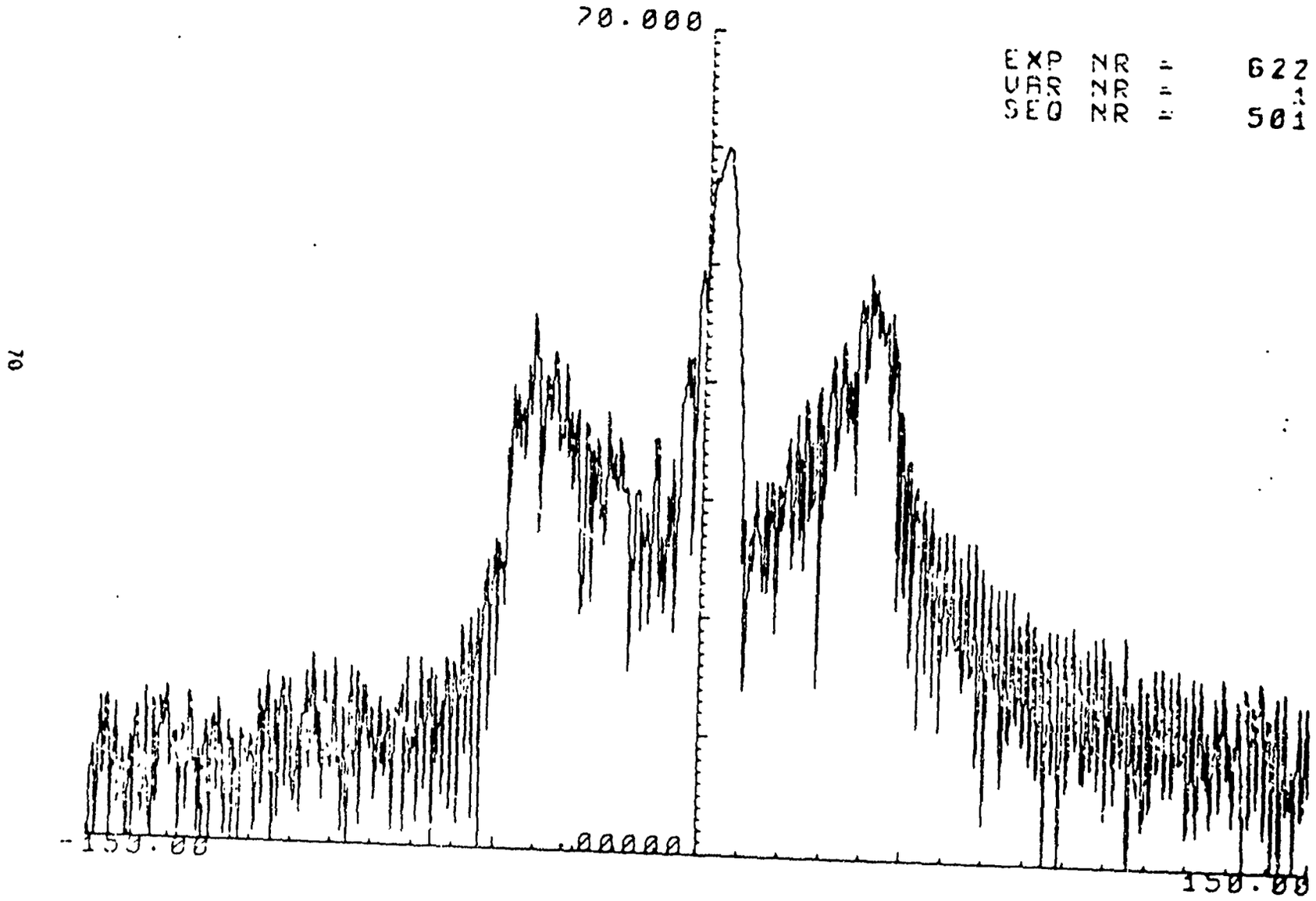

Figure 3.12. Normal Spectra

3.1.8.1 Glint Reflections (Appendix B)

Two isolated experiments are summarized here to illustrate the effect of glint reflections upon the program.

The first experiment, Number 845, was conducted to resolve the differences between the calculated cross section of a stationary parked aircraft and the measured cross section of this aircraft. Figure 3.13 is a representation of the problem. The aircraft presents a flat surfact target perpendicular to the ground.

The glint equation is as follows:

$$G = \frac{16 \pi A^2}{\lambda^2} \sin^2 (90^\circ - \delta) \qquad (3.28)$$

A = target area, perpendicular to the ground

λ = wavelength of the transmitter energy

δ = depression angle to the target

An estimate of the aircraft's surface area was determined from a photograph and a scaling factor applied.

A = side area = 224 square feet

δ = 14.7 degrees

$$\sigma_G = \frac{16 \pi (224)^2}{49} \sin^2 (90^\circ - 14.7^\circ) + 48,157 \text{ square feet}$$

For Experiment 845, the raw data value of its maximum cross section was 46,741 square feet. The difference between the glint and the raw data values indicate an error of only 2%. Therefore, the large value for the previous test was probably caused by the geometry of the data gathering, where glint return can change depending on the range gate and the aircraft's altitude.

During the lake tests the measured cross section value of the square corner reflector (from Experiment 619) was 3276 square feet. Calculating the theoretical value, using the depression angle of 19 degrees and the position of the corner reflector, the maximum radar cross section should have been 600 square feet.

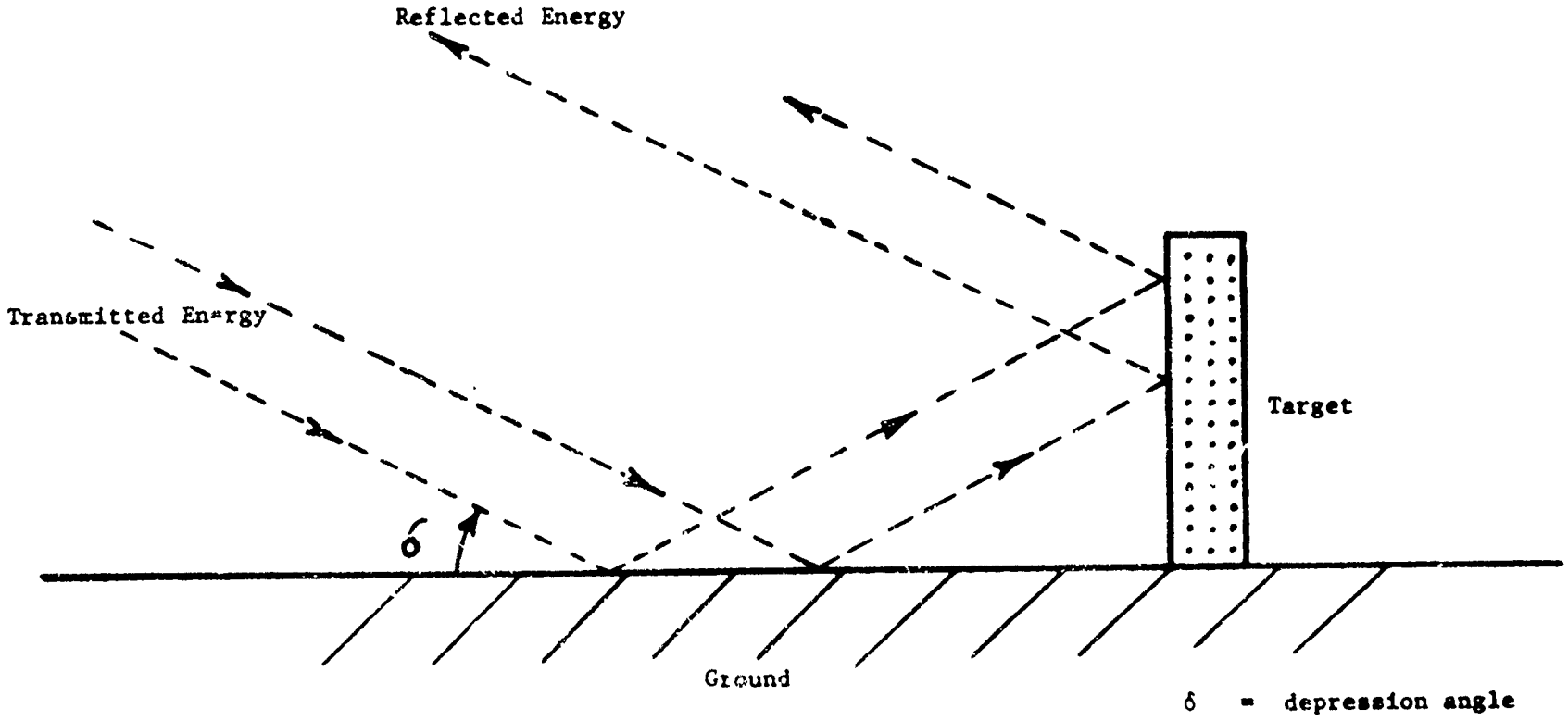

Figure 3.13. Glint Reflection

This large raw data value could have been caused by glint. The following is the glint cross section equation:

$$\sigma_G = \frac{16\pi}{\lambda^2} A^2 \sin^2 (90^\circ - \delta) \qquad (3.28)$$

δ = depression angle

A^2 = aperture squared

λ^2 = wavelength squared

For this problem, the aperture of the SCR can be determined by the flat plane equation

$$\sigma = \frac{4\pi A^2}{\lambda^2}$$

$$A^2 = \frac{\sigma \lambda^2}{4\pi} \qquad (3.29)$$

Substituting A^2 from Equation (3.29) into Equation (3.28) we have:

$$\sigma_G = 4 \sigma_C \sin^2 (90^\circ - \delta)$$

if δ equals fifteen degrees, then the glint cross section is:

$$\sigma_G = 2799.6 \text{ square feet}$$

The normal reflected energy should be added to the glint energy to produce the final reflected cross section of the target.

Normal maximum cross section of the corner reflector is 750 square feet and the maximum glint cross section is 2799.0 square feet.

$$\text{Total } \sigma = \sigma_G + \sigma_{CR}$$

$$\sigma = 3549 \text{ square feet}$$

Therefore, the very large value of the cross section data could have been caused by the addition of glint reflection to the normal returned signal.

3.2 Data Processing (UNIVAC)

Concurrent with the development of the radar signal processing hardware described in Section 2.0, radar data was collected and analyzed using a general purpose digital computer. The data collection effort is described in detail in Section 4.0. In this section we shall describe the software used to process the data and give some examples of the output obtained from the computer programs.

3.2.1 Description of UNIVAC Software

Developmental analysis of the radar data base was performed on the UNIVAC 1706 computer with the aid of software that utilized the interactive capabilities of the CRT and keyset peripheral devices. The primary intent of this section is to document the existence of the various computer programs and give a brief summary of their usage and capabilities rather than to completely describe the coding and operation. Much of the software used on the UNIVAC for this contract was developed under previous efforts, and has been described in other reports*. In particular, the tape handling and display programs, and the summary and reporting programs are virtually unchanged from their previous versions. The data reduction program, which forms the condensed data tapes (CDT's) from the raw (field) data tapes has been improved and is described in the March 1973 letter report**. The remaining programs to be described are PPQUA3, XSECT, and SIATAN.

3.2.1.1 PFQUA3

PPQUA3 is the fundamental spectral analysis program for converting sampled time domain data into the frequency domain using the Fast Fourier Transform (FFT). Power spectrum estimates are displayed on the CRT, and information relating to the absolute power reference of the received signals is calculated and printed for later use. The parameters used in forming the power spectrum estimate are very flexible and may be varied at the user's request. The basic difference between this program and the spectral analysis programs of the previous contract is that both in-phase and quadrature phase

---

* See "Moving Platform Investigation for FOPEN Radar," SURC TR-71-249 November 1971, pp. 59-65.

** Letter Report, "Moving Platform FOPEN Radar Prototype Development," Contract DAAD05-72-C-0229, March 1973, Section 2.1.

data is used to form double-sided spectral estimates rather than using only a single channel of doppler information at a time.

The program operates in two distinct, independent phases. In phase 1, time data from a CDT is processed via the FFT algorithm -- either the software or hardware version -- and subjected to a Hanning window to help eliminate sidelobe distortion. Each time-data sample is a complex number which is determined by simultaneously sampling both the in-phase and quadrature phase channel of the demodulated doppler signal from a given range gate. The number of points used for each FFT, along with the overlap between successive sets, is variable and controlled by the user. Each set of Hanned FFT coefficients is then subjected to a magnitude squaring operation and, along with appropriate header information, is written onto magnetic tape for later processing either by the phase 2 logic or by other programs. This frequency domain data set is commonly known as a modified periodogram.

In phase 2, frequency data is read from magnetic tape, smoothed and then displayed on the CRT under the interactive control of the user. Smoothing, accomplished by averaging a number of successive periodograms, reduces the statistical variability of the estimate at the expense of processing resolution. The result is a double-sided power spectrum estimate of the doppler frequencies returned from a segment of terrain as determined by the range gate, aircraft altitude and velocity, and the duration of the time data contained in the average.

3.2.1.2 XSECT

The UNIVAC program XSECT computes the radar cross section of either a target, distinguished by a prominent peak in the power spectrum estimate, or a given patch of clutter, as determined by a specified azimuth angle. Spectral estimates generated by the first phase of PPQUA3 are utilized by XSECT to perform the indicated operations. An absolute power reference, taking into account all system gains and losses, is established by performing a calibration experiment using a single-sideband generator. Actual received signals, with the gains unchanged, can then be compared to the calibration data and adjusted according to the magnitude of the power spectrum estimates. (See Tab B).

The program uses the principle that the power reflected by a given patch of terrain (or a target) is equal to the integral of the power spectral density over appropriate frequencies corresponding to the azimuth extent of the patch. The analyst can thus measure clutter cross section at any azimuth angle and compare it to observed target cross sections. The target cross sections are calculated for various azimuth angles, which change according to the motion of the aircraft, and rise to a maximum when the radar illuminates the largest area. These measurements are useful for determining the probability of target detection.

3.2.1.3 STATAN

The UNIVAC program called STATAN attempts to enhance the detection of a target utilizing sequences of power spectrum estimates generated by phase 1 of PPQUA3. A matrix of power spectral density values with frequency in one dimension and time in the other is formed within core memory. Taking into account the changing doppler frequency of a target, a diagonal average is computed along the matrix. In principle, the target reflections should exhibit a greater degree of coherency than returns from clutter, and the presence of the target should be easier to detect. This program is continually undergoing modifications in its basic algorithm, and is generally thought of as experimental.

PARAGRAPH 3 - TAB A

Spectra Averaging

To average spectra from the same section of ground, data must be obtained at different times. Assuming one range bin, a matrix of spectral amplitudes can be written with each row corresponding to a particular frequency bin and each column to a particular time. Referring to Figure 3.14 it can be seen that a target takes on a range of azimuthal values, hence a range of doppler frequencies as it is passed over by the range gate. If the range of frequencies is broken into discrete bins the target will pass through several of these bins. If time increments are properly chosen the target will pass through one time increment while being contained in one frequency bin. Moving downwards, Fig.3.14 yields higher frequencies corresponding to angles more forward of the normal to the platform velocity vector. Moving toward the right yields later times. Moving diagonally upward and to the right corresponds to the amplitude returns from a single stationary point object on the ground.

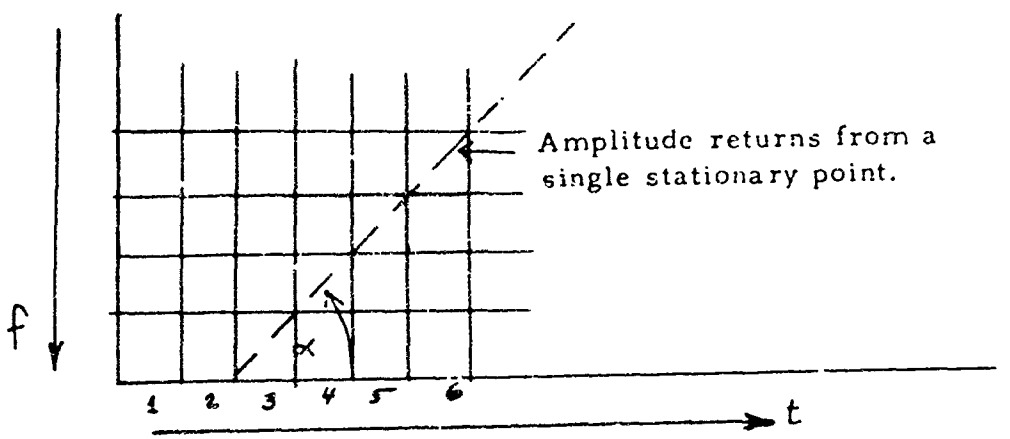

Figure 3.14. Target Averaging Relationship

The speed of the aircraft, the sampling rate, and the number of samples used to obtain a spectra can be adjusted such that the angle of the locus of the returns from an object will be 45° to the horizontal, or 30°, etc. For example, increasing the speed of the aircraft will increase the angle α. For ease of manipulation, α = 45°, or 30° is chosen.

Calculation of the sampling rate which will cause the locus of returns from a single object to fall on a path of 45° to the horizontal follows. Doppler frequency is given by:

$$f_D = \frac{2v}{\lambda} \cos\theta \sin\psi$$

v = velocity of platform

λ = wavelength

θ = depression angle

ψ = azimuth angle (straight ahead = 90°, right broadside = 0° to the rear = -90°)

Let Δf be the spacing between frequency bins and T the time used to gather data for one spectrum, then

$$\Delta f = \frac{1}{T}$$

Define $\Delta\psi$ by

$$\Delta f = \frac{2v}{\lambda} \cos\theta \sin\Delta\psi$$

Distance = (velocity) (time)

$$d = vt$$

if $\alpha = 45^\circ$,

$$d = (GR)\,\Delta\psi = vT$$

$$\Delta\psi = vT/(GR)$$

where GR = ground range

and SR = slant range

$$\Delta f = \frac{2v}{\lambda} \cos\theta \sin(vT/(GR))$$

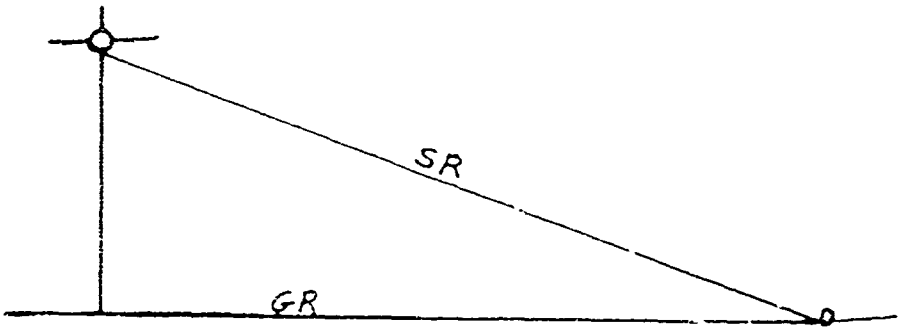

$$\cos\theta = GR/SR$$

$$\sin\frac{vT}{(GR)} \cong \frac{vT}{(GR)}$$

$$\Delta f \cong \frac{2v}{\lambda}\frac{(GR)}{(SR)}\frac{vT}{(GR)}$$

$$\Delta f = \frac{2\,v^2\,T}{\lambda\,(SR)}$$

$$\frac{1}{T^2} = \frac{2\,v^2}{\lambda(SR)}$$

$$\frac{1}{T} = \frac{1}{n\,\Delta t} = \frac{s}{n}$$

n = number of samples used to obtain one spectrum

Δt = time between samples = 1/s

s = sampling rate

$$\frac{s^2}{n^2} = \frac{2\,v^2}{\lambda(SR)}$$

$$s = n\,v\sqrt{\frac{2}{\lambda(SR)}}$$

λ = 7 ft

n = 512

v = 120 mph = 176 ft/sec

SR = 1500 ft

then

$$s = 512 \cdot 176 \sqrt{\frac{2}{7\ (1500)}}$$

s = 1242.9 for slant range 1500 ft

s = 879.14 for slant range 3000 ft. $\alpha = 45^{\circ}$, v = 120 mph

We can also compute the velocity required to obtain the same 45° locus for a given sampling rate s

$$v = \frac{s}{n} \sqrt{\lambda(SR)/2}$$

For example, v = 66.4 ft/sec.

when s = 468.75

n = 512

λ = 7

SR = 1500

For a locus with $\alpha = 60^{\circ}$, simply set $vT = 2(GR)\ \Delta\psi$

$$\Delta\psi = \frac{1}{2}\ vT/(\text{illegible})$$

$$\Delta f = \frac{2v}{\lambda} \cos\theta \sin\left(\frac{2\ vT}{2\ (GR)}\right)$$

$$\frac{1}{T} \simeq \frac{2v}{\lambda} \frac{(GR)}{(SR)} \frac{2\ vT}{2(GR)}$$

$$\frac{1}{T^2} \approx \frac{v^2}{\lambda\ (SR)}$$

$$\frac{s^2}{1^2} \approx \frac{v_2}{\lambda\ (SR)}$$

$$S \approx nv\ \sqrt{1/\lambda\ (SR)}$$

$$v \approx \frac{s}{n}\sqrt{\lambda\ (SR)}$$

for $s = 468.75$, $\lambda = 7$, $n = 512$, $SR = 1500$

$$v = \frac{468.75}{512}\sqrt{7\ (1500)}$$

$$v = .915\ \sqrt{10500}$$

$$v = 94 \text{ ft/sec. for SR} = 1500 \text{ ft}$$

$$= 133 \text{ ft/sec.} = 90.5 \text{ mph for R} = 3000 \text{ ft.}$$

The same effect can be obtained by shifting forward on the time data, by the right amount, before taking each spectra; this, in effect, is an adjustment of n.

$$s = nv\ \sqrt{\frac{2}{\lambda\ (SR)}}$$

$$v = \frac{s}{n}\sqrt{\lambda\ (SR)/2}$$

let $s = 468.75$

$\lambda = 7$

$SR = 1500$ ft

$$v = \frac{468.75}{n}\sqrt{5250}$$

$$v = \frac{34000}{n} \text{ ft/sec.} \qquad SR = 1500 \text{ ft}$$

$$v = \frac{48000}{n} \text{ ft/sec.} \qquad SR = 3000 \text{ ft}$$

If v = 118 knots = 136 mph = 200 ft/sec.,

$$n = \frac{34000}{200} = 170 \qquad SR = 1500 \text{ ft}$$

$$n = \frac{24000}{200} = 120 \qquad SR = 3000 \text{ ft}$$

When more than one range bin is present, we can construct a three-dimensional matrix where the additional dimension is range. See Figure 3.15.

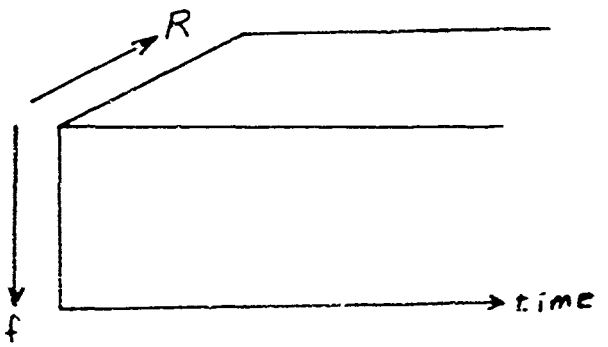

Figure 3.15. Three-Dimensio al Diagonal Averaging

Averaging diagonally within a range plane can be done just as before. We can take into account the variation in range with azimuth by averaging elements of our matrix from different range planes.

Signal Injection Calibration

Calibration of injected signal was accomplished through the use of a beacon with known characteristics. For these tests both an omni antenna and a directional antenna with 6 dB gain was used on the beacon.

The beacon was placed on a platform approximately 30 feet off the ground. Range to the beacon was determined by summing the beacon delay, the radar delay and the two-way cable delay and subtracting the total from the delay of the radar return. This method was checked for a 1000-foot actual range and was found to be accurate. The effective range to the beacon was found to be 840 feet.

The video signal resulting from the transmitting beacon was measured (photographed). The receiving antenna was then disconnected and a calibrated RF source connected to the radar. The RF power level needed to make the video due to the injected RF source equal to the video due to the transmitting beacon was measured.

Applying the radar equation to the beacon data where:

$$P_R = \frac{P_T G_T G_R \lambda^2}{(4 \pi R)^2}$$

and

P_R = power received

P_T = power transmitted by beacon

G_T = gain transmitting (beacon) antenna

G_R = gain receiving antenna

λ = wavelength

R = range

when

P_T = 10 watts

G_T = 6 dB

G_R = 6 dB

λ = 7 feet

R = 840 feet

$P_R = 7.04 \times 10^{-2}$ mW

P_R = -11.52 dBm

The calculated power incident on the radar antenna is -11.52 dBm. The magnitude of the injected signal was measured as -11.0 dBm indicating a successful technique of signal injection. The experiment was repeated with an omni antenna on the beacon and again the results closely correlated.

4.0 DATA COLLECTION

Data collection was accomplished using an airborne mounted FOPEN radar. The doppler output of the radar was converted to a 12-bit digital signal, recorded on magnetic tape and later processed on the UNIVAC 1206 computer.

Selection of clutter environments for data collection included:

a) lakes

b) farm land

c) coniferous woods

d) deciduous woods

e) open areas

A corner reflector was constructed and used as a calibrated target. The ability to compute the radar cross section of a target or patches of clutter directly from the doppler data was provided through signal injection procedures.

The following sections will describe in detail the radar hardware, instrumentation, and data collection techniques used in the actual data collection.

4.1 Description of the Data Collection System

The data collection system* is comprised of

1. A FOPEN radar with three range gates
2. A horizontally polarized antenna
3. A data recording system
4. A data processing system.

Figure 4.1 depicts the system instrumentation in block diagram form. Data was collected and processed in the following manner:

The transmitter is used to transmit a horizontally polarized signal.

The return signal is received and processed through three adjacent range gates with the center range gate used as the reference for range settings.

*See also "Moving Platform Investigation for FOPEN Radar," SURC TR-71-249, November 1971. Section 2.0 Data Collection

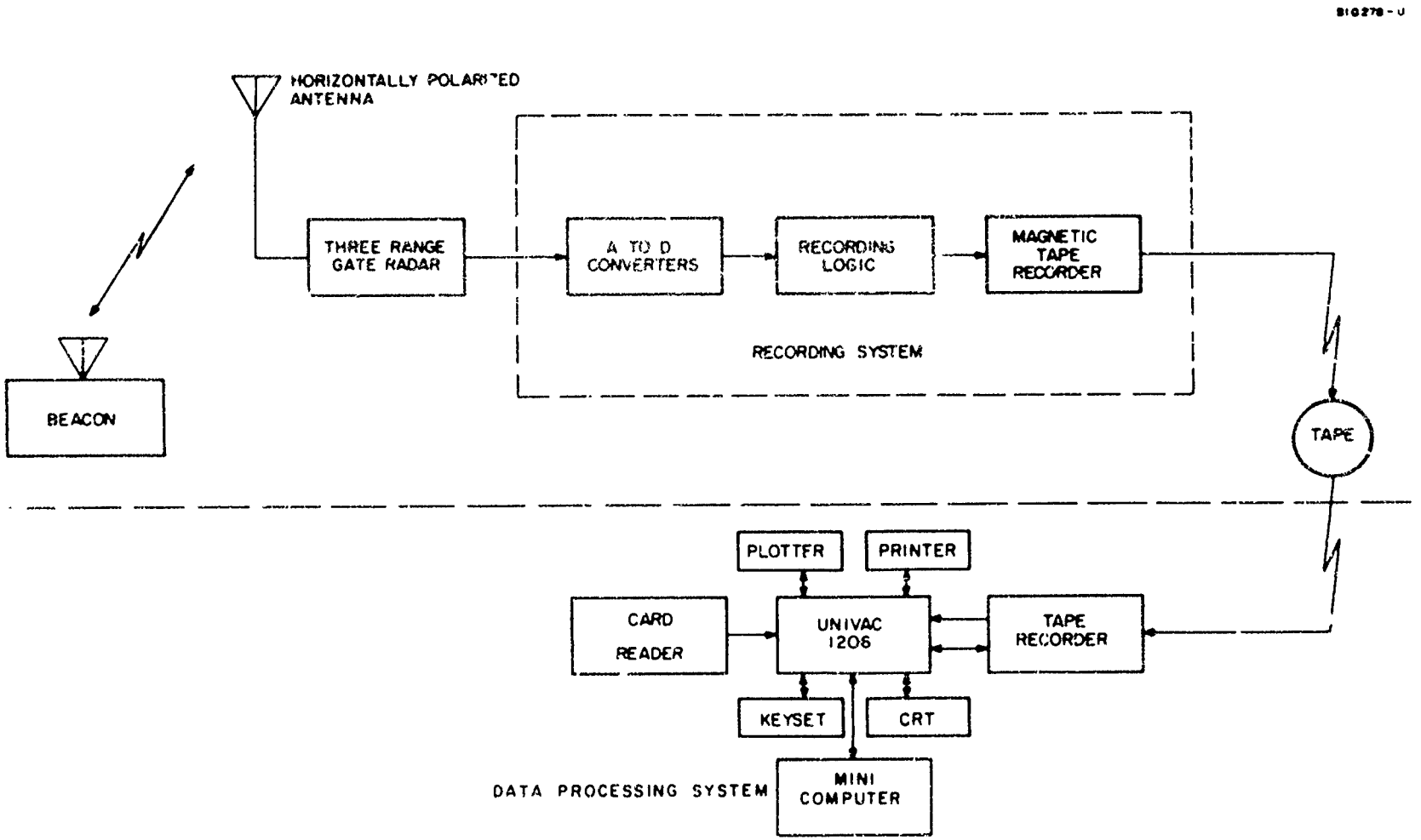

Figure 4.1. System Instrumentation Block Diagram

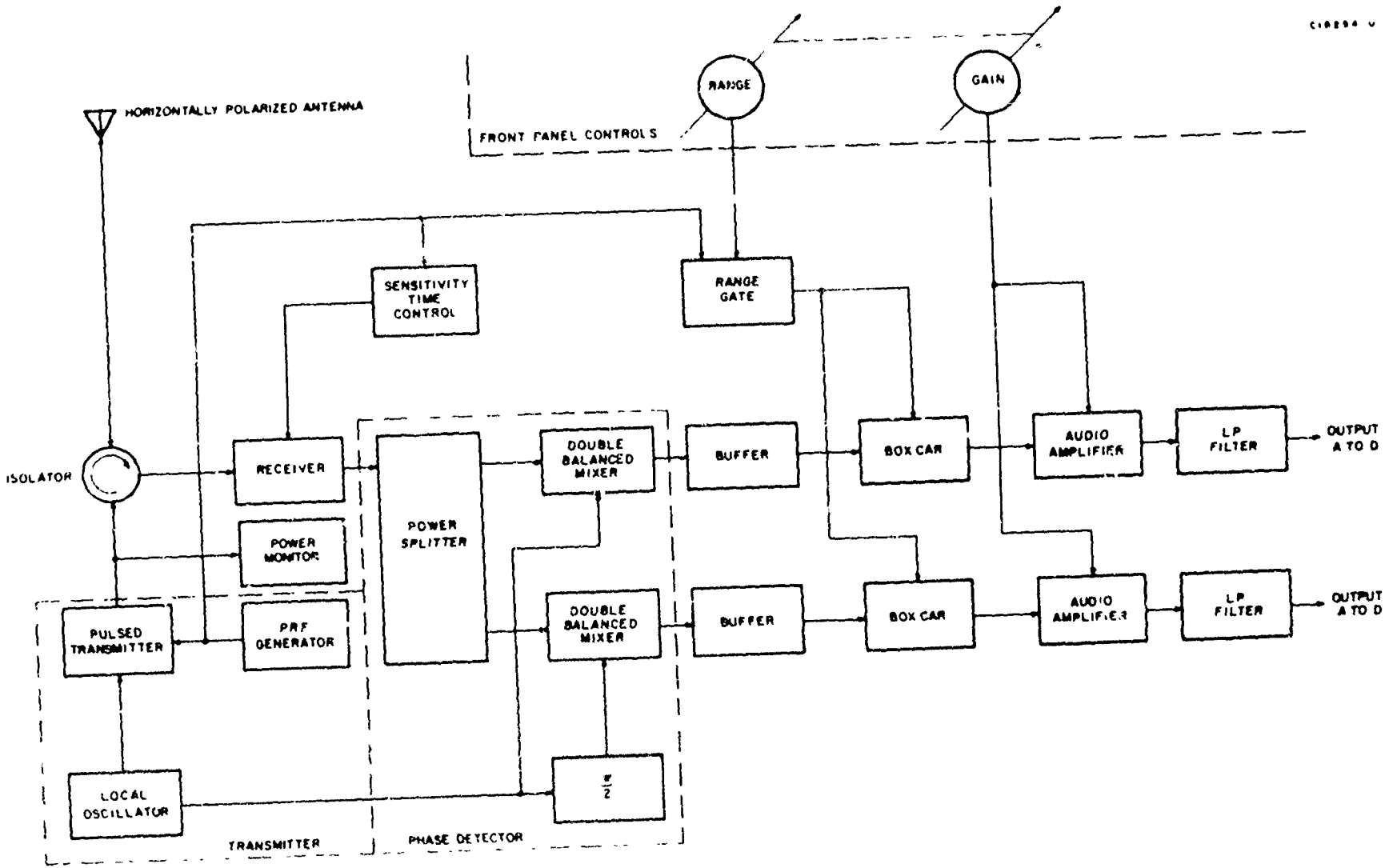

Figure 4.2. Instrumentation FOPEN Radar

The data recording system accepts six analog doppler outputs which were multiplexed, digitized and recorded on magnetic tape in a preselected format. These tapes are referenced as field data tapes.

Data from the field data tapes were read into the UNIVAC 1206 computer where they are sorted, compressed, reformatted and stored on new tapes referenced as condensed data tapes. This process involved using an IBM compatible tape transport and formatter.

To facilitate locating the given target from the aircraft, a beacon (cransponder) was positioned at the target site. Interference with the target spectrum by the beacon was suppressed by delaying its response.

4.1.1 FOPEN Radar

The instrumentation FOPEN radar is shown in Figure 4.2. It differs from the radar utilized on Contract DAAD05-71-C-0156 "Moving Platform Investigation for FOPEN Radar" in the following ways:

1) the addition of a block of audio gain

2) a change in the radar frequency and PRF

3) the addition of Post boxcar amplifiers to insure utilization of the full range of the analog to digital converters.

4) the addition of the Sensitivity Time Control (STC) to insure a reasonable gain distribution over the ranges of interest.

4.1.1.1 Transmitter

The transmitter includes the local oscillator, the PRF generator, pulse amplifier and power amplifier. Its maximum power output is 5 kW at a center frequency of 143 MHz. It operates with a pulse width of 200 nanoseconds at a PRF of 10 kHz. As noted in Figure 4.2 the transmitter also provides a local oscillator reference signal to the phase detector.

A second operating frequency was also used. The change of frequencies required retuning the transmitter a receiver to operate at a center frequency of 51 MHz, 10 kW maximum power output, a pulse width of 200 nanoseconds at a PRF of 10 kHz.

4.1.1.2 Antenna

The antenna used in the data collection system was an American Electronics Lab (AEL) log periodic antenna with a bandwidth of 100 to 1000 MHz. This wideband antenna was chosen because of a severe video ringing problem associated with long antenna feed cables.

Free space antenna patterns indicate a 3 dB beamwidth of 72 degrees (see Figure 4.3). The antenna gain is 6 dB.

Radiation patterns were obtained after mounting the log periodic array on the aircraft while the aircraft was on the ground and in flight. These patterns are presented in Figures 4.4 and 4.5, respectively.

Figure 4.4 exhibits a large perturbation on the left side of the pattern which is attributable to reflections from the air frame. Due to physical problems involved, the rotation of the airframe could not be held exactly constant which results in the azimuth scale of the pattern representing only approximate azimuths.

Figure 4.5 indicates an increase in magnitude of the distortions which can only be a result of the change in attitude of the aircraft in respect to the RF source. Higher frequency components in perturbations are attributed to either propeller modulation or antenna vibration.

4.1.1.3 Video Amplifier/Buffer

The original video amplifiers were duty cycle sensitive which put a severe limitation on the operator's target location capabilities. The design and implementation of a non-duty cycle limited DC coupled video amplifier has resolved this problem. Figure 4.6 is a schematic of this circuit.

4.1.1.4 Sensitivity Time Control (STC)

The system AGC was replaced by the STC to control RF gain as a function of range (see Figure 4.7).

4.1.1.5 Audio Amplifiers

An audio amplifier was added to the radar to insure sufficient dynamic range in the recorded data. It is a dual stage amplifier with a fixed gain of 10 dB in the first stage. The gain of the second stage is controlled from the front panel in eight (8) unequal increments. The maximum gain of the second stage is 31 dB. Figure 4.8 schematically presents this circuit.

4.1.2 Data Recording Equipment

The data recording equipment, shown in Figure 4.9, includes the analog control logic, 8-channel multiplexers, buffer amplifier, analog-to-digital (A/D) converters, recorder control logic and the magnetic tape transport.

The analog control logic controls all the timing required to present the digital data to the tape transport in the format shown in Figure 4.10.

The sampling rate of 468.75 Hz is generated in the recorder control logic by dividing the 60 kHz clock by 128. It is synchronous with the clock and is the input to the sync logic.

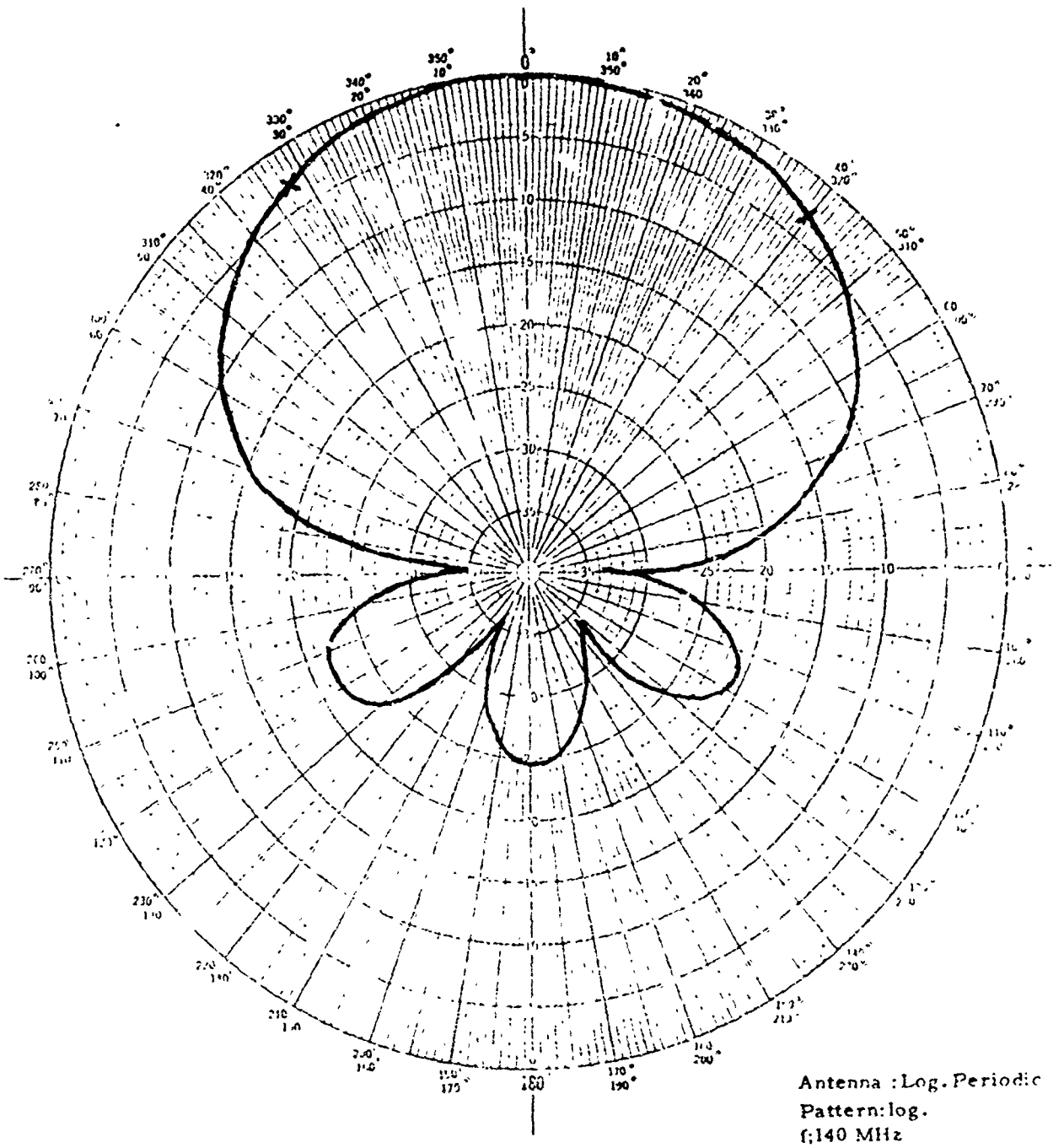

Figure 4.3. Free Space Antenna Pattern

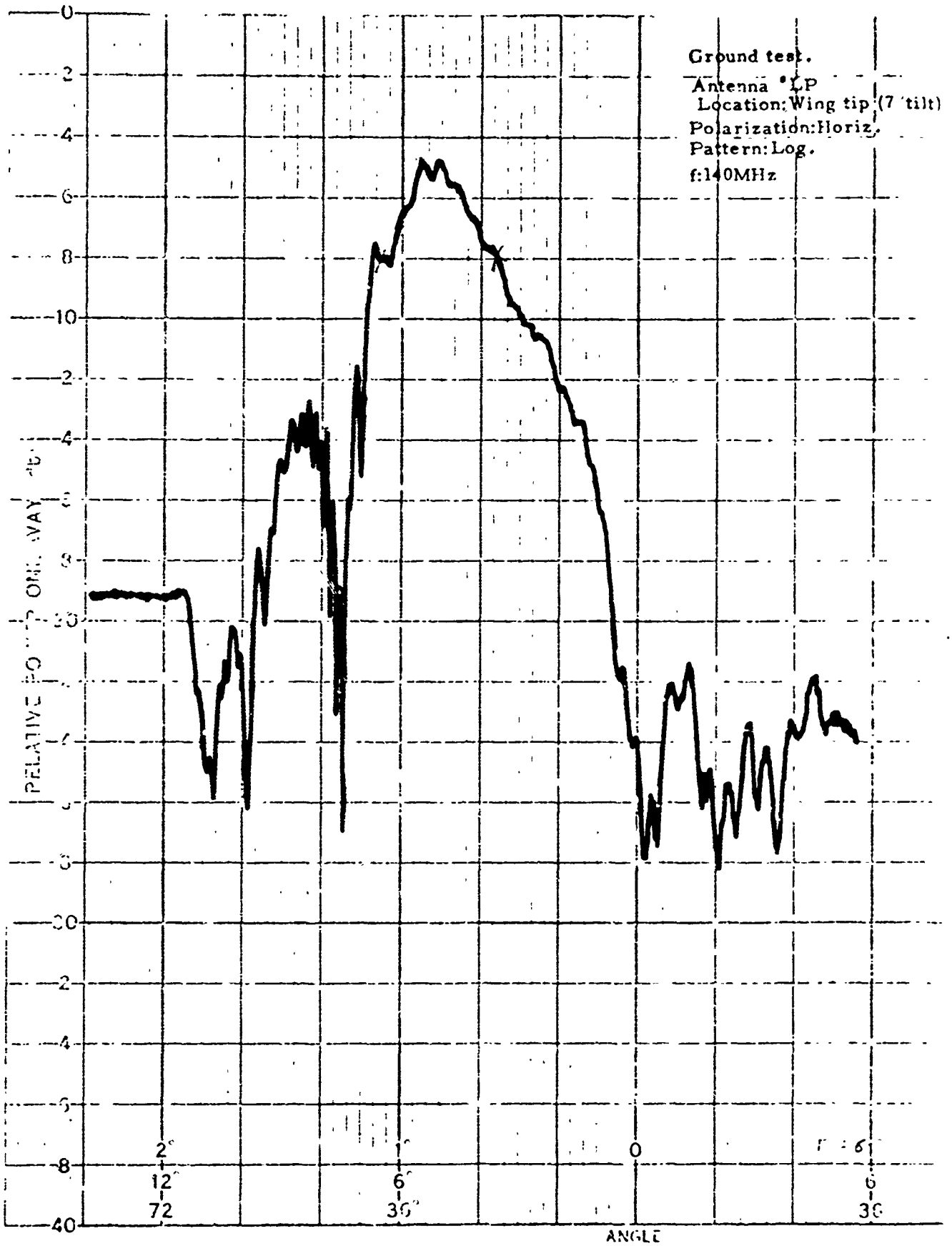

Figure 4.4. Aircraft Mounted Antenna Pattern

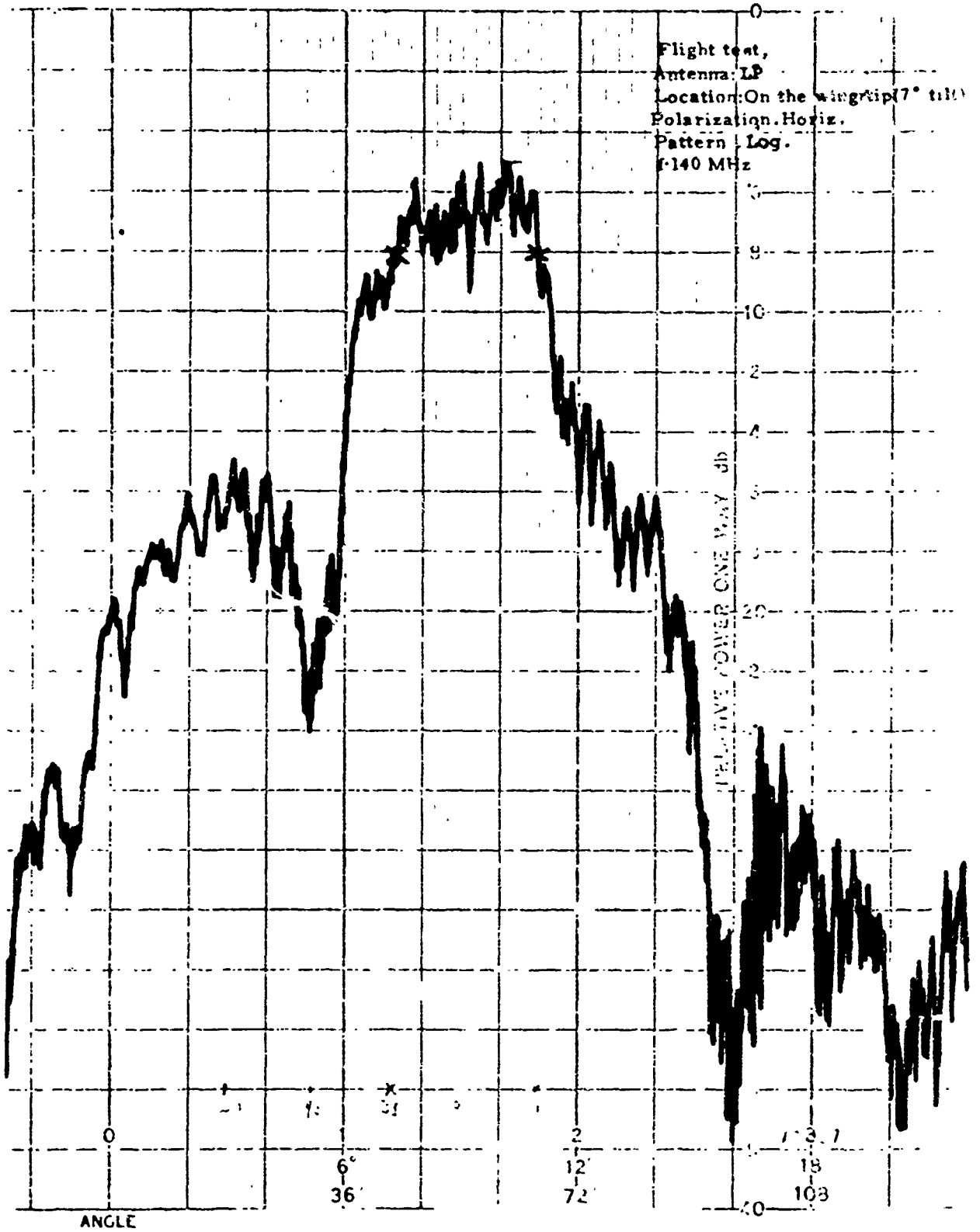

Figure 4.5. Aircraft Mounted Antenna Pattern

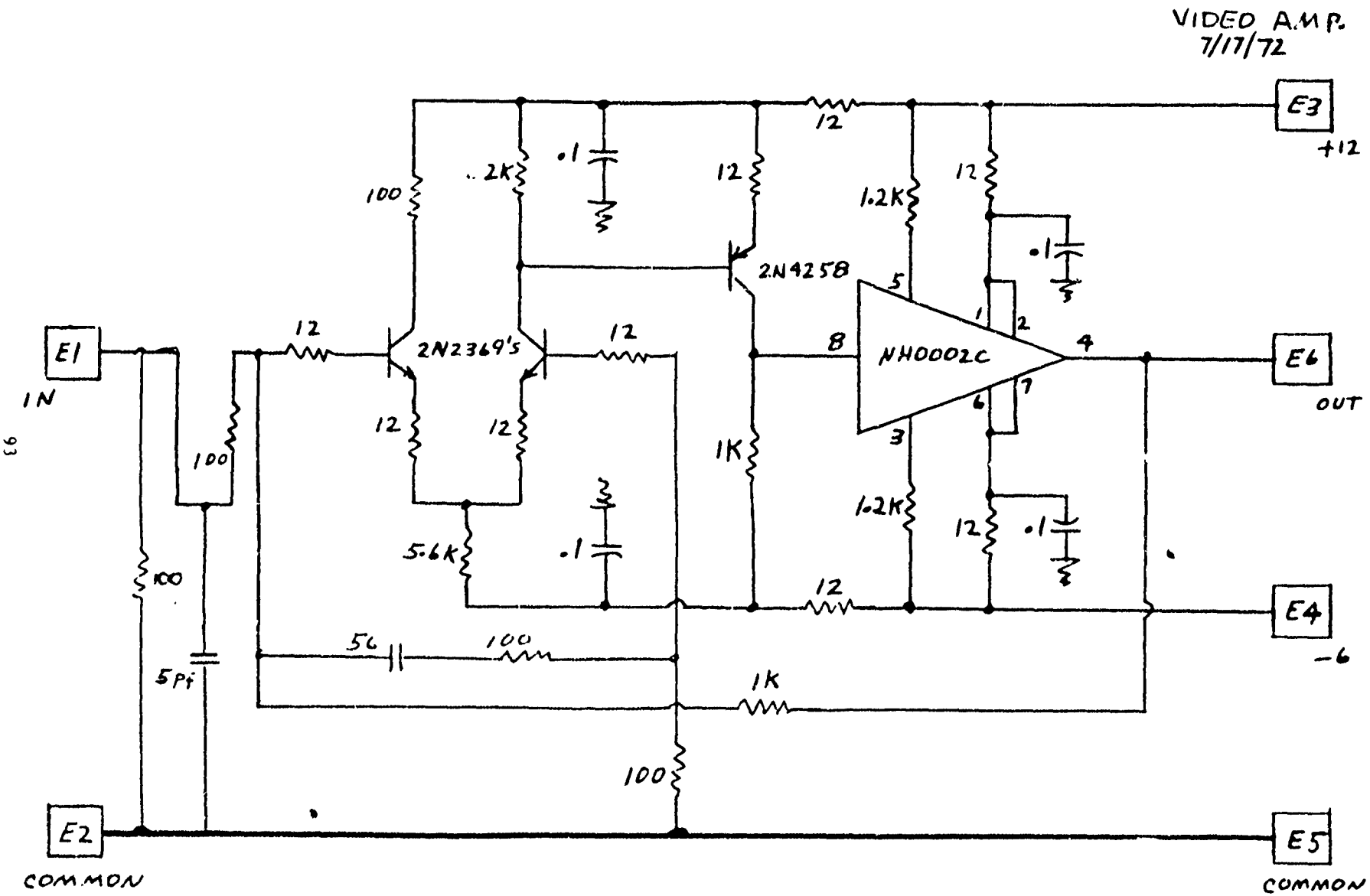

Figure 4.6. Video Amplifier Schematic Diagram

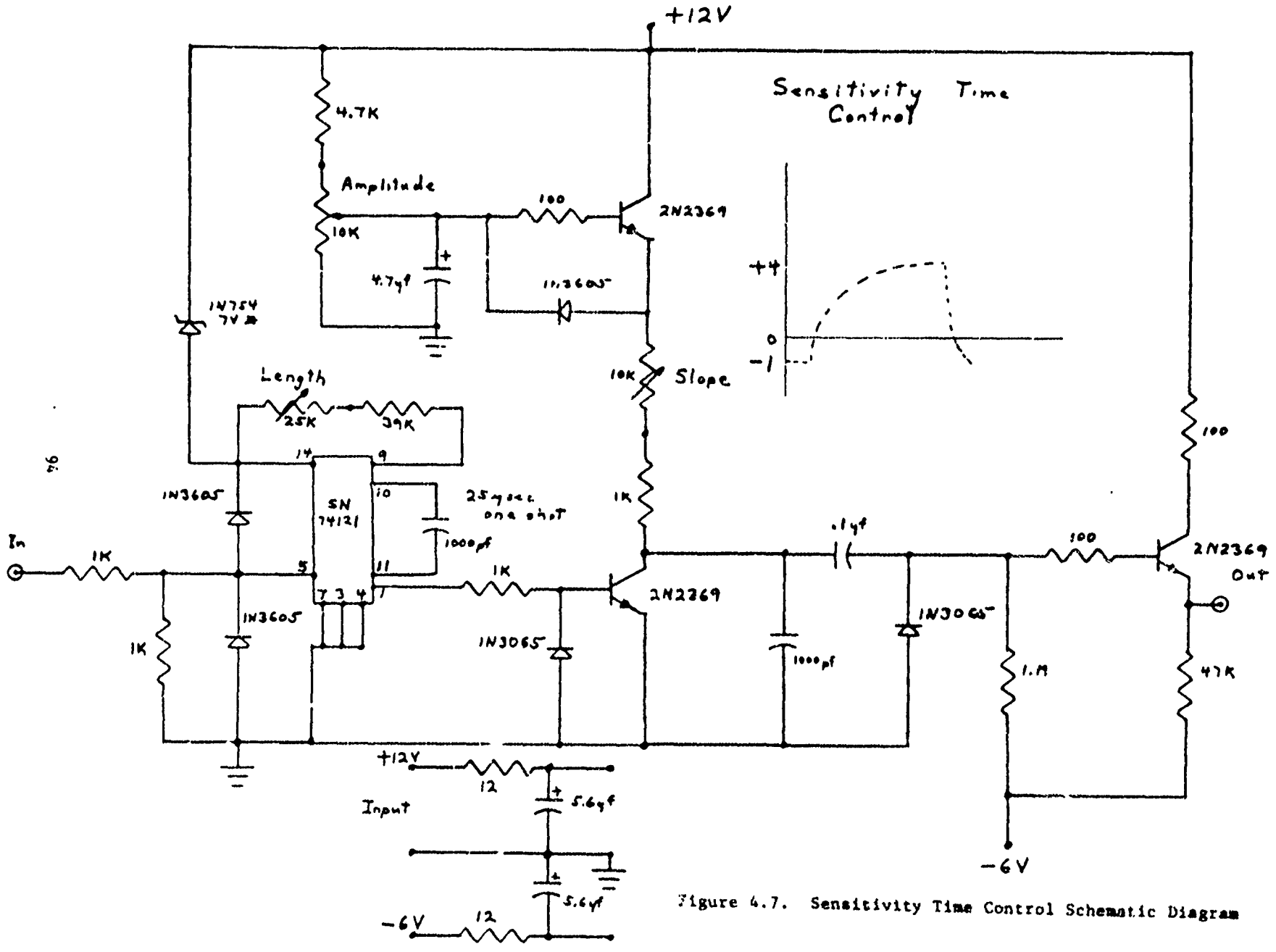

Figure 4.7. Sensitivity Time Control Schematic Diagram

Audio Amplifier

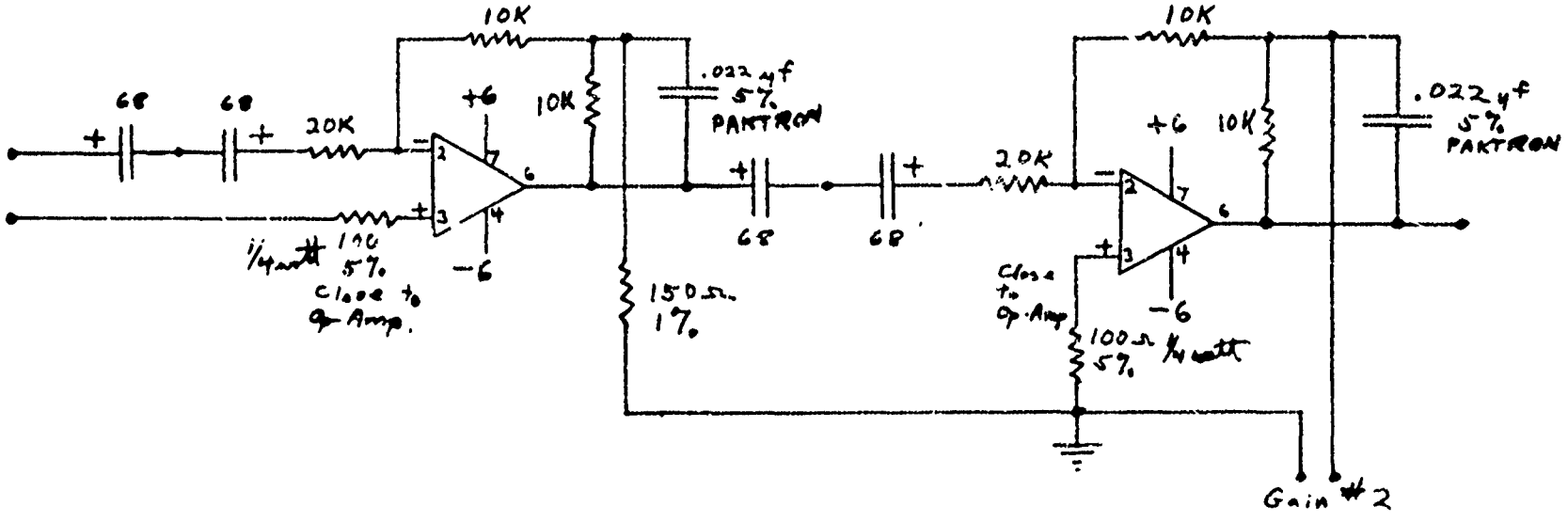

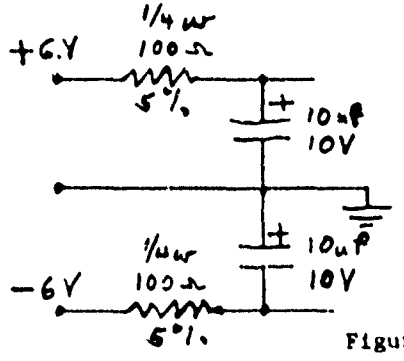

Figure 4.8. Audio Amplifier Schematic Diagram

ALL UNMARKED RESISTORS 1%
CORNING TYPE RN55D

Op-Amps. RCA CA6741T

P.C. Connector
ELCO SERIES DUAL PIN 1/4"
00-6007-012-980-002

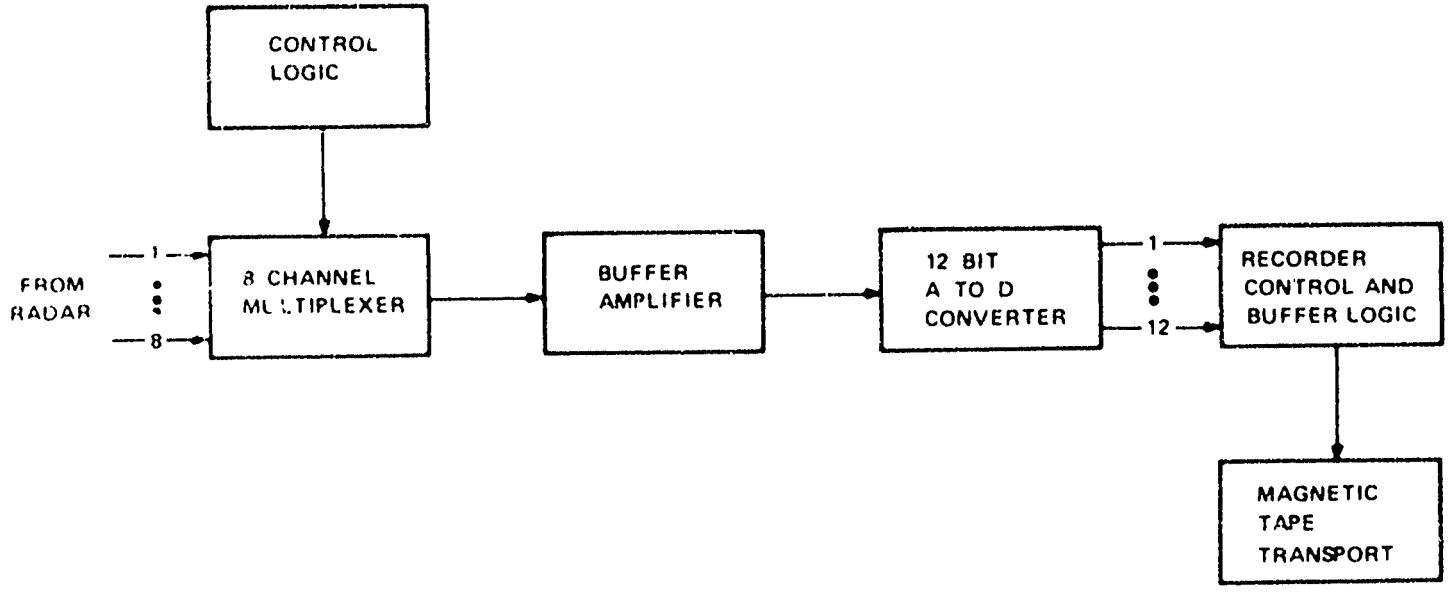

Figure 4.9. Data Recording Equipment

← Tape Direction

16	15	14	13	12	10	8	6	4	2	1
O	O	D	T	A to D bits						

1. Most significant byte first on tape
2. Most significant bit first
3. The A to D sign bit is bit 12
4. D represents the data instruction position
5. T represents the target instruction position
6. D = 1 implies data are present
7. T = 1 implies target is present

Tape Sequence

Word	Clock	Bit Weights 2^7	2^6	2^5	2^4	2^3	2^2	2^1	2^0	P	Functions
	0	0	0	0	0	0	0	0	0		
1	1	0	0	1	$\frac{T=1}{T=0}$	X	X	X	X		Boxcar 1 Range 1 Q
	2	X	X	X	X	X	X	X	X		
2	3	0	0	1	T	X	X	X	X		Boxcar 2 Range 1 I
	4	X	X	X	X	X	X	X	X		
3	5	0	0	1	T	X	X	X	X		Boxcar 3 Range 2 Q
	6	X	X	X	X	X	X	X	X		
4	7	0	0	1	T	X	X	X	X		Boxcar 4 Range 2 I
	8	X	X	X	X	X	X	X	X		
5	9	0	0	1	T	X	X	X	X		Boxcar 5 Range 3 Q
	10	X	X	X	X	X	X	X	X		
6	11	0	0	1	T	X	X	X	X		Boxcar 6 Range 3 I
	12	X	X	X	X	X	X	X	X		
7	13	0	0	1	T	X	X	X	X		
	14	X	X	X	X	X	X	X	X		
8	15	0	0	1	T	X	X	X	X		Range
	16	X	X	X	X	X	X	X	X		
	17	0	0	0	0	0	0	0	0		
	18	0	0	0	0	0	0	0	0		

Figure 4.10. Field Tape Format

The sync logic interrogates the A/D converter and inserts the target present bit into the data.* The analog counter and the control matrix combine to sequentially switch the multiplexer through the eight input channels. The output of the multiplexer is connected through a high input impedance buffer amplifier to the A/D converter. When a command is given by the sync logic the digital conversion is made. At the completion of the conversion the digital word is gated to the recorder by the control gate logic. Eight conversions are made for each PRF interval recorded. Data is recorded every six PRF intervals.

The three following units are manufactured by Analog Devices, Inc.:

1) Model MOSES 8, multiplexer, an eight-channel device with 100 nanosecond switching time.

2) Model ADC 12U5B, A/D converter, a 12-bit converter capable of accepting a bipolar input with a maximum conversion time of 10 microseconds.

3) Model 148, FET differential operational amplifier used as a buffer amplifier for its parameters of 0.01% in 1 μs settling time and a slew rate of 100 volts per μs.

The recorder is a Recording Designs Limited (RDL) series 10500, continuous, IBM compatible, nine-track magnetic tape transport. The dynamic range of the recording system is ±2 dB. Maximum recording time for the eight and one-half inch reel of tape is about three minutes.

4.1.3 Beacon

The beacon aids the radar operator in differentiating the test vehicles from other targets in the test area and is the only means of insuring that the recorded test data includes the target data.

The beacon, acting as a transponder, is interrogated by the radar and sends back an R.F. burst delayed by about 1200 nanoseconds. The delay is included so that the radar may sample the data without interference from the beacon and the delayed beacon signal produces an unmistakable blip on the video monitor for assurance that the control target has been located during the airborne tests. The beacon's transmitted frequency is offset from the radar's transmitted frequency by 3 MHz to reduce the possibility that the beacon may appear to be a large target.

---

*The radar operator, upon receiving the beacon return from the controlled target, may insert a marker bit in the digitized data words under control of a manual pushbutton.

Figure 4.11 is a block diagram of the beacon. Received signals are amplified, square law detected and used to actuate the delayed trigger (receiver sensitivity is pre-set). The delayed trigger keys the transmitter to produce the return signal. The included status circuit and meter indicates when the beacon is being interrogated and is operational by coupling a portion of the transmitted energy into the metering circuit.

4.2 System Calibration

Calibration of both the analog and digital equipments in the data collection system is essential to accurate data collection and subsequent processing of the data. To accomplish this purpose a calibration procedure was devised to assure daily operational parameters.

This procedure included a pre-collection and post-collection injection of a single side band RF test signal* of known amplitude and modulated at a known frequency into the front end of the system. This signal is processed by the radar and its resultant test data recorded on the magnetic tape for special processing on the computer.

The procedure provides a total system test and calibration, in effect a documented means of accounting for changes in system parameters due to temperature changes and aging, in addition to a complete system functional check.

Figure 4.12 is an example of a typical processed test data spectrum. It indicates a sideband separation of greater than 38 dB (at the modulation frequency of 11 Hz) and incidental 60 Hz components more than 50 dB below the amplitude of the test signal (no 60 Hz visible). System gain may be calculated by comparing the area under the curve with the known input power of -12 dBm.

4.2.1 Signal Strength Estimation

In order to properly set the various system gains, it is necessary to establish expected signal strength from the radar environment. Both minimum and maximum signal levels are required to set dynamic range. The following section will show in some detail the derivation of the system gain parameters.

4.2.1.1 Input Power from a Point Target

From the radar equations:

$$P_{sig} = P_t G_t G_R \sigma \lambda^2/(4\pi)^3 R^4 L$$

---

*See "Moving Platform Investigation for FOPEN Radar, SURC TR-71-249, November 1971.

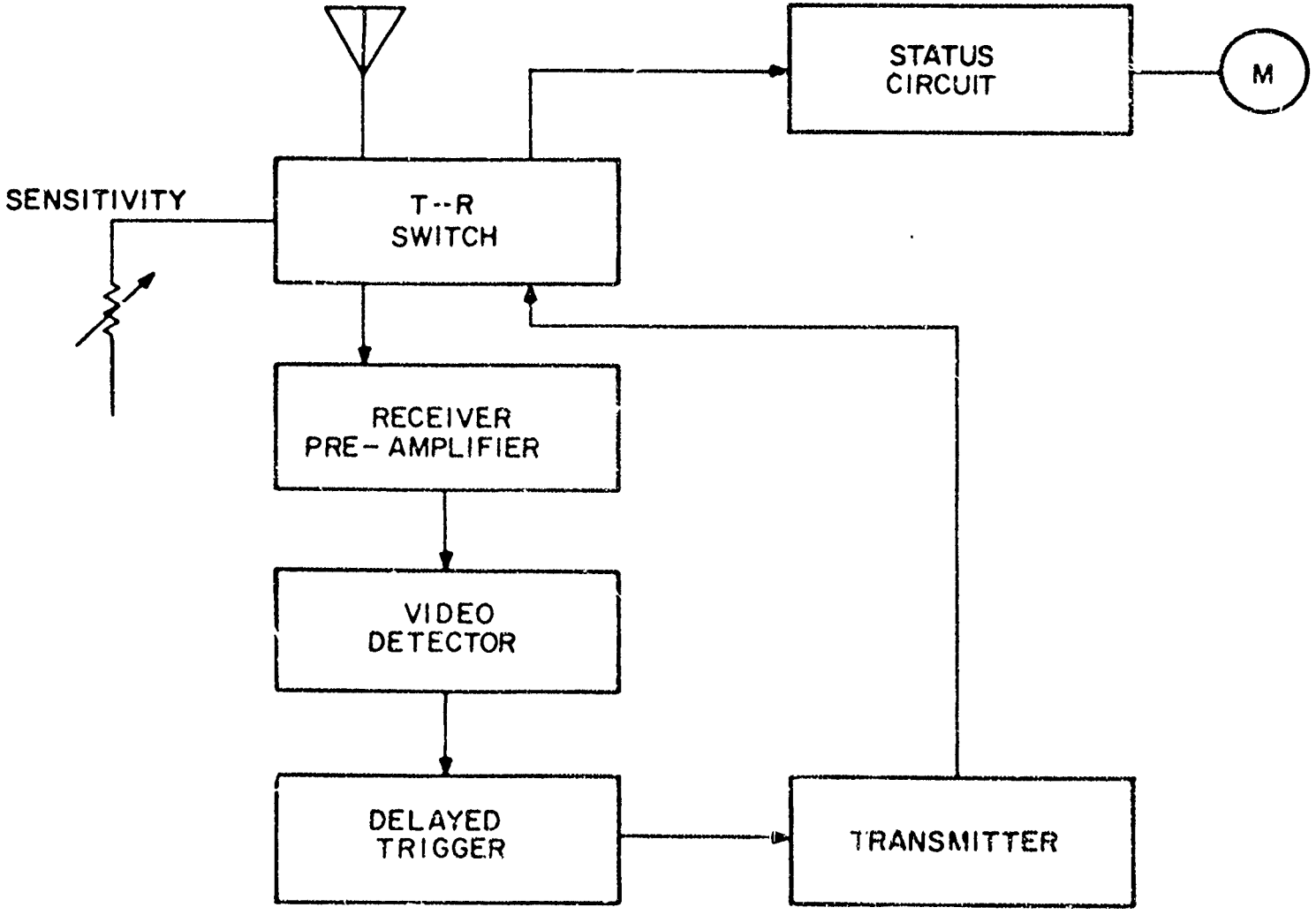

Figure 4.11. Beacon Block Diagram

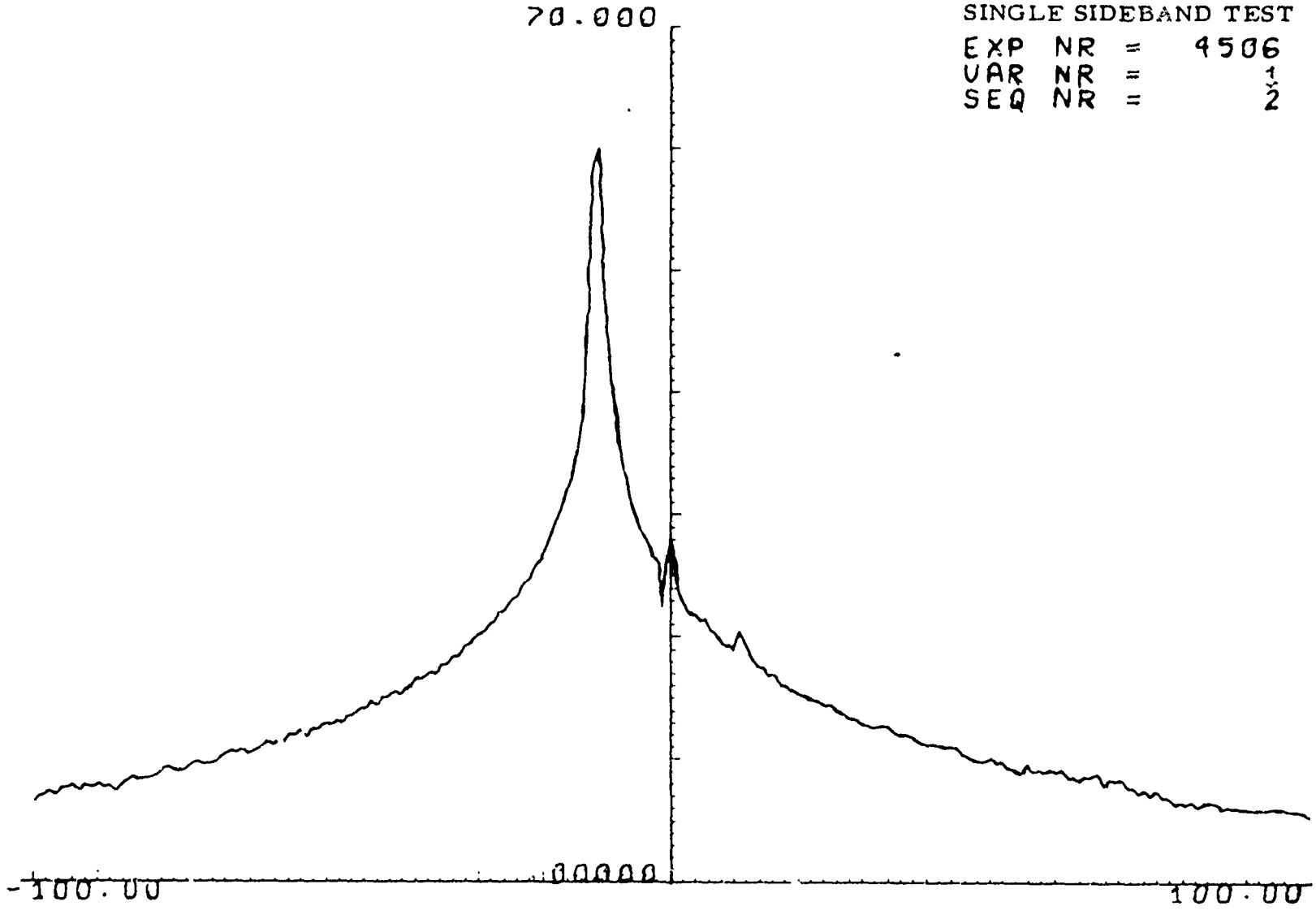

Figure 4.12. Single Side Band Test Data Spectrum

where

P_{sig} = system input power

P_t = 1 kW = 10^6 MW = 60 dBm

G_T = gain transmitting antenna = 8 dB = 6.3

G_R = gain receiving antenna = 8 dB = 6.3

σ = radar cross section = 1 m

λ = wavelength = 2.1 m

R = range = 1000 m

L = system loss

Assuming a range of 1000 meters, input power (P_{sig}) to the system from a one square meter target is:

$$P_{sig} = -(70.5 + L) \text{ dBm}$$

System losses consist of:

1) Isolator loss = 4 dB

2) Cable loss = 6 dB

If the total system loss, L = 10 dB, then:

P_{sig} = - 80.5 dBm for a target of one square meter at 1000 meters.

Input signal power as a function of Range is plotted (solid lines) in Figure 4.13.

4.2.1.2 Input Power Due to Instantaneous Clutter Signal

The effective cross section, σ_{BIN}, represented by a single frequency bin[1] can be expressed as:

$$\sigma_{BIN} = \sigma_o A_g$$

[1] A frequency bin relates to the elemental filters of a discrete Fourier Transform. The Fourier transform is the principal processing technique used in the radar processor. Refer to Section 3.1.2.

where

$\sigma_{BIN} = \sigma_o R_s \Delta\phi (c\tau/2)$

A_g = ground area represented by one bin = 1175 m^2

σ_o = square meters radar cross section per square meters area

R_s = slant range = 1000 meters

$\Delta\phi$ = frequency beamwidth = 2.25^o = .03925 radians

$c\tau/2$ = gate width = 30 meters

τ = pulse width = 200 nanoseconds

$c = 3 \times 10^8$ m/sec

Clutter was assumed to have a radar cross section, σ_o, of one square meter per 20 to 40 square meters of deciduous forest

For $\sigma_o = \frac{1}{20}$

$\sigma_{BIN} = \frac{1}{20}(1175) = 58.75\ m^2$

$= 17.7$ dB above 1 m^2

For $\sigma_o = \frac{1}{40}$

$\sigma_{BIN} = \frac{1}{40}(1175) = 29.375\ m^2$

$= 15.7$ dB above 1 m^2

$\sigma_{BIN} = 29\ m^2$ to $59\ m^2$

---

[1]Butler, J.E., Reflection and Doppler Characteristics of Targets and Clutter, ECOM-00263-F, (DSD 0209-0011), June 1967, pg. 56, Figure 3.

The total instantaneous clutter cross section is represented by σ_c and is calculated by multiplying σ_{BIN} by the number of bins. Since the antenna pattern is not an omni each successive bin will have a decreasing weight. It was estimated that ten bins at full weight could be used to approximate the total cross section, σ_c. Therefore,

$$\sigma_c = 10\ \sigma_{BIN} = 590\ m^2$$

or σ_c for all frequency bins is 27.7 dB above 1 m^2.

Since the system input power, P_{sig}, due to σ = 1 m^2 is -80.5 dBm, then the system input power, P_{sig}, due to clutter cross section σ_c = 590 m^2 is:

$$P_{sig} = -82.5 + 27.7\ dB$$

$$P_{sig} = -54.8\ dBm\ .$$

Input clutter signal as a function of range is plotted as a dashed line in Figure 4.13.

4.3 Modification of Radar - 140 MHz to 50 MHz

The decision to reduce the operating frequency of the radar resulted in changes in components of the radar.

The major problem involved in this change on both transmitter and receiver was the bandwidth requirement in that a 5 MHz bandwidth at 50 MHz is more difficult to attain than a 5 MHz bandwidth at 140 MHz. As would be expected changes have occurred in the frequency sensitive parts and are well documented in the research notebooks at SURC.

After all changes were accomplished the radar was bench tested and reinstalled in the aircraft.

Changing the Log Periodic Antenna caused concern over vibration problems as well as antenna patterns These problems were resolved by stiffening of the mount, reseating all the elements and subjecting the antenna to a fast taxi experiment when it was again aircraft mounted.

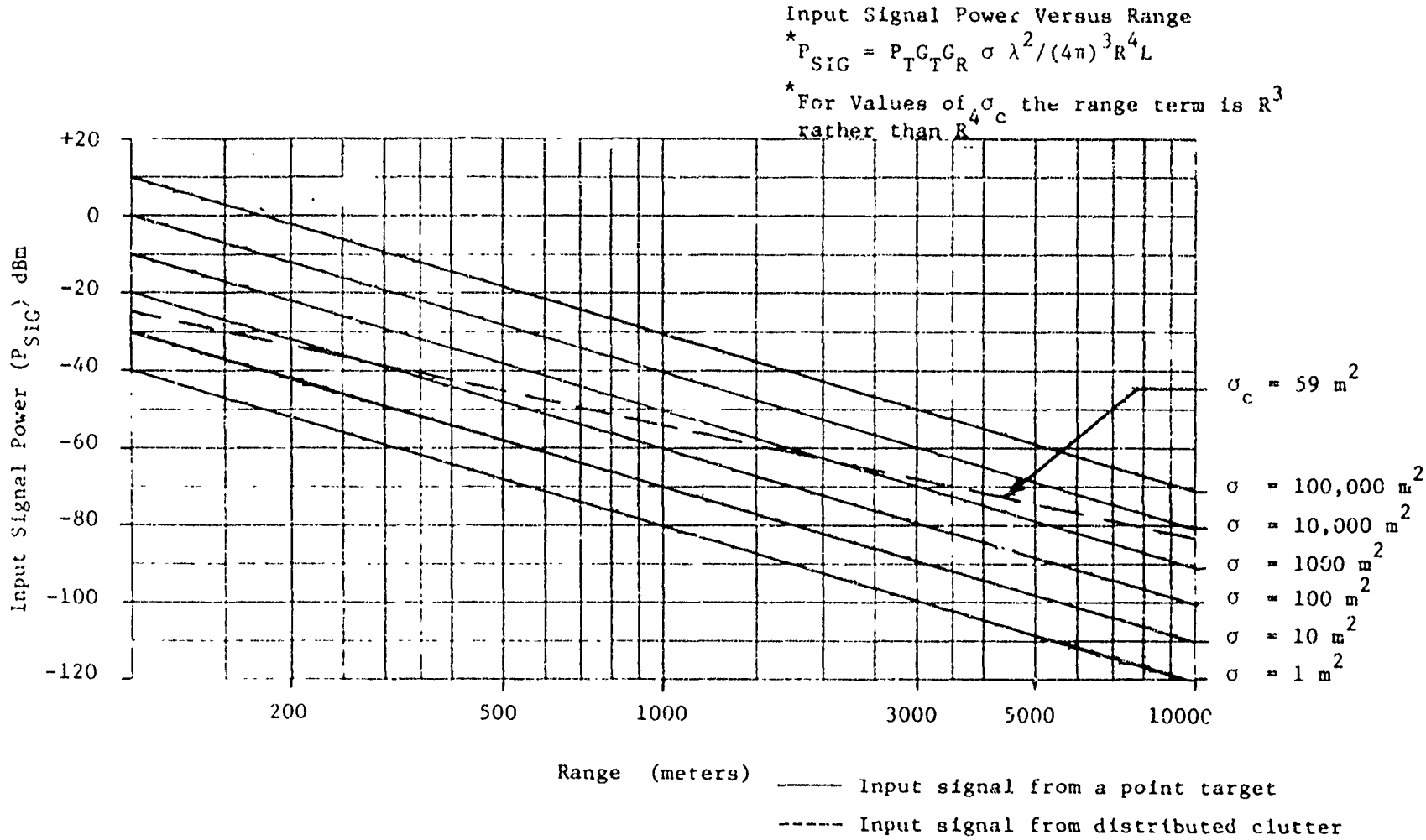

Figure 4-13. Relationship of Input Signal Power to Range

5.0 TESTING

5.1 Airborne Data Collection and Testing

Several tests and periods of data collection were required to calibrate the equipment used and collect sufficient data to fulfill the requirements of the study. This section will describe the tests and data collection efforts.

The "Instrumentation Test Plan", SURC document TR-72-223, provides a detailed description of the test procedures. Where differences occur between the test plan and actual data collection, this section will describe the rationale for those differences.

The objectives of the flight tests were:

1) to gather data to support the analytical model

2) to extend the data base to include side-looking radar data

3) to use the data to determine the detection probability of targets of interest in various environments

and 4) to use the data to obtain a statistical model of clutter for each of the various environments.

The collected data is also used to evaluate the operation and effectiveness of the developmental processor.

The radar and instrumentation system used to collect the data is described in Section 4.1 of this report.

5.1.1 Corner Reflector Tests

One of the objectives of the flight tests was to obtain data from which the effective cross section of both distributed clutter and point targets could be determined. To meet this objective a corner reflector with a known theoretical cross section was constructed for use as a standard target. The use of this target allowed data collection and processing techniques to be evaluated against a known reference point. The standard target plus the use of the beacon transponder provided an increased confidence factor in the data.

The cross section of the square corner reflector was determined analytically to be 1849 ft^2.

The experimental radar cross section of standard corner reflector (7 ft) was determined by supporting the corner reflector on a hillside 700 feet from the radar. The returned video was monitored by oscilloscope while the corner reflector was positioned for maximum video. This was done for both positive and negative video to assure a true peak-to-peak measurement. The time and value of the video was then recorded.

To determine the level of energy necessary to produce this video, the antenna was disconnected and the antenna end of the coaxial cable was reconnected to a calibrated RF source. While observing the video, the generator was adjusted until the peak-to-peak level of the video was the same as the measured video due to the corner reflector. The RF generator output was recorded. This corresponds to the energy input at the antenna end of the coaxial cable due to the corner reflector.

Test data was substituted in the radar equations and the effective radar cross section of the target calculated.

$$P_R = \frac{P_T G^2 \lambda^2 A_t}{(4\pi)^3 R^4}$$

$$A_t = \frac{P_R (4\pi)^3 R^4}{P_T G^2 \lambda^2}$$

where

$P_R = 4.47 \times 10^{-5}$ milliwatts

$P_T = 15 \times 10^{3}$ milliwatts

$R = 1400$ nanoseconds * c = 700 feet

$\lambda^2 = 49$ feet^2

$G^2 = 16$

$(4\pi)^3 = 1981$

$$A_t = \frac{4.47 \times 10^{-5} \times 1981 \times 24 \times 10^{10}}{15 \times 10^{3} \times 16 \times 49}$$

$$A_t = \frac{212,521.68 \times 10^2}{11760} = 18.071 \times 10^2 \text{ feet}^2$$

$A_t = 1807.1$ square feet radar detected target cross section

The radar cross section of the square corner reflector was found to be 180 square feet. The theoretical area of the corner reflector is 1849 square feet.

5.1.2 Tests of Aircraft Mounted Antenna*

5.1.2.1 Ground Tests

A series of tests were conducted to provide information on the changes in radiation patterns of the log periodic array when it was mounted on the aircraft (wing tip mount). (See Figure 5.1)

Testing was conducted at the airport facilities. An RF source was connected to a transmitting antenna about 8 ft above the ground and 1000 feet from the mounted LPA. The aircraft was then taxied in a circle (approximately 100 feet in diameter).

5.1.2.2 In-Flight Tests

Changes in radiation patterns while in flight are obviously of interest; therefore, a series of tests were conducted to gather this information.

The RF source and transmitting antenna were mounted at the SURC antenna test range. The aircraft was flown to an altitude of 2500 feet and a position of about 10 miles from the RF source. Test runs were conducted by flying the aircraft past the transmitter in a standard rate turn with a diameter of about two miles.

5.1.3 Airborne Data Collection

5.1.3.1 Skaneateles Lake Tests

The site of the lake tests was changed to Skaneateles Lake due to its proximity to SURC and the availability of boat launching and docking facilities. Figure 5.2 is a map of this test site.

The tests were divided into three separate subsets. Data collection was accomplished with the aircraft heading north at various altitudes, velocities and radar ranges. These parameters are listed in Table 5.1.

The first subset was composed of clutter tests made from the middle of the lake at three different depression angles.

The second subset duplicated the first but utilized the floating standard target as a radar target.

The third subset consisted of single sideband calibration tests in which signals of various known levels are injected into the system and data recorded. Calibration data was recorded for each of the first two subsets.

*Details of the tests are given in Section 4.1.1.2.

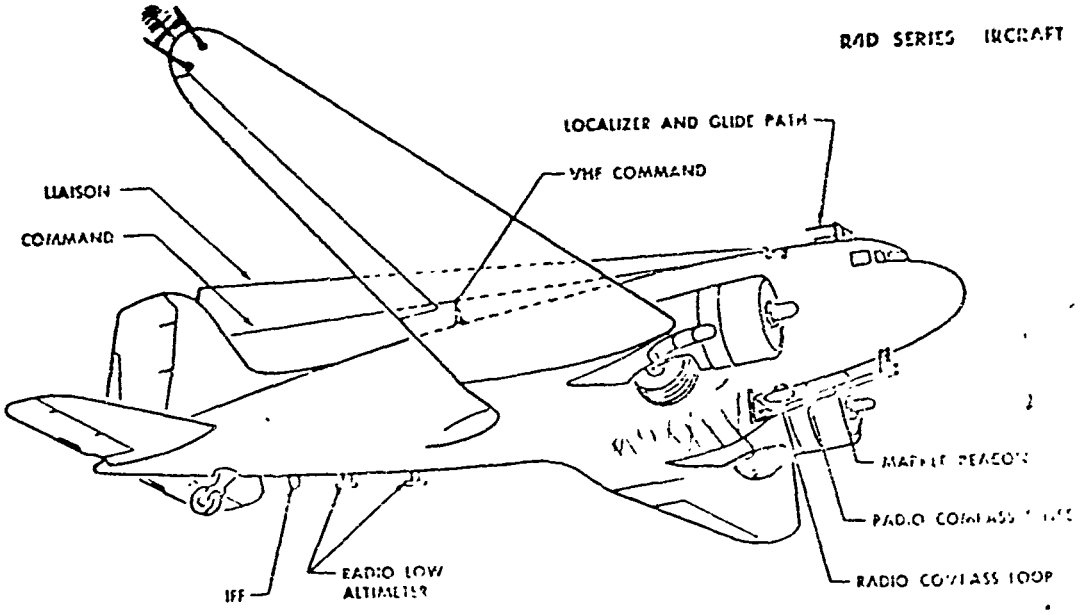

A. Antenna mounted on the wing tip.

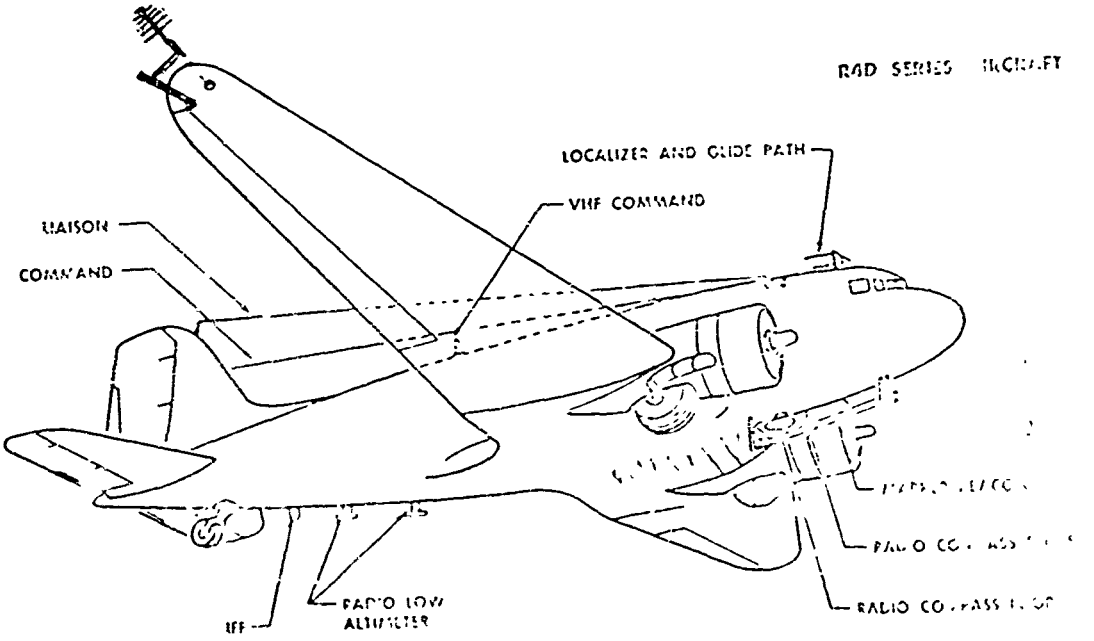

B. Antenna mounted on the supporting structure.

Figure 5.1. Alternate Methods of Mounting LPA

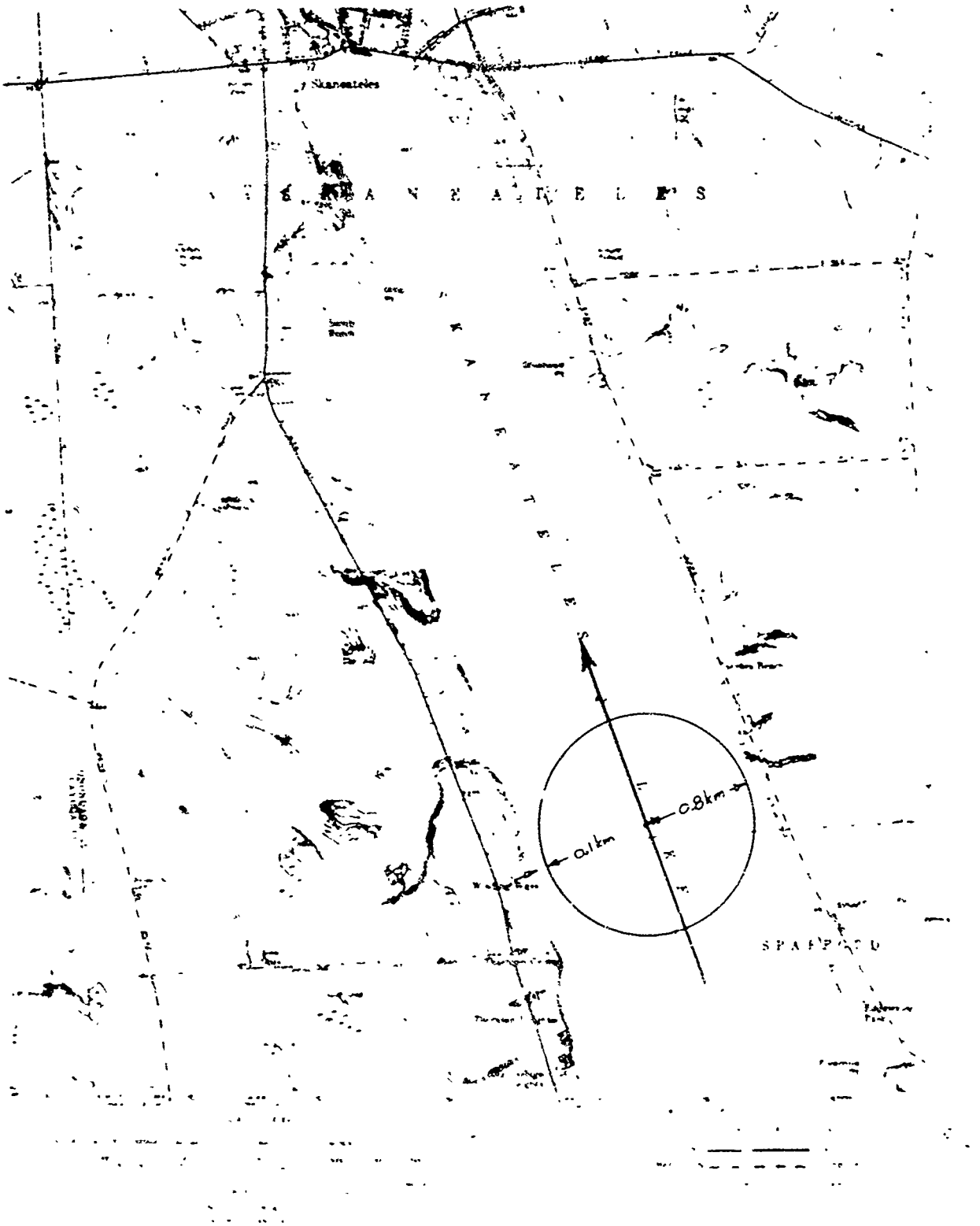

Figure 5.2. Lake Test Site

Table 5.1. Lake Test Parameters

Slant Range in meters	Ground Range in feet	Altitude in feet	Depression Angle in Degrees	Corner Reflector Tilt in feet
500	1565	500	17.6	4.6 back up
500	1159	1159	45	flat
500	1000	1300	52.5	1.2 front up
1000	3130	1000	17.6	4.6 back up
1000	2318	2318	45	flat
1000	2000	2600	52.5	1.2 front up

The standard target was floated on a raft-like platform. The mounting bracket allowed adjustment of the reflector to three different positions. For these tests the platform and reflector were towed into position by an outboard motor boat and during the tests the standard target was a minimum of 100 meters from the shore.

5.1.3.2 Farm Lands

The area chosen for these tests is approximately 20 miles southeast of SURC, near Fabius, New York. It may be characterized as flat with few trees and no power or telephone wires. Our designation for this test is the Vincent Corners Site. Figure 5.3 is a map of this area.

The standard target was utilized as a radar target in ground clutter for these tests. The single sideband calibration data was taken for each set of tests.

The aircraft was flown parallel to New York State Route 80 with test parameters listed in Table 5.2 to provide data for a variety of depression angles.

TABLE 5.2

TEST PARAMETERS

Exp #	Dep Angle	Altitude	Slant Range
686	12	700	2954
688	13	700	2954
685	12	700	2954

5.1.3.3 Coniferous Forest

The area selected for this test is called Highland Forest and is located two miles east of Fabius, New York on New York Route 80.

The test area is a reforestation area where trees are about one foot in diameter, approximately 35 feet tall and planted in a definite grid pattern.

Data was collected from the airborne radar using the standard target in a large ground clutter as the radar target. The standard target was first located in a small open area surrounded by evergreens; data was taken and the standard target was then moved into the evergreens for further data gathering. Although the areas in which the standard target was placed were relatively flat areas immediately adjacent had very steep slopes.

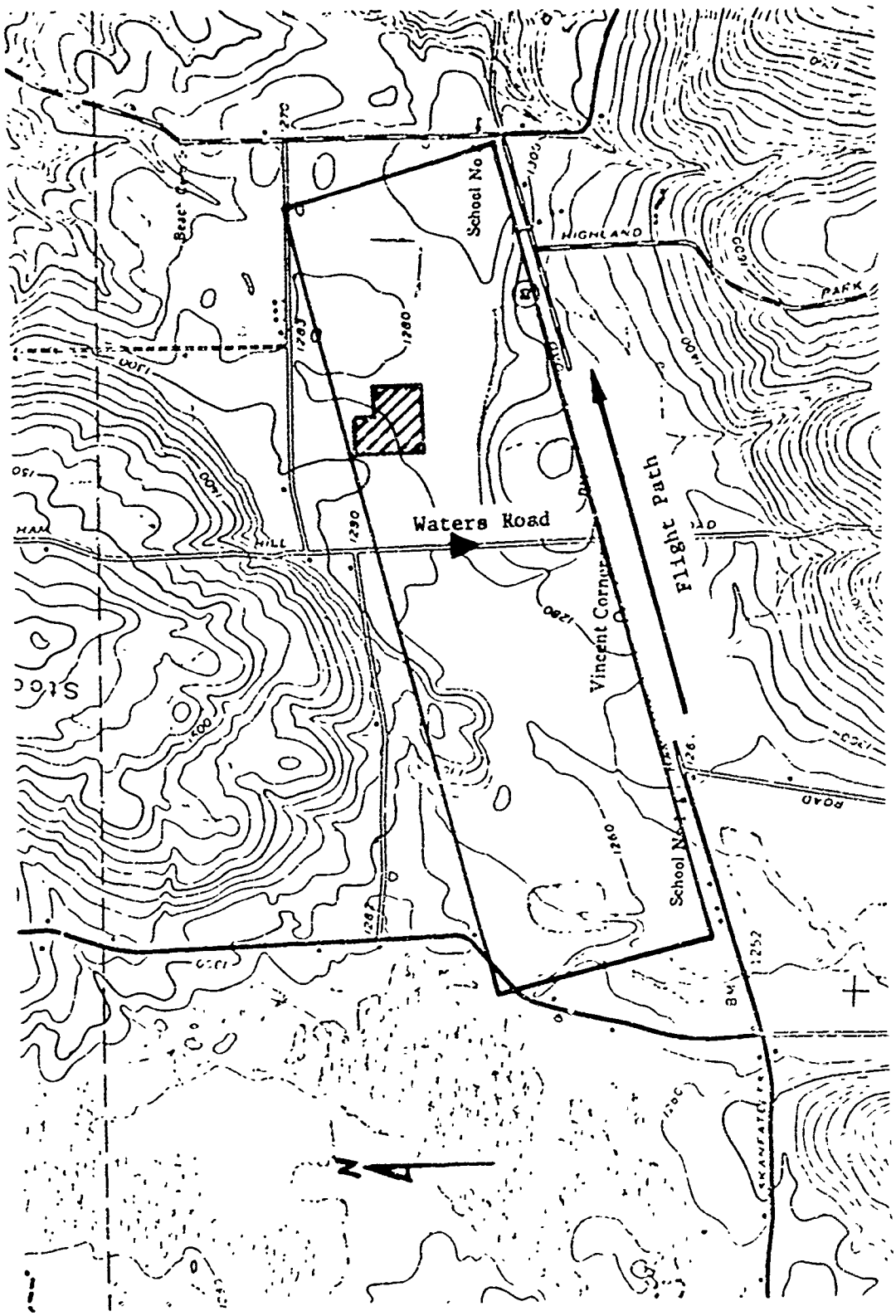

Figure 5.3. Vincent Corners Test Area

Difficulty was encountered in maintaining constant flight paths due to the paucity of landmarks.

As in previous tests the single sideband calibration data was taken after each set of data.

Figure 5.4 is a map of the area and Table 5.3 lists the pertinent test parameters.

TABLE 5.3

CONIFEROUS FOREST TEST PARAMETERS

Exp #	Dep Angle	Alt	Slant Range
792	21	950	2661
793	21	950	2661
795	21	950	2661
798	22	1000	3108

5.1.3.4 Deciduous Forest

An area known as Happy Valley Game Management Area was selected for this test. It is located approximately 10 miles north of Oneida Lake, New York and 6 miles east of Route 81 (Figure 5.5).

This site was selected for its level surface covered with young first growth deciduous trees about 4 to 6 inches in diameter and approximately 30 feet high. There is heavy underbrush in the area.

Flight tests were made over part of this area located one mile east of Howardville, New York on Route 126. Two flight paths were used, one with the aircraft following a northwest course approximately parallel to Churchill Road and Barber Road. The second path required the aircraft to fly approximately east northeast nearly bisecting the first flight path.

The radar target for these tests was a jeep and the standard target.

Table 5.4 outlines the test parameters for the Deciduous Forest Tests.

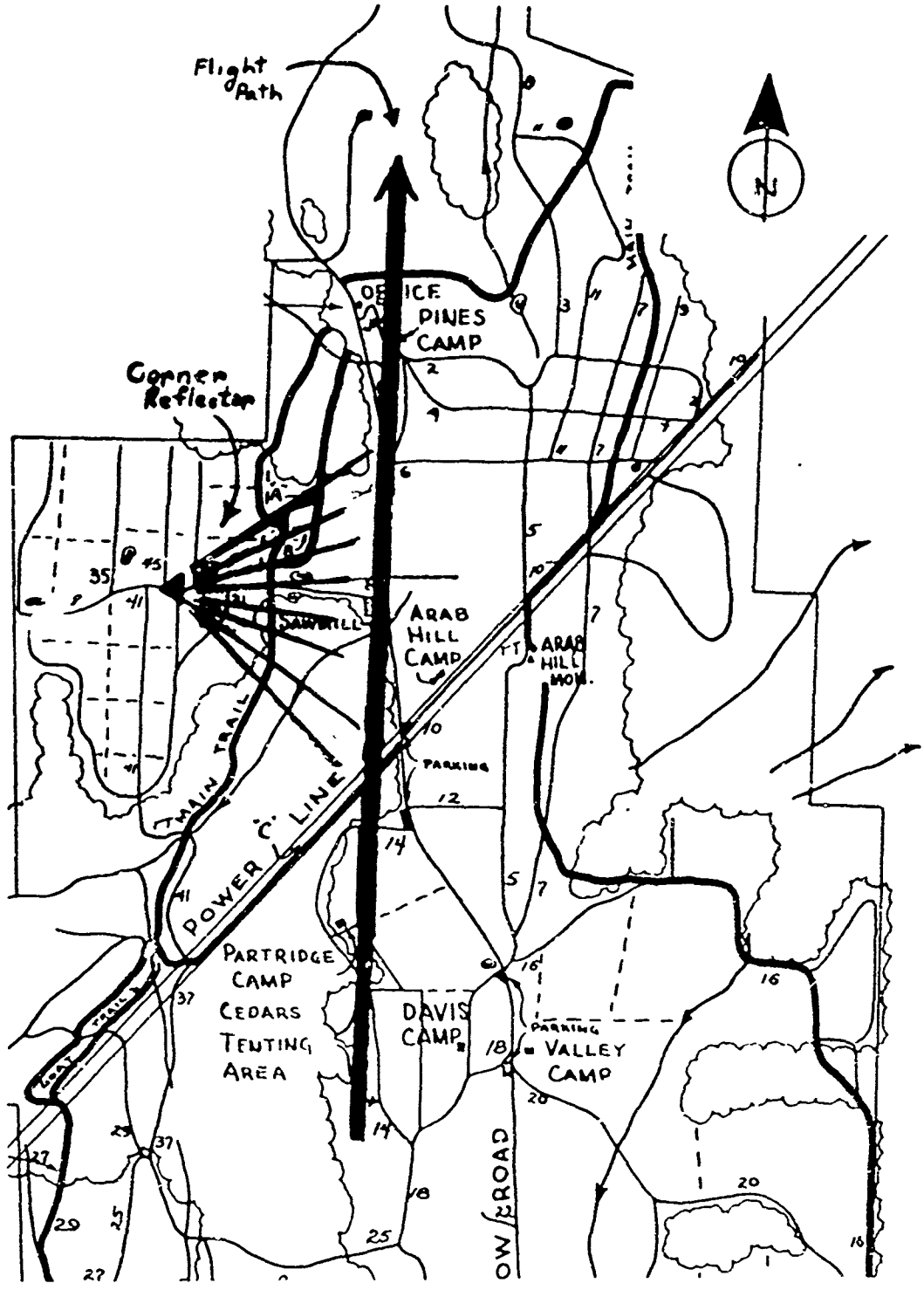

Figure 5.4. Highland Park Test Site

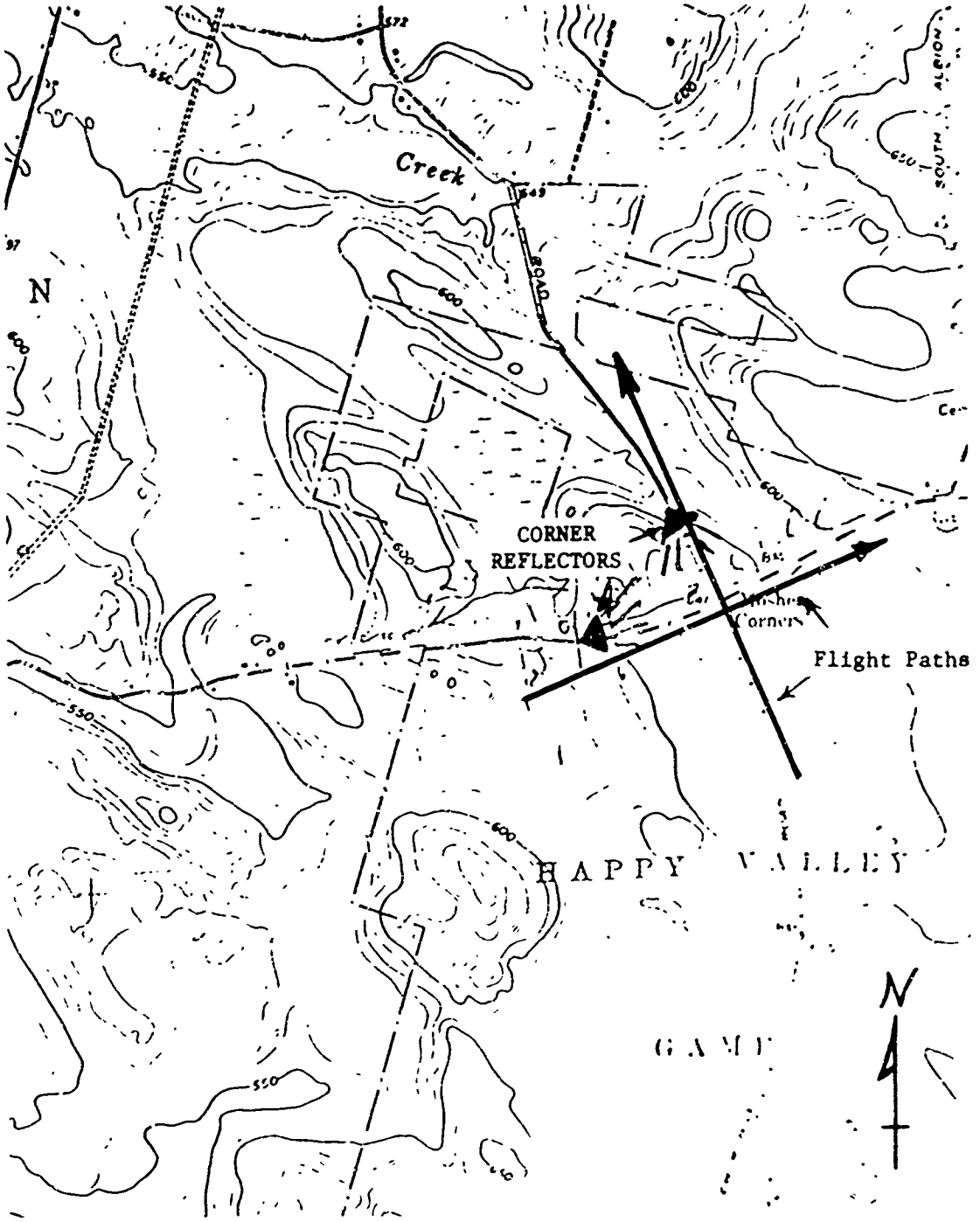

Figure 5.5. Happy Valley Test Area

TABLE 5.4

DECIDUOUS FOREST TEST PARAMETERS

Exp #	Dep Angle	Alt	Slant Range
880	15	500	1960
881	20	700	2040
882	25	900	2100
883	30	1100	2200
884	34	1300	2300
885	38	1500	2420
886	42	1700	2540

5.1.3.5 Aberdeen Proving Ground

Airborne radar tests were conducted at Aberdeen Proving Ground, Maryland to determine the effective radar cross section of selected targets.

As in previous tests the target area was verified by using the ground beacon. For each of two targets, placed in an open area at the end of the runway shown in Figure 5.6, data was collected for 3 depression angles while flying the aircraft in an approximate southerly direction. Data collection, in this case, occurred when the targets were approximately perpendicular to the port side of the fuselage.

Clutter data was collected of the runway 22 area and the forested area between range 9 and the dynamometer course on the tank access road. The first of the clutter data collection tests of the forested area was made with an extended range gate while subsequent data collection was accomplished at normal ranges and altitudes.

Data was collected using a UHID helicopter, setting on the ground, as the radar target. The turning rate of the rotors and altitude of the radar platform were used as changing parameters for the tests. Data was collected at 1500, 1000 and 700 feet, The tail rotor was turning at a rate of approximately nine times that of the main rotor. The main rotor was turning at one of two fixed speeds (275 or 325 rpm). The UHID helicopter was positioned on a pad near the south end of runway 22. During the first data run an Aero Commander (N 2268B) was on a pad just south of the target helicopter.

As in all previous tests data from the calibrated single sideband source was recorded.

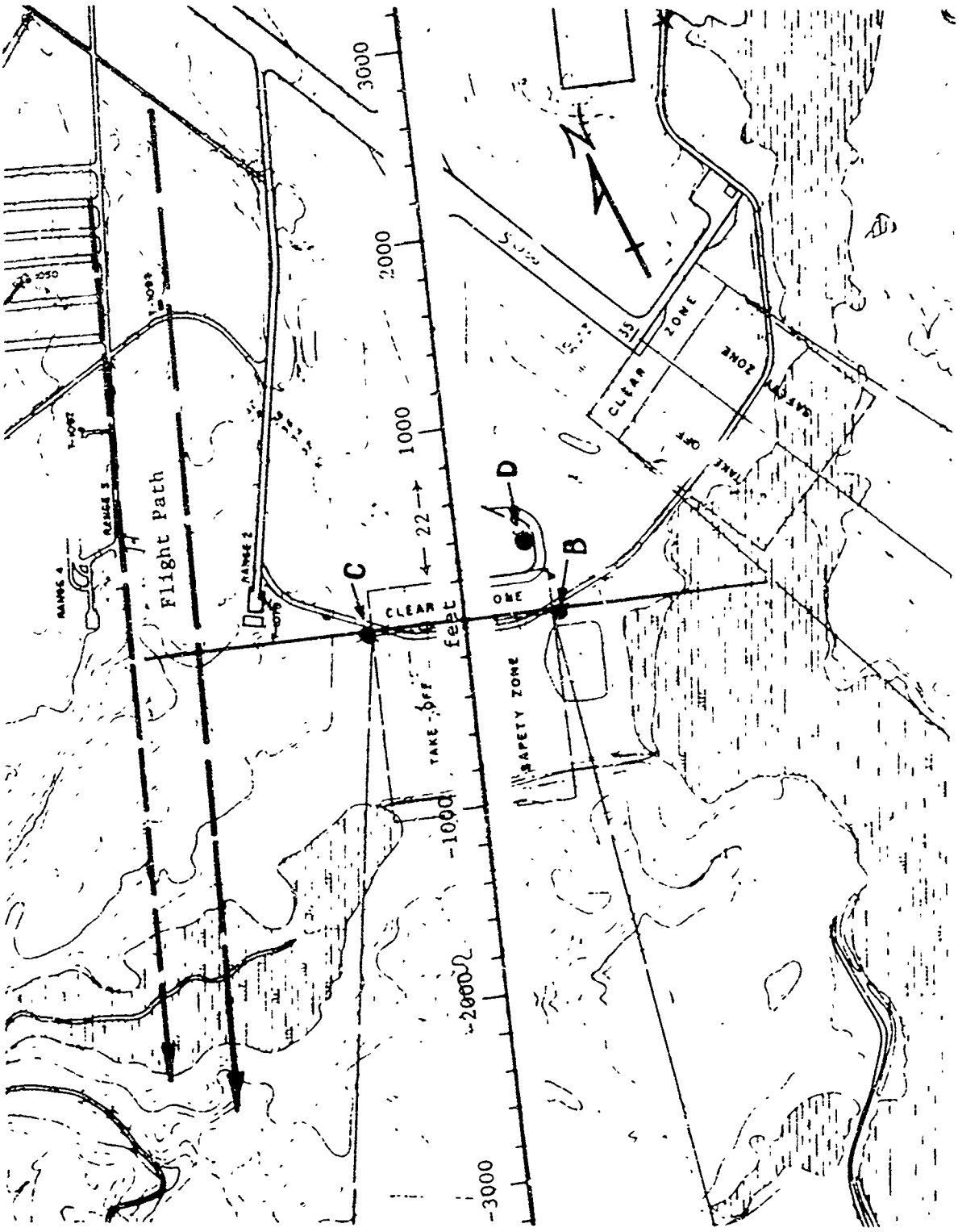

Figure 5.6. Aberdeen Test Area

Table 5.5 is a list of the Aberdeen Proving Ground Test Parameters:

TABLE 5.5

ABERDEEN PROVING GROUND TEST PARAMETERS

Exp #	Dep Angle	Alt	Slant Range
835	16	700	2970
836	16	700	2970
845	17	700	2760
815	27	700	2220
820	53	1000	1813

5.2 Data Collection at 50 MHz

Late in the program a carrier frequency change allowed airborne data collection to be accomplished at 50 MHz over the tests areas designated as the Vincent Corners area and the Swamp Road area. The Vincent Corners area is described in Section 5.1.3.2.

The Swamp Road area is a heavily wooded, swampy area with a well defined clearing (a small grass airfield) as shown in Figure 1.6. A dipole was positioned in this clearing for use as a standard target.

The objective of the test was to compare the cross section from these areas with the cross section as derived from the tests conducted at 140 MHz.

The following tables outline valid flight tests parameters made at 50 Mhz. Table 5.6 encompasses the Swamp Road Tests and Table 5.7 the Vincent corners data.

TABLE 5.6

SWAMP ROAD AREA TEST PARAMETERS

Experiment No.	2047	2048	2049	2050	2051	2052	2053
Velocity A/C	187	187	187	187	187	187	187
Altitude	690	760	820	820	820	860	1000
Slant Range	2115	2327	2542	2343	2159	2650	3063
Ground Range	2000	2200	2400	2200	2000	2500	2900
Depression Angle	19°	19°	19°	20°	22°	19°	19°
Flight Path*	A	A	A	A	A	B	B

*Two flight paths were used; flight path, A, was along Swamp Road; flight path B was offset 500 feet and parallel to Swamp Road.

TABLE 5.7

VINCENT CORNERS AREA TEST PATAMETERS

Experiment No.	2054	2055	2056
Velocity	187	187	187
Altitude	995	920	860
Slant Range	3064	2850	2650
Ground Range	2900	2700	2500
Depression Angle	19°	19°	19°

6.0 AIRBORNE DATA COLLECTION

The objectives of the flight test portion of the study were to gather data to support the analytical model, to expand the data base, to determine the detection probability of targets of interest in various environments and to establish a statistical model of clutter for each of the various environments. The radar used for the data collection should be an integral part of the fieldable prototype system.

6.1 Cross Section Measurements

Although it is common to speak of "the" radar cross section of an object, it is well known that radar cross section depends upon the target shape and material, the angle at which the target is viewed, the frequency of the radar and the polarization of the radar system antennas. In making cross section measurements on this program a concerted effort has been made to keep these parameters fixed, however, it is acknowledged that flight paths and depression angles may vary between successive experimental runs. These variations may markedly change the clutter echoes and the glint reflections which causes apparent erratic results. The change of radar frequencies was proposed as an aid in resolving the target to clutter resolution problem.

6.1.1 Cross Section of the Standard Target

The reliable measurement of a standard (point) target in a cluttered background (distributed target) is of particular interest to this program. Utilizing the results of the Skaneateles Lake and Vincent Corners tests it is obvious that the standard target radar reflections can be discussed and are separable from the different background clutter echoes. As described in section 5, the backgrounds are (1) a lake surface, and (2) open fields with hedge rows, fence lines, roads and small forested areas. (See Table 6.1 for comparative test results.)

6.1.2 Lake Tests

The processed lake data exhibited horn-like peaks at high doppler frequencies. The peaks were attributed to wave crests which are perpendicular to the direction of the radar transmission and occur for those signals transmitted directly to the front and to the rear of the aircrafts flight path. This wave motion on the lake can produce higher frequency doppler returns which approximate the expected doppler from the standard target. A method of averaging successive spectra was devised to eliminate the horn-like peaks from the processed data.

6.1.2.1 Elimination of Horn-Like Peaks in Processed Lake Data

The following series of spectra show the peak due to the corner reflector on the lake sliding from positive to negative frequencies. The spectra were computed such as to minimize the horn-like peaks at large ($\pm$50 Hz) doppler frequencies. These horn-like peaks were experimentally shown to be due to

TABLE 6.1

MEASURED CROSS SECTION OF THE STANDARD TARGET

Exp #	Dep Angle	Alt	Slant Range	Cross Section Theo. ft^2	Cross Section Meas. ft^2
619[1]	19	1000	1150	600	3276
622	31	1150	700		840
632	40	2000	800	200	181
685[2]	12	700	900	300	1532
686[2]	12	700	900	300	1547
688[2]	13	700	900	300	1286

[1]Glint cross section is computed as 2799 ft^2 which may account for the large measured value.

[2]Glint reflections or the addition of the cross section of the truck on which the standard target is resting accounts for the large measurement.

wave crests which are perpendicular to the direction of the radar transmission and occur for those signals transmitted directly to the front and to the rear of the aircraft's flight path.

A method used to eliminate the distracting horns is described below. Compute the average of K successive spectra (K = 16 was used), where successive spectra may use partly redundant time data -- 7/8ths redundant in the case being considered. Then compute the average of the next L successive spectra (L = 16), and subtract the two averages. This procedure is repeated for the second subtracted spectrum by taking the starting point for the first subtracted spectrum and moving forward I data records before starting on the second, for the spectra shown in Figures 6.1, 6.2, and 6.3 for I = 4.

Averaging 16 spectra yields a wide peak as shown in Sequence 85*. The second subtracted spectrum, Sequence 88, has the peak due to the corner reflector slightly closer to the origin. Sequences 91, 94, 97, 100, 103 and 106 show the peak moved to the left. Sequence 106 shows a reduction in subtracted clutter signal from the previous spectrum, indicating that the target is starting to slip out of the range bin. Sequence 109 shows an even greater decrease in the peak due to the corner reflector; in addition, a peak at positive frequencies corresponding to a direction slightly ahead of the port wing of the aircraft is beginning to build up. This may be due to the edge of the lake beginning to get into the range bin toward the end of the run. Sequence 112 shows little residue from the target; no edge of lake peak is apparent. The rest of the spectra have no significant peaks.

6.1.2.2 An Examination of the Variation of Lake Clutter

The following series of clutter spectra show the effect of using nearly the same data for adjacent spectrum estimates. These spectra are from Experiment 622 (lake data) prior to the time at which the corner reflector appears. Seven eights of the time data used for one spectrum is also used for the next.

Figure 6.4 shows the average of all 89 spectra. The peaks on either side are due to the strong return from wave crests which are perpendicular to the radar. The center peak is primarily due to the presence of the target in the latter spectra.

Figure 6.5 is the first of 89 spectra obtained from Experiment 622, and Figure 6.6 is the second. Seven-eights of the time data used to form the spectrum of Figure 6.5 is also used to form the spectrum of Figure 6.6, and these two curves are overlayed in Figure 6.7. Note that the difference in power at various frequencies averages to about 2 or 3 dB, but varies by as much as 30 dB at some frequencies. Now compare Figure 6.5 with Figure 6.8. These two spectra are obtained from blocks of time data which are adjacent. A comparison of these two spectra reveals an average difference in power of 3 or 4 dBm, as shown in Figure 6.9. This is comparable to the difference in the spectra obtained with data which was seven eights redundant. The reason for only a

*Sequence (SEQ NR) regers to the group number located in the upper right hand corner of all spectral plots.

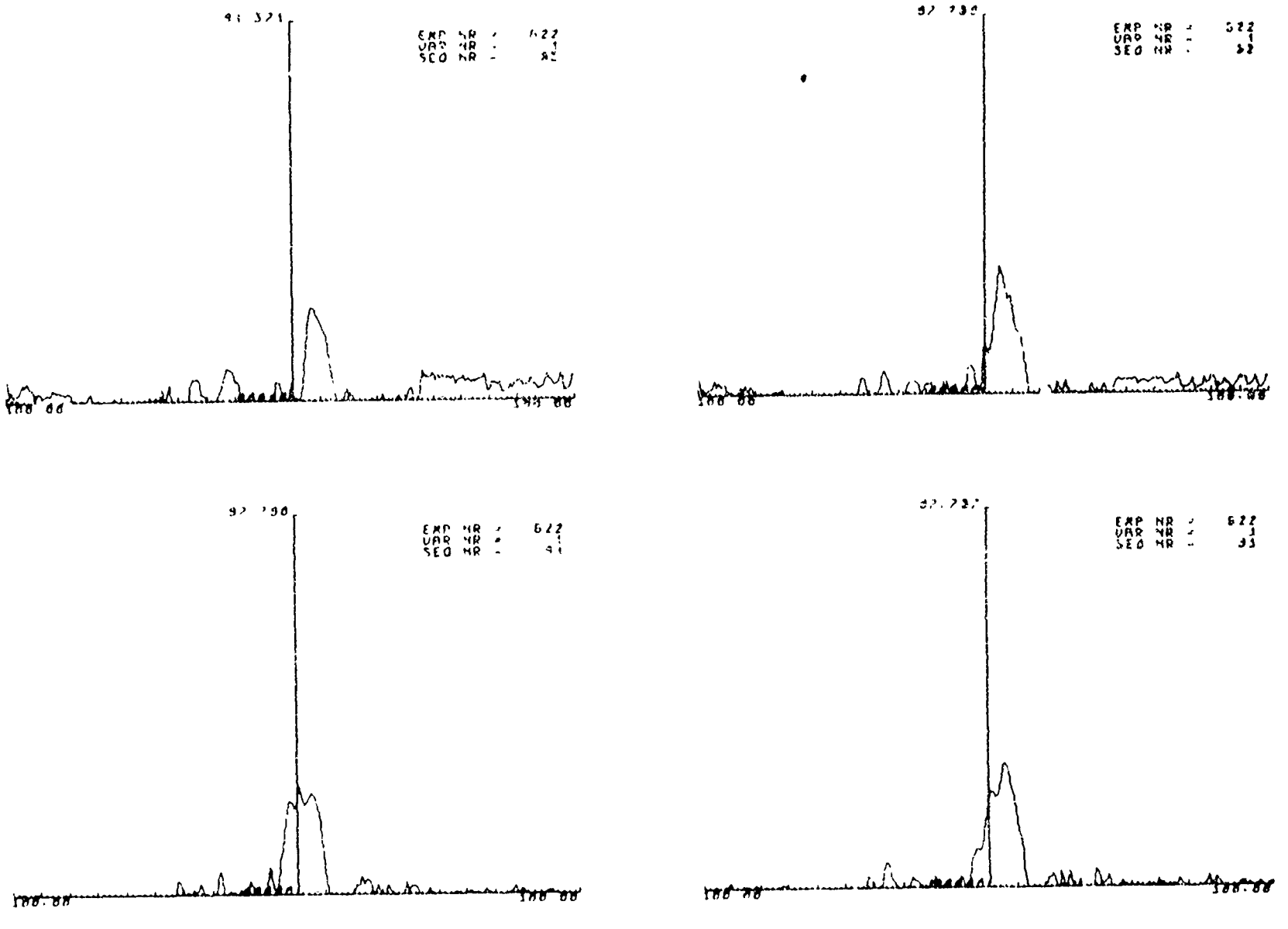

Figure 6.1 Clutter Spectra using Adjacent Estimates

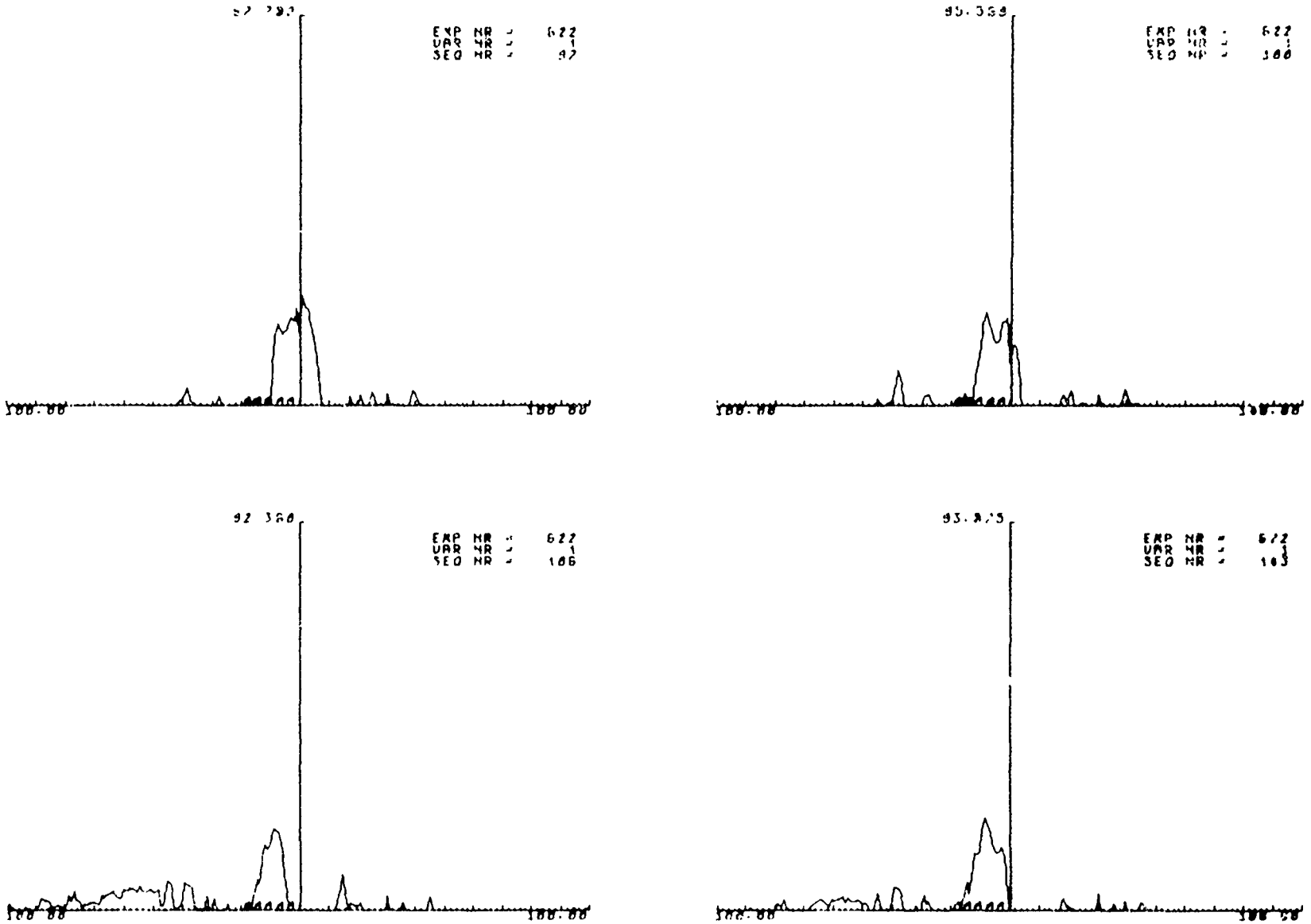

Figure 6.2 Clutter Spectra using Adjacent Estimates

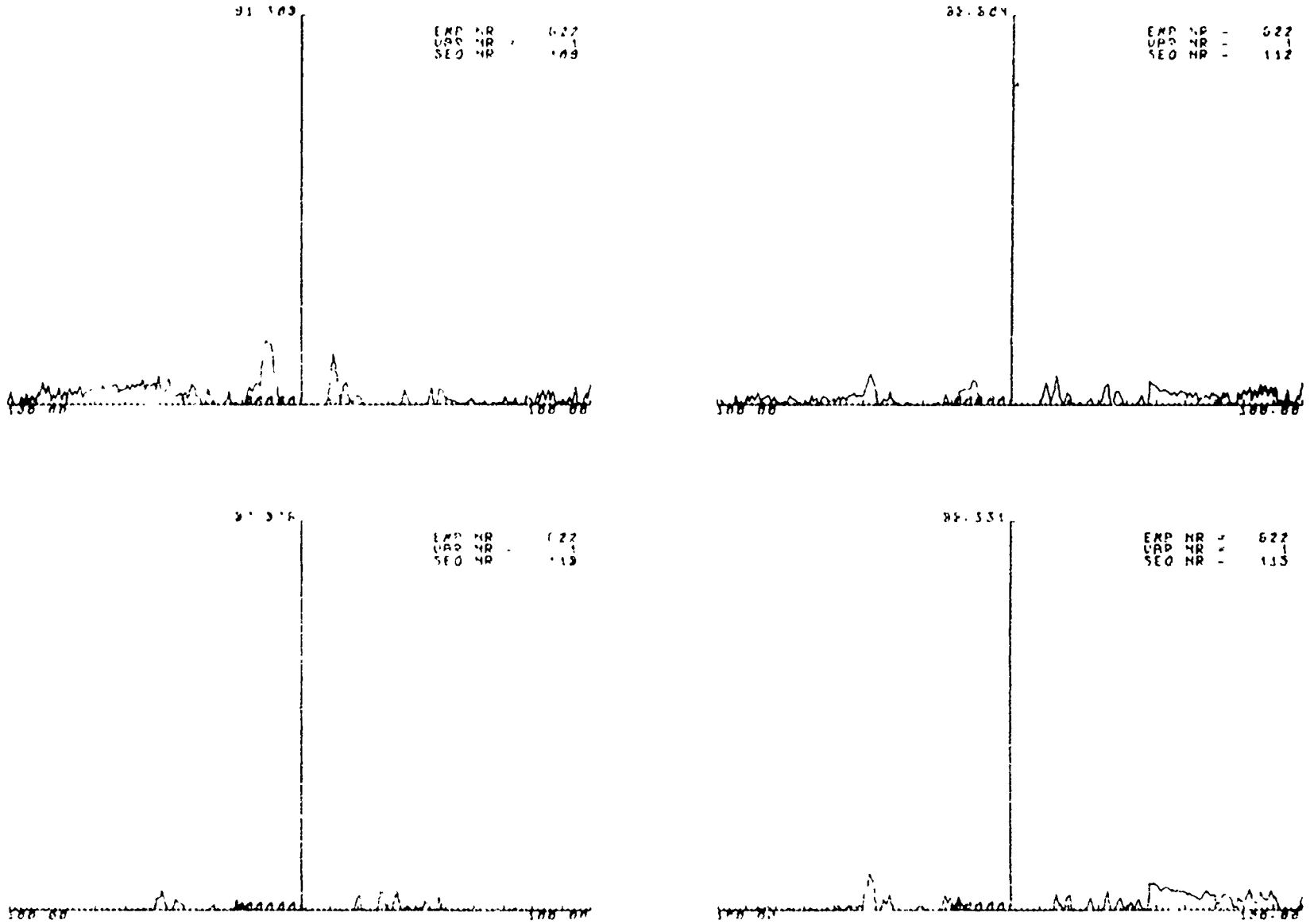

Figure 6.3 Clutter Spectra using Adjacent Estimates

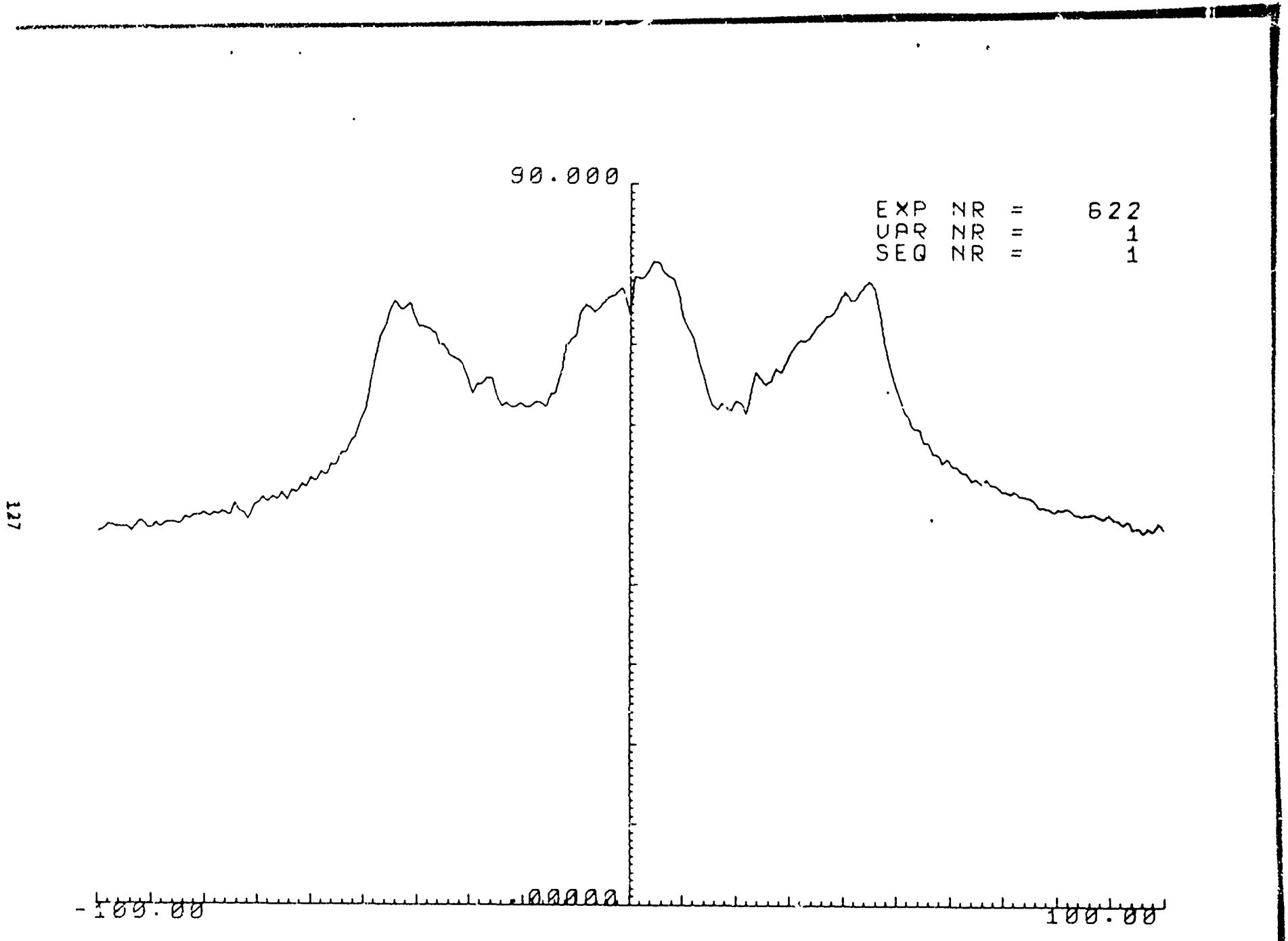

Figure 6.4 Average Spectra Estimates for Experiment 622

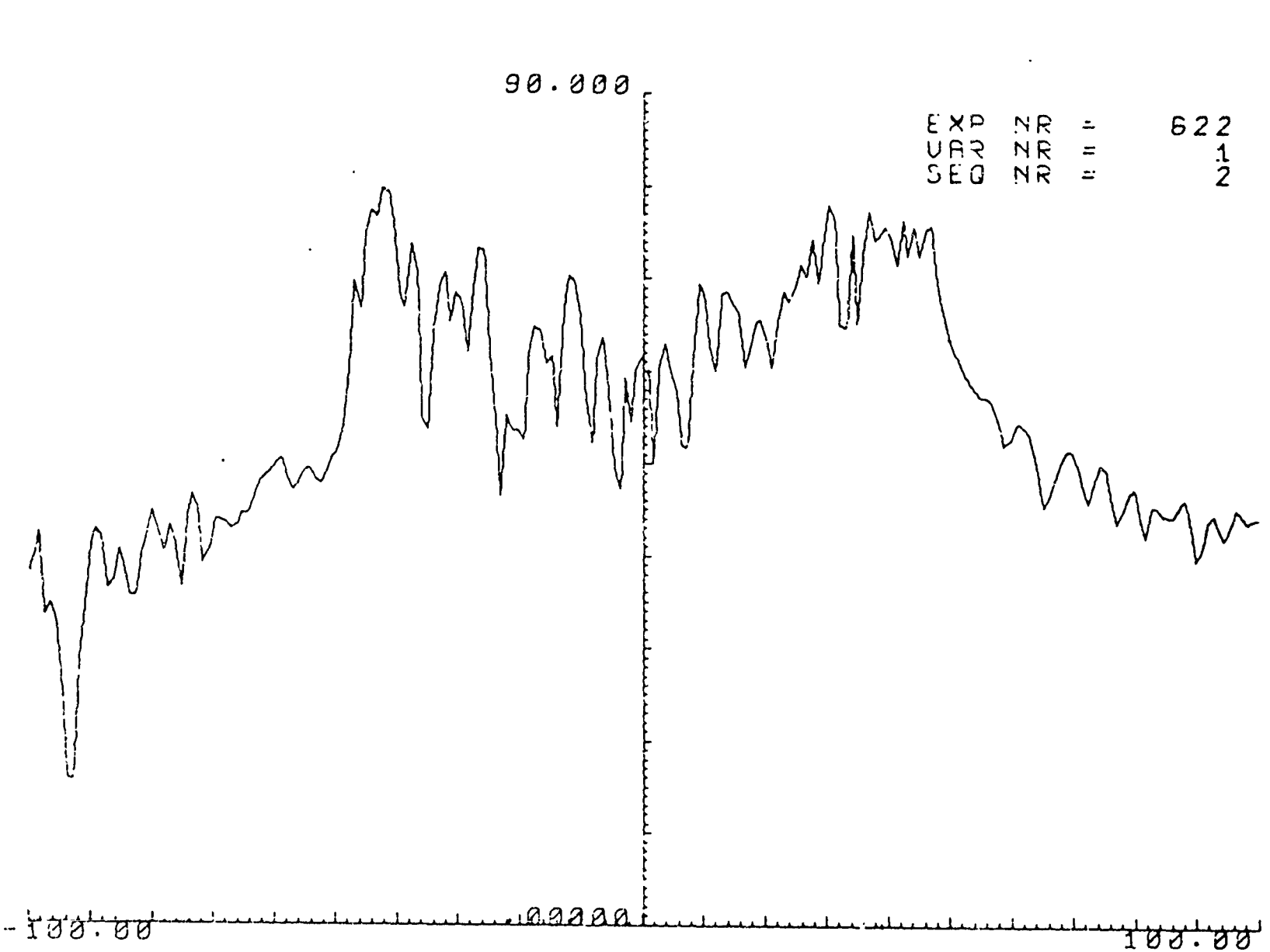

Figure 6.5 Average Spectra Estimates for Experiment 622

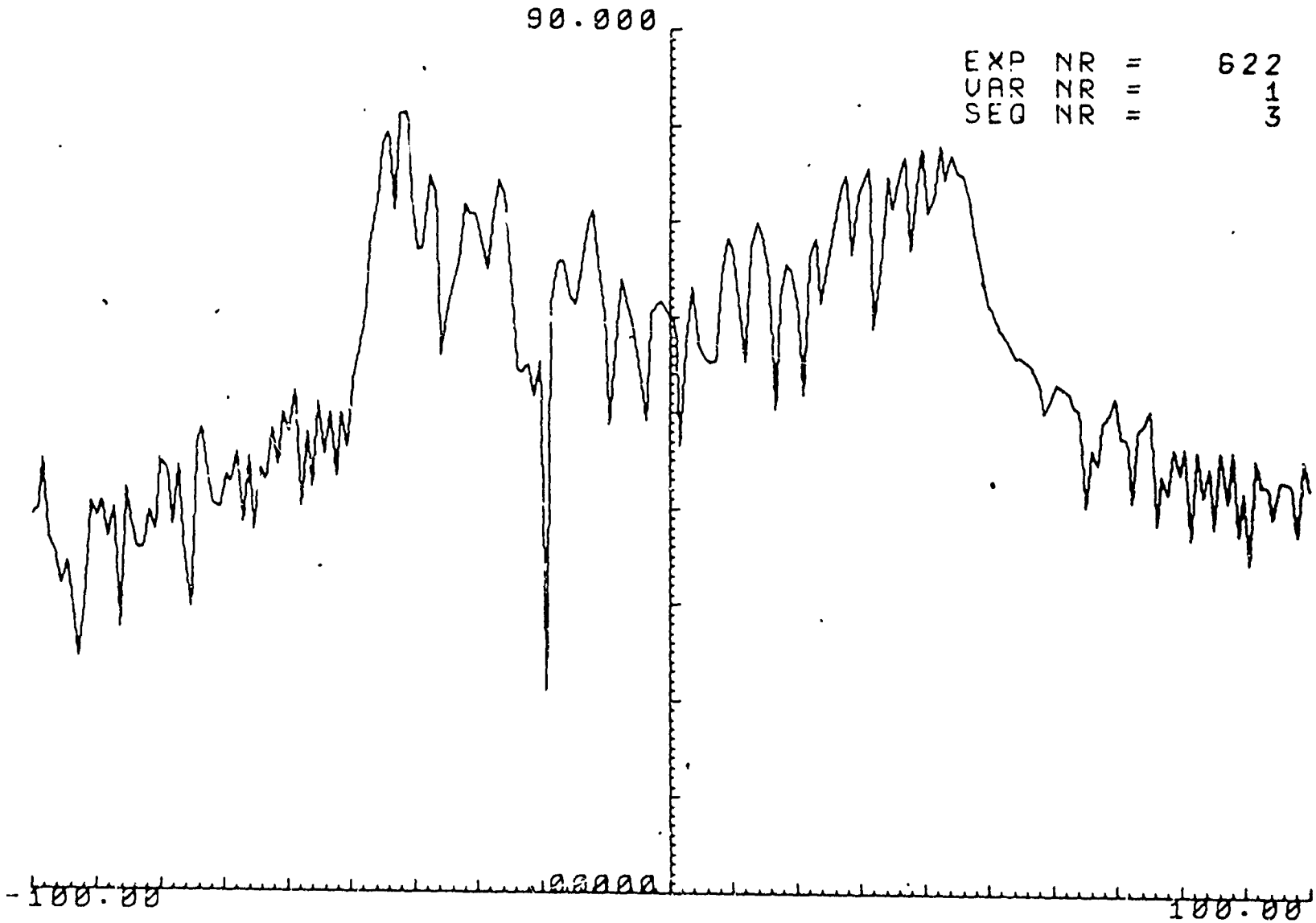

Figure 6.6 Average Spectra Estimates for Experiment 622

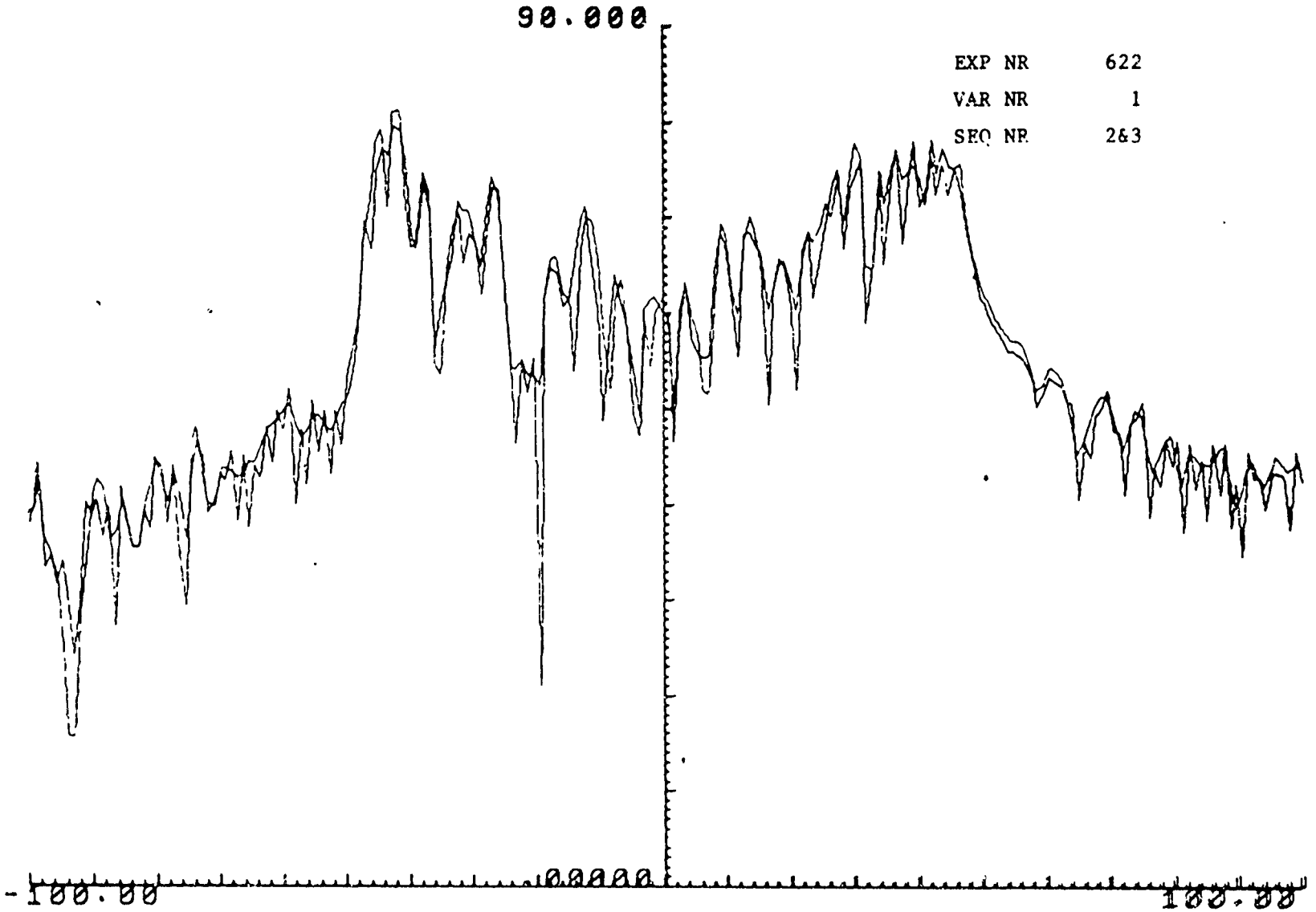

Figure 6.7 Average Spectra Estimates for Experiment 622

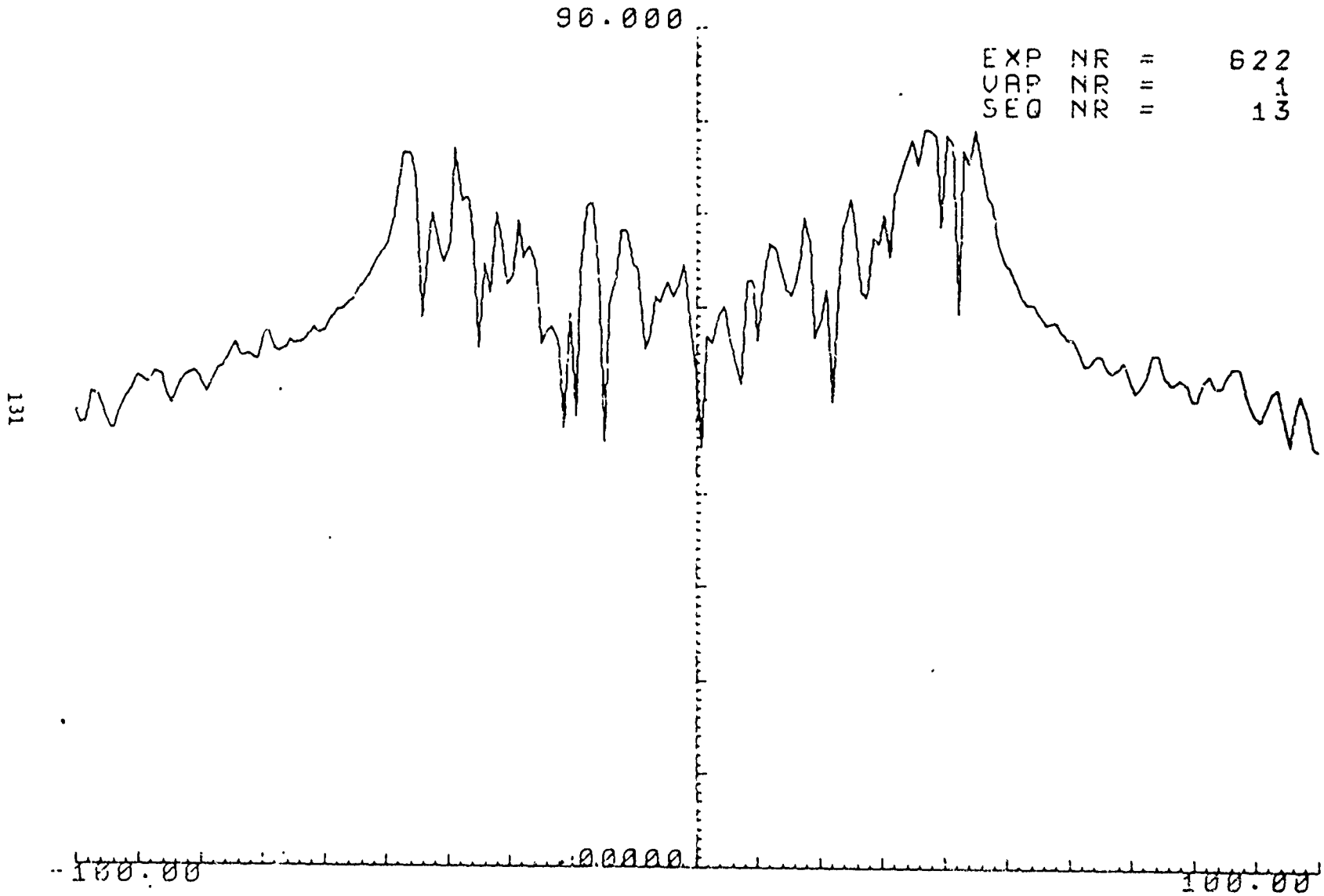

Figure 6.8 Average Spectra Estimates for Experiment 622

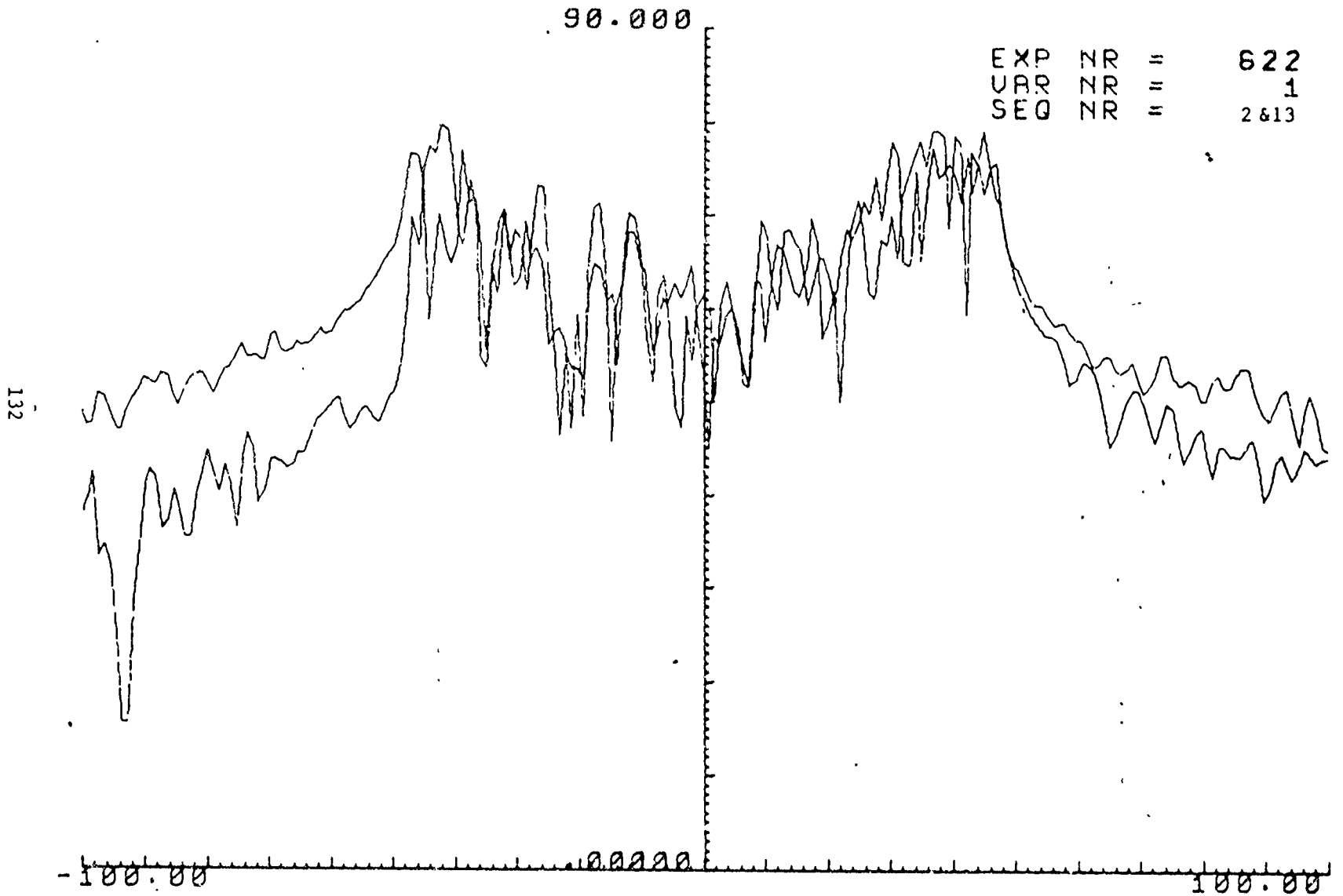

Figure 6.9 Average Spectra Estimates for Expe iment 622

slight increase in the difference in the power spectra is that this particular clutter has a degree of short-term stationarity. The clutter in this case is due to lake return.

6.1.3 Vincent Corners Tests

Data is included in section 6.3.

6.1.4 Highland Forest Tests

A set of four tests were performed at the same depression angle over the same area (approximate) in an effort to obtain repeatable clutter cross sections. The results of these tests are:

Table 6.2 Highland Forest Data

Exp #	Dep Angle	Mean (ft^2)	σ_o	Var (ft^2)	Exp Dev
792	21	24711	.461	16377	$\pm$.058
793	21	30204	.564	16118	$\pm$.057
795	21	32874	.613	21368	$\pm$.075
798	22	38650	.613	24246	$\pm$.073

The repeatable measurement of σ_o was not attained which may be attributed to (1) difficulties in flying exact paths, (2) the effect of wind on the trees and backscattered energy, (3) differing reflections from steep slopes and (4) perhaps an RFI condition.

In this case the collected data did not correlate with the statistical model while similar measurements of coniferous trees in the Vincent Corners area did fit the model. Therefore, either the resulting data from these experiments or the model for this environment are suspect.

6.1.5 Happy Valley Tests

These tests were conducted to determine the effect of depression angle (therefore aspect angle) on the clutter cross section of a deciduous forest. The results are:

Table 6.3 Happy Valley Data

Exp #	Dep Angle	Mean (ft^2)	σ_o	Var	Exp Dev.
880	15	5141	.134	3313	$\pm$.0163
881	20	1411	.036		
882	25	8677	.199	6153	$\pm$.027
883	30	5793	.121		
884	34	4635	.089	2459	$\pm$.009
885	38	1806	.031		
886	42	9363	.145	5685	$\pm$.017

As may be expected there appears to be no correlation between depression angle and cross section. The widely varying cross section is attributable to the inability to fly over the same path each time.

6.1.6 Aberdeen Proving Ground Tests

The tests performed at the Aberdeen Proving Ground (APG) were hampered by poor flying conditions, however, some interesting results are presented here.

6.1.6.1 Runway Clutter

Clutter cross section measurements were taken of a runway and the area immediately beyond. The aircraft was flown at 1000 feet at 127 miles per hour. The pertinent calculations revealed,

Table 6.4 Runway Data

Dep Angle	Mean (ft^2)	Var	Slant Range
53°	481	664	1813

6.1.5.2 Tank

The radar was utilized in this case to illuminate the tank and record the return signal. In this case no attempt has been made to define its cross section because (1) the dimensions of the tank are unknown, and (2) the many reflecting surfaces cause irregularities in the returns. Figure 6.10

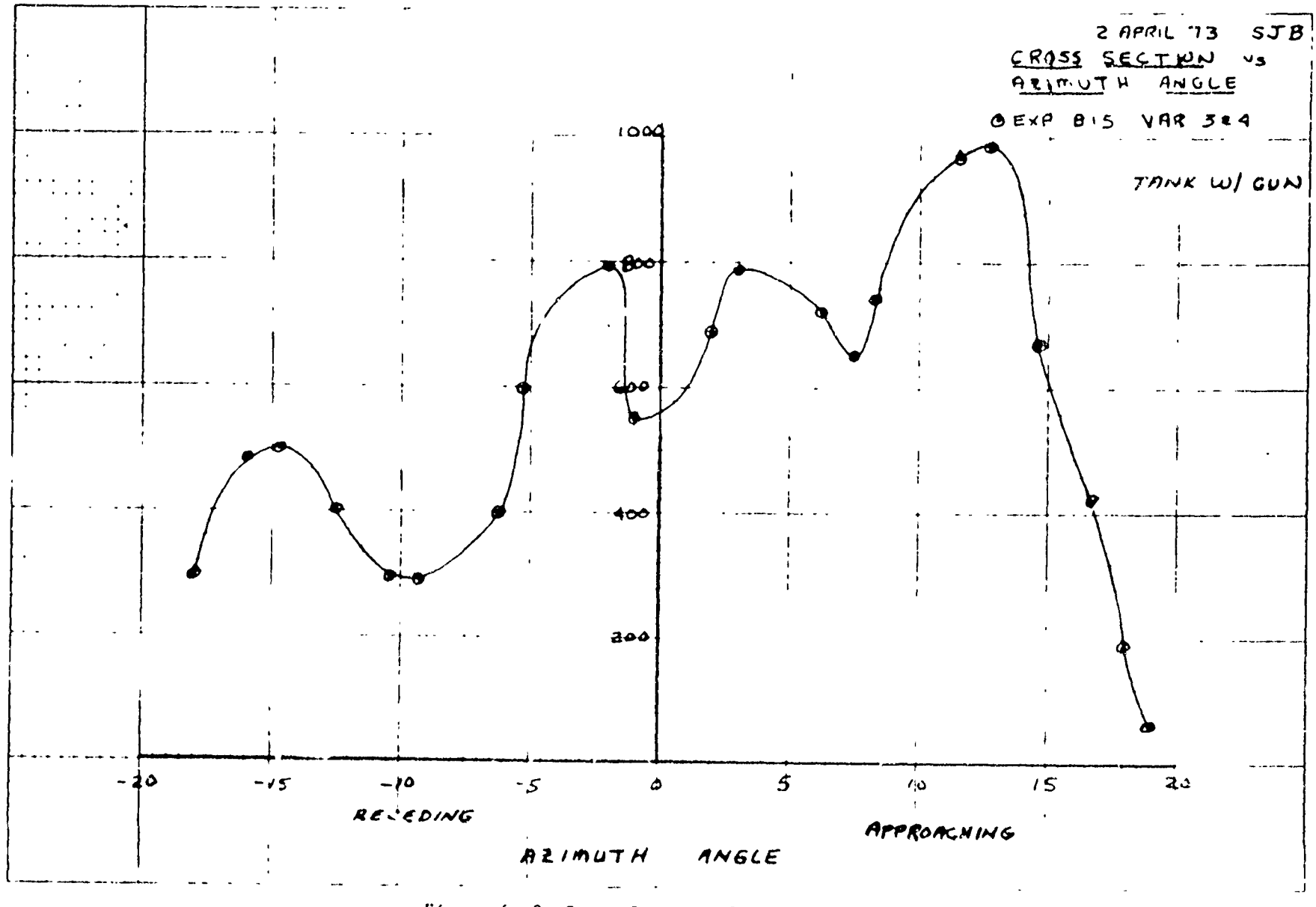

Figure 6.10 Cross Section of Tank with Gun

is a plot of cross section values versus azimuth angles.

6.1.6.3 Aircraft Tests

This series of experiments indicated that Glint Cross Section measurements are repeatable and large. Figure 6.11 indicates the results of the tests which had the following parameters,

Table 6.5 Aircraft Test Parameters

Exp #	Dep Angle	Alt	Slant Range
835	16	700	2970
836	16	700	2970
837	17	700	2760

The high value cross section measurement shown in Figure 6.11 agrees closely with the theory presented in Appendix A and therefore is attributed to Glint Cross Section.

6.2 Correlation of Targets

Experiments show a close correlation between the observed terrain and the processed data. The following figures are but one example. Figure 6.12 is a map of the Vincent Corners test area. Figure 6.13 is a photograph of the test area showing the range bin position just prior to reaching the target. Figure 6.14 is a photograph showing the range bin positioned directly on the corner reflector target. The two photographs show the flight path and position of the standard target. Figures 6.15a and b are corresponding spectra of the data taken at the time of the photo. The first spectra (Figure 6.15a) shows little radar return over pasture land and then a large point target when the standard target is in the range gate.

6.3 Data Reduction by Observed Terrain Type

To confirm the correlation between the observed terrain and the collected data, the Vincent Corners Experiment (685) data was further reduced and tabulated as follows in Table 6.6:

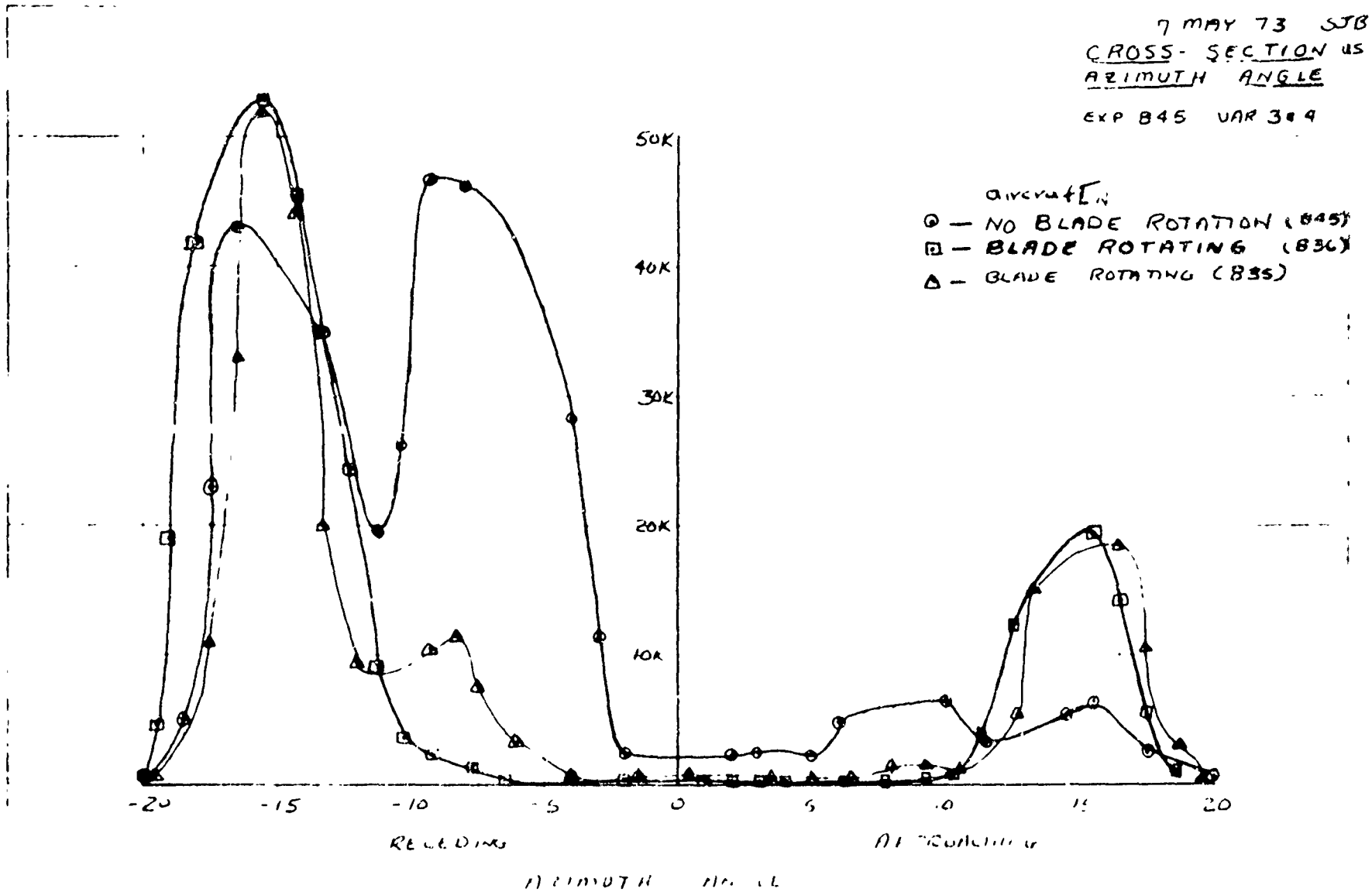

Figure 6.11 Cross Section of Helicopter

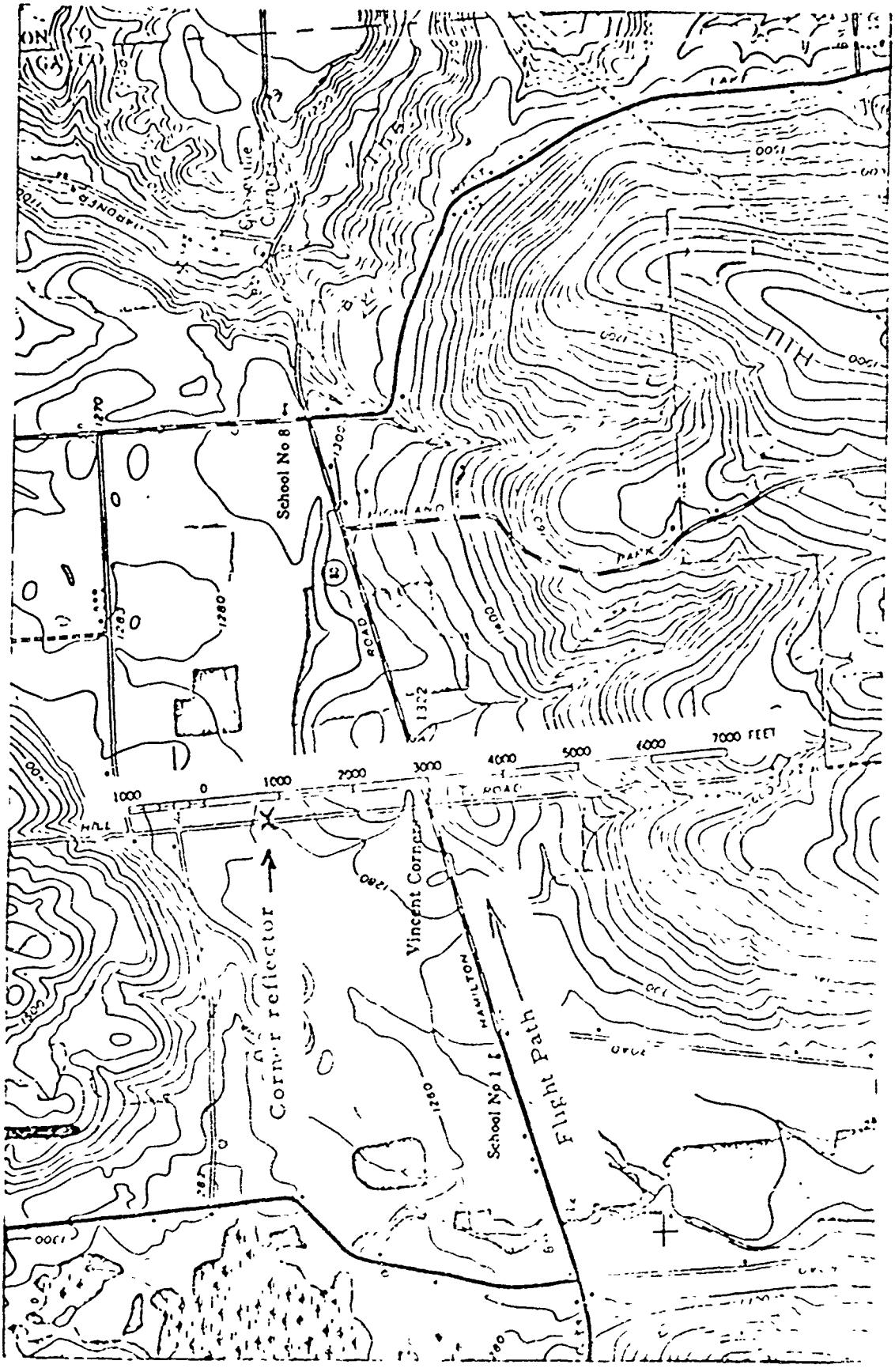

Figure 6.12 Vincent Corners Test Area

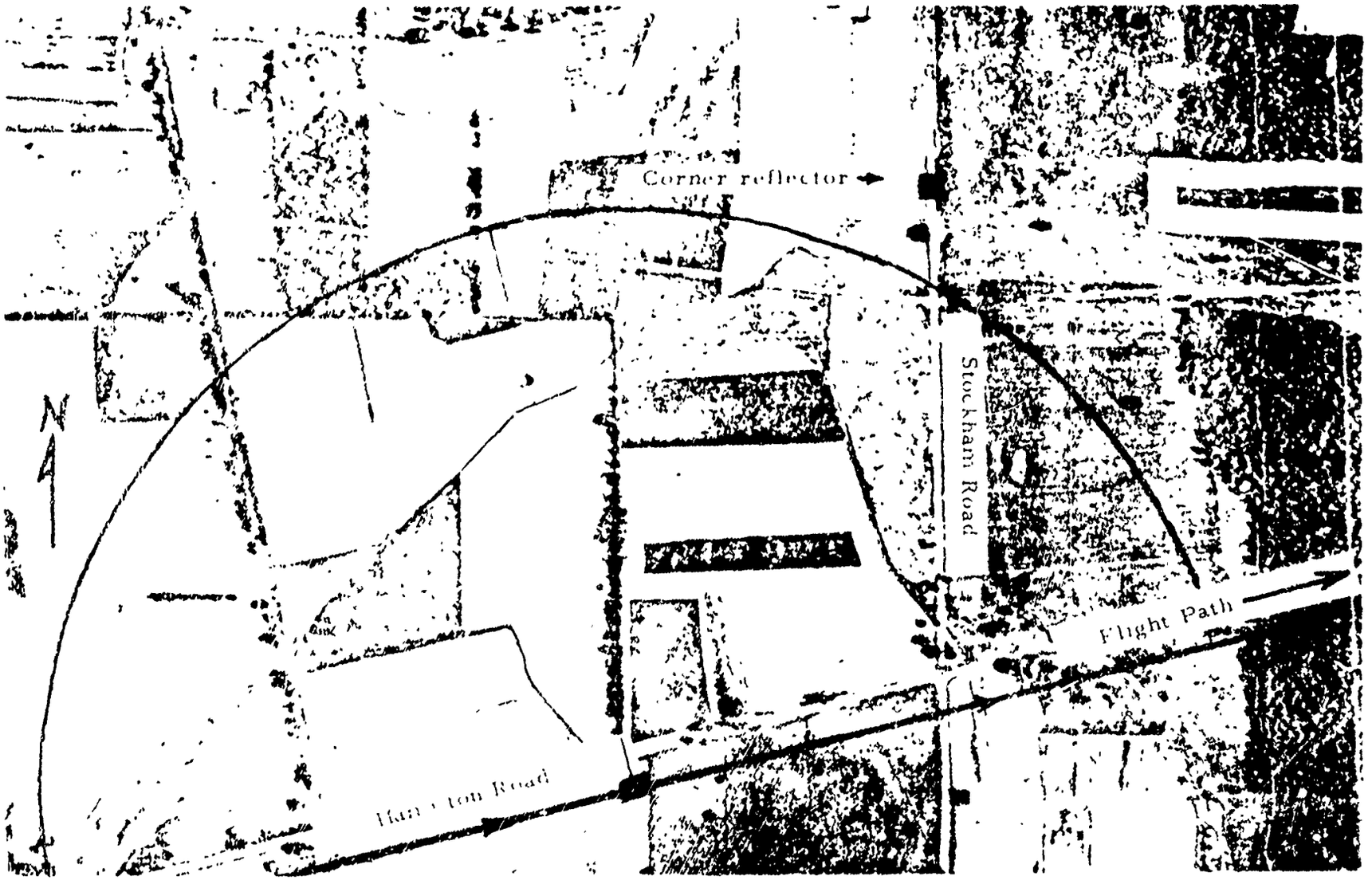

Figure 6.13. Photograph of Vincent Corners Test Area

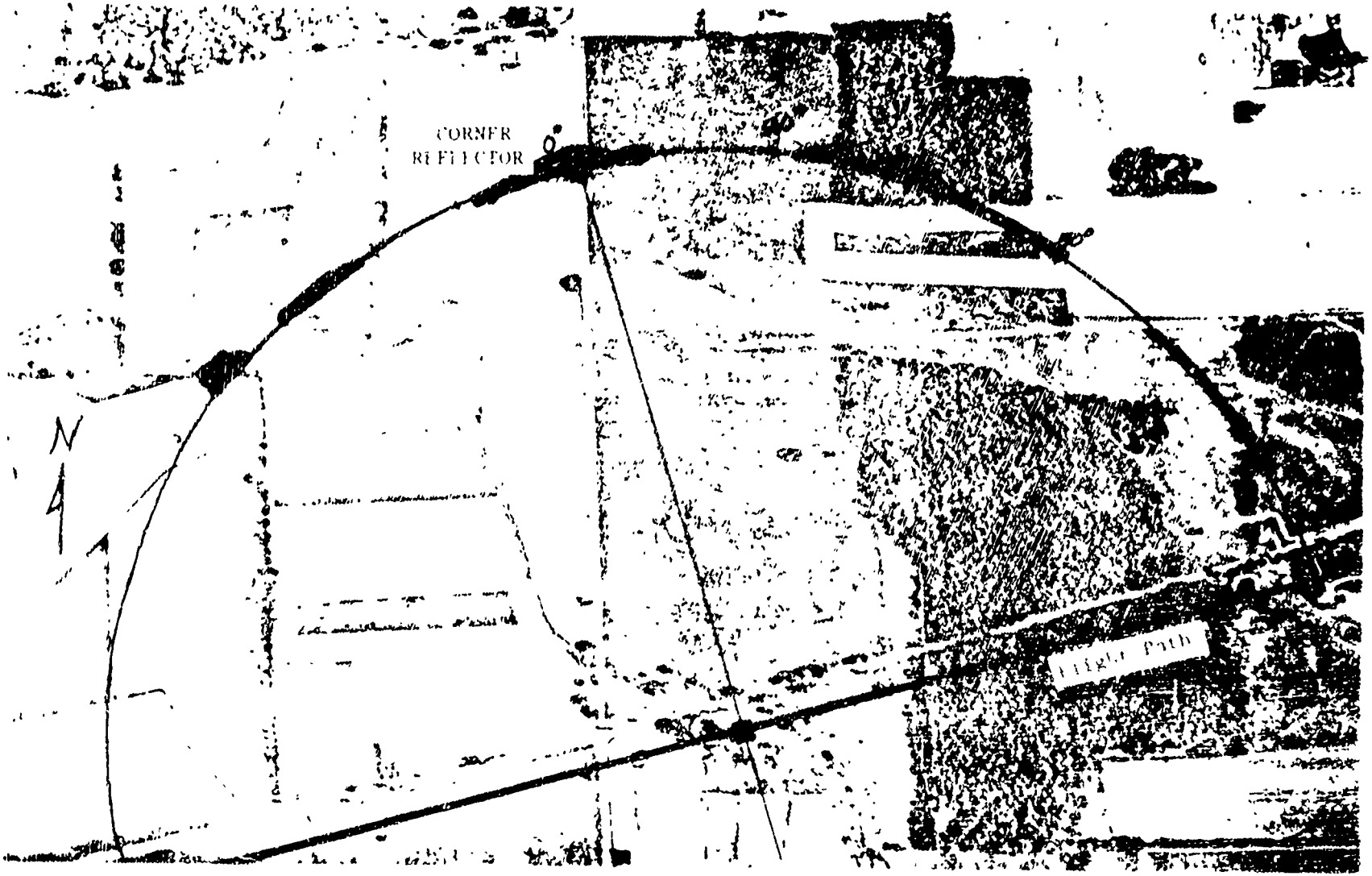

Figure 6.14. Photograph of Vincent Corners Test Area

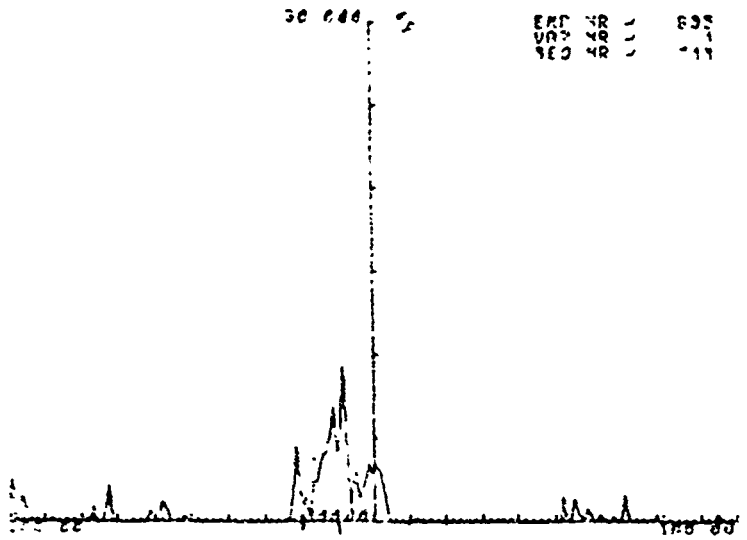

(a)

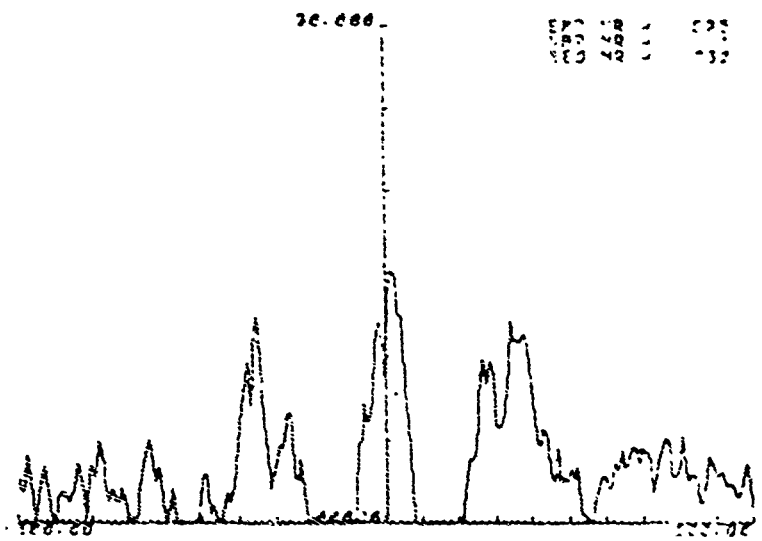

(b)

Figure 6.15 Spectra-Vincent Corners Test Area

Table 6.6 Vincent Corners Data

Terrain Description	First Record	Freq. Range cps.	σ_o
1. Open field-flat	49	-10 to 10	0.000013
2. Open field-rolling	49	20 to 50	0.0013
3. Woods	81	15 to 25	0.17
4. Same	89	5 to 15	0.15
5. Same	97	-5 to 5	0.10
6. Hill with scattered trees	17	-10 to 10	0.046
7. Same	25	-25 to -5	0.032
8. Field (unknown target)	65	-40 to -30	0.019
9. Same	73	-35 to -25	0.028

σ_o is the radar cross section per unit area of terrain surface.

Each cross section shown is the post square average of all frequency points within the frequency range shown. Each frequency point is the post square average (over time) of 8 FFTs with I shift=64.

The terrain may be further described as follows:

1. Open field-flat. The lowest cross section observed at the Vincent Corners sight and apparently represents very flat land free of vegetation, buildings, fences, etc.

2. Open field-rolling. Pasture land with very few trees and no buildings. The land was gently rolling, the maximum angle of inclination being about 10-15°. There were several small ravines or gullies, about 8 ft. deep, with sides sloping at an angle of 20 or 30 degrees with respect to the horizontal. There were several small fences of the electrical type. The radar cross section values measured here are typical of those found for pasture land in the Vincent Corners area.

3. Woods. A rather heavy stand of hardwood trees. The trunk diameters were about 1 ft. at the base and they were about 35 to 45 ft. tall. The mean spacing between trunks was about 8 to 10 ft. There was very little undergrowth.

6. Hill with Scattered Trees. Really two little hills, about 300-400 ft. high with a scattering of fairly large trees at the top. The slopes were quite steep, perhaps 60° or so.

8. Field (unknown target). This field yielded a somewhat larger radar cross section than most fields in the area. There were no hills, trees, or other obvious targets on the field. This field was not searched on foot (as were most of the other areas in this study), however, the topographical map shows some indication of a ravine type structure which may be responsible for the larger cross section.

Terrain samples marked "same" are adjacent and of very similar type to the preceding sample.

The expected standard deviation due to random scattering may be computed (at least for uniformly wooded terrain) from statistical theory, as shown in the report 'Moving Platform FOPEN Radar Systems'. For example, for target number 3- woods-, the final average contains about 80 FFTs. Since they are overlapping in time, about one half of them may be taken to be statistically independent. The expected standard deviation is therefore $1/\sqrt{40}$ or $\pm$ 16%. This is about the standard deviation of the three points reported for wooded terrain, hence, one may attribute the observed difference between points to random scatterings effects rather than vegetation density variation. The expected standard deviation for the other targets is more difficult to compute but is probably of about the same magnitude.

It is clear then that the large difference in cross sections measured for different terrain samples actually reflects differences in terrain type and is not just due to the random nature of the scattering process.

6.4 Cross Section Measurements at 50 MHz

6.4.1 Standard Target at 50 MHz

The standard target chosen for these tests was a halfwave dipole. The simplicity and small size were governing factors in this choice. The characteristics of this target are as follows:

Length = .47 = 9.02 feet
Diameter = 2.0 inches
Bandwidth = 18% (approximately)
Cross Section (dipole) = $\sigma_d = G(.83\lambda^2) = G(309)$ ft^2

Ground Effect = $G = 16 \sin^4\left(\frac{2\pi H \sin\theta}{\lambda}\right)$

where H = height of dipole above ground
θ = elevation angle of aircraft.

as an example: $G = 16 \sin^4\left(\frac{2\pi H \sin\theta}{\lambda}\right)$

when H = 8 ft; λ = 19.3 ft; θ = 20°
then G = 5.83
and σ_d = (5.83)(309) = 1802 ft^2

The following (Table 6.7) are typical results from data collected during a Swamp Road flight test at 50 MHz (experiment 2049). During this experiment the one-half wavelength dipole was placed in an open flat area. The dipole was suspended 12 feet above the ground and can be expected to provide a target with a calculated (ground plane effect included) cross section of 4,421 square feet.

For experiment 2049 the outer range gate was positioned such that the target passed through the range gate twice (the normal range from the target to the flight path was less than the actual range gate setting - see Figure 3.3 where X_o is less than R_8). The following cross section values of the dipole were determined from the data.

Table 6.7 Swamp Road Data

Deg. of Wavelength	Cross Section Ft^2
+17	2040
+14	3415
+11	3287
+ 8	2029
.	
.	
.	
- 2	1820
- 5	3300
- 8	2060

The data shows an experimental cross section ranging from 1820 square feet to 3415 square feet. Expected angular dependence[1] of incidence from normal yields σ_d varying roughly as $\cos^5$ -. Since the experimental and theoretical data correspond fairly well, it is reasonable to assume that the radar calibration is correct and that clutter cross section measurements are therefore valid at 50 MHz. Validity of the measurements at 140 MHz was thoroughly established as described in Section 3.1.5.

6.4.2 Processed Results at 50 MHz Tests

Data collected during the various experiments was processed in two different ways. The data was displayed and cross sections were computed.

[1] Reference - Methods of Radar Cross Section Analysis - Cuspen & Siegel, Academic Press, 1968, p. 109, angular distributions of wire responses.

6.4.2.1 Displayed Data

The radar map of the target area was encouraging. The dipole target was definitely discernible from the surrounding clutter. Prior experiments (at 140 MHz) to observe a target in the same clutter had been marginal.

6.4.2.2 Cross Section Computations

An inspection of the computed cross section measurements indicated an improvement in the clutter cross section of at least one order of magnitude. The measurements of clutter cross section must be termed relative measurements at this time due to (1) the limitations of time restricted flight test time and, (2) it was not possible to locate the dipole target in more than one area to establish a confidence factor in repeatable measurements.

6.4.2.3 Vincent Corners Measurements

Experiment 2055 yields typical data for Vincent Corners (See Section 5.1 3.2 for description of test area). Of particular interest is the radar cross sections of a boot-shaped forest just east of Waters Road, which is well known from the test data at 140 MHz.

The average of eight (8) power spectral density estimates of a simple frequency bin was used to find the mean radar cross sections per frequency bin of the woods at Vincent Corners. The mean was determined from the averages of four (4) adjacent frequency bins.

The results are an arithmetic mean of the equivalent clutter cross section per bin of σ bin = 330 ft^2.

Table 6.8 is a list of computer calculated cross sections for frequency bin number minus two (-2). The bracketed numbers include the boot-shaped woods which on the average are significantly larger than for the pasture which precedes and follows the forest data.

The clutter cross sections per unit area (σ_o) calculated from the mean cross sections is 0.022 as compared to σ_o = .15 at 140 MHz (See Section 6.3). This is a reduction in cross section by approximately a factor of 7.

6.4.2.4 Swamp Road Measurements

Experiment 1019 represents data collected at 140 MHz over the Swamp Road site. The arithmetic mean of the equivalent clutter cross sections per bin for this experiment is σ bin = 4650 ft^2. The maximum value of σ bin is about 7600 ft^2. This is equivalent to a σ_o of about .84.

Data from approximately the same geographic area at 50 MHz is represented by experiment 2049. The arithmetic mean of the equivalent clutter cross section per bin for this experiment is σ bin = 400 ft^2. The maximum σ bin

Table 6.8. List of Computed Cross Sections

EXP NO. 2055 VAR NO. 5 .. NO. POINTS 256 PRI(MSEC) 4.26
IPOINT= 2 ISHIFT= 171

SEQ NO.	NO.OF REC	1ST REC	NORM. CONSTANT	SCAN LIM.	CROS SEC.	REC. POWER	AZ. ANG.	DOP. FREQ.	NBIN
126	1	20	48.24						
				-2 TO -2	41.019	-67.71	-8.66	-2.75	1
127	1	21	48.69						
				-2 TO -2	2.198	-80.42	-8.66	-2.75	1
128	1	22	52.03						
				-2 TO -2	74.581	-65.11	-8.66	-2.75	1
129	1	23	49.64						
				-2 TO -2	13.155	-72.65	-8.66	-2.75	1
130	1	24	48.45						
				-2 TO -2	134.625	-62.55	-8.66	-2.75	1
131	1	25	53.21						
				-2 TO -2	532.538	-56.57	-8.66	-2.75	1
132	1	26	54.04						
				-2 TO -2	3.080	-78.95	-8.66	-2.75	1
133	1	27	53.34						
				-2 TO -2	930.151	-54.15	-8.66	-2.75	1
134	1	28	52.19						
				-2 TO -2	126.254	-62.82	-8.66	-2.75	1
135	1	29	51.63						
				-2 TO -2	43.225	-67.48	-8.66	-2.75	1
136	1	30	51.99						
				-2 TO -2	134.163	-62.56	-8.66	-2.75	1
137	1	31	51.31						
				-2 TO -2	220.250	-60.29	-8.66	-2.75	1
138	1	32	49.13						
				-2 TO -2	14.984	-72.08	-8.66	-2.75	1
139	1	33	50.34						
				-2 TO -2	9.962	-73.85	-8.66	-2.75	1
140	1	34	54.35						
				-2 TO -2	20.751	-70.67	-8.66	-2.75	1
141	1	35	52.43						
				-2 TO -2	7.646	-75.00	-8.66	-2.75	1
142	1	36	49.67						
				-2 TO -2	145.260	-62.21	-8.66	-2.75	1
143	1	37	48.13						
				-2 TO -2	3.127	-78.89	-8.66	-2.75	1
144	1	38	51.42						
				-2 TO -2	10.379	-73.67	-8.66	-2.75	1
145	1	39	50.59						
				-2 TO -2	10.837	-73.49	-8.66	-2.75	1
146	1	20	48.24						
				-1 TO -1	144.557	-62.12	-5.76	-1.83	1
147	1	21	48.69						
				-1 TO -1	50.722	-66.67	-5.76	-1.83	1
148	1	22	52.03						
				-1 TO -1	48.448	-66.87	-5.76	-1.83	1
149	1	23	49.64						
				-1 TO -1	83.206	-64.52	-5.76	-1.83	1
150	1	24	48.45						
				-1 TO -1	96.919	-63.87	-5.76	-1.83	1

value is about 900 ft^2. The equivalent σ_o is about .03 with a maximum value of σ_o being .07. This represents a reduction in clutter cross section by a factor about 28 due to the frequency change.

6.5 Comparison with Existing Data

It should be mentioned that the cross section results quoted in this report are seriously in conflict with those obtained by Control Data Corporation.[1] For example, the value of σ_o reported by CDC for dense trees at 20° depression angle and a carrier frequency similar to 51 MHz is about 10^{-4}. This is two to three orders of magnitude smaller than the results obtained here. The system used for the SURC measurements was carefully calibrated and good agreement was obtained in a measurement of a standard dipole. Hence, it is not considered likely that our measurements are seriously in error.

Of course, there is a great deal of difference between woods and the label "dense" is rather vague, however, SURC results seem to be, in general, several orders of magnitude larger than CDC's.

The source of this discrepancy is not at all understood. It should be noted that the CDC results were taken without any focusing and from an altitude of about 10,000 ft., making each measurement bin about 5 miles wide. Therefore, it must be very hard for them to know just what is in the measurement cell. In the SURC experiment, the measurement cell is only a few hundred feet on a side and the targets stands of trees were carefully checked from the ground. Hence, it is felt these results are somewhat more reliable than CDC's. However, the discrepancy remains disturbing.

[1] "Backscatter Analysis," by R.A. Zuck, Control Data Corporation, Report Number AFCRL-TR-73-0212.

7.0 STATISTICS OF CLUTTER SIGNALS

7.1 The Model

This section is a review of the basic theorems dealing with the addition of random signals. This information is used to describe the statistical properties of the backscattered radar signal from vegetated terrain. It is in order first, therefore, to construct and work within a model of the vegetated surface.

The surface should be flat or gently rolling. Perfectly flat ground produces no backscatter except at vertical incidence. If the terrain is slowly rolling, such that the tangent to the surface changes little over distances of the order of a wavelength and no portion of the surface is steep enough so as to be normal to the direction of propagation of the incident radiation, the backscattered energy is still very small. If such terrain is covered with reasonably dense woods, the backscatter from the trees greatly exceeds that from the surface of the ground itself. Therefore, we will neglect the contour of the land and assume it to be flat. For very rough terrain, there is large ground backscatter and therefore the vegetation may be neglected. This problem is treated in standard works and will not be dealt with here.

It seems reasonable to take as a model, then, a flat surface with scattering objects distributed randomly upon its surface. The nature of these objects need not be specified, they could be trees, rocks, etc.

The assumptions we must make are as follows:

1) The location of the objects on the surface is truly random. This means their positions are uncorrelated; the position of one object has no effect on the position of any other. This is probably a very good assumption for a forest but would be no good at all for an orchard.

2) That it is possible to specify an average radar cross section for each species of object under consideration and that this average be stable. Since the radar cross section is a positive definite quantity, this condition is always met in practice.

3) That the number of each significant species of object per resolution cell will be large. By significant species, we mean those species which contribute a significant portion of the total radar backscatter. For example, the trunks of large trees are the dominant scatterer in many cases of interest. Since there are usually a fairly large number of trees in a resolution cell, the condition is satisfied. On the other hand, an object with a large vertical facet, such as a cliff or a ravine, can easily have a radar cross-section larger than many trees. As there would probably be one such object in the resolution cell, the condition is now not satisfied.

4) The question of just how large a number is required is a difficult one. The answer depends on how far out on the tail of the distribution one requires the theory to be valid. If one is only interested in the central portion of the distribution, 20 or 30 objects per cell is enough. In radar work one often requires a false alarm probability of 10^{-6} or less. Hence (if no post-detection averaging is being used), the distribution must be known accurately out to four or five times the mean signal (voltage) value. This requires that the number of objects be at least 100 preferably 300 or more. If post-detection averaging is used, this requirement is greatly reduced. The resolution cell of the existing system will probably contain at least 100 trees, when operating in fairly dense, homogeneous forest. Hence, the theory presented here is usable for false alarm analysis in most cases. For systems having resolution much greater than that of the present system, the theory may not be usable for radar purposes.

5) That the scattering objects are spread evenly throughout the cell. The distribution is stationary, at least over the width of the cell.

6) That the resolution cell be much larger than a wavelength. We shall show later that only two or three wavelengths are necessary. This is always met in practice.

All of the conditions are quite reasonable and are probably all satisfied in the case of reasonably flat forest terrain.

7.1.1 Distributions

Consider the voltage received from a single scattering object. Let the amplitude of the received signal be s and the phase be v. Represent this signal, using the usual complex polar diagram, as a vector of length, s, making an angle, v, with the positive real axis. The total received signal for one resolution cell is the vector sum of the signals from all of the scattering objects in that cell. A diagram of the sum of three signals is shown in Figure 7.1.

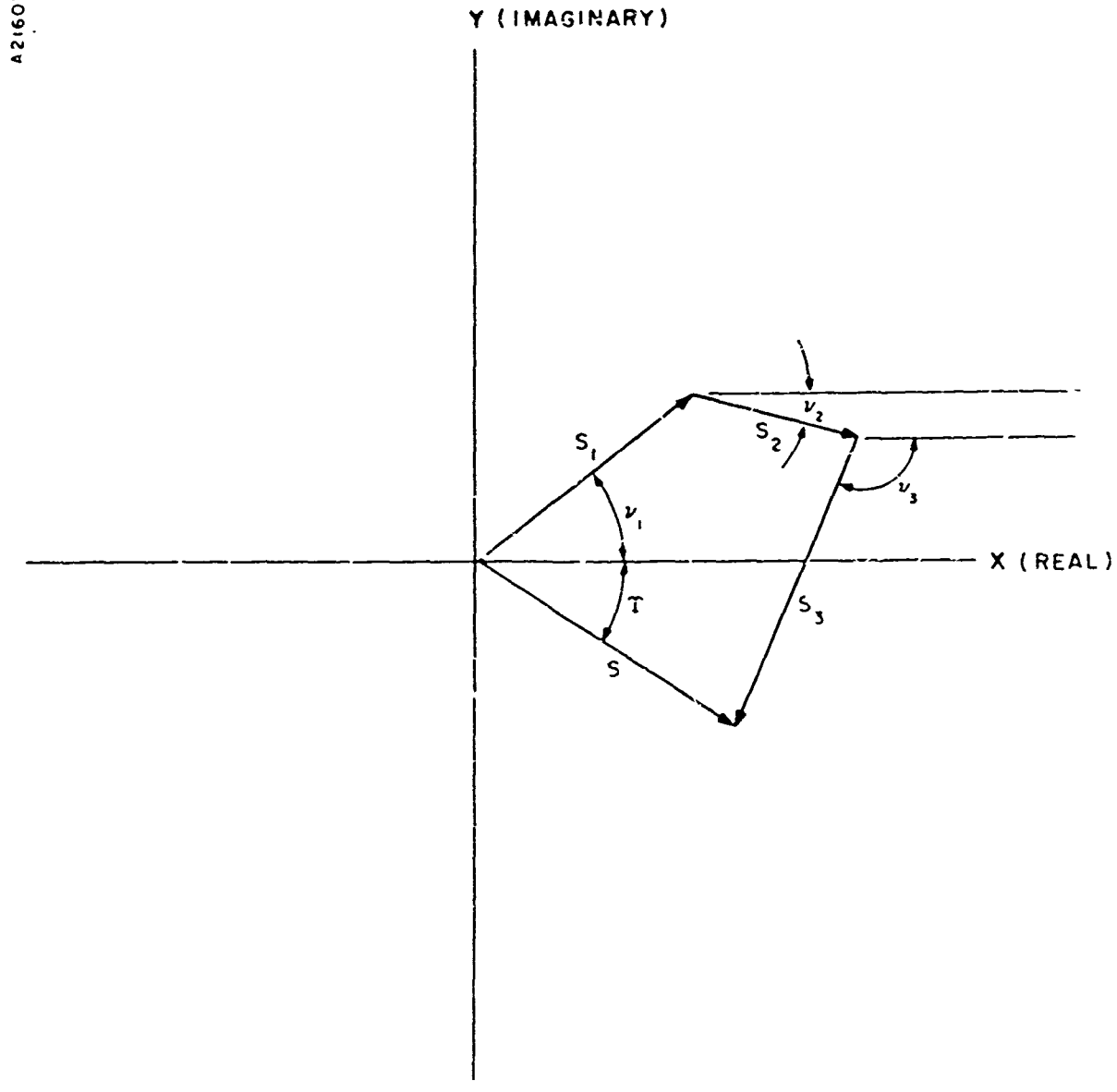

Figure 7.1 Vector Diagram of a Single Scatterer

Now the phase of the backscattered signal from each object is $\upsilon = 2\frac{2\pi}{\lambda} R + \phi$, where λ is the wavelength of the radiation, R is the distance from the radar to the object, and ϕ is the phase shift inherent in the scattering process. Since the objects in question are randomly spread over a range cell larger than λ, it can be shown that the phases must be spread randomly over the range $-\pi$ to π. In other words, the vectors to be summed are pointed randomly in all possible directions. The solution for the probability distributions for the length and direction of the sum vector is the famous random walk problem and the solution can be found in any text on this subject. The distribution for the projection of S on either axis is

$$P(S_x) = \sqrt{\frac{1}{\pi\zeta}}\ e^{-\frac{S_x^2}{\zeta}} \tag{1}$$

where

$$\zeta = \sum_{k=1} \bar{N}_k\ s_k^2 \tag{2}$$

The projections on the two axis are independent. Here S_x is the real or imaginary part of the sum vector. This would correspond to the voltage in the in phase or quadrature phase channel of a balanced processor radar receiver. P is the probability density for finding the projection of the sum amplitude near S_x. $\bar{N}_k$ is the mean number of the k'th species in the resolution cell and s_k is the signal amplitude for that species.

In the case of most interest here, i.e., trees, the major scatterers are the trunks. For a given stand, most of the trunks are about the same size. Therefore, in order to make the meaning of these equations clearer, we will replace the summation with a mean amplitude a_0 and an average number $\bar{N}_s$,

$$\zeta = \sum_{k=1} \bar{N}_{s_k}\ s_k^2 = \bar{N}_s\ a_0^2$$

These quantities may be replaced by the summation in any of the following work if it is so desired Equation (1) may now be rewritten

$$P(S_x) = \frac{1}{a_0}\sqrt{\frac{1}{\pi\bar{N}_s}}\ e^{-\frac{S_x^2}{\bar{N}_s a_0^2}} \tag{3}$$

This is a Caussian distribution of zero mean and standard deviation $\langle S_x^2\rangle$:

$$\sigma_s = \sqrt{\langle S_x^2\rangle} = \frac{1}{\sqrt{2}}\ a_0\sqrt{\bar{N}_s}$$

$$\langle S_x\rangle = 0 \tag{4}$$

Now the standard deviation is the same as the root mean square, so the rms value of the clutter signal is proportional to the square root of the number of objects.

To obtain the two-dimensional distribution for the vector amplitude of the sum signal multiply the distribution for the real projection by that for the imaginary projection.

$$P(S_x, S_y) = \frac{1}{\pi \overline{N_s} a_0^2} e^{-\frac{S_x^2 + S_y^2}{\overline{N_s} a_0^2}}$$

transform into polar coordinates using

$$S^2 = S_x^2 + S_y^2$$

$$d S_x \, d S_y = S \, d S \, d T$$

Since the distribution does not depend on the phase angle, T, integrate T from 0 to 2π, thus obtaining the probability density for an arbitrary phase angle. This yields the well known Rayleigh distribution for the amplitude

$$P(S) = \frac{2 S}{\overline{N_s} a_0^2} e^{- S^2 / \overline{N_s} a_0^2} \qquad (5)$$

Of much greater interest is the distribution for the square of the a amplitude, since this is the quantity usually found at the output of a radar. To find this let

$$W = S^2$$

and using $d W = 2 S \, d S$

results in $$P(W) = \frac{1}{\overline{N_s} a_0^2} e^{- W / \overline{N_s} a_0^2} \qquad (6)$$

This formula is very important for the theory of foliage penetration radar. Note that it is a simple exponential with a mean of $\overline{N_s} a_0^2$. Interpreting the squares of the amplitudes as power, just say that the total average power received is $\overline{N_s}$ times the power received from an individual scatterer.

We will call this quantity $\overline{W}$,

$$\langle W \rangle = \overline{N_s}\, a_0^2 = \overline{W}$$

The distribution may then be written

$$P(W) = \frac{1}{\overline{W}}\, e^{-W/\overline{W}} \tag{8}$$

The standard deviation about the mean, σ_W, is given by

$$\sigma_W^2 = \langle (W - \langle W \rangle)^2 \rangle = \langle W^2 \rangle - \langle W \rangle^2 = 2\overline{W}^2 - \overline{W}^2 = \overline{W}^2$$

or

$$\sigma_W = \overline{W} \tag{9}$$

Therefore, the standard deviation is equal to the mean. This indicates that the scatter in the data will always be large. A single measurement is not a good estimate of the mean, even when the number of objects in the cell is large. This can also be seen from the shape of the distribution because the exponential decreases smoothly and has no peak. It should be emphasized that this variation is entirely due to the random interference of the wave trains backscattered and has nothing to do with any variation of the density of the clutter. This large variation is a serious problem for the designer of a radar system.

One notices that all of the distributions discussed above are exactly the same as would be obtained for Gaussian random noise. The similarity arises because the noise is the sum of a large number of independent waves. Note, however, that this is not true for all types of clutter. For example, rough terrain clutter is often non-Gaussian. This is because such clutter is usually due to single surfaces glinting. Thus, in many ways, a homogeneous forest represents an ideal type of clutter. The signal backscattered has the simplest possible statistical properties.

7.1.3 Averaging

One of the simplest methods of reducing the variance of a random signal is averaging. One averages over several different measurements of the same cell, either at different carrier frequencies or from different angles. A review of a few of the pertinent theorems concerning the averaging of random variables is in order.

Consider N random variables, X_i, all having the same mean, $\overline{X}$, and

Consider N random variables, X_i, all having the same mean, $\bar{X}$, and the same variance σ^2. let the average of these be X_{AV}:

$$X_{AV} = \frac{1}{N} \sum_{i=1}^{N} X_i \tag{10}$$

The mean of X_{AV} is still $\bar{X}$,

$$\langle X_{AV} \rangle = \frac{1}{N} \sum_{i=1}^{N} \langle X_i \rangle = \bar{X} \tag{11}$$

Let the variance of the average be σ^2_{AV},

$$\sigma^2_{AV} = \langle X^2_{AV} \rangle - \langle X_{AV} \rangle^2 = \langle \frac{1}{N^2} \sum_{i}^{N} \sum_{j}^{N} X_i X_j \rangle - \bar{X}^2$$

$$\sigma^2_{AV} = \frac{1}{N} \langle X^2 \rangle - \frac{1}{N} \bar{X}^2 + \frac{1}{N^2} \sum_{i \neq j}^{N} \sum^{N} \langle X_i X_j \rangle - \frac{1}{N^2} (N^2 - N) \bar{X}^2$$

$$\sigma^2_{AV} = \frac{1}{N} \sigma^2 + \frac{1}{N^2} \sum_{i \neq j}^{N} \sum^{N} \mathrm{Cov}(X_i, X_j) \tag{12}$$

If the N variables are statistically independent, the convariance is zero

and

$$\sigma_{AV} = \frac{\sigma}{\sqrt{N}} \tag{13}$$

The standard deviation about the mean decreases as the square root of the number of points averaged, regardless of the type of distribution.

To find the distribution function for the averaged variable use the fact that the distribution function for the sum of two random variables is the convolution of the individual distribution functions. Let the N random variables, X_i, be independent and have identical distribution functions, $P(X_i)$. The distribution function for the sum of two of these is then

$$P_2(X) = \int_{-\infty}^{\infty} P(X') \; P\;(X - X')\; d\;X' \tag{14}$$

by repeating this process the distribution for the sum of any number of variables may be found. We then make the transformation $X_{SUM} \rightarrow NX_{AV}$ because the sum has been divided by N to obtain the average.

This may be applied to the problem of averaging the clutter signals in the in-phase or the quadrature phase channel of the receiver, i.e., before they are absolute squared. The distribution for these signals is given by Equation (3). The convolution of a Gaussian is another Gaussian therefore, the distribution function for the average of N of these signals is

$$P(S_{X-AV}) = \frac{1}{a_0}\sqrt{\frac{N}{\pi \bar{N}_s}}\; e^{-NS^2_{X-AV}/\bar{N}_s\, a_0^2} \tag{15}$$

This is exactly the same as Equation (3) except that $\bar{N}_s$ is replaced by $\bar{N}_s/N$. Thus, averaging before squaring does not change the shape of the distribution but reduces the rms value of the clutter signal by $1/\sqrt{N}$. If this signal is subsequently absolute squared, the mean and the standard deviation of the resulting signal are reduced by a factor of 1/N from the unaveraged values.

Now turn to the more interesting case where the signal is averaged after the absolute square has been taken. Perform the same operations on the distribution for the amplitude squared (Equation 8) and obtain

$$P(W_{AV}) = \frac{N^N}{(N-1)!} \frac{W_{AV}^{N-1}}{\bar{W}^N} e^{-N\frac{W_{AV}}{\bar{W}}} \tag{16}$$

This looks rather formidable, however, it is easy to show that the mean and standard deviation have the expected values

$$\langle W_{AV} \rangle = \bar{W} \tag{17}$$

$$\sigma_{W_{AV}} = \bar{W}/\sqrt{N}$$

As N becomes larger, this distribution becomes more and more peaked around $\bar{W}$. In the limit of large N it goes over into a Gaussian

$$P(W_{AV}) = \sqrt{\frac{N}{2\pi}} \frac{1}{\bar{W}} e^{-N(W_{AV}-\bar{W})^2 / 2\bar{W}^2} \tag{18}$$

Note that N must be on the order of 1,000 if it is desired to use the Gaussian limit to predict radar false alarm rates. This is because the Gaussian approximation is weaker in the high amplitude tail of the distribution. Equation (16) may be used for any value of N.

It is interesting to compare the process average before absolute square with the process absolute square before average. The first process does not change the final distribution function from its unaveraged form but reduces the mean and standard deviation by 1/N. The second process yields a very different distribution function from the unaveraged case. The mean is not affected but the standard deviation is reduced by $1/\sqrt{N}$. Thus, the first process is superior for clutter reduction purposes.

7.2 Data Analysis

In this section, comparisons are made of the results of the previous section with data from the LWL-SURC airborne radar system. The main objective will be to test the probability distribution for the absolute square of the amplitude of the clutter signal (Equation 8). If this formula is found to represent the data, it follows that the other distributions derived in the previous section should also be valid.

The stationarity of the clutter is also tested. Stationarity indicates that the mean and the autocorrelation function of the clutter object density are constant over the area in question. In other words, stationarity indicates that the distribution of clutter objects is homogeneous. Of course, if the clutter objects occur in clumps or patches they cannot be stationary. If the clutter object density is stationary, the backscattered radar signal is also stationary. Since the positions of the scattering objects are of interest and (trees) are almost certainly uncorrelated, the question of the stationarity of the clutter object density autocorrelation function as no meaning.

Note that stationarity was not assumed in the previous section. Stationarity was not needed there because the averages were really ensemble averages. Therefore, the shape of the distribution does not depend on the stationarity. Of course, ensemble averaging and spatial averaging must give the same result as we assume all natural processes are ergodic regardless of stationarity. If is important to test the stationarity of the data as this property is viral for some of the clutter reduction systems under consideration.

For our immediate purpose, the details of the radar system are ignored, consider it as a black box which gives an output proportional to the absolute square of the signal received from a given element of terrain surface. The radar, as used here, has only one range bin, about 100 feet wide, and a large number of azimuth bins or elements, which vary in size. These azimuth elements are formed by a digital filter and are sometimes designated by the frequency of the filter element. Note that a linear operation does not change the distribution of a Gaussian variable. Therefore, the spectrum weighted digital filter at the output of the radar does not affect the shape of any of the distributions predicted in the previous section. As the radar flies along it makes records of the signals received. For this data, one output is available every second. In this time the aircraft moves about two cell widths. Designate a single output number as W_{ij}, where i refers to the azimuth filter element number and j to the sequential record number. The fact that individual trees are moving into and out of the cell during the measurement also has no effect on the form of the distribution. The motion of the range cell has the same effect as pre-absolute square averaging. This will be shown in greater detail in the next section.

Now the output for different azimuth elements vary greatly in average value, because the azimuth elements are not all the same size nor are they illuminated equally by the antenna. Therefore, in order to put the data in a more usable form, normalize the output of each elemental filter by

dividing it by its own average over all records in an experiment. Call this normalized quantity w_{ij}, then

$$w_{ij} = \frac{W_{ij}}{\frac{1}{M}\sum_{j=1}^{M} W_{ij}} \tag{19}$$

where M is the number of records in an experiment. Since M is fairly large (usually on the order of 20 or so), we are effectively dividing W_{ij} by its own average. Therefore, the mean (ensemble average) of any of the w_{ij} is unity

$$\langle w_{ij} \rangle = 1 \tag{20}$$

By this normalization we have divided out the effects of the antenna pattern and the variation in azimuth element size. Figure 7.2 shows a plot of w_{ij} for Experiment 352, Variable 1, Record 1, made with the SURC UNIVAC computer. Here w is plotted against filter element frequency. This data was taken front-looking so that the clutter data lies between 0 and 50 Hz on the X axis; this corresponds to the entire 180° forward azimuth sector. Note that the data do scatter quite markedly.

The w_{ij} are proportional to the absolute squares of the received clutter amplitudes, therefore, their distribution should be governed by Equation (8). Since the mean of all the w_{ij} is one, Equation (8) reduces to

$$P(w) = e^{-w} \tag{21}$$

This must hold for all of the w_{ij}, in spite of the fact that the azimuth element size and therefore the number of scattering objects measured per sample varies with the index i. Since they all have the same distribution, consider all of the w_{ij} as one set of equivalent samples of the random variable w. This is the only way to obtain enough points to plot a distribution from the data of one experiment.

The distribution is computed in the usual way. The w range is divided into a number of sectors or binds and the number of data points in each

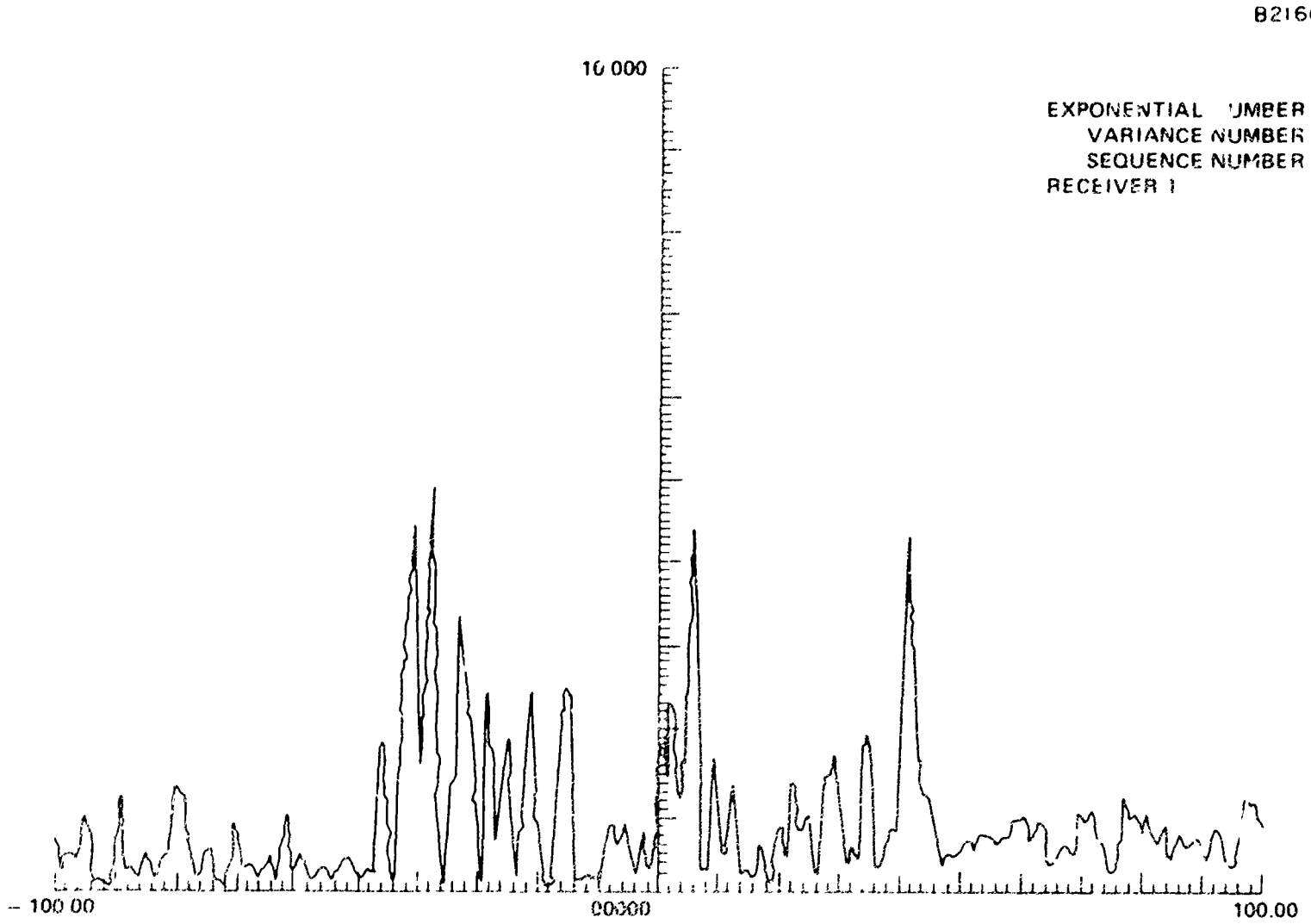

Figure 7.2. Plot of a Normalized Power Spectrum

bin is counted. The probability density corresponding to the midpoint of a bin is

$$P = \frac{(\text{number of points in bin})}{(\text{total number of points}) \times (\text{width of bin})} \quad (22)$$

Each point thus obtained has an uncertainty given by its standard deviation

$$\sigma_P = \frac{\sqrt{(\text{number of points in bin})}}{(\text{total number of points}) \times (\text{width of bin})} \quad (23)$$

Ignore the small additional term in the standard deviation arising from the uncertainty in the normalizing factor for the W_s. This term is always small compared to the uncertainties given above.

The data probability distribution for w from Experiment 352, Variable 1, is shown in Figure 7.3.The probability density, (P(w), is shown plotted against w. The data from the entire forward 180° sector of records 1 through 9 is used. The vertical marks at the bottom of the page show the limits of the bins into which the data has been divided. The error bars indicate the standard deviation. The solid line in Equation (21), the theoretical distribution. Note that this line has not been adjusted or fit to the data in any way. The fit is seen to be remarkably good; all of the points are within or very close to a standard deviation from the theoretical line.

In order to test the data for stationarity, we shall compute N point averages of sections of the data and compare these. If the data is truly stationary, these averages should all be within a standard deviation of the mean. Deciding how many points to take in an average is difficult. On one hand, N should be large enough to make the standard deviation small compared to the mean. On the other hand, if N is too large, any possible inhomogeneity in the clutter density may be missed. After some experimentation, it was decided to use averages of 15 points. We utilize the small normalized data which was used for plotting the distribution. Let us call these averaged quantities w_{AV}. We then have from Equation (17) that

$$\langle w_{AV} \rangle = 1$$

$$\sigma_{w_{AV}} = \frac{1}{\sqrt{15}} = .26 \quad (24)$$

We would like the region averaged to be more or less rectangular in shape.

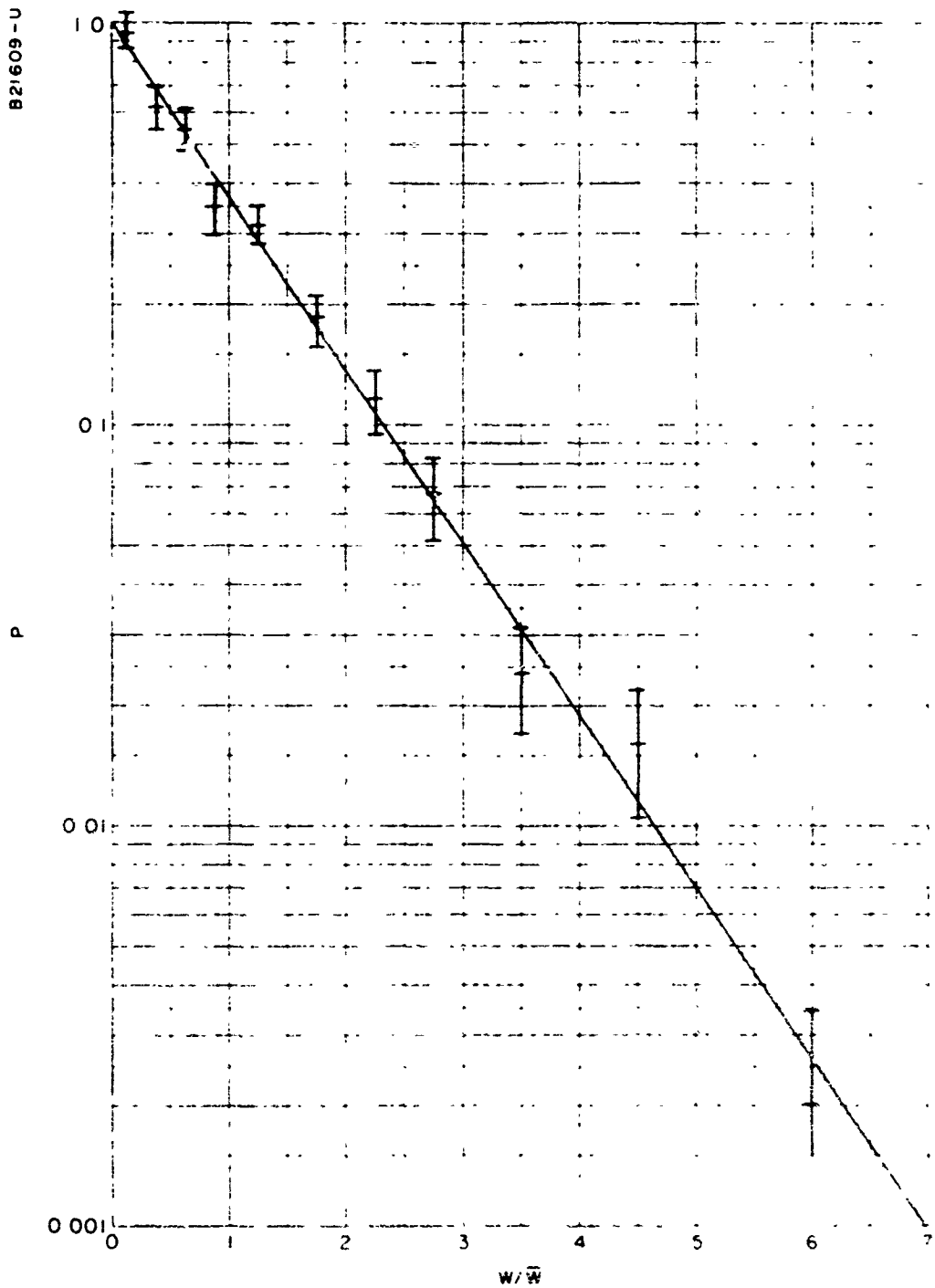

Figure 7.3. Probability Distribution for Experiment 352

Clearly, a long strip is not appropriate as one expects inhomogeneities in the vegetation density to occur in clumps. The averages used here are five contiguous azimuth elements taken for three contiguous records and located at a skew angle with respect to the direction of flight. For example, one average might consist of azimuth (doppler frequency) elements 20 through 25 of records 1 through 3. Thus the area included in one average would look something like Figure 7.4, where the rough dimensions are shown for Experiment 352. Of course, the upper and lower boundaries are slightly curved and the side boundaries are ragged. Also, as most of the data presented here is front-looking, there will be two such areas, one on either side of the aircraft, included in each average. Also, since the aircraft travels about two cell widths per record, there is a complicated overlapping of the individual area elements. None of these qualifications is very serious and this method should be adequate to give some idea of the clutter density in the area covered by each average.

Averaged data from Experiment 352, Variable 1, are shown in Figure 7.5. Values of w_{AV} are shown plotted against average number. Average number is an arbitrary designation for a given 15-point average. The error bar at the left hand side of the page represents the standard deviation above and below the mean. The data used are records 1 through 9, elemental filters +14.6 Hz through +41.2 Hz. It can be seen that most of the points are within, or nearly within, one standard deviation of unity.

To see whether the observed scatter was really within the expected bounds, χ^2 test was performed. This resulted in a χ^2 of 18.7 for the 18 points. The probability that the χ^2 could be as large or larger than this by chance is 42%. This is very reasonable and we may state that the results of this test are compatible with the assumption that the clutter density is stationary to within 26%. The variation in the data is comparable with what is to be expected from wave interference alone, therefore, any additional variation due to changes in the clutter object density must be smaller than this.

Experiment 352 was performed at Camp Drum, which is described as broken woods. The region is described as flat with woods of density varying from light to moderate; the density variations were like patches, several acres in area. This is about half the area of a 15-point average cell, therefore, such variations should be seen. The fact that they do not seem to indicate that mild variations in clutter density will have small effect on this radar. Note that the experiment described above was made with a large depression angle, approximately 32°, therefore, the signal travelled through relatively little vegetation before being backscattered. This data was from Variable 1, which means that it was both transmitted and received with horizontal polarization.

Shown in Figures 7.6 and 7.7 are the amplitude squared distribution and stationarity test for Experiment 352, Variable 3. This is cross-polarized data. This data was taken simultaneously with the Variable 1 data, however, it was received on a vertically polarized antenna. This data also seems to

A21610-J

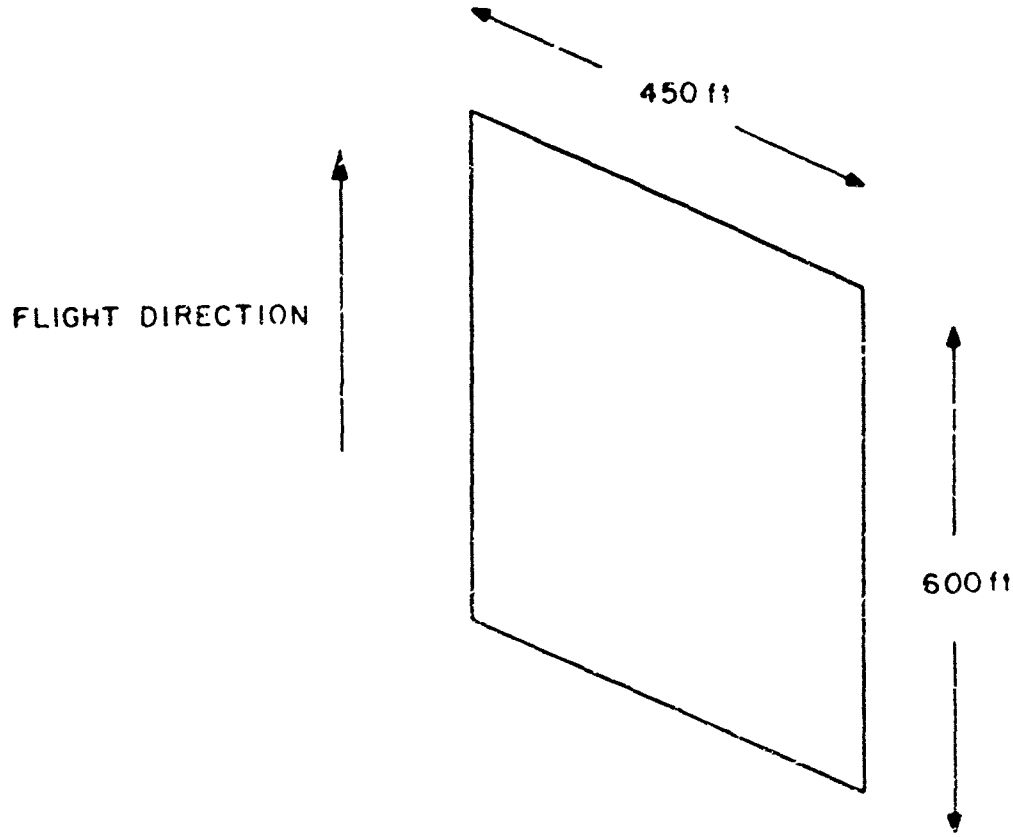

Figure 7.4 Typical Shape of Area Included in an Average Structure

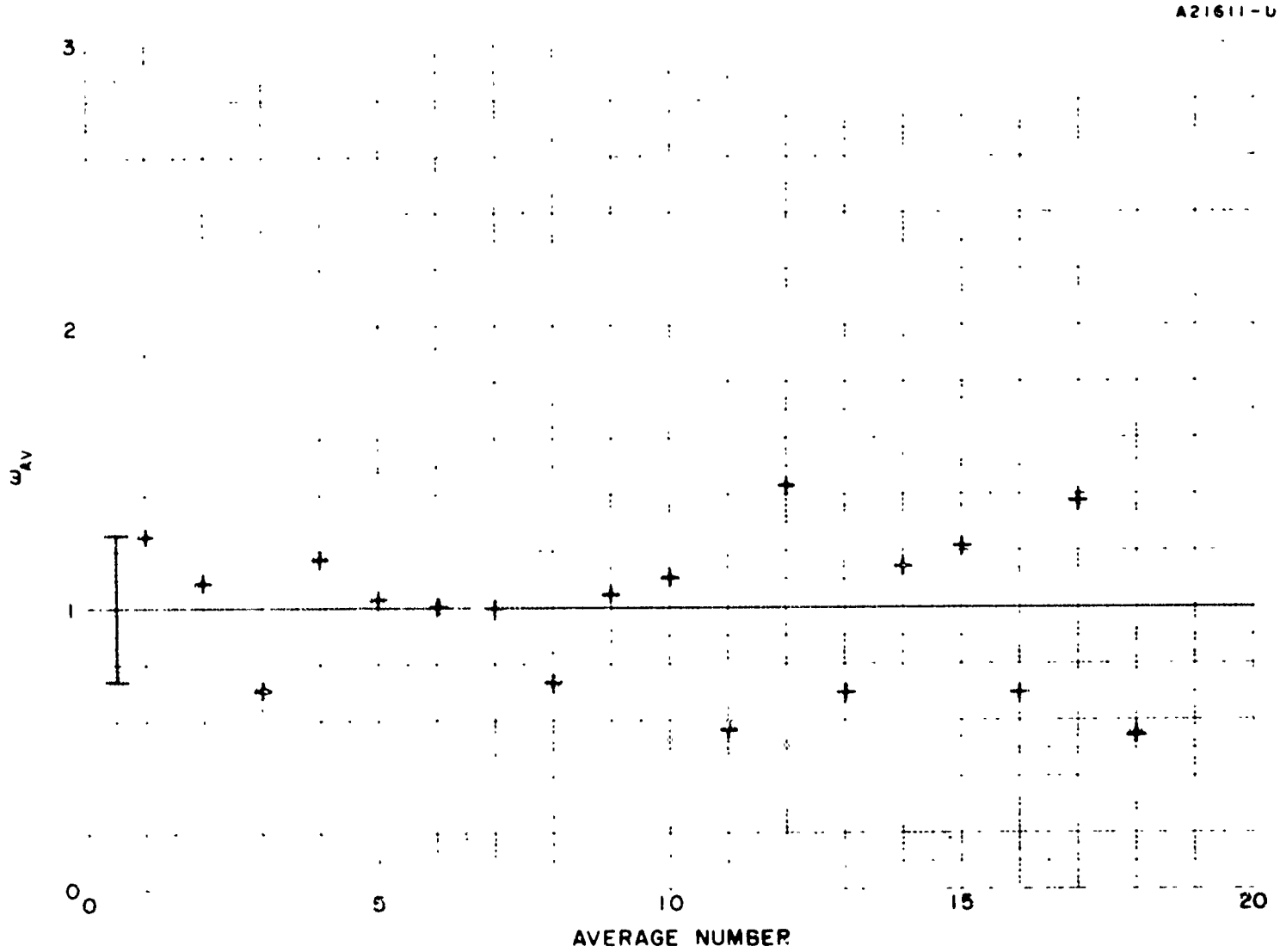

Figure 7.5. Stationarity Test Data for Experiment 352, Variable 1

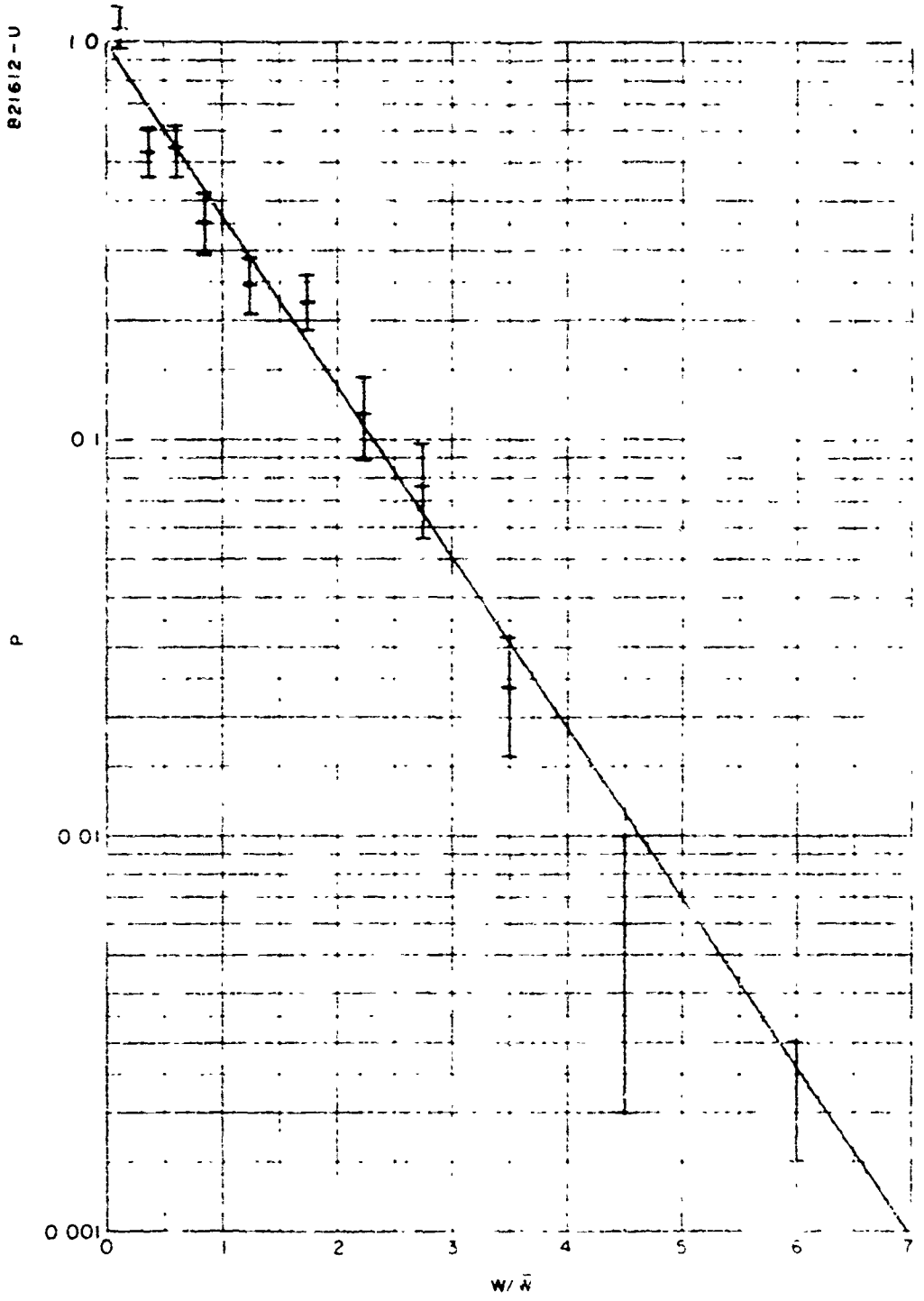

Figure 7.6. Amplitude Squared Distribution for Experiment 352

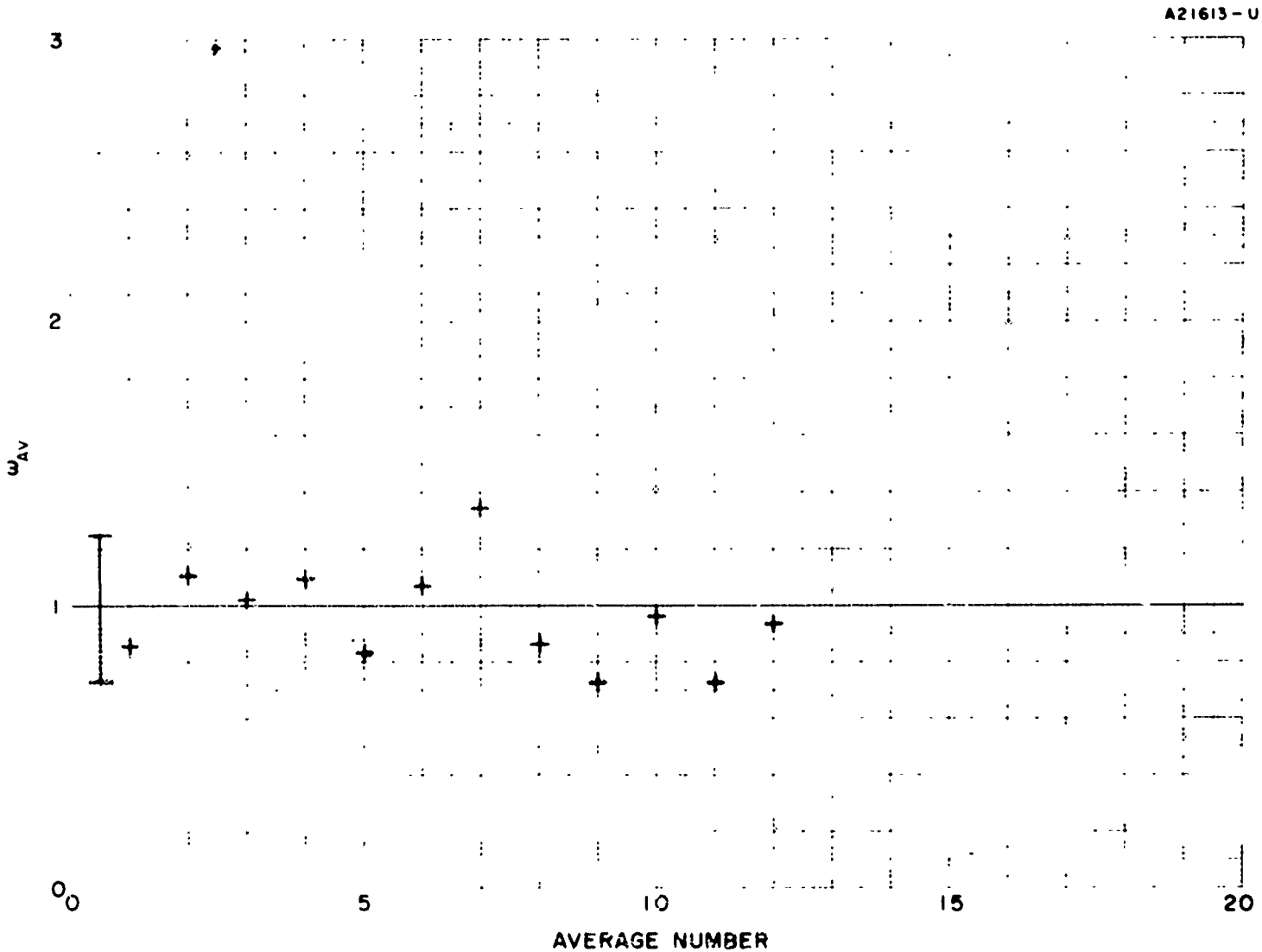

Figure 7.7. Stationarity Test Data for Experiment 352, Variable 3

follow the theoretical distribution. The distribution plot suffers somewhat from the fact that not enough data points were used. The χ^2 for the stationarity test is 5.40 for 12 points. The probability of a χ^2 this large or larger by chance is 93%. Therefore, the cross-polarized data also seems to be stationary.

Figures 7.8 and 7.9 show the distribution and stationarity test for Experiment 248, Variable 1. This is horizontal polarization data taken at low depression angles, about 3.5°. Therefore, the signal travelled through much vegetation before being backscattered. This data was also taken at Camp Drum. With the exception of one point, the data follows the theoretical distribution quite well. Note, however, that the stationarity test plot shows very large deviations from the mean. The very large point at the far right is probably a target of some kind. Excluding this point, the χ^2 was 37.8 for 17 points; there is only about 0.2% probability this could be due to chance. Therefore, this data seems to be non-stationary. We cannot say now whether this is due to the low depression angles used or to the terrain.

Figures 7.10 and 7.11 show data from Experiment 647, Variable 1. This data was taken in Tully Forest, in the rolling hill region south of Syracuse, New York. The depression angle for this experiment is about 30°. Figure 7.11 shows that the data is clearly very non-stationary. The distribution from the theoretical line, in the form of a tail at large values of W. Both of these effects are probably associated with backscatter from sharp facets of the hillside or ravines. As was pointed out earlier, the theory is not expected to work in such a case.

We conclude then that the clutter can be taken as stationary to within about $\pm$25% in some realistic cases. When the vegetation is very patchy or in hilly terrain, the clutter will be non-stationary. The theoretical probability distribution obtained in the previous section fits the data very well, except in the case of hilly terrain. Hence, the theory may be used with some confidence for evaluating signal processing systems.

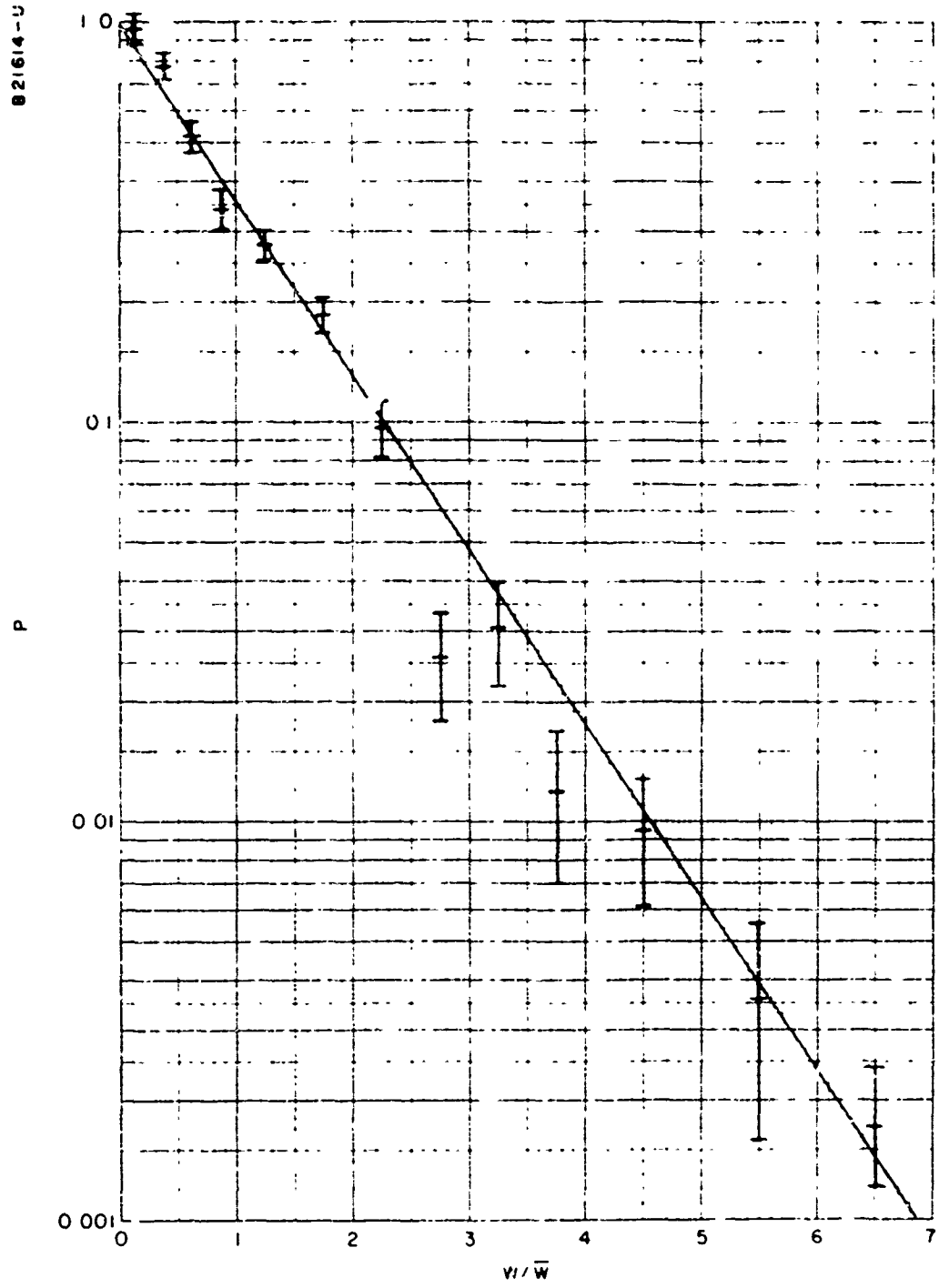

Figure 7.8. Amplitude Squared Distribution for Experiment 248

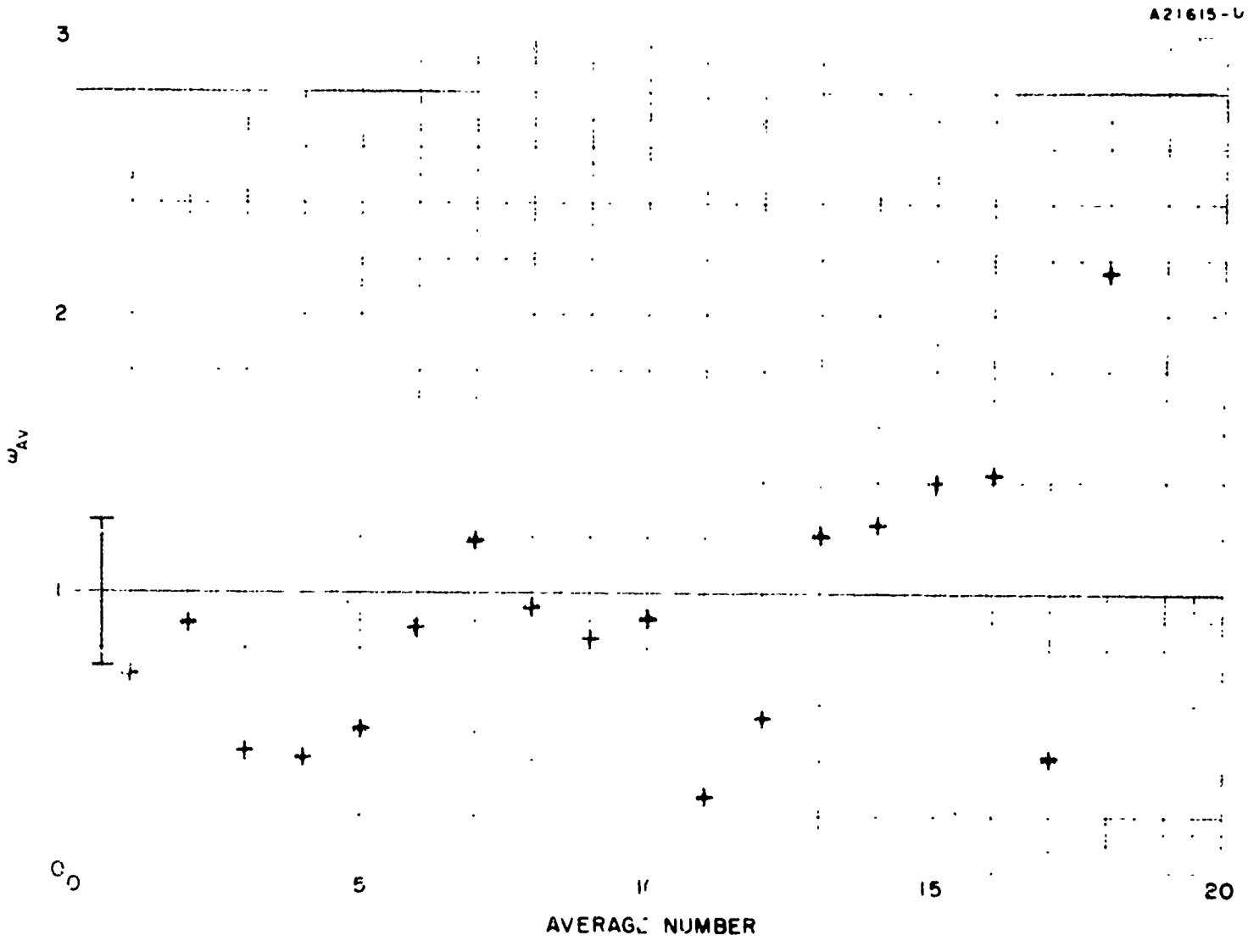

Figure 7.9. Stationarity Test Data for Experiment 248, Variable 1

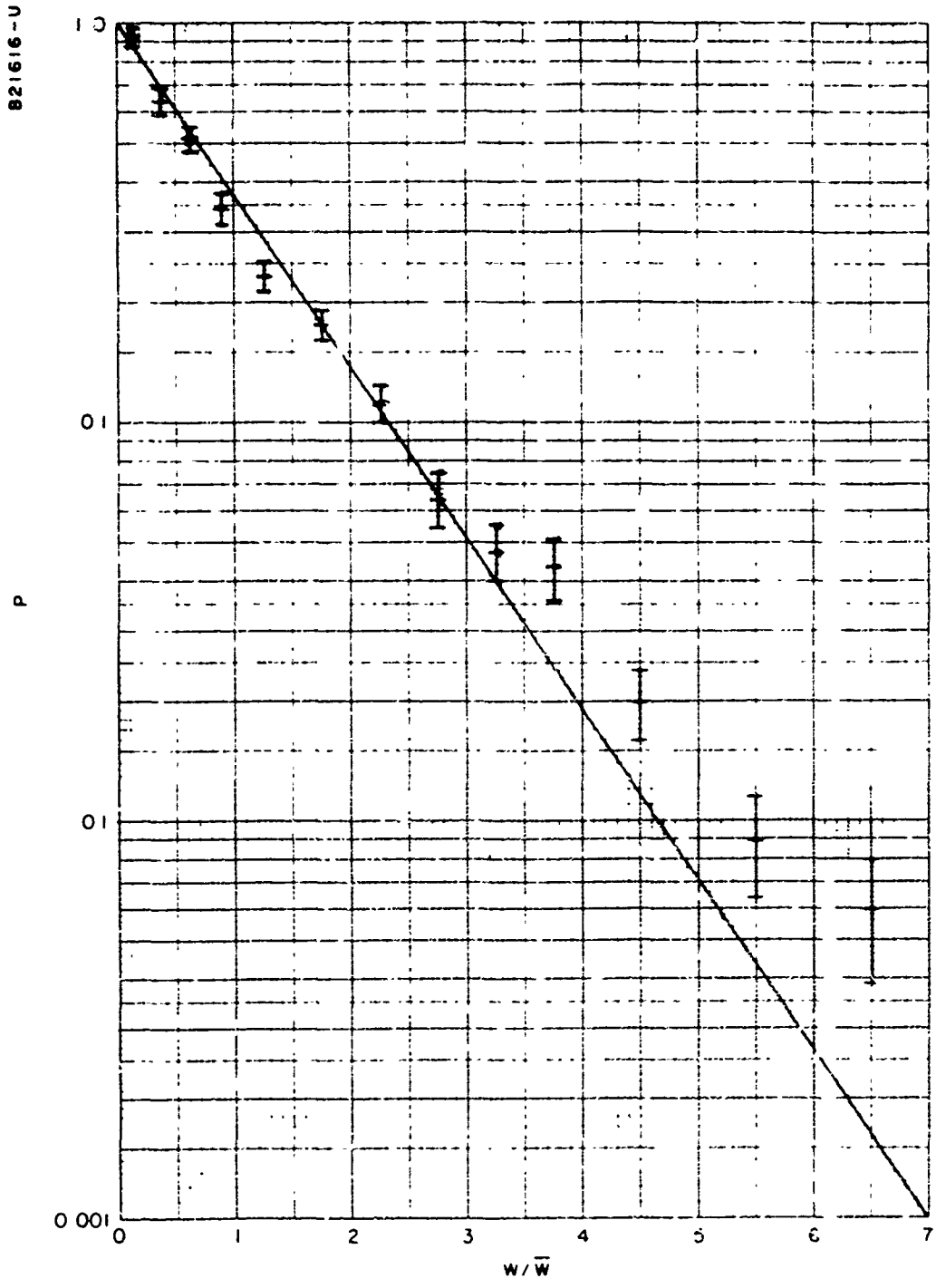

Figure 7.16. Amplitude Squared Distribution for Experiment 647

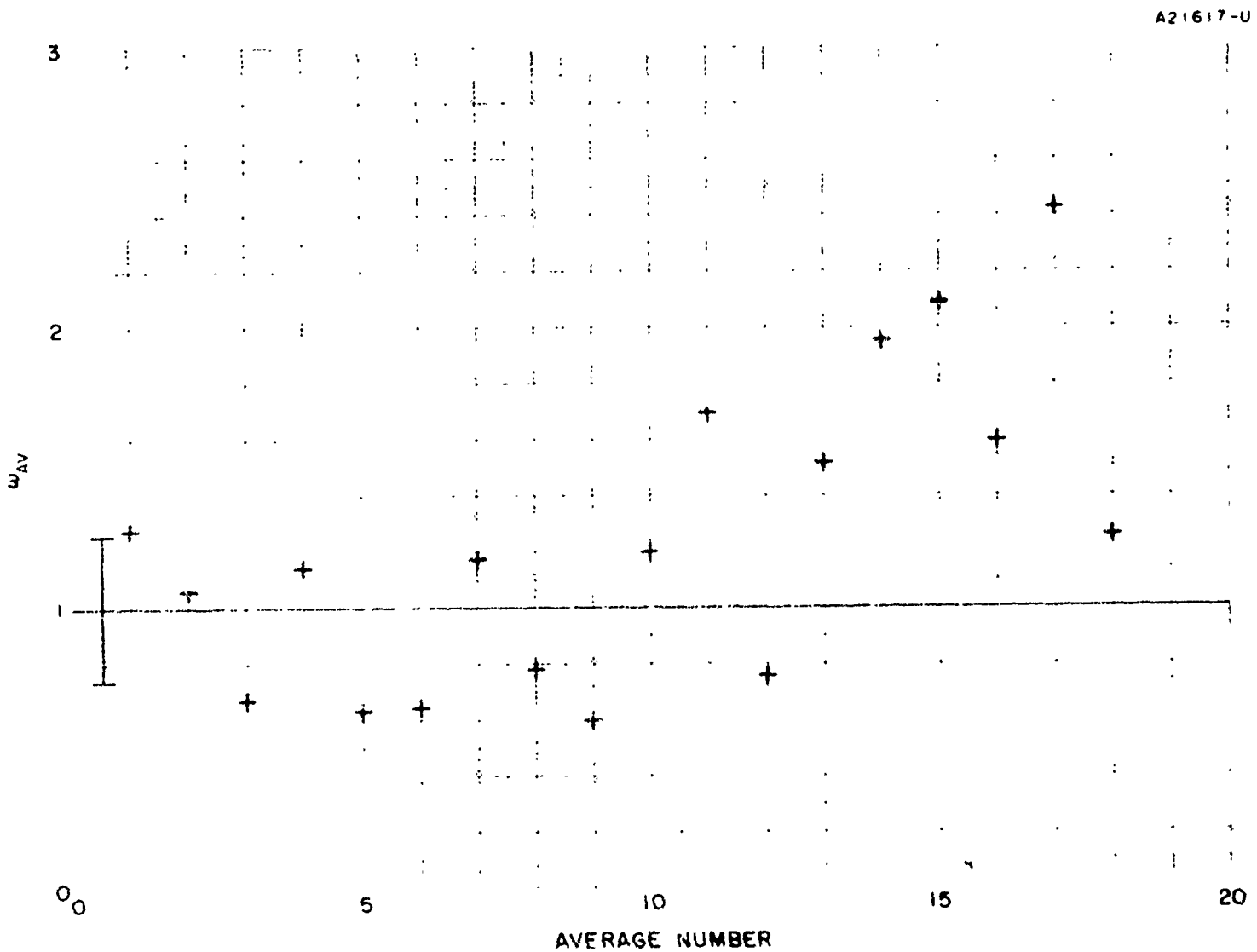

Figure 7.11. Stationarity Test Data for Experiment 647, Variable 1

8.0 MAJOR RESULTS - OVERALL PROGRAM

A prime objective of the program, that of developing an inexpensive airborne radar for data collection and utilization on a real time basis was accomplished. The data collected indicated a change of frequencies would be beneficial. This change has progressed in orderly, planned increments.

Data collection accomplished after the frequency change indicates that further work should be considered. A statistical model (presented in Section 7.0) was theoretically derived which adequately describes the statistical data collected.

The concept of an airborne foliage penetration radar has been economically demonstrated. An unfocused synthetic aperture was utilized in conjunction with a successfully implemented hardwired FFT to form in a small package a real time data collection and processing system.

The use of 140 MHz in measurement of clutter returns was accomplished. Cross sections of lakes, pastures and woods have been determined.

The lake data reinforces the data from other programs that indicates the cross section is a function of wind velocity and direction of the measurement since the returns are a function of the wave fronts and crests. Of particular interest is the method of reducing the effect of the "horns" in the processed data, i.e., the method of computation can result in the elimination of an expected, but undesired result.

Pasture data indicates that returns from fences, occassional trees and perhaps a slight roll to the land provide the majority of clutter cross section of this environment. As shown in the following table, the large differences in cross sections measured for different terrain samples actually reflects differences in terrain type and is not just due to the random nature of the scattering process.

Table 8.1 Cross-Section Data

Terrain Description	Freq. Range cps.	σ_o
1. Open Field-flat	-10 to 10	0.000013
2. Open field-rolling	20 to 50	0.0013
3. Woods	15 to 25	0.17
4. Same	5 to 15	0.15
5. Same	-5 to 5	0.10
6. Hill with scattered trees	-10 to 10	0.046
7. Same	-25 to -5	0.03?
8. Field (unknown target)	-40 to -30	0.019
9. Same	-35 to -25	0.028

σ_o is the radar cross section per unit area of terrain surface.

Each cross section shown is the post square average of all frequency points within the frequency range shown. Each frequency point is the post square average (over time) of 8 FFTs with I shift = 64.

Of more significance is the forest cross section data since it is not obtainable from current available literature. Included in the data base is a substantial amount of data on the cross sections of northern forests both coniferous and deciduous. The cross section of the forests, as measured, varies in σ_o between 0.1 and 0.2 at 140 MHz.

The utilization of the FOPEN system combined with the theoretical work accomplished has led to the following results. The output of the radar, when flying over vegetated terrain, is always a rapidly fluctuating, noise like signal. These fluctuations are of two kinds. First, a rapid fluctuation which is due to the random interference of waves scattered from different trees. Secondly, a slower modulation of the rapid fluctuations by an envelope which is due to the actual variation of vegetation density.

It is shown theoretically that the clutter voltage signal from a uniform, random forest should be Gaussian White noise over a passband of doppler frequencies corresponding to the center of the antenna pattern (for a side-looking antenna). The signal at the output of the radar (after absolute squaring) should therefore have an exponential distribution of amplitudes.

This conclusion was tested against SURC radar data. The data was found to fit the expected distributions to within the expected standard deviation for all valid cases studied. This fact allows one to find the expected target detection probability and false alarm rate for any given threshold setting and target to mean clutter ratio, simply by using the graphs published in most radar handbooks.[1] In this way it can be seen that acceptable radar performance demands that the target signal be about 13 dB above the mean clutter signal in order that the large upward random fluctuations of the clutter do not cause excessive false alarms.

Signal processing methods for a radar such as this may seemingly be divided into three groups, averaging methods, subtraction methods, synthetic aperture and focusing methods. Synthetic aperture and focusing aim at reducing the clutter by reducing the size of the resolution cell. Unfocused synthetic aperture is in use on the present system. Focusing could improve the resolution to about 15 ft. by 15 ft., which would yield a 15 dB increase in target to clutter ratio. However, it seems that focusing is too complex and expensive for the present system requirement. Synthetic aperture methods are well known and the present system is described elsewhere, hence this

[1] "Radar Handbook" by Merrill Skolnik, page 2-21.

method will not be discussed further here.

Subtraction methods attempt to reduce the clutter signal with respect to the target signal by subtracting the signal from itself at some later time. Such methods were studied theoretically in the report by Foster and found to yield little improvement for the present system, and such methods were studied using real data and obtained only marginal results. It is concluded that such methods have little to offer for the present problem.

The most useful signal processing method for the present problem seems to be averaging. Several radar amplitude signals from the same patch of ground but taken at different times are averaged together. This requires that the signals be taken from different doppler frequency bins if the target is near zero azimuth (measured from the side-looking direction) and at different range bins of the target is at larger azimuth. In this way the size of the random amplitude fluctuations of the clutter signals are reduced, hence the target to clutter ratio required for good detection is also reduced. This averaging is equivalent to the post detection integration used in many conventional radar systems. Hence the curves published in radar handbooks may be used to predict the performance of averaging systems. It is found that the target to mean clutter signal ratio required for good detections decreases as 1/N, where N is the number of points averaged, as long as N is less than about .5. For larger values of N, the ratio tends toward $1/\sqrt{N}$. Of course, these statements require that each value averaged by statistically independent of all the others. It is shown theoretically in the report by Foster that this requires a minimum time lapse of T/2 between points averaged. Here T is the time length of data in each discrete Fourier Transform. In other words, about half the data in each discrete Fourier Transform should be made redundant in order to obtain the maximum number of independent points for averaging. Much larger redundancy factors have been experimented with using real data at the SURC computer. There seems to be some slight indication that redundancies larger than 50% are of use, but the issue is not clear. In any case, the difference is small.

Most of the theoretical results quoted above are computed on the basis of a uniform forest with no other forms of clutter present. Nonuniformity makes little difference as long as the variation is slow with respect to a resolution cell. The computational results are not changed for N less than about 5, which is the case of most practical interest.

The actual improvement to be expected from averaging with the present system is hard to estimate as it depends on many factors. If the target is directly broadside of the aircraft, it remains in the range cell a long time and many independent points are available for averaging. If the target is

ahead of or behind the aircraft, it passes through the range cell quickly and several range cells are necessary if the target is to be tracked. Summing the target signal as it passes through several range cells is quite difficult. Assuming this can be done and taking the number of range cells to be the present number of 3, the number of independent points available for averaging (over the entire arc of the range cell) is 3. Hence about 5 dB less target signal is required for good detection than for a system without averaging. No such processor has been made to operate at present due to the difficulties involved in tracking the target through several range cells. Several methods of accomplishing this are being considered at the present time.

8.1 Major Results - Detection Analysis

The main object of the radar is to detect tactical targets in foliated environment. It appears to be possible to detect large tactical targets in all but the heaviest types of woods using the present system operating at 51 MHz. Unfortunately the present test program was not able to demonstrate this due to lack of time and funds. However, since the radar cross section of the vegatation has been measured and the cross section of tactical targets is known from other work, it is possible to predict the performance of the radar from theory.

The radar cross section of a small truck has been measured at a frequency fairly close to 51 MHz.[2] The maximum value is 2,000 sq. ft. and occurs at 50° depression angle. The average value for depression angles is the range 20° - 40° is about 1,000 sq. ft. These values are said to be the median values of measurements taken over all aspect angles. These values are in rough agreement with a simple theoretical model used to predict radar cross section at these frequencies.

The radar cross section (with the targets at broadside aspect) will increase roughly as the square of the target dimensions. Hence a medium-large truck might be expected to have a cross section of about 5,000 sq. ft. We shall rather arbitrarily take this as the size of the target to be detected in this example. A target of this size might also be made up of several smaller trucks or tanks in a group.

It must be recognized that, at this frequency, trucks can only be detected at aspect angles fairly near to broadside. Since the width of a truck is less than a half wave, the cross section is very small off the ends. Hence, in order to search an area, it would be necessary to fly over it from several different azimuth angles.

---

[2] "Long Range Standoff Radar Surveillance Study" by W. Chudleigh and S. Moulton, Control Data Corporation report AFCRL-TR-73-0145, Figure 3-1.

For the sake of this example, we will assume the truck to be hidden in a medium density forest, such as that found at Vincent Corners. This woods is described in Section 6.3. This woods was very uniform and had a mean σ_o of 0.02 at 51 MHz, measured at 20° depression angle. A study of σ_o vs. depression angle was not performed at 51 MHz, however, experience at 140 MHz, as well as general results from the theory of random scattering, led us to believe that σ_o varies only slowly with depression angle. Hence the above value of σ_o can probably be used at 30° - 40° depression angle, which is the optimum range for detecting trucks.

Let us assume that the aircraft flies at a height of 2,000 ft. and a depression angle of 40° is used. The slant range is then 3,100 ft. and the area within a single resolution cell is 20,000 sq. ft. This area is then multiplied by σ_o to obtain 400 sq. ft. mean clutter cross section per resolution cell. The target to mean clutter ratio is therefore +11 dB.

We must now calculate the probability that the target may be detected and an expected false alarm ratio. Even at 11 dB above the mean, there is an appreciable upward fluctuation of the clutter signal may cause a false alarm. This calculation is made simple by the fact that the signal backscattered from a reasonably uniform forest is a Gaussian process.[3] The detection probability and false alarm rate may therefore be computed from the graphs published in most radar handbooks. Using the curves given in Skolnik's Radar Handbook[4], we find that for a 90% detection probability and an 11 dB target to clutter ratio, the false alarm probability is 10^{-3}. This is the false alarm probability for a single measurement of a single cell. If the forest covers the entire radar screen, the false alarm rate for the total presentation must be computed. About 15 resolution cells are displayed for each presentation. In order that any target will be in the range cell for at least most of one DFT period, 2 presentations must be computed per one second DFT period. Hence 30 resolution cells per seoond are displayed. Therefore the false alarm rate for the entire display is .03 per second or about 2 false alarms per minute.

This is too high for most practical use, however, this is computed for the display system as it now stands with only one range gate displayed. When all 3 presently available range gates are displayed, a certain amount of averaging will take place in the refresh buffer of the display system. This is analogous to the video integration which takes place in a conventional PPI radar. There are some difficult questions involved with the fact that the target will

---

[3] G.M. Foster, "A Study of Clutter in Moving Platform FOPEN Radar." SURC TD 73-190.

[4] Merrill Skolnik, "Radar Handbook," pages 2-19 to 2-23. These curves are for linear detection rather than square law detection as used here, however, the difference is only a fraction of a dB.

straddle two range bins part of the time, however, it is felt that the loss due to this fact will be small. We will take the performance of the system with 3 range cells to be equivalent to 3 pulse video integration. We then find that a 90% detection probability, an 11 dB target to clutter ratio yields a false alarm probability of 10^{-10}. This is a false alarm rate for the entire display of only 10^{-5} per hour. This is clearly negligible and the system could be used effectively in this situation. About 2 dB of target signal could be sacrificed and acceptable performance still obtained.

The clutter we have been discussing here is distributed clutter, i.e., the clutter is distributed more or less evenly over the resolution cell. One must also consider discrete or point target clutter. This clutter is caused by objects of large cross section which are much smaller than the resolution cell. Examples of such objects are small, very dense stands of very large trees, small but steep hills, man made objects such as power lines or buildings. Such clutter is indistinguishable from the objects we wish to detect and cannot be reduced by averaging. Very little can be said about such objects as their occurrence cannot be predicted. However, such objects can usually be visually seen from the aircraft and can then be disregarded.

If we now turn to a more dense type of forest, such as that found at Swamp Road, we find the situation is more difficult. This region contained some very large trees and the vegetation was in general very uneven. Some of the larger returns observed were probably discrete type targets. The average returns in the denser areas were about 5 dB higher than at Vincent Corners. Acceptable radar performance here would require a target cross section of about 10,000 sq. ft. or an increase in the number of range gates to 8 (for a 5,000 sq. ft. target).

It should be mentioned that these estimates of detectability do not include the important factor of operator training. A trained operator can often pick out targets of interest even when they are not detectable by the usual threshold criterion. For this reason, the above calculations should be considered conservative estimates.

8.2 Major Results - Radar

A prototype radar was assembled, tested, and utilized for the required data collection.

8.2.1 Side Looking vs. Forward Looking Radar

Additionally it was determined early in the program that to reduce the clutter return the antenna had to be shifted from forward looking to side looking. This change effectively reduces the clutter that impinges on the filter elements therefore the signal to clutter ratio is improved. As indicated in Section 8.5, "Polarization Study Results," the forward looking radar was utilized and data presented, however, the balance of the data presented was collected using the side looking radar.

8.2.2 Focusing

The tests also indicated that the use of 140 MHz does not seem appropr ate for this type radar without more sophisticated techniques of beam focusing to reduce the resolution cel! to 15 feet by 15 feet. When operating at 140 MHz the clutter return and the standard target return were inseparable. The need for an additional 10 dB for reliable target resolution was indicated.

Going to a focused synthetic aperture system would yield considerable improvement in target detectability as indicated in SURC TD-73-190. Although such systems could probably be made to yield acceptable detection rates, they involve considerable more complexity and cost. Thus focusing was outside the scope of the program, but may be worthy of consideration for future effort.

8.2.3 Carrier Frequency

In the search to further improve the target to clutter ratio a modification was made to the radar to change the carrier frequency to 50 MHz. Theory indicates that when considering tree trunks to be dielectric cylinders with diameters much less than a wavelength, their cross section should vary as the fourth power of the frequency (in this frequency range). Therefore, for a threefold frequency reduction a 20 dB reduction in clutter cross section should result.

This modification was completed and a comparison of results of the processing of test data at both frequencies are presented here:

Test Area	σ_o at 140 MHz	σ_o at 50 MHz
Swamp Road	0.84	0.3
Vincent Corners (boot shaped woods)	0.15	0.022

These results indicate a significant improvement in the target to clutter ratio at 50 MHz. These results warrant a recommendation that further work be funded for this promising avenue of investigation.

8.3 Major Results - Data Analysis System

A complete prototype data analysis system was devised, fabricated and tested for use as the processing portion of the airborne foliage penetration radar. In doing so, the concept of a real time reliable detection and analysis system was demonstrated.

An operators position complete with display and keyboard was developed

and utilized. As pictured in Figure 1.1 the position provides for real time airborne monitoring of data collection.

The processing routines developed for the data analysis and display systems are illustrated in Section 2.8 and completely described in the operation and maintenance manual provided with the system. These routines have been shown to be necessary and extremely useful when utilizing the system.

8.4 Major Results - Data Collection

The airborne data collection experiments have shown:

1) A close correlation between the known terrain and the collected data.

2) That the collected data was sufficiently reliable to include in the data base.

3) The ability to experimentally determine radar cross sections of both point targets and distributed clutter.

4) At 140 MHz certain background environments result in poor target resolution.

5) That operation of the radar at 50 MHz enhances the clutter to target ratio.

The Vincent Corners Tests yielded the most significant results, they were:

1) Fence lines and large stands of woods can give returns as strong as the standard target.

2) The use of a simple threshold detector in this environment is not practical.

3) Man-made objects and natural objects with sharp changes in cross sections cannot be separated from other corner reflector-like objects such as trucks.

4) The standard target return is discernible and measurable (Although tests were conducted with the target in open areas and not shaded by trees).

5) The calculated spectra and observed terrain are closely correlated.

In addition, the other tests provided results which included:

1. The close correlation of the calculated and measured glint radar cross section of a helicopter was very encouraging. It is noted that the tactical usefulness of glint radar cross sections is probably minimal since it is highly dependent angle of arrival the broadside illumination of a vehicle. Other attempts to correlate the recorded returns with expected returns were less successful than at the Aberdeen Proving Grounds due to test conditions.

   While experimentally unsuccessful, during the test period, it should be emphasized that the magnitude of the glint cross section of a panel truck or armored personnel carrier should be sufficient to discern from the background clutter of the environments tested.

2. During the contract period significant portions of the collected data were included into the data base. Especially noteworthy are cross section measurements of forest environments that are not currently found in the available literatures (for northern forests are on the order of 0.1 and 0.2 at 140 MHz).

8.5 Major Results - Polarization of Signals Backscattered from Forest Terrain

The analysis has been derived from data collected under contract DAAD05-71-C-0156, but not analyzed at that time.

For this experiment a cross-polarized antenna was mounted on the front of a DC-3 aircraft in which the LWL-SURC FOPEN Radar, operating at 140 MHz was mounted. The transmitter was connected to the horizontal element via the usual duplexer system. The backscattered signal was received on both the vertical and the horizontal antenna elements and recorded on separate channels of the digital tape recorder. On the ground the data from each channel is fast Fourier transformed and the amplitude found in the usual way.

The experiments analyzed are numbers 299 and 300 taken at Camp Drum in Northern New York State and numbers 180 and 181 taken at Pompey Center Road near Syracuse, New York. The terrain at Camp Drum was flat and fairly heavily wooded with northern pine. These pines are a small pine with trunk diameter 6-12 inches and very thin branches. The region around Pompey Center Road is unevenly wooded, mostly with deciduous type trees. This region is not a forest, but contains steep hills, pasture land, houses and fences as well as trees. This region has not been checked in detail from the ground, hence it is not known exactly what is within the measuring cell at a given time. It is probable that most of the backscattering comes from trees of the deciduous type.

In most of the data analysis done at SURC, only the horizontal received channel has been considered. In what follows, the vertical channel will also

be considered. First, the possibility of correlation between the two channels will be considered. This is important because, if there were correlation, it could be used to subtract out or reduce the clutter signal. Amplitude correlation was checked for by superimposing a graph of the vertical channel amplitude output over the graph for the horizontal output taken at the same time. The two graphs are then viewed with a transparency viewer. In this way it is easy to notice any correlation between the fluctuations.

It is observed that there is no correlation between the rapid amplitude fluctuations of the two channels for any of the data. In cases where the envelope varies appreciably, it is approximately the same for both channels. This is expected since trees cause the signal for both channels, however, different parts of the tree contribut to different channels didferently. No attempt was made to test for phase correlation. It seems unlikely that there would be phase correlation of there is no amplitude correlation. No numerical correlation analysis was performed, since small correlations were of no interest.

The next step of the analysis is the comparison of the absolute magnitude of the signal amplitude in the two channels. This is done by taking the average of the amplitude of the same four points from each channel. The ratio of these values is then found and corrected for the difference in receiver gain between the two channels. The ratio (in decibels) of the horizontal channel amplitude to the vertical channel amplitude for 5 such averaged points from Experiment 299 (Camp Drum) data are shown below.

	+30.8
	+23.4
	+25.1
	+37.0
	+34.5
Average	+30.2 dB

The points were selected at random from the region around maximum envelope amplitude[6]. Points from Experiment 300 (also Camp Drum) gave very similar results. It is seen that the horizontal signal is much larger than the vertical. It is hard to know if the average ratio of 30 dB has any meaning. This ratio is so large that the small vertical signal observed might well be due to depolarization effects of the aircraft. One may conclud. that the

[6]It should be mentioned that points taken at low azimuth angles (toward the side of the aircraft) tended to have horizontal to vertical amplitude ratios smaller than indicated above. This is thought to be due to the difference in antenna patterns for the horizontal and vertical elements. The antenna is pointed forward, so points taken to the side are in the edge of the main lobe. The horizontal element should have a sharper pattern in the horizontal plane than should the vertical element, hence the horizontal to vertical ratio appears smaller than it should.

average vertical backscatter is at least 30 dB smaller than the horizontal. This result is not too surprising, since the type of trees involved, northern pine, tend to have very straight, vertical trunks and thin branches extending out from the trunks at almost right angles. Since the backscattering cross section of a dielectric cylinder, much smaller (in diameter) than a wavelength varies as the fourth power of the diameter, the thin branches have negligible scattering cross section in comparison with the trunk. This result has some practical importance. Any target which depolarizes strongly can easily be detected in a pine or similar forest. Any target which has elements at an acute angle with respect to the horizontal will depolarize. Examples of such targets are rocket launchers in launch position, howitzers, men carrying rifles, etc. Note that a 100 foot by 100 foot resolution cell of fairly dense forest usually has a horizontal cross section of about 2,000 sq. ft. The corresponding cross polarized vertical signal cross section for a pine type forest would only be about 2 sq. ft. A man carrying a rifle has a cross section of about 30 sq. ft. If the rifle is carried in any attitude other than perfectly horizontal or vertical, a large fraction of the energy will be scattered into the cross-polarized channel. Therefore, even a small group of men carrying rifles should be detectable in a pine or similar type forest.

Finally, the polarization characteristics of trees other than pine must be considered. It is clear that a tree whose branches are thick and reach out at an acute angle will respect to the vertical, such as an oak, must backscatter nearly as much energy into the vertical channel as into the horizontal. Most deciduous trees fall somewhere in between the branch dominant type (oak) and the trunk dominant type (pine).

An analysis was made of Experiments 180 and 181 taken on Pompey Center Road. This region contains many deciduous type trees but unfortunately also contains steep hills, farm land, buildings, etc. The average horizontal to vertical power level ratio, computed as before, was +6 dB. Clearly, here the backscattered signal is greatly depolarized. However, one cannot be sure this depolarization is due to trees, as it might be the result of hills or buildings. Hence the question of the depolarization ratio for deciduous type trees is still open. All that can be said is that it seems likely that branch dominant trees will depolarize the scattered signal strongly.

In conclusion, it has been found that trunk dominant type trees preserve the polarization of the incident wave when backscattering. For a forest of northern pine at Camp Drum, New York, the cross-polarized component average was at least 30 dB below the polarization conserving component. This means even very small targets which depolarize, such as men carrying rifles, can be detected in such a forest. Other depolarizing targets which could be detected include howitzers and rocket launchers in launch position. The case for branch dominant type trees is still unclear, however, it seems such trees must depolarize the backscattered signal strongly. If this is ture, polarization methods will be of little use in the presence of such a forest. It has been found that there is little or no correlation between

the fluctuation envelopes for the two channels. This could be used to subtract or reduce the clutter signal if the rapid fluctuation could first be averaged out.

There does not appear to be any significant correlation in the fine structure of the variation of the signals from the vertical and horizontal receive channels. When horizontal wave is transmitted and the target is deciduous forest, the horizontally received and vertically received signals are of the same average amplitude. When the target is conifer forest, the vertically polarized received signal is about 20 dB weaker. This means that certain types of targets which depolarize a radar wave strongly, such as missile launchers, field guns, etc., could be detected in a conifer forest by the use of polarization ratios. The detection of personnel does seem feasible from this platform by using polarization ratios.

9.0 RECOMMENDATIONS FOR FUTURE WORK

Every program being brought to a successful conclusion has areas of interest that deserve additional effort. Based upon this program and previous efforts, the following recommendations are presented for future effort.

9.1 Continuation of the 50 MHz Effort

Based upon the improvement in target-to-clutter ratio resulting from the reduction of the carrier frequency to 50 MHz a continuation of this effort is recommended.

The benefits which may accrue from this continuation include: data collected could fill a void in defining typical forest clutter. Measurements of σ_o have been made by SURC at 140 MHz. Lower frequency values, σ_o, theoretically derived, indicated an improvement of at least 15 dB should be expected. Initial measurements indicated an actual reduction of 15 dB in heavy forests. Further measurements could confirm these computations and such a continuation would provide a complete in-flight test program of the system.

9.2 Continuation of Glint Cross Section Measurements

The application of this technique may be of limited value; however, the close correlation of expected returns and actual returns indicates that its potential value for specialized applications merits continuing the effort.

9.3 Addition of Focusing

It has been mentioned that a focused synthetic aperture system would yield some improvement in target detectability, but involves considerable complexity and cost. However, this system is small and inexpensive and may well provide the basis for an inexpensive focused system. An initial feasibility study is recommended with the ultimate objective of adding focusing to this system.

It is felt that additional work with multiple range gate averaging would sharply improve detectability in distributed clutter. This work could be initially accomplished with the existing data base through injection of simulated target signature into the clutter data base currently available. This simulation would be used to gauge the effectiveness of additional multiple range gate averaging.

9.4 Polarization Studies

It has been found that the cross-polarized backscattered component from a forest of trees of the vertical trunk dominant type (such as pines) is very small. This allows the detection of even very small targets which depolarize a signal (such as men carrying rifles, field guns or rocket launchers) in this type of vegetation. If there is need for this type of detector, it is recommended that this method be further investigated.

APPENDIX A

MODEL CALCULATION OF BACKSCATTERER FROM VEHICLES AT VERY HIGH FREQUENCIES

by G.M. Foster

Introduction:

This report presents a simple model calculation of the VHF radar cross section of land vehicles such as cars, tanks, and trucks. The object is to obtain a rough estimate of the magnitude of the average and glint radar cross section rather than to perform an accurate calculation.

The Target Model:

At VHF the wavelength is of the order of several meters and is therefore somewhat smaller than the vehicles taken as a whole but larger than any "substructure" such as windows, tracks, wheels, etc. Therefore, at this wavelength, the side of the vehicle presents effectively a flat plane which makes a right angle with the ground plane. Consider the diagrams shown in Figure A1 on the following page.

The side of the vehicle and the ground plane form a two-sided 90° corner reflector. If the radar illuminates the target at right angles to the vehicle side-ground plane intersection line, i.e., $\emptyset = 0$, the target will glint as shown in Figure A2.

The term glint here is used in its exact sense, meaning specular reflection from a flat surface of dimensions greater than a wavelength. It will be shown that, for cases of interest here, this glint cross section is much larger than the off-glint cross section. In fact, the glint region dominates the average over all angles so that the glint characteristics determine both the glint cross section and the average cross section. Now the top and far side surfaces are never illuminated at an angle where they might glint (the $\emptyset \approx 0$ case is of no interest), therefore, they may be neglected for the purposes of this calculation. The front and back of the vehicle are also neglected as they are much smaller than the sides. The problem to be solved is then that of a flat plate of height b and length a set at right angles to an infinite ground plane. The gap between the bottom of the vehicle and ground will be ignored as it is much less than a wavelength.

To proceed with the calculation, the type of radiation incident upon the target must be specified. If the vehicle stands upon a bare plane, it is clear that this radiation is a transverse plane wave. However, if the target is in a region of dense vegetation or other obstacles, very complex wave shapes may develop. This calculation will be done assuming plane waves incident in order to keep things simple. The results may be expected to be valid for a vehicle on bare, flat ground or in light to moderate density

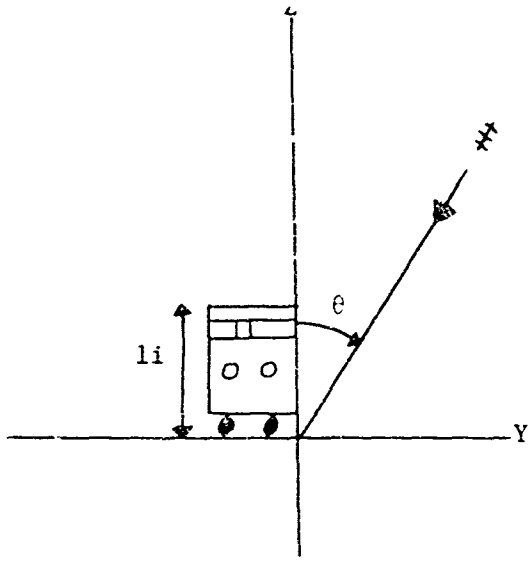

FRONT VIEW

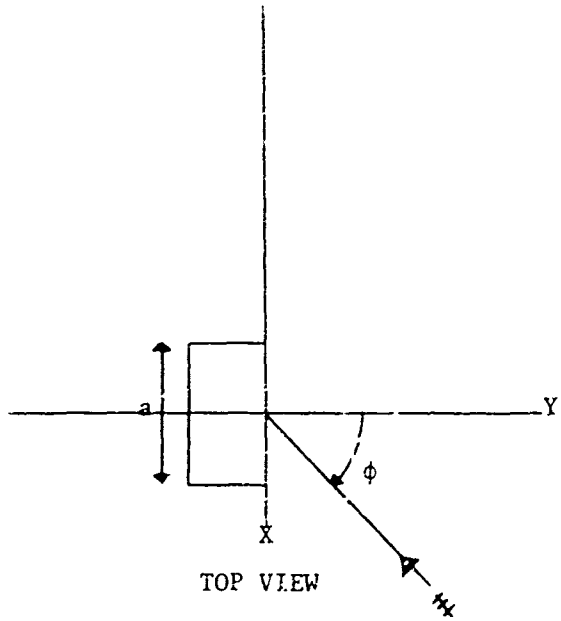

TOP VIEW

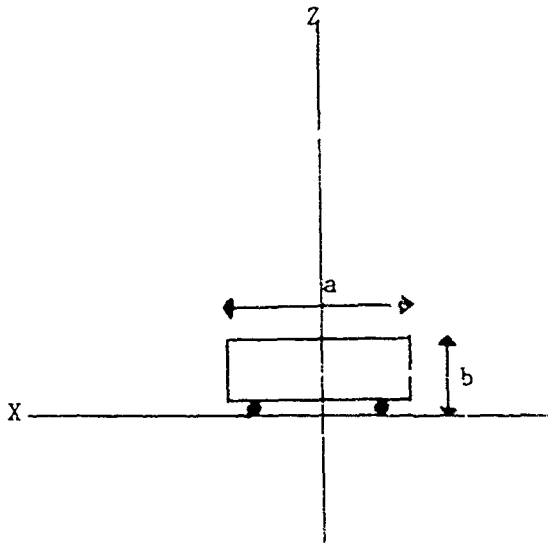

SIDE VIEW

Here R, θ, ϕ, are the spherical coordinates of the radar's position.

Figure A.1 Target Model for Backscatter Calculation

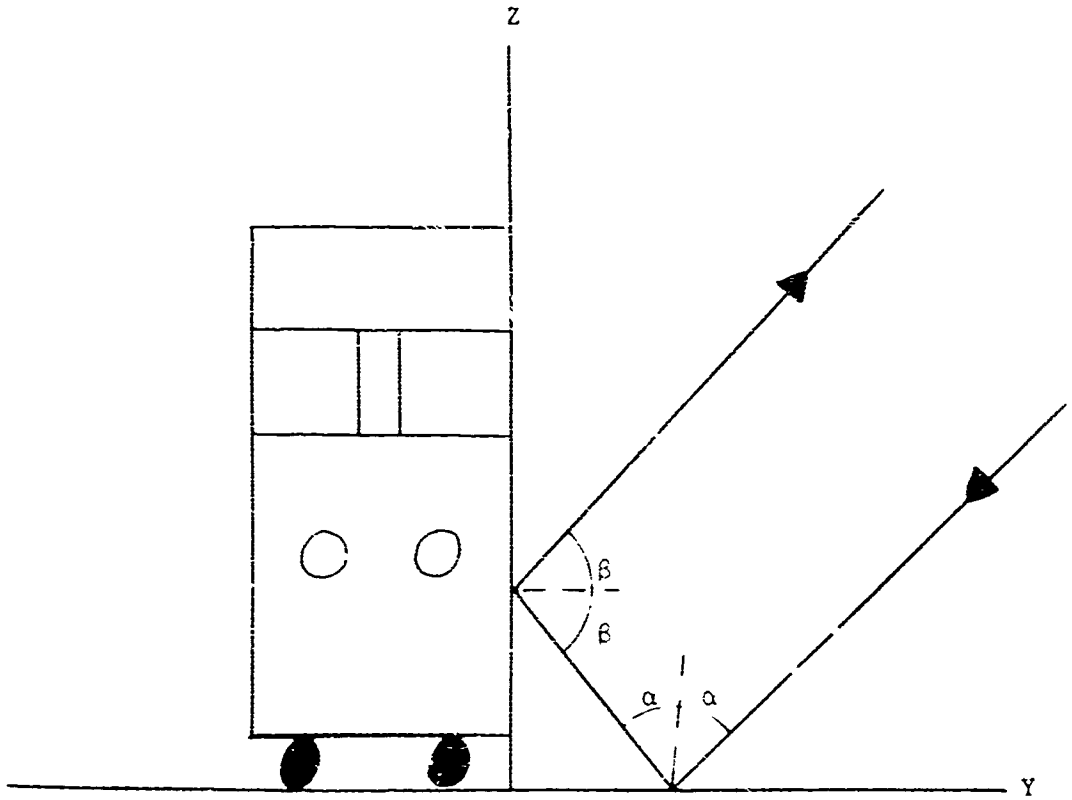

Figure A.2 Target Model for Glint Calculation

vegetation if the depression angle is fairly large (= small). It is very difficult to estimate how valid the calculation might be for small depression angles or very dense vegetation.

Calculation for Flat Plate:

To perform the calculation one evaluates the field scattered from a flat plate (neglecting the ground plane for the moment) using the vector Kirchoff integral.

$$\vec{E}(\vec{R}) = \int_S [(\vec{n} \times \vec{E}) \times \vec{\nabla}' G + (\vec{n} \cdot \vec{E}) \vec{\nabla}' G + ik(\vec{n} \times \vec{B}) G] \, dA' - i\frac{1}{k} \oint \vec{\nabla}' G \, \Delta\vec{B} \cdot d\vec{S}' \qquad (1)$$

where

$$G = \frac{1}{4\pi} \frac{e^{ikR_2}}{R_2} \qquad k = \frac{2\pi}{\lambda}$$

R_2 is the positive distance from the point x', y', z' to the observer point.

$\vec{E}$ and $\vec{B}$ are the fields at the point of integration. $\vec{n} = \vec{i}_y$ is the unit vector normal to the plate. dA' is the element of area.

The first integral is over S, the entire XZ plane including the surface of the plate. The second integral is a line integral used to represent the line charge which occurs at the edge of the plate. This integral is taken around the edge of the plate. $\Delta\vec{B}$ is the difference in the B field between the left and the right hand sides of the path of integration. This term arises due to the highly artificial boundary conditions used in Kirchoff theory.

The fields on S may be taken to be the sum of the incident plane wave E_0, and the scattered field E_s.

$$\vec{E} = \vec{E}_0 + \vec{E}_s \qquad (2)$$

$$\vec{B} = \vec{B}_0 + \vec{B}_s$$

If the incident plane wave term is put into Equation 1 and integrated, one must just get back the incident plane wave, therefore, this term is of no interest. Since the plate is somewhat larger than a wavelength, the Kirchoff approximation may be expected to be roughly valid and may be used to find $\vec{E}_s$ and $\vec{B}_s$ on S. According to this approximation, the scattered field on the plate is equal to that which would be obtained if the plate were infinite and the scattered field off the plate equal to zero. This gives:

$$\vec{E}_s \times \vec{n} = -\vec{E}_0 \times \vec{n}$$
$$\vec{E}_s \cdot \vec{n} = \vec{E}_0 \cdot \vec{n} \qquad \text{on the plate}$$
$$\vec{B}_s \times \vec{n} = \vec{B}_0 \times \vec{n}$$

and (3)

$$\vec{E}_s = 0$$
$$\text{off the plate}$$
$$\vec{B}_s = 0$$

Placing these values in Equation 1, integrating and assuming the distance of the observer point from the target, R_2, is much greater than the target dimensions, $R_2 >> a, b$, yields

$$E_\theta = A\,[\sin\alpha \sin\theta_1 \cos\phi_2 + \sin\alpha \sin\theta_2 \cos\phi_1 - \cos\alpha \sin\theta_2 \cos\theta_1 \sin\phi_1 + \cos\alpha \sin\theta_1 \cos\theta_2 \sin\phi_2]$$

$$E_\phi = A\,[\cos\alpha \sin\theta_2 \cos\phi_1 + \cos\alpha \sin\theta_1 \cos\phi_2 \sin\alpha \sin\theta_2 \cos\theta_1 \sin\phi_1 - \sin\alpha \sin\theta_1 \cos\theta_2 \sin\phi_2]$$

$$A = -i \frac{|E_\theta|}{R\lambda R_2} e^{i\frac{2\pi}{\lambda}(R_1 + R_2)} \times \frac{\sin\left[\frac{\pi}{\lambda} b\,(\cos\theta_1 + \cos\theta_2)\right]}{\frac{\pi}{\lambda}(\cos\theta_1 + \cos\theta_2)} \times \frac{\sin\left[\frac{\pi}{\lambda} a\,(\sin\theta_1 \sin\phi_1 + \sin\theta_2 \sin\phi_2)\right]}{\frac{\pi}{\lambda}(\sin\theta_1 \sin\phi_1 + \sin\theta_2 \sin\phi_2)} \qquad (4)$$

where R_1, θ_1, ϕ_1 and R_2, θ_2, ϕ_2 are the spherical coordinates of the transmitter and the receiver. α is the polarization angle of the transmitted signal, i.e., $\alpha = 0$ for horizontal and $\alpha = 90°$ for vertical.

Note that these solutions obey the reciprocity theorem, that is, the signal received is not changed by interchanging receiver and transmitter points. The solution is also invarient with respect to simultaneous rotation of receiving and transmitting polarizations.

In order to find the backscattered signal, one takes $\theta_1 = \theta_2$, $\phi_1 = \phi_2$. Because of the symmetry, ϕ may be equal to zero without loss of generality. This gives:

$$E_\theta = 0$$

$$E_\phi = -i \frac{|E_\theta|}{\lambda R} e^{i\frac{4\pi}{\lambda}R} \sin\theta \cos\phi \quad X$$

$$\frac{\sin\left(\frac{2\pi}{\lambda} b \cos\theta\right)}{\frac{2\pi}{\lambda}\cos\theta} X \frac{\sin\left(\frac{2\pi}{\lambda} a \sin\theta \sin\phi\right)}{\frac{2\pi}{\lambda}\sin\theta \sin\phi} \qquad (5)$$

The first equation shows that there is no cross-polarized backscatter. Evaluating the cross section in the usual way gives:

$$\sigma = \frac{4\pi}{\lambda^2} \sin^2\theta \cos^2\phi \left[\frac{\sin\left(\frac{2\pi}{\lambda} b \cos\theta\right)}{\frac{2\pi}{\lambda}\cos\theta}\right]^2 X$$

$$\left[\frac{\sin\left(\frac{2\pi}{\lambda} a \sin\theta \sin\phi\right)}{\frac{2\pi}{\lambda}\sin\theta \sin\phi}\right]^2 \qquad (6)$$

One sees that in this case glint occurs at broadside incidence or $\theta = 90°$, $\phi = 0$. The cross section in this case simplified to:

$$\sigma_\alpha = \frac{4\pi}{\lambda^2} a^2 b^2 \qquad (7)$$

A more detailed treatment of the scattering from a flat plate has been given by R.A. Ross.[1] Ross calculates the radar cross section of a plate using a more accurate theory and compares the results with physical optics theory as well as the experimental measurements. It is shown that the approximations used in this report are valid for angles within about 30° of specular reflection, which is the case of interest here.

Effect of Ground Plane:

The effect of the ground plane must now be included. In order to simplify the calculations, it is convenient to take the ground to be a perfect reflector. For horizontal polarization at VHF, this is a quite good approximation. For vertical polarization, it is a poor approximation except at small incidence angles. As horizontal polarization is the case of greatest practical interest, perfect reflectivity will be assumed and vertical polarization neglected. The problem may now be solved simply by the method of images The field above a perfect ground plane may be found by mirror reflecting all objects and radiation sources in the ground plane and then ignoring the ground plane. The reflected sources must have their polarities reversed. Thus, the problem of a plate set at right angles to the ground is solved simply by doubling the height of the plate and placing an image radiator, of opposite sign to the real radiator, at position R_1, $180 - \theta_1$, ϕ_1. Using the previous result for a plate, Equation 4, the backscattered field is found to be:

$$E_\theta = i \frac{|E_\theta|}{\lambda R} e^{i \frac{4\pi}{\lambda} R} \; 2b \sin\theta \cos\theta \sin\phi \quad X \quad \frac{\sin\left(\frac{2\pi}{\lambda} a \sin\theta \sin\phi\right)}{\frac{2\pi}{\lambda} \sin\theta \sin\phi} \tag{9}$$

$$E_\phi = -i \frac{|E_\theta|}{\lambda R} e^{i \frac{4\pi}{\lambda} R} \sin\theta \cos\phi \quad X \quad \left[2b - \frac{\sin\left(\frac{4\pi}{\lambda} b \cos\theta\right)}{\frac{2\pi}{\lambda} \cos\theta} \right] \frac{\sin\left(\frac{2\pi}{\lambda} a \sin\theta \sin\phi\right)}{\frac{2\pi}{\lambda} \sin\theta \sin\phi}$$

[1] Ross, R.A., "Radar Cross Section of Rectangular Plates as a Function of Aspect Angle," IEEE Transactions of Antennas and Propagation, Volume AP-14, Number 3, May 1966, page 329.

It is seen that there is depolarization backscatter in this case, however, it does not glint and is therefore always small and is of no interest here. The desired cross section is then found to be

$$\sigma = \frac{4\pi}{\lambda^2} \sin^2\vartheta \cos^2\theta \left[2b - \frac{\sin\left(\frac{4\pi}{\lambda} b \cos\theta\right)}{\frac{2\pi}{\lambda}\cos\theta}\right]^2 \left[\frac{\sin\left(\frac{2\pi}{\lambda} a \sin\theta \sin\phi\right)}{\frac{2\pi}{\lambda}\sin\theta \sin\phi}\right]^2 \qquad (10)$$

This is the final result for the radar cross section of a vehicle-like object. It is of interest to analyze this expression further. When the depression angle is small, $\theta \tilde{\approx} 90°$, the two terms in the first bracket tend to cancel. The limiting form for small depression angles is:

$$\sigma = \frac{1024}{9}\pi^5 \frac{b^6}{\lambda^6} a^4 \cos^2\phi \left[\frac{\sin\left(2\frac{\pi}{\lambda} a \sin\phi\right)}{2\frac{\pi}{\lambda}\sin\phi}\right]^2 \qquad (11)$$

where

$$a << \frac{\lambda}{4\pi b}$$

Here a is the depression angle, $90 - \theta$. This cross section falls off as the fourth power of a, therefore, the cross section is very small at small depression angles. Of much greater interest is the value for large depression angles which is given by

$$\sigma = \frac{16\pi}{\lambda^2} b^2 \sin^2\vartheta \cos^2\phi \left[\frac{\sin\left(\frac{2\pi}{\lambda} a \sin\vartheta \sin\phi\right)}{\frac{2\pi}{\lambda}\sin\vartheta \sin\phi}\right]^2 \qquad (12)$$

where

$$a = 90 - \theta \gtrsim \frac{\lambda}{4\pi b}$$

This has no small terms and is much larger than the small α case. This formula indicates glint for $\phi = 0$ at <u>any angle θ</u>. The glint cross section is

$$\sigma_b = \frac{16\pi}{\lambda^2} a^2 b^2 \sin^2 \theta \qquad (13)$$

This glint should occur for angles ϕ smaller than $\lambda/4a \sin \theta$, for angles much larger than this one obtains the off-glint cross section which has average value

$$\sigma_{0b} = \frac{2}{\pi} b^2 \cot^2 \phi \qquad (14)$$

The average cross section is obtained by averaging Equation 12 over all angles.

$$\sigma_{AV}(\theta) = \frac{1}{\pi} \int_{-\pi/2}^{\pi/2} \sigma(\theta, \phi)\, d\phi$$

$$\sigma_{AV} = 8b^2 \frac{a}{\lambda} \sin \theta \qquad (15)$$

where the fact that $a/\lambda >> 1$ has been used.

Numerical Results:

To give some idea of the size of the cross sections to be expected in practice, values are given below for a more or less typical truck:

Radar cross section for a vehicle 18 feet long and 9 feet high at a depression angle of 30° at 145 Mcs.

σ_G (glint cross section, $\phi = 0$) = 20,000 feet^2

σ_{OG} (average off-glint cross section, $\phi \approx 45°$) = 54 feet^2

σ_{AV} (average over all ϕ) = 1,500 feet^2

width of glint peak (azimuth) 1/2 power points) = 14°

minimum depression angle for glint ~ 3°

One sees that the glint cross section is much larger than the average value, by 11 dB. The glint occurs for all depression angles greater than about 3°, however, the azimuthal angle, ϕ, must be within about 7° of broadside incidence. Therefore, the probability of obtaining glint for arbitrary illumination angle is about 14/180 = .08. However, this probability could be made much larger if one knew the direction of the road upon which the vehicles travelled. The very small off-glint cross section should probably not be taken too seriously as it depends on complicated interference which is beyond this model to compute. However, it is probably quite small. The small size of these off-glint cross sections provide the justification for neglecting the top and front facets of the vehicle.

Comparison with Experimental Results:

The only experimental values for the radar cross section of a truck, below microwave frequencies, available to the author are those of Steele and Barnum.[2] These workers have measured the radar cross section of a truck 22 feet long, 11 feet high and 8 feet wide. The measurements were performed at 26 Mcs., using a standing wave method. They report free space values, having subtracted out the ground plane effect in an approximate manner. Therefore, their results must be compared with the plate without ground plane solutions, Equations 6 and 7. These measurements are made with the antenna on the ground, therefore $\theta = 90°$.

[2] Steele, J.C., and Barnum, J.R., "High Frequency Measurements of Radar Cross Section Using the Standing Wave Method," Stanford Electronics Laboratories, Radio Science Laboratory, Technical Report # 127, March 1966.

Radar cross section of a truck at 26 Mcs.

Aspect Angle, ϕ	Stanford Value	This Calculation
0°	300 feet^2	480 feet^2
45°	21 feet^2	20 feet^2

The rather good agreement is probably somewhat fortuitous as the dimensions of the truck are somewhat smaller than a wavelength and Helmholtz theory is only truly valid when the wavelength is much smaller than the target.

Conclusions:

In conclusion, this analysis has shown that glint is an important factor in detecting targets with VHF radar. The glint cross section is quite large, 20,000 feet^2 for a moderate sized truck and on the order of 10 dB larger than the average cross section. The glint occurs for aspect angles within about $\pm 7°$ of broadside incidence and is approximately independent of depression angle. In order to have a high probability of obtaining a glint return from a given vehicle it would be necessary to illuminate a given piece of ground from all azimuth angles from 0° to 180°. This could be done by utilizing a number of range gates and flying over the region of interest and observing each segment of land at different times. The number of range gates required could be reduced by making several passes over the same territory from different directions. The problem would be much simpler if one knew in advance the approximate direction of the road on which the vehicles travelled. One would then simply fly parallel to the road (if sidelooking antennas were being used).

The theory given here is very approximate. The short wavelength approximation has been used extensively in spite of the fact that the target is only slightly larger than a wavelength. All of the details of the structure of the vehicle have been ignored as has been the gap between the bottom of the vehicle and ground. In spite of this, the calculation probably will give reasonable estimates of cross sections at frequencies of interest. The largest approximation is to ignore the diffusing effect of the vegetation on the incoming wave. It is very hard to estimate this effect but it probably may be ignored if the vegetation density is not too high and the depression angle is fairly large, i.e., if the incoming wave only has to penetrate a few hundred feet of vegetation.

APPENDIX B

MAP DISPLAY GEOMETRY

The map displays are generated from a single range gate using the doppler frequency dependence on azimuth. Since the range gate describes a circle on the ground, the relationship between the x and y coordinates is known. The expression required then is the doppler frequency of each point on that circle.

Figure B1 shows the geometry of the situation. The aircraft at point Z is looking at a target at point T on the ground. The aircraft has a velocity along the y-axis toward the left. This is equivalent to a ground velocity of equal magnitude but opposite directions. A line is drawn from the target and perpendicular to the x-axis. A third line drawn from point x to the aircraft forms the right triangle XTZ.

The doppler frequency, F_D, is given by the following expression.

$$F_D = \frac{2 V_r}{\lambda} \tag{1}$$

where V_r is the radial velocity of the target and λ is the wavelength of the radar. Since the velocity vector triangle is similar to the triangle XTZ we have,

$$V_r = V_g \sin \phi \tag{2}$$

Where V_g is the ground velocity and ϕ is the angle shown in Figure 1. We can eliminate the angle ϕ from the expression by using the large triangle, XTZ.

$$\sin \phi = \frac{y_g}{R_s} \tag{3}$$

where y_g is the y-coordinate of the target and R_s is the slant range of the radar. Combining these expressions gives the following equation for the doppler frequency as a function of the y-coordinate of the point along the circle described by the range gate.

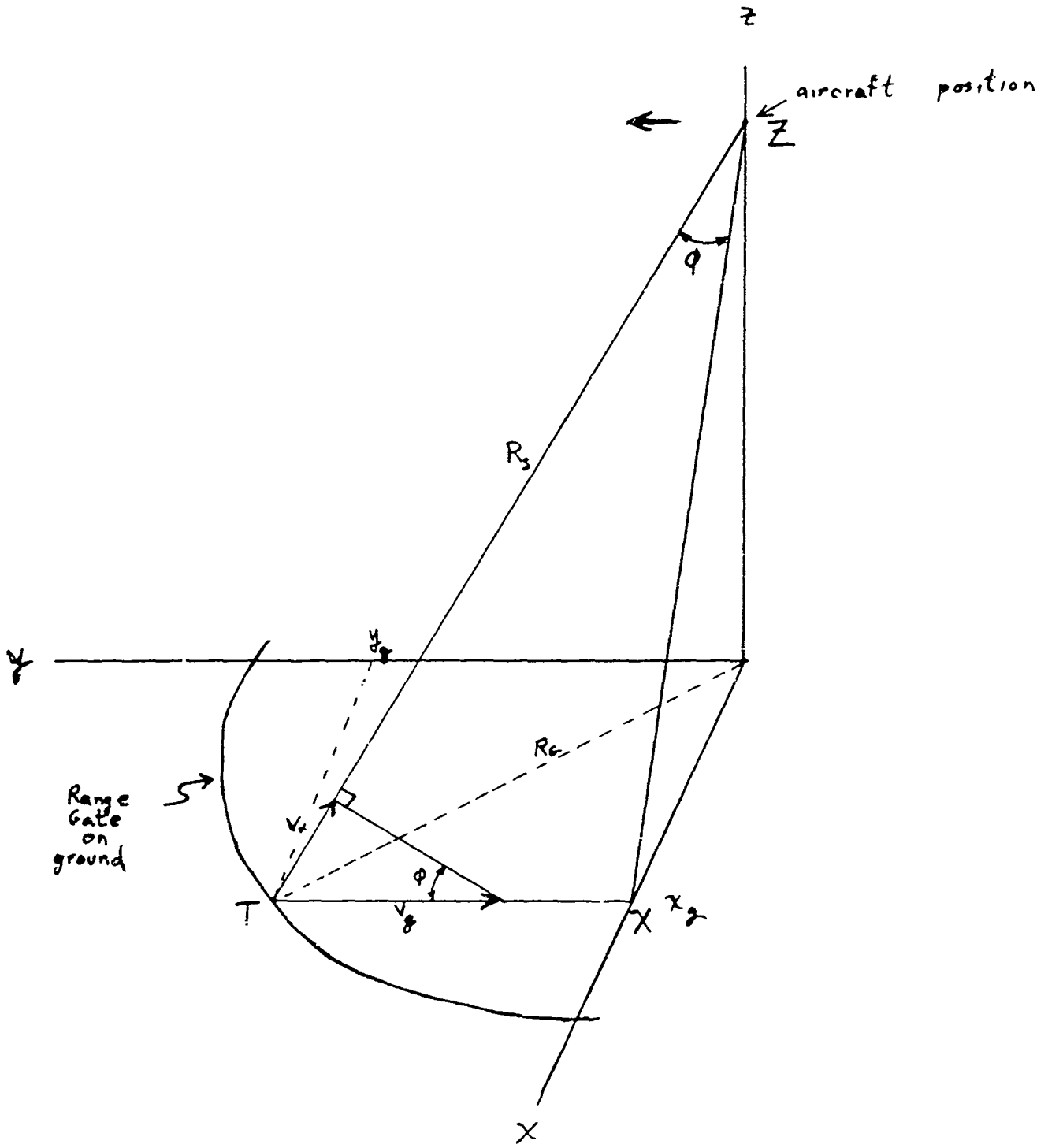

Figure B.1 Aircraft Geometry

$$F_D = \frac{2 V_g y_g}{\lambda R_s} \tag{4}$$

Equation (4), then, gives the doppler frequency caused by any point along the circle. The range gate projection on the ground is given by,

$$x_g^2 + y_g^2 = R_g^2 \tag{5}$$

The map on the display is generated as an arc of a circle with a variable grey scale. The arc is defined by the following equation.

$$y_D = + \sqrt{r_D^2 - (r_D - x_D)^2} \qquad \text{for } 0 \leq x_D \leq r_D/2$$

or

$$y_D = + \sqrt{2x_D r_D - x_D^2}$$

Note that the origin of the circle is at $(r_D, 0)$. X_D, y_D are the display coordinates and r_D is the radius of the circle on the display. (See Figure B2.) The limits for x restrict the display to a 60° arc.

Equation (6) defines the path of the display element. The grey scale used at each point is determined by the signal strength at the given doppler frequency. This doppler frequency is derived from Equation (4) with a change of units to display position units. This is done as follows

$$y_g = \frac{R_G}{r_D} y_D \tag{7}$$

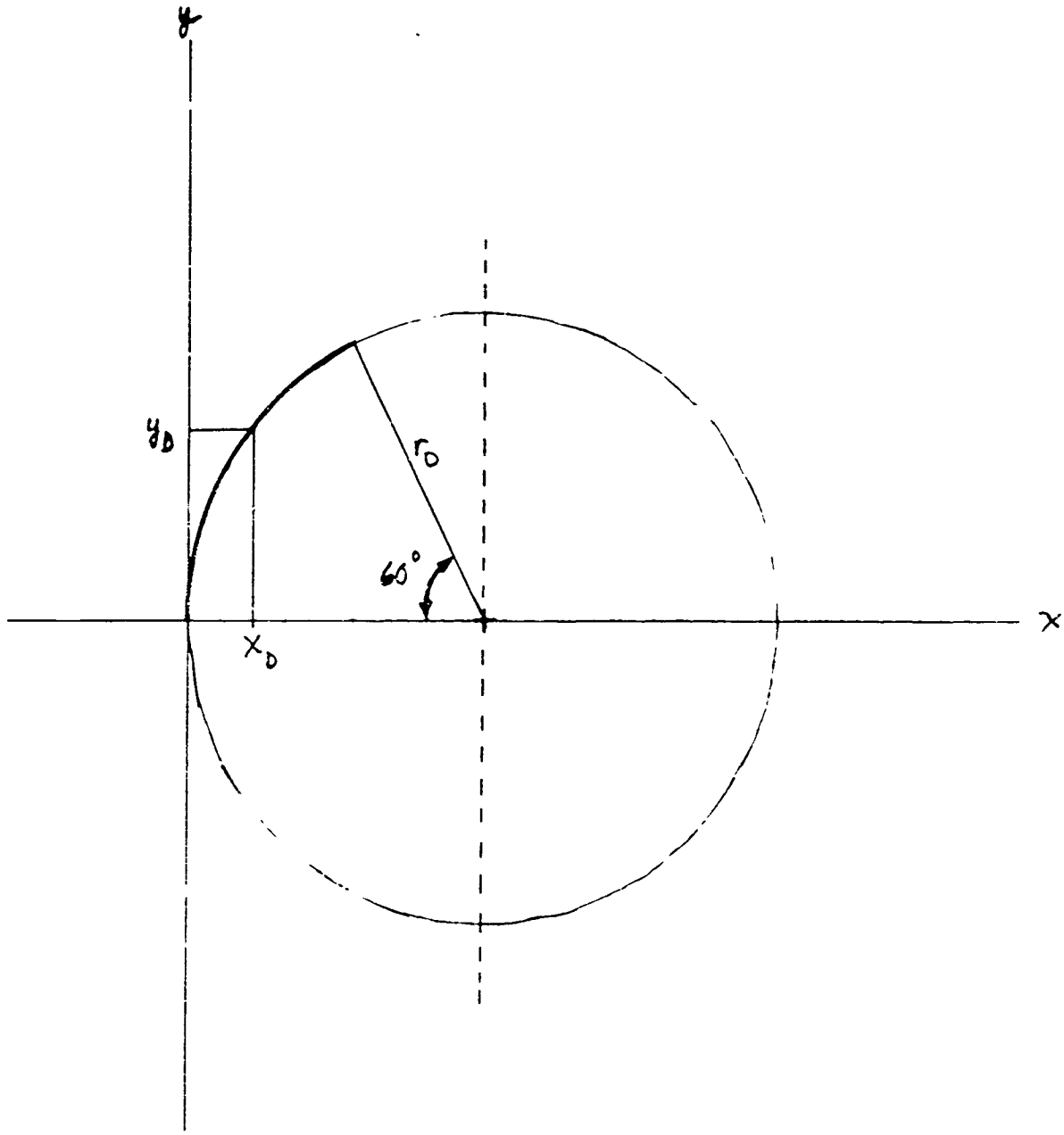

The heavy section of the circle is the arc used to generate the display

Figure B.2. Map Display Arc

where R_G is the target ground range. Then Equation (4) becomes

$$F_D = \frac{2 V_g R_G}{\lambda R_s r_D} y_D$$

or, in terms of X_D

$$F_D = \frac{2 V_g R_G}{\lambda R_s r_D} \sqrt{2X_D r_D - X_D^2} \tag{8}$$

The FFT of N data points produces N frequency bins. Each of these bins have a frequency width, ΔF_B, as follows.

$$\Delta F_B = \frac{1}{N t_s} \tag{9}$$

where t_s is the sample rate (the time delay between individual sample points). The grey scale of a point on the display arc is, then, determined by the contents of frequency bin j.

$$j = \frac{2N t_s V_g R_G}{\lambda R_s r_D} \sqrt{2 r_D x_D - x_D^2} \tag{10}$$

and

$$y_D = \sqrt{2 r_D x_D - x_D^2} \tag{6}$$

These two equations, (6) and (10), define a single arc on the display. The display is shifted between arcs in order to correspond to the aircraft motion. This shift, in display units, is given by

$$d_s = \left(\frac{r_D}{R_G}\right) V_g (n_s t_s) \tag{11}$$

where n_s is the shift count (the number of samples which the data is shifted before the next calculation).

APPENDIX C

ANALYSIS OF MOVING TARGET CASE

For the purpose of this discussion, a moving coordinate system is chosen with the origin on the aircraft. All angles are measured from a line perpendicular to the motion of the aircraft. (See Figure C.1.). The target velocity is assumed to be constant.

The doppler frequency of the target is given by:

$$f_D = \frac{2 \cos \theta_D}{\lambda} V_R$$

where:

f_D = doppler frequency

θ_D = depression angle

λ = wavelength

V_R = total radial velocity

for simplicity, the variable K will be used as follows:

$$K = \frac{2 \cos \theta_D}{\lambda}$$

and

$$f_D = K V_R$$

The radial velocity is given by the following equation as derived from Figure C.1.

$$V_R = V_g \sin \rho - V_T \cos (\psi - \rho)$$

where:

V_g = velocity of the ground due to motion of the aircraft.

V_T = target velocity

ρ = angle to target

ψ = angle of target velocity

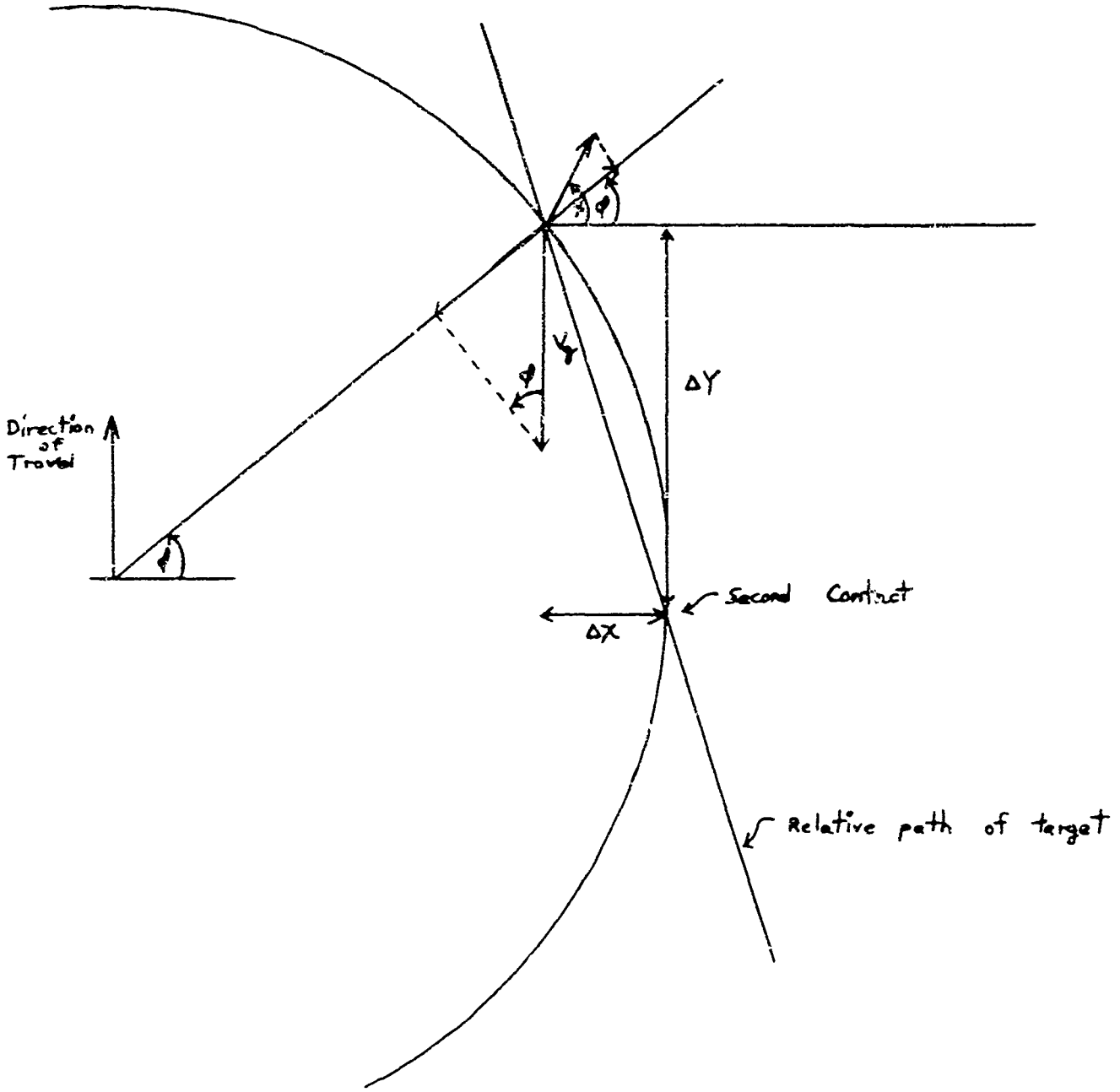

Figure C.1 Model for Derivation of Velocity Equation

In this case, two measurements are made. One at first contact, ahead of the aircraft; the second at last contact, after the aircraft has passed the target. This yields two measurements of doppler frequency.

$$f_{D1} = V_g K \sin \rho_1 - V_T K \cos(\psi - \rho_1) \quad (1)$$

$$f_{D2} = V_g K \sin \rho_2 - V_T K \cos(\psi - \rho_2) \quad (2)$$

The distance traveled is also of interest and can be given in two ways, geometry and, velocities and time.

$$\Delta X = R \cos \rho_2 - R \cos \rho_1$$

$$\Delta Y = R \sin \rho_1 - R \sin \rho_2$$

and

$$\Delta Y = V_g \Delta T - V_T \Delta T \sin \psi$$

$$\Delta X = V_T \Delta T \cos \psi$$

or

$$V_g \Delta T - V_T \Delta T \sin \psi = R \sin \rho_2 - R \sin \rho_1 \quad (3)$$

$$V_T \Delta T \cos \psi = R \cos \rho_1 - R \cos \rho_2 \quad (4)$$

Expanding Equation (1) yields:

$$\frac{f_{D1}}{K} = V_g \sin \rho_1 - V_T \cos \psi \cos \rho_1 - V_T \sin \psi \sin \rho_1$$

substituting for $V_T \cos \psi$ and $V_T \sin \psi$ from Equations (3) and (4) gives

$$\frac{f_{D1}}{K} = V_g \sin \rho_1 - \frac{R}{\Delta T} (\cos \rho_1 \cos \rho_2 \cdot \cos^2 \rho_1 - \sin^2 \rho_1 + \sin \rho_1 \sin \rho_2) - V_g \sin \rho_1$$

or

$$\frac{f_{D1}}{K} = \frac{R}{\Delta T} (1 - \cos (\rho_1 - \rho_2)) \quad (5)$$

Similarly for Equation (2)

$$\frac{f_{D2}}{K} = -\frac{R}{\Delta T}\,(1 - \cos(\rho_1 - \rho_2)) \tag{6}$$

Therefore

$$f_{D1} = -f_{D2} \tag{7}$$

The two doppler frequencies measured are equal in magnitude and opposite in sign.

Now subtracting Equation (2) from Equation (1),

$$\frac{f_{D1} - f_{D2}}{K} = V_g(\sin\rho_1 - \sin\rho_2) - V_T[\cos(\psi - \rho_1) - \cos(\psi - \rho_2)]$$

Expanding:

$$\frac{f_{D1} - f_{D2}}{K} = V_g(\sin\rho_1 - \sin\rho_2) - V_T[\cos\psi(\cos\rho_1 - \cos\rho_2) + \sin\psi(\sin\rho_1 - \sin\rho_2)]$$

Substituting again from Equations (3) and (4), but this time for $(\cos\rho_2 - \cos\rho_1)$ and $(\sin\rho_1 - \sin\rho_2)$.

$$\frac{f_{D1} - f_{D2}}{K} = V_g\frac{\Delta T}{R}(V_g - V_T\sin\psi) + V_T\frac{\Delta T}{R}[V_T\cos^2\psi - V_g\sin\psi + V_T\sin^2\psi]$$

or

$$\frac{R}{K\,\Delta T}(f_{D1} - f_{D2}) = (V_g - V_T\sin\psi)^2 + V_T^2\cos^2\psi \tag{8}$$

Summarizing then, the following equations are of interest:

$$\frac{f_{D1}}{K} = \frac{R}{\Delta T}\left(1 - \cos\left(\rho_1 - \rho_2\right)\right) \tag{5}$$

$$\frac{f_{D2}}{K} = -\frac{R}{\Delta T}\left(1 - \cos\left(\rho_1 - \rho_2\right)\right) \tag{6}$$

$$\frac{R}{K\Delta T}\left(f_{D1} - f_{D2}\right) = \left(V_g - V_T \sin\phi\right)^2 + V_T^2 \cos^2\phi \tag{8}$$

Note that the right hand side of Equation (8) is nothing more than the magnitude of the resultant target velocity relative to the aircraft. Equations (5) and (6) show that the two measured doppler frequencies are not independent but are equal in magnitude.

The true azimuth of the target is the one piece of information missing here. The magnitude of the resultant velocity and the subtended angle (or equivalently the distance of closest approach) are both given.

A discussion of detection criteria follows.

Assume that the spectra of the processed clutter has a Gaussian distribution.[1]

$$f_0(v) = \frac{1}{\sqrt{2\pi\sigma^2}}\, e^{-v^2/2\sigma^2}$$

Where:

- v = amplitude in volts
- σ = standard deviation
- f_0 = probability when no target present
- A = amplitude of signal due to target

[1] Schwartz, M., "Information Transmission, Modulation and Noise," Second Edition, Brooklyn Polytechnical Institute Series, McGraw Hill Book Company, New York, 1970, pp. 330-338.

Probability of false alarm is given by

$$P_{fa} = P_{\text{false alarm}} = \int_{A/2}^{\infty} f_0(v)\, dv$$

$$\frac{1}{\sqrt{2\pi\sigma^2}} \int_{\frac{A}{2}}^{\infty} e^{-v^2/2\sigma^2}\, dv$$

Let $y^2 = v^2/2\sigma^2$

then $y = v/\sqrt{2\sigma^2}$

$dy = dv/\sqrt{2\sigma^2}$

$$P_{fa} = \frac{1}{\sqrt{\pi}} \int_{\frac{A}{2\sqrt{2}\sigma}}^{\infty} e^{-y^2}\, dy$$

$$= \frac{1}{2}\left(1 - \frac{2}{\sqrt{\pi}} \int_{0}^{\frac{A}{2\sqrt{2}\sigma}} e^{-y^2}\, dy\right)$$

Since $\text{erf}(x) = \frac{2}{\sqrt{\pi}} \int_0^x e^{-y^2}\, dy$

$$P_{\text{false alarm}} = \frac{1}{2}\left(1 - \text{erf}\frac{A}{2\sqrt{2}\sigma}\right)$$

The following information pertains to Figure C.2.

d is the threshold level.

d_{opt} is the optimum threshold level.

for $P_{no\ target} = \frac{1}{2}$ $P_{target} = \frac{1}{2}$

$d_{opt} = 0$ This is the crossover point of the two probability distributions

$$\text{In general } d_{opt} = \frac{\sigma^2}{2A} \ln_e \frac{P_0}{P_1} \tag{9}$$

P_0 = probability no target (clutter only)

P_1 = probability of a target

$$P_{error} = P_0 \underbrace{\int_a^{\infty} f_0(v)\, dv}_{P_{e0}} + P_1 \underbrace{\int_{\infty}^{d} f_1(v)\, dv}_{P_{e1}} \quad \text{(see Fig. C.3)}$$

P_{e0} mistaking clutter for target

P_{e1} Mistaking target for clutter

A proof of Equation (9) follows:

Minimize P_{error}

$$\frac{\partial P_{error}}{\partial d} = 0 = -P_0 f_0(d) + P_1 f_1(d)$$

$$\frac{f_1(d)}{f_0(d)} = \frac{P_0}{P_1}$$

$$f_1(d) = \frac{1}{\sqrt{2\pi\sigma^2}} e^{-(d - A/2)^2/2\sigma^2}$$

$$f_2(d) = \frac{1}{\sqrt{2\pi\sigma^2}} e^{-(d + A/2)^2/2\sigma^2}$$

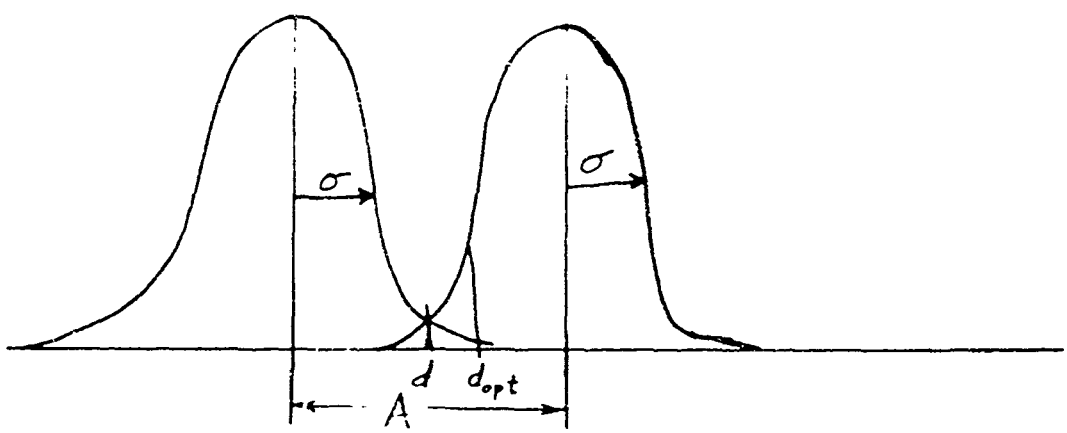

Figure C.2 Probability Curves

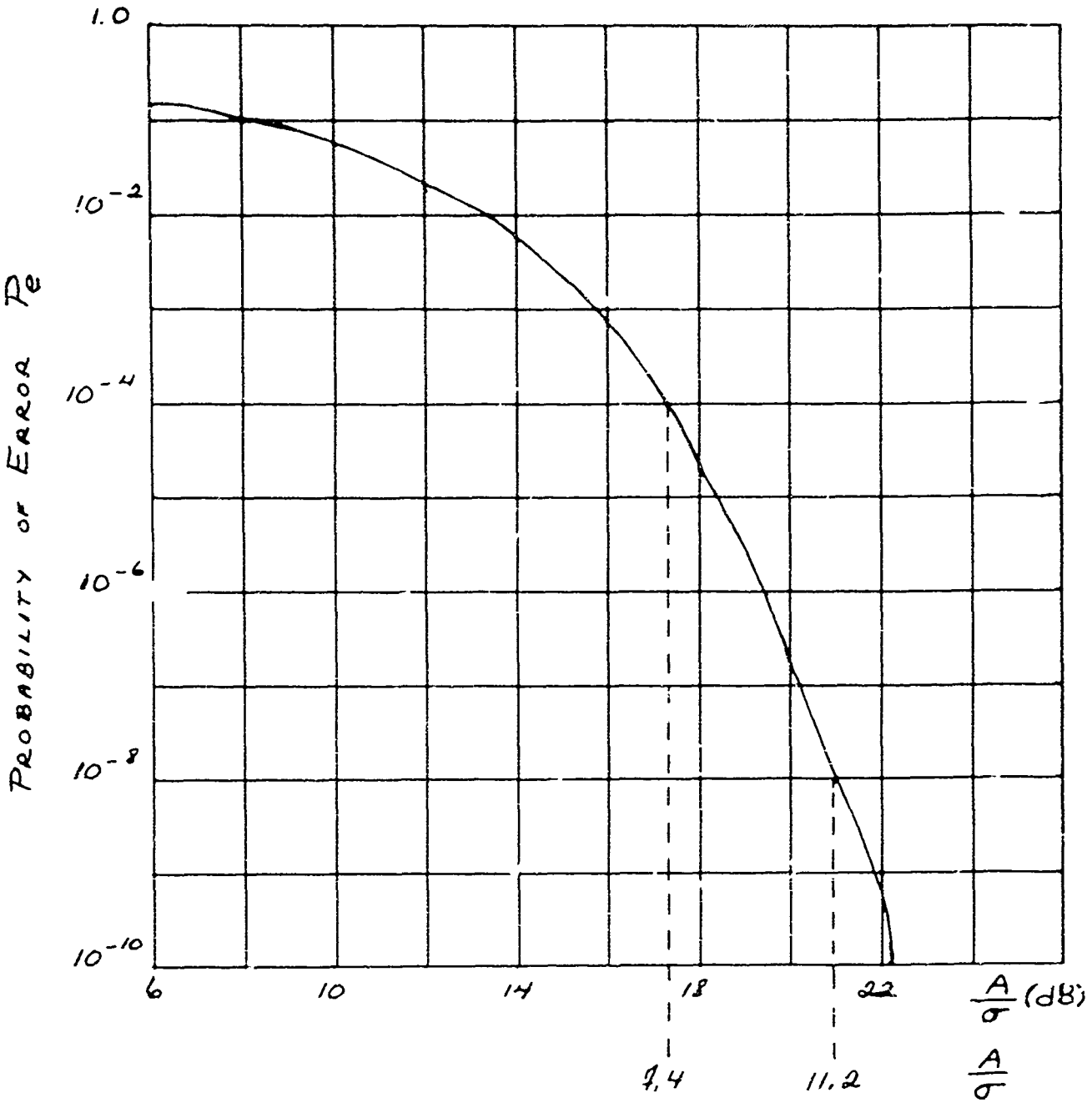

If a probability of error of 10^{-4} is desired, then the signal-to-noise ratio must be 7.4. This means that the signal, A, must be greater than the standard deviation, σ, for acceptable probability of error.

Figure C.3. Error Distribution Curve

$$\frac{f_1(d)}{f_2(d)} = e^{-\frac{(d - A/2)^2 + (d + A/2)^2}{2\sigma^2}} = \frac{P_0}{P_1}$$

$$\frac{-\left[d^2 - 2\frac{dA}{2} + \frac{A^2}{4}\right] + \left[d^2 + 2\frac{dA}{2} + \frac{A^2}{4}\right]}{2\sigma^2} = \ln_e \frac{P_0}{P_1}$$

$$\left(2\frac{dA}{2} + 2\frac{dA}{2}\right) / 2\sigma^2 = \ln_e (P_0/P_1)$$

$$\frac{dA}{\sigma^2} = \ln_e \frac{P_0}{P_1}$$

$$d_{opt} = \frac{\sigma^2}{A} \ln_e \frac{P_0}{P_1}$$

This is the optimum threshold level where main (noise clutter) lies at $-\frac{A}{2}$ and means signal plus clutter lies at $+\frac{A}{2}$.

P_0 = probability of clutter only

P_1 = probability of signal plus clutter.

APPENDIX D

TARGET-CLUTTER SIMULATIONS

A FORTRAN program package exists which creates a fake condensed data tape (CDT) of computer generated data. This format is compatible with all LWL spectral analysis programs, and thus can be used to test the programs and to simulate various target-clutter situations. The two main programs in the package are DATGEN and FAKCDT. DATGEN, which can be easily modified at the experimenter's option, is executed first, and creates a scratch tape of data for use by FAKCDT. FAKCDT, which operates relatively quickly, properly converts and formats the data to create a fake CDT.

DATGEN

DATGEN writes 512-word recores of one's complement integers onto FORTRAN Unit 1. The maximum absolute value allowed is 2047_{10}. A file mark is written after each group of records representing a variable, with a final file mark at the end to provide an end-of-tape designator.

FAKCDT

FAKCDT uses the data on FORTRAN Unit 1 to create a fake CDT. For each data record, a validity check is performed to insure that the maximum absolute value of each data work is 2047. (If not, the error is reported and the program stops.) Each data word is then converted to a 12-bit two's complement word (sign + 11 bits). A 513-th and 514-th word are added to the 512-word record, as follows: Word 513 is the integer 512_{10}, designating the number of data words in the CDT record, and word 514 is the suncheck of the first 512 words. The converted and formatted record is then written onto FORTRAN Unit 4 in the 2-byte mode. Appropriate header information is required by FAKCDT as input and is written out as required on the CDT. As currently configured, the fake CDT has two experiments, each of which has seven variables.

24 August 1973

Experiment 1

Variable	
1	Gaussian random noise*
2	Gaussian random noise*
3	50 Hz cosine wave + Gaussian random noise*
4	50 Hz sine wave + Gaussian random noise*
5	In-phase channel of target simulation no. 2
6	Quadrature-phase channel of target simulation no. 2
7	Gaussian random noise*

Experiment 2

Variable	
1	In-phase channel of linearly swept sinusoid going from +15 Hz to -15 Hz
2	Quadrature-phase channel of above signal
3	In-phase channel of target simulation no. 1°
4	Quadrature-phase channel of target simulation no. 1°
5	Cosine on the 45-th line of a 512 point DFT
6	Sine on the 45-th line of a 512 point DFT
7	Sum of two sinusoids, with frequencies 17 Hz and 50 Hz The 17 Hz signal is 20 dB down from the 50 Hz signal.

*: The Gaussian random noise is generated with a mean of zero and standard deviation of

$$2046/(2.5^* \ 2.4) = 528.3 ,$$

which, given the mechanism of the Gaussian random number generator (see the writeup on NOISEPAK), guarantees numbers having absolute value less than or equal to 2046.

°: Target simulation no. 1 has a maximum absolute value of 500.

Δ: Target simulation no. 2 has a maximum absolute value of 2047.

All other sines and cosines have a maximum absolute value of 2047.

All variables have 20 records of 512 words each.

Target Simulation

Two cases of target simulation data are provided, and the exact results depend on the relative numbers chosen. The following input data card is required by DATGEN:

RS, DELRS, H, VG, XO1, XO2

where all numbers are floating-point.

RS is the slant range in feet

DELRS is the range gate width in feet, normally 100

H is the altitude in feet

VG is the ground speed of the aircraft in feet/second

XO1 is the x-coordinate of target no. 1

XO2 is the x-coordinate of target no. 2

The user must take into account that the current version of the program (24 August 1973) computes 20 records of 512 points with a sampling interval of 2.13 ms, for a total of 21.8 seconds. Time t = 0 is chosen as the time that the target would enter the range-gate if the x-coordinate were zero. (Refer to Figure D.1.). Thus, VG should be chosen so that the target is covered by the range-gate during the desired simulation time. XO1 and XO2 are chosen after computing the ground range at the inner and outer edges of the range gate, designated by RG and RGPD, respectively. Although this calculation must really be done by the user before executing the program, the computer will re-calculate and print these values. If the x-coordinate is greater than RGPD, no data (other than zero) will be generated; if the x-coordinate is less than RGPD but greater than RG, the target enters the range gate tangentially, does not intersect the inner edge of the range gate, and leaves at a negative azimuth angle. If the x-coordinate is less than RG, the target enters the range gate, leaves, re-enters, and leaves for good. These last two cases are illustrated as XO1 and XO2 in Fig.D.1; however, during the simulation, XO1 and XO2 can be chosen arbitrarily.

Theory

The instantaneous doppler frequency for a target within the range gate is given by

$$f_d = \frac{2 v_g}{\lambda} \frac{y}{(x_o^2 + y^2 + h^2)^{1/2}} ,$$

where

$$y = R_g + \Delta R_g - v_g t .$$

The instantaneous phase $\theta(t)$ is given by

$$\theta(t) = \int f_d \, dt ,$$

subject to the arbitrary initial condition that $\theta(0) = 0$. It is easily shown that

$$\theta(t) = K - \frac{2}{\lambda} \sqrt{x_o^2 + h^2 + y^2} ,$$

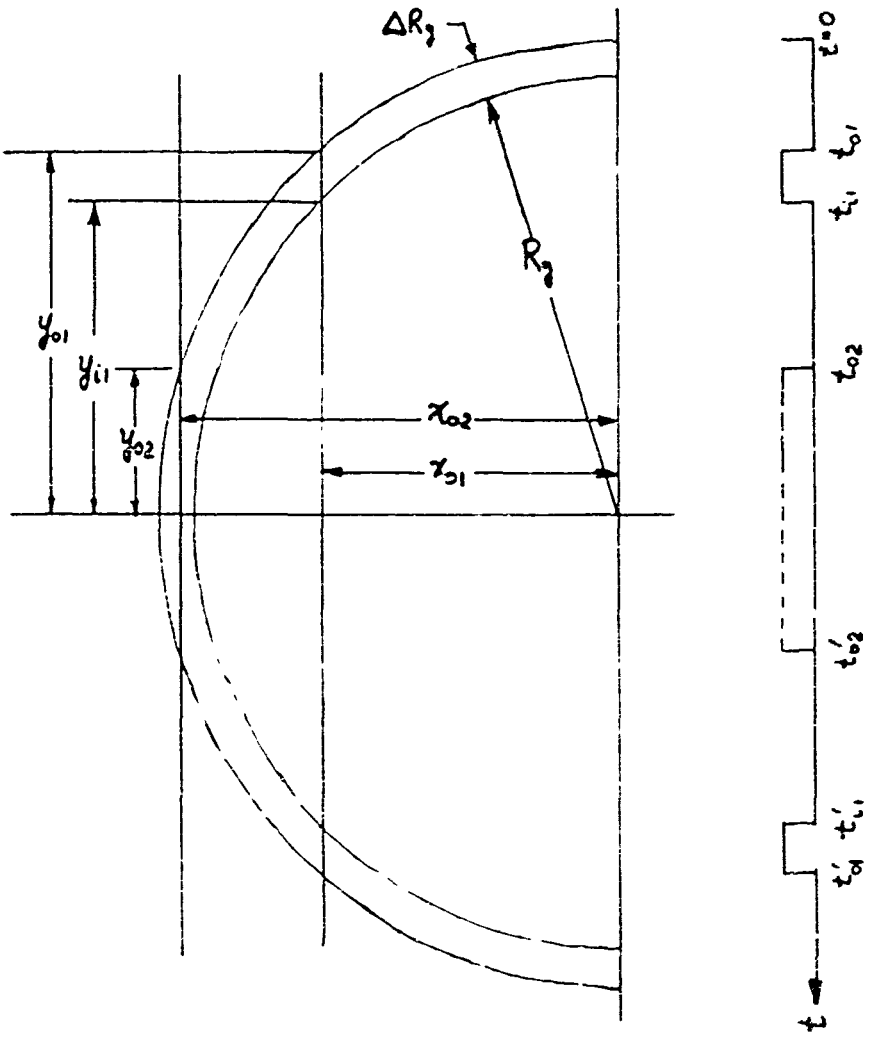

Figure D.1. Target Simulation Geometry

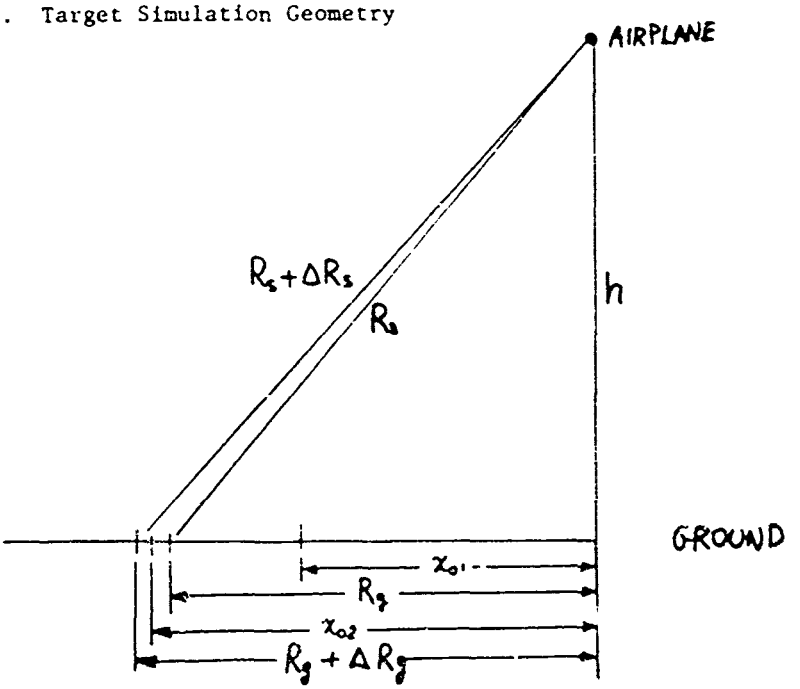

where

$$K = \frac{2}{\lambda}\sqrt{x_o^2 + h^2 + (R_g + \Delta R_g)^2}\,.$$

Note that $\theta(t)$ increases as y goes from $R_g + \Delta R_g$ to zero, and then decreases as y grows more negative (See Figure D.2).

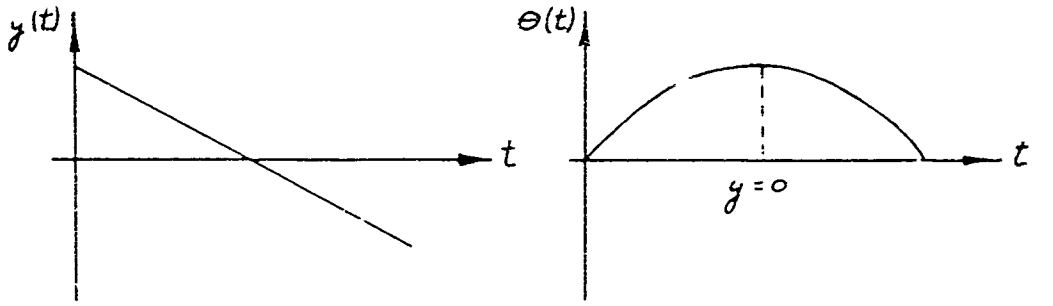

Target Position vs. Time

Instantaneous Phase Velocity vs. Time

Figure D.2. Position and Phase Relationship as Target Passes Through the Range Gate

Experiments involving target simulation no. 1

For this experiment the following data was used:

R_s = slant range = 3000 feet

h = altitude = 1000 feet

R_g = ground range = 2828.4 feet

v_g = ground speed = 250 feet/second

The simulated data (see Figure D.3) is recorded on condensed data tapes. The first point of the first 512 word record is t = 0, and there are a total of 20 records. The sampling rate is 469 Hz, for a Δt = 2.13 ms. The target enters the range gate at t = 9.9 seconds (record 10) and leaves at 13.5 seconds (record 13). Since there is no noise, all other records are identically zero. During the time that the target is in the range gate, a complex exponential is generated with an instantaneous frequency as dictated by the geometry of the airplane and the ground (and the ground speed of the airplane).

The Univac program INTERP was used to generate a time-domain plot of the in-phase channel (variable 3), which is presented in Figure D.3. The program PPQUA3 was then used to view the data in the frequency domain. Figure D.4 illustrates the segments of data utilized to calculate the spectral estimates shown in Figures D.5 through D.9. Note that the original data records 9 and 14 are identically zero. Figures D.5, D.6 and D.8 are average spectral estimates covering the same data, but calculated using 6 512-word records, 12 256-word records, and 24 128-word records, respectively. The results change dramatically as the smoothing changes, illustrating that this method of smoothing is <u>not</u> suitable for this type of target data. The main objection to averaging of this type is that the target data is non-stationary over the time period of interest, since the frequency is changing relatively quickly with time.

One possible conclusion from this analysis is that the method of processing targets tangential to the range gate should be different from those targets located closer in to the flight vector. This is not to say that the software must be changed, but rather that the input processing parameters must be optimized for the targets of interest.

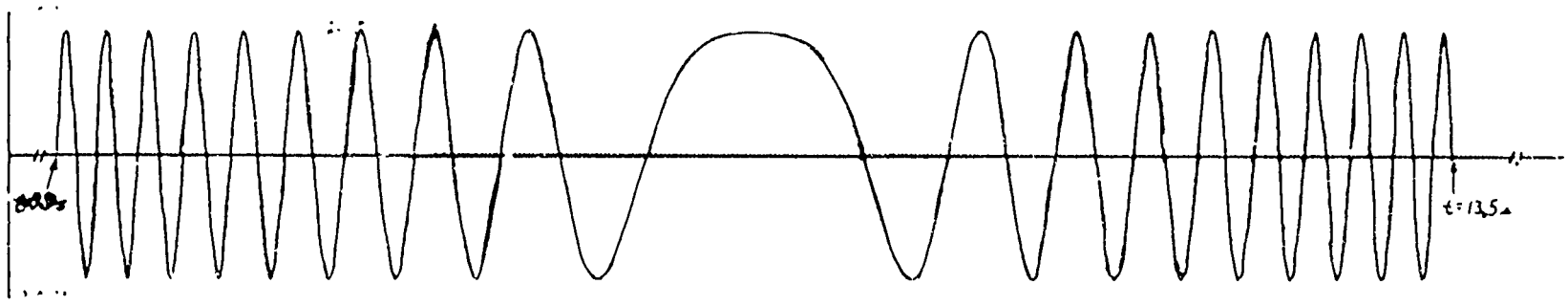

Figure D.3. Time-domain data from the in-phase channel (variable 3) of target simulation number 1 (Experiment 2, Tape 901, 24 August 1973).

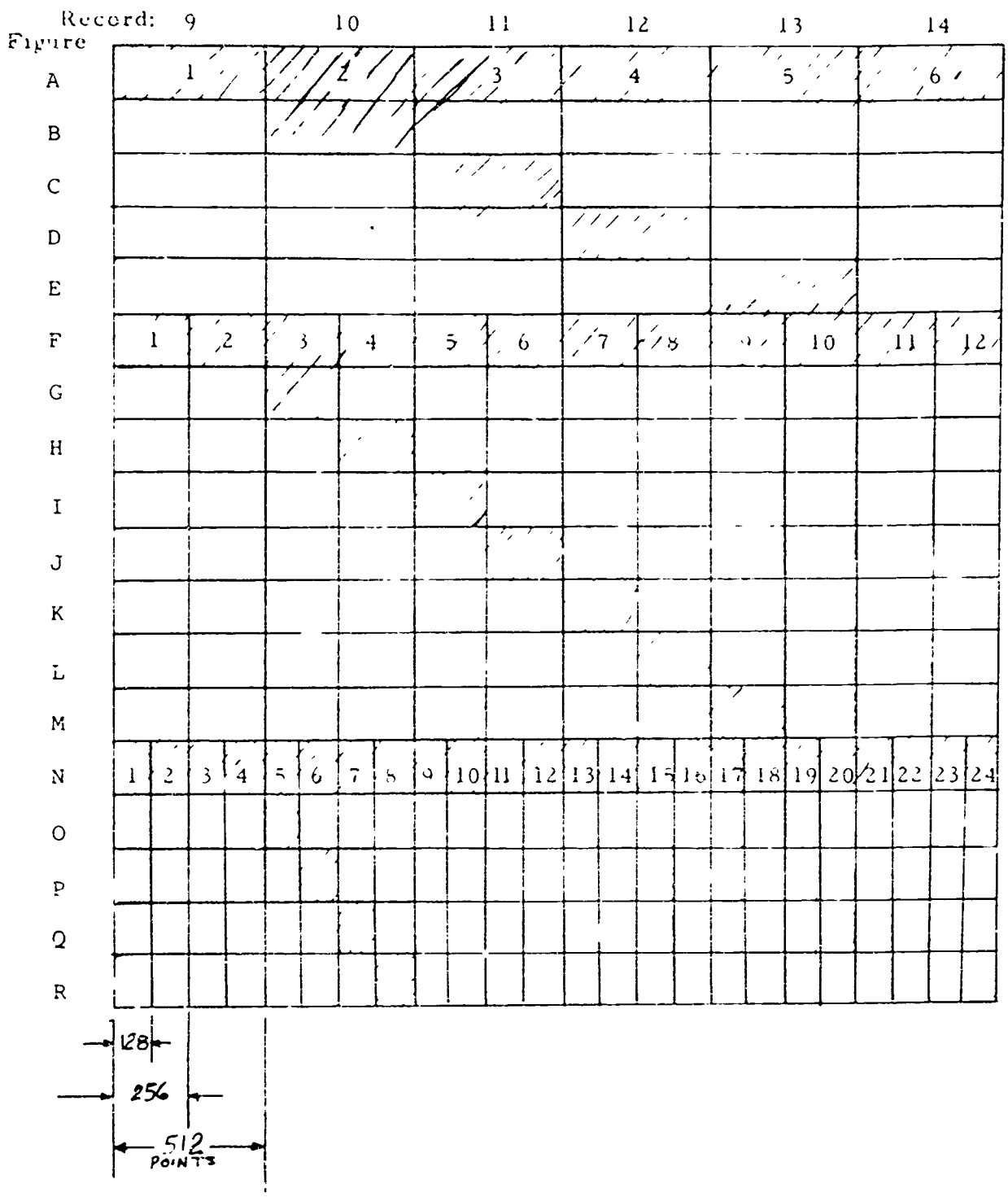

Figure D.4. Graphic illustration of data used in Figures D.5 through D.9; Shaded areas represent data used in each figure. Where more than one block is shaded, the spectral estimate is calculated as an average of the individual estimates for each block.

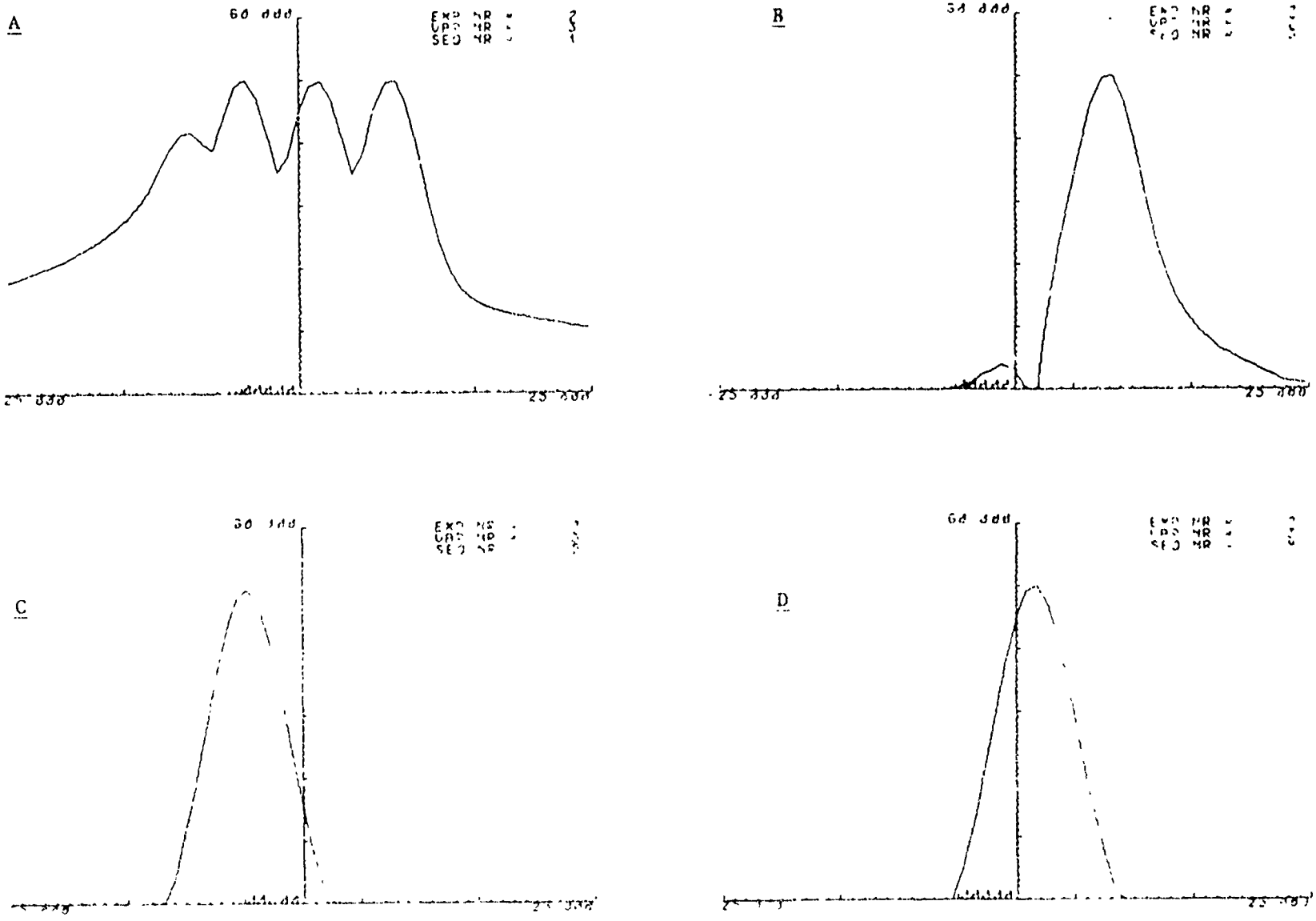

Figure D.5. Spectra Illustrating Various Smoothing Constants

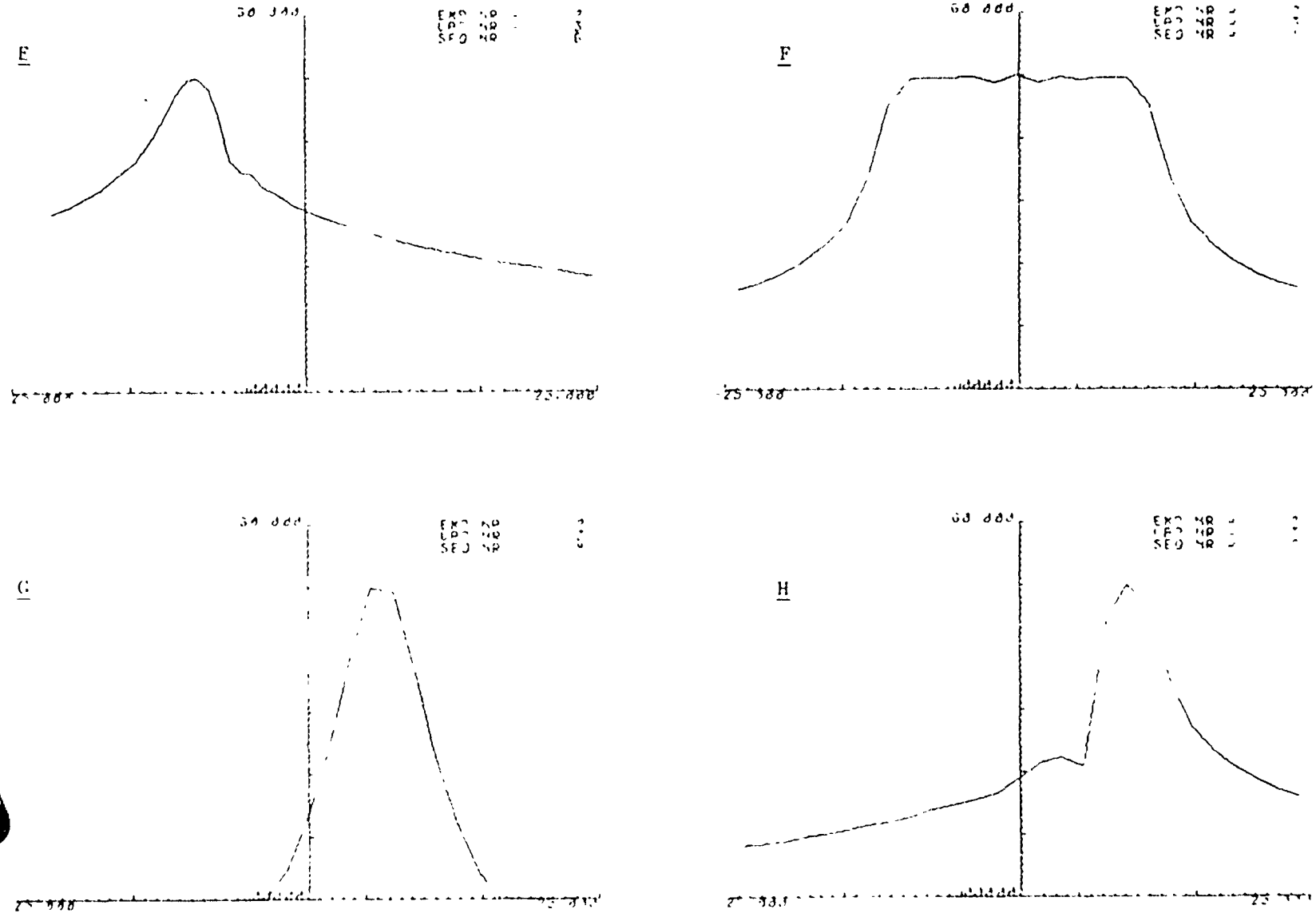

Figure D.6. Spectra Illustrating Various Smoothing Constants

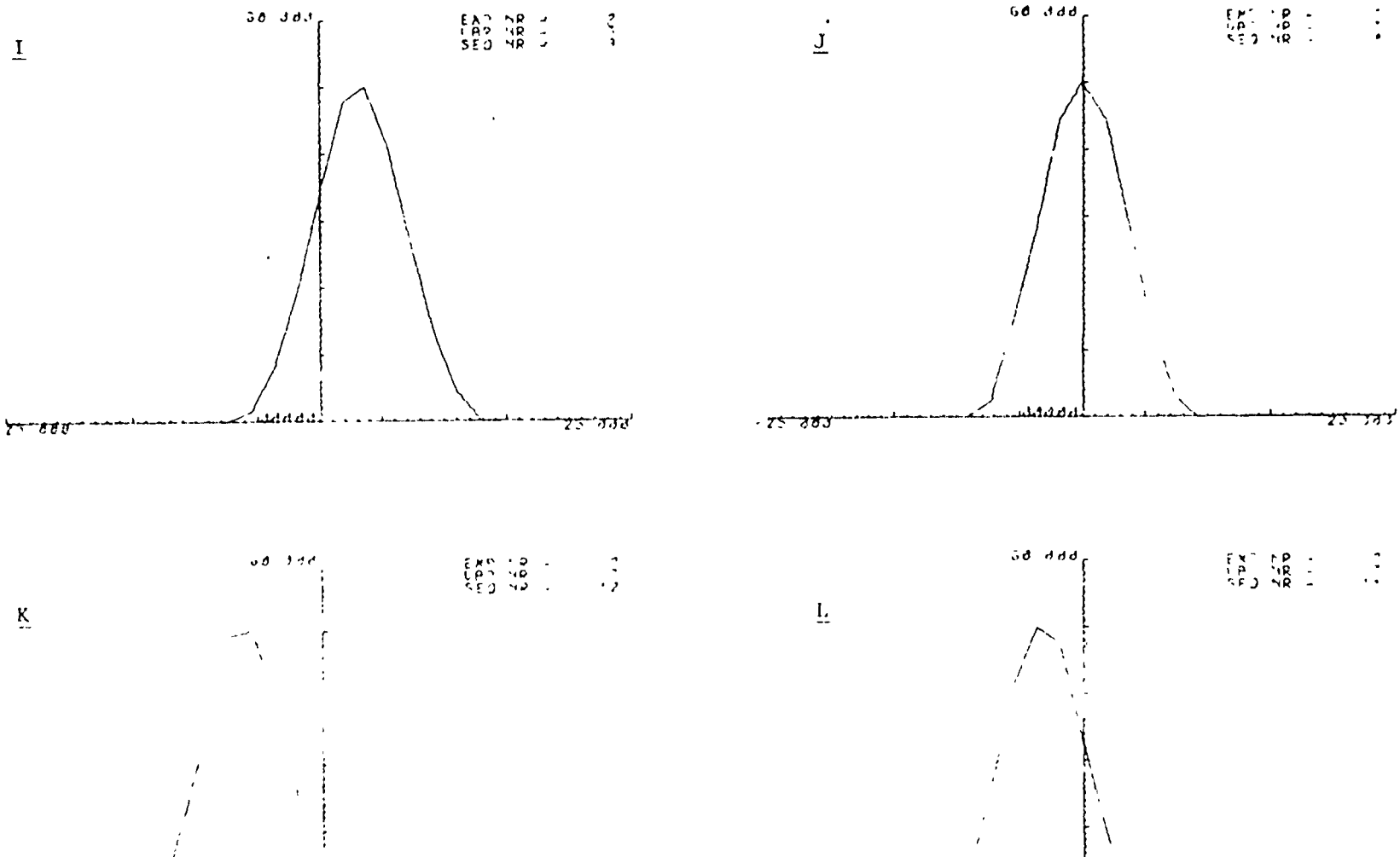

Figure D.7. Spectra Illustrating Various Smoothing Constants

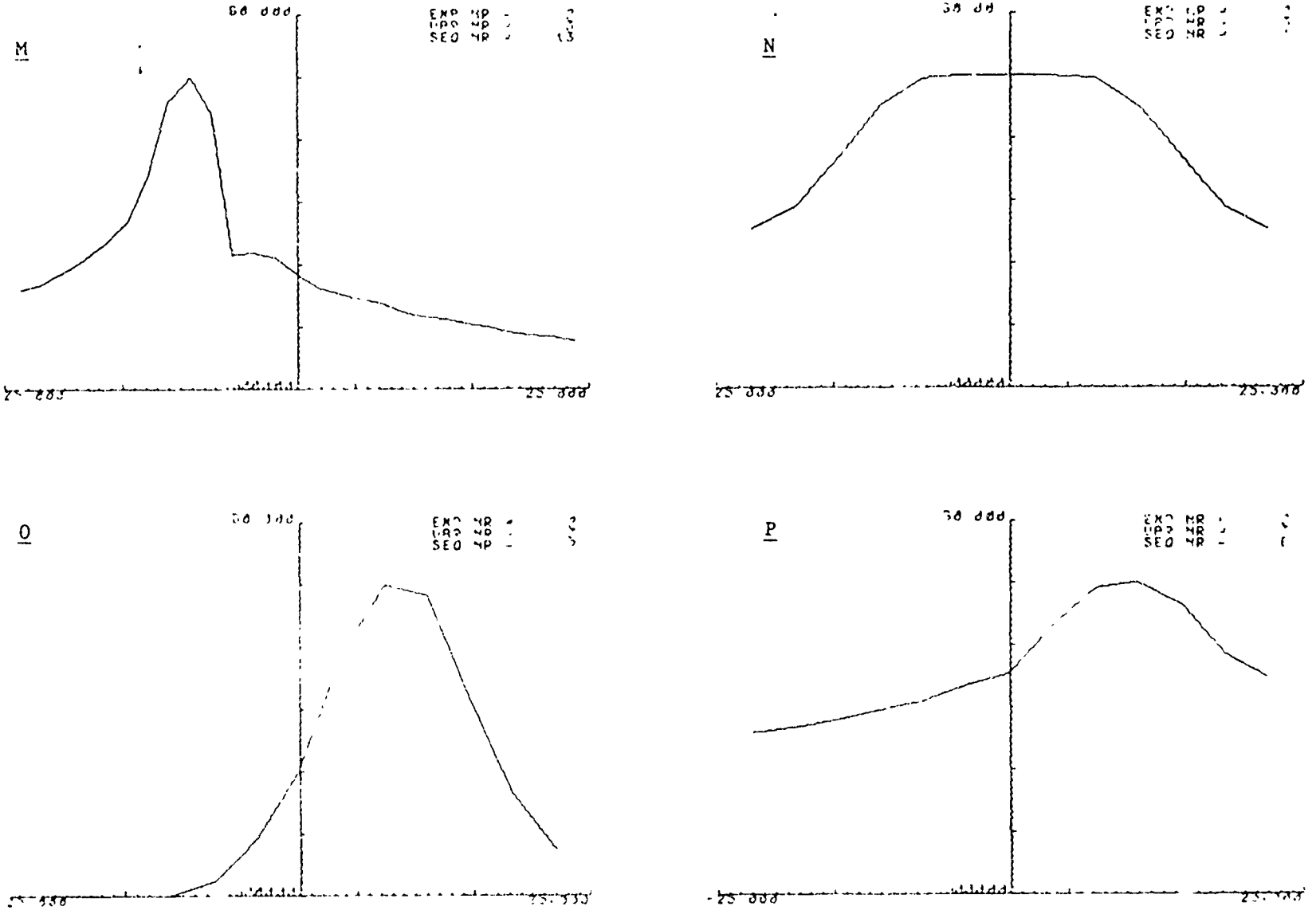

Figure D.8. Spectra Illustrating Various Smoothing Constants

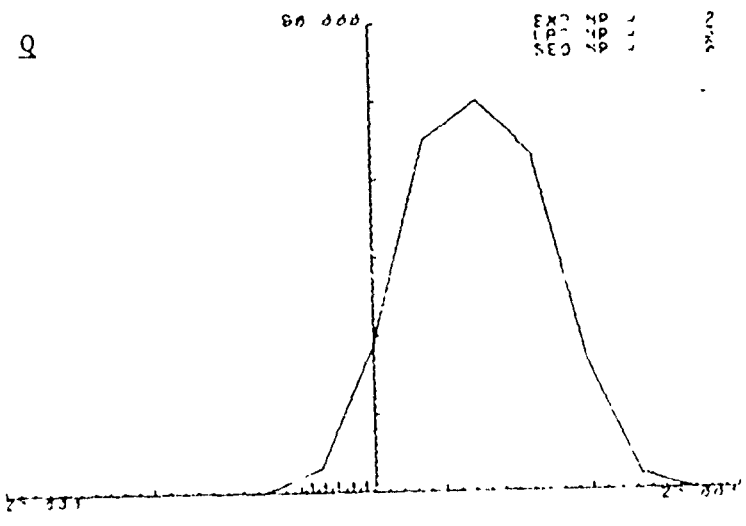

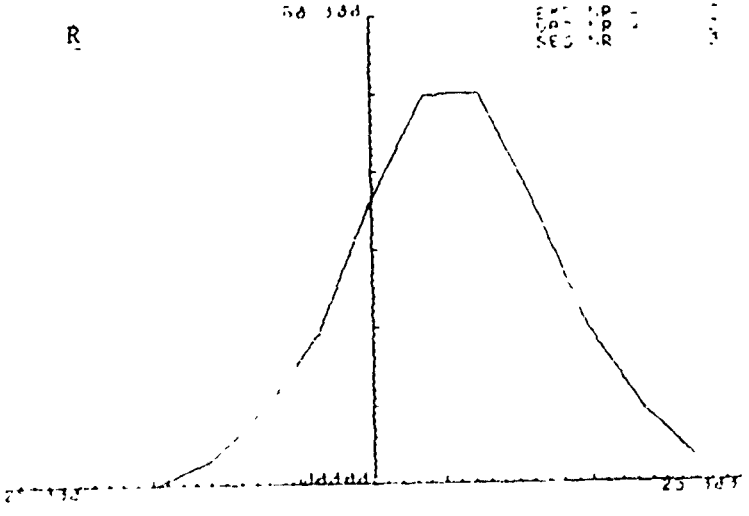

Figure D.9. Spectra Illustrating Various Smoothing Constants

APPENDIX E

SPECTRAL ANALYSIS

Effect of Jitter on Spectra

The sampling aperture used is roughly Gaussian in shape. The time between the beginning of the main pulse and the sampling event, $\Delta T = (t_{transmit} - t_{sample})$, can jitter by an amount τ. Let $r(t)$ be the received pulse, $c(t_s)$ the output of the sampling process and $g(t)$ the sample signal. See Figure E.1.

Assume that the sampling occurs during a time when the received pulse has a constant slope of s volts/nanosecond.

Assume that $g(t)$ is a finite duration rectangular pulse such that $\int g_p(t)\,dt = \int g(t)\,dt$. The variation in amplitude of $c(t)$ due to time jitter between the sampling aperture $g(t)$ and the received signal $r(t)$, is:

$$\Delta c(\tau) = c(t)\,\Big|_{t = t_s} - c(t)\,\Big|_{t = t_s + \tau}$$

Ideal sampling works like this

$$\int r(t)\,\delta(t_s - t)dt = r(t_s) = c(t)\,\Big|_{t = t_s}$$

When the sampling is not ideal $\delta(t)$ is replaced with $g(t)$ where $g(t)$ is the aperture.

$$\int r(t)\,g(t_s - t)dt = c(t)\,\Big|_{t = t_s}$$

$$\int r(t)\,g(t_s - t + \tau)dt = c(t)\,\Big|_{t = t_s + \tau}$$

Thus $\Delta c(\tau) = c(t)\,\Big|_{t = t_s} - c(t)\,\Big|_{t = t_s + \tau}$

$$c(t)\,\Big|_{t = t_s} \simeq \int r(t)\,g_p(t_s - t)\,dt = \int_a^b r(t)dt$$

$$c(t)\,\Big|_{t = t_s + \tau} \simeq \int r(t)\,g_p(t_s - t + \tau)\,dt = \int_{a+\tau}^{b+\tau} r(t)\,dt$$

The area shaded in Figure E.2 is the first integral and the area shaded in Figure E.3 is the second integral.

$$\Delta c(\tau) \cong \int_a^b r(t)\,dt - \int_{a+\tau}^{b+\tau} r(t)\,dt$$

$$= I_1 - I_2$$

I_1 and I_2 are shown graphically in Figure E.4

$$(I_1 - I_2) = \tau \cdot s \cdot (b - a)$$

Also,
$$I_1 \cong r(t) \cdot (b - a)$$

$$I_1 = r\left(\frac{b+a}{2}\right) \cdot (b - a)$$

$$\frac{\Delta c(\tau)}{c(t)\big|_{t = t_s}} = \frac{I_1 - I_2}{I_1} = \frac{\tau \cdot s \cdot \text{aperture}}{r\left(\frac{b+a}{2}\right) \cdot \text{aperture}}$$

If $r\left(\frac{b+a}{2}\right) = 1$ volt, and

$$s \cong \frac{1}{4} \text{ volts/100 ns.}$$

$$\cong .0025 \text{ volts/ns.}$$

$$\tau \cong 4 \text{ nanoseconds}$$

then
$$\tau s \cong .01 \text{ volts}$$

$$\frac{\Delta c(\tau)}{c(t)\big|_{t = t_s}} \cong .01$$

$$(\Delta c(t)/c(t))_{max} = .06$$

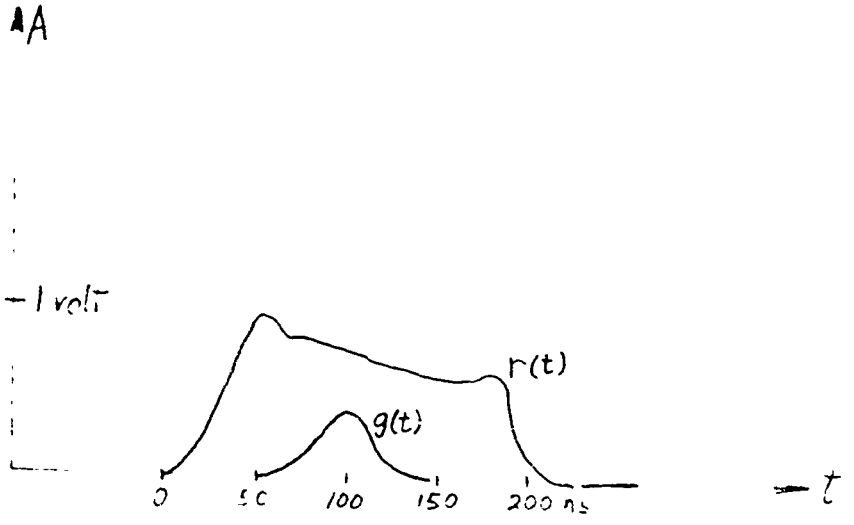

Figure E.1. Relationship of Received Pulse and Sample Signal

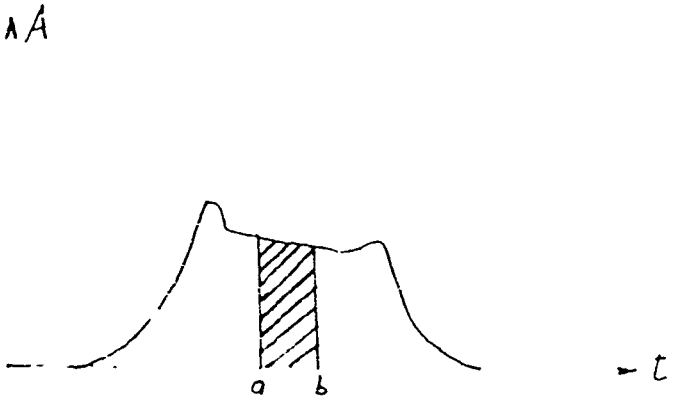

Figure E.2. Graphical Representation of Equation E.1.

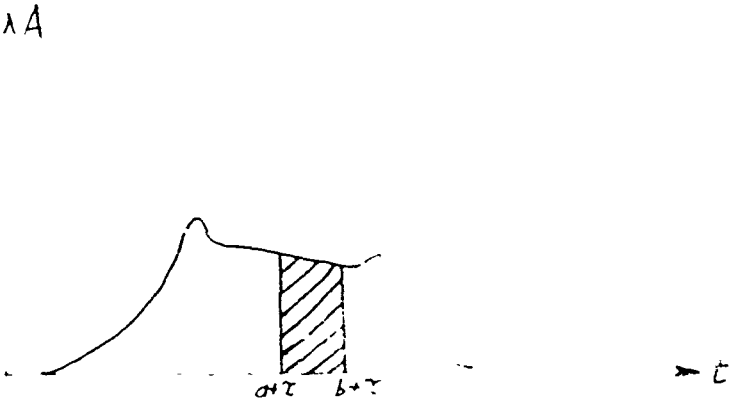

Figure E.3. Graphical Representation of Equation E.2.

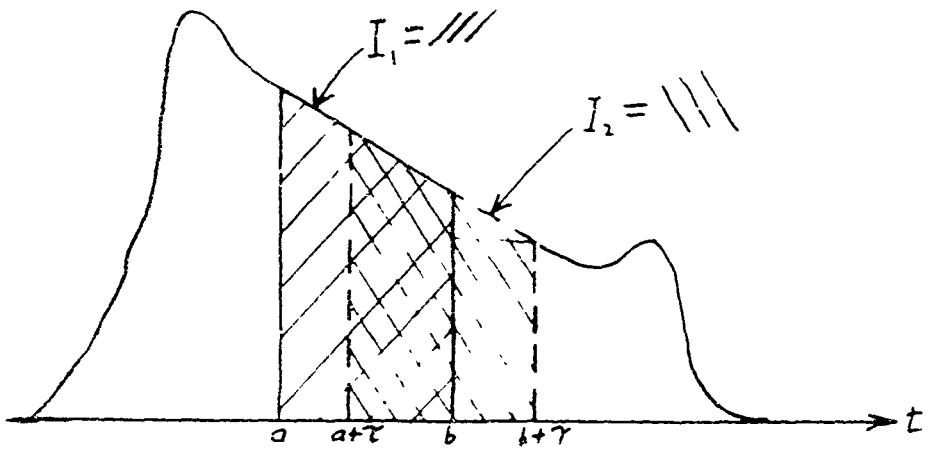

The area represented by I_2 can be shifted to the left τ seconds so that the beginning of I_2 lines up with the beginning of I_1.

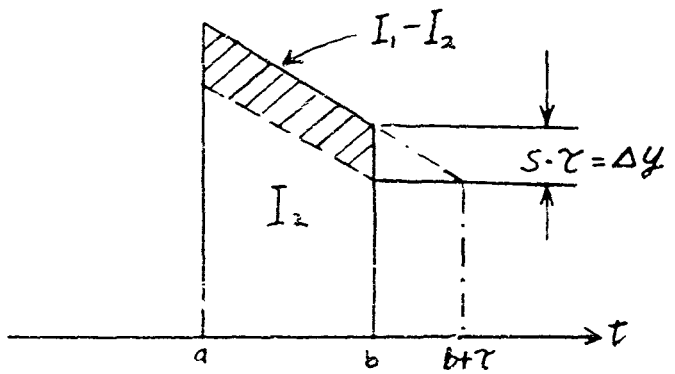

I_2 can be moved up so that the sloping line of I_2 lies on the sloping line of I_1.

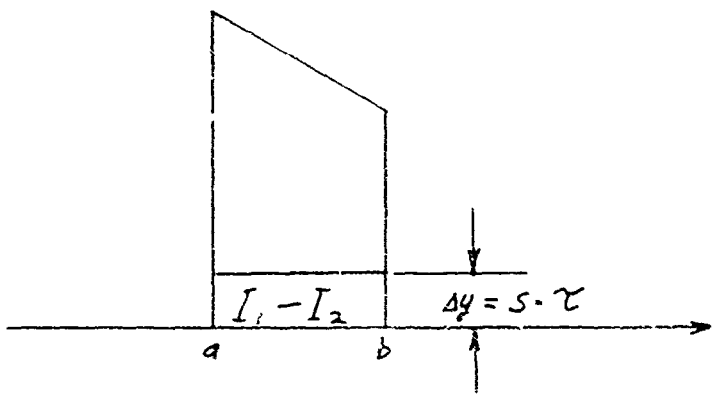

Figure E.4. Graphical Presentation of I_1 and I_2

If the jitter is represented by a single sinusoid $\tau = A \sin 2\pi ft$ and if the frequency spectrum is evenly distributed over 30 frequency bins, then the jitter will cause the frequency spectrum to look like that of Figure E.5.

If the frequency of the jitter is greater than 100 Hz, the strength of the signal component due to jitter will be severely attenuated by the 100 Hz low pass filter.

If the frequency of the time jitter is evenly distributed over all frequencies from 0 to 9 Hz , the spectral energy will be increased by $10^{-4})(1/30)$ at all frequencies.

FMing on the pulse is shown in Figure E.6. When the aperture occurs during this part of the pulse the signal will be modulated not only by the motion of the target but also by ΔA. If FMing is a single frequency $\Delta A \sin 2\pi ft$ and this frequency is within the region of interest, then $\Delta A/A = 5\%$ could be in one frequency bin but A might be in all 30 frequency bins yielding a spurious peak 30/400ths times greater than the clutter. If FMing was distributed in frequency, then that portion of the FMing spectra within the band of interest would add to the clutter.

F.2 Artificially Generated Data

In debugging spectrum analysis programs it is useful to have a data set whose properties are known and, hence, whose spectrum can be predicted and compared to the actual output. One such set consists of Gaussian random variables, with mean zero and standard deviation σ. Suppose we have N such random variable,s all having identical distributions; label these X(0), X(1), . . . , X(N-1). Assume they are independent, and therefore, uncorrelated. The discrete Fourier coefficient defined by the relation:

$$A(n) = \sum_{k=0}^{N-1} X(k) W_N^{kn}$$

where $W_N = e^{-j2\pi/N}$, defines a new random variable. When the discrete Fourier series is used to calculate a periodogram* as part of a spectral estimate, a quantity of interest is the expectation of the magnitude

---

*A periodogram is defined to be the set of squared magnitude discrete Fourier coefficients.

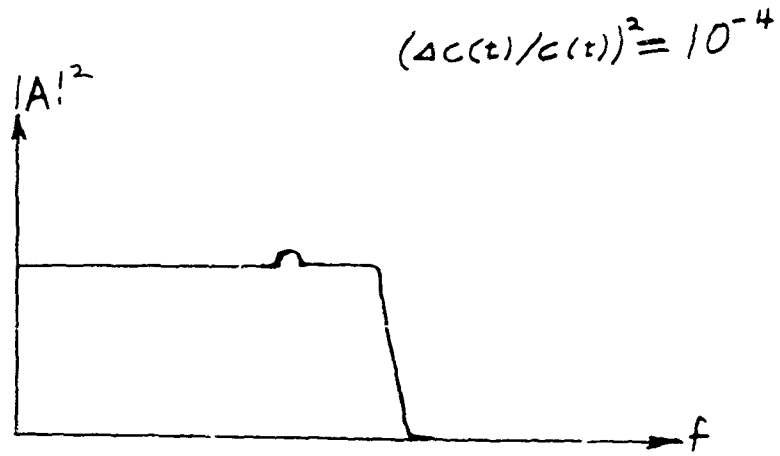

Figure E.5. Graphical Presentation of Frequency Spectra Caused by Jitter

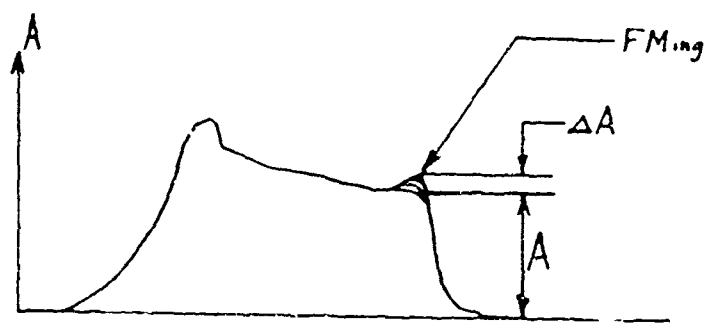

Figure E.6. Graphical Presentation of Frequency Spectra Caused by FM

squared A(n), $E\{ |A(n)|^2 \}$, which we shall now compute:

$$E\{ |A(n)|^2 \} = E\{ A(n)\,\overline{A(n)} \}$$

$$= E\left\{ \sum_{k=0}^{N-1} X(k)\, W_N^{kn} \cdot \sum_{i=0}^{N-1} X(i)\, W_N^{-in} \right\}$$

$$= E\left\{ \sum_{k=0}^{N-1} \sum_{i=0}^{N-1} X(k)\, X(i)\, W_N^{(k-i)n} \right\}$$

$$= \sum_{k=0}^{N-1} \sum_{i=0}^{N-1} E\{ X(k)\, X(i) \}\, W_N^{(k-i)n}$$

Now, $E\{ X(k)\, X(i) \} = E\{ X(k) \}\, E\{ X(i) \}$ for $k \neq i$, since the random variables are uncorrelated. Since each random variable has zero mean and variance σ^2 we have

$$E\{ X(k)\, X(i) \} = \begin{cases} 0 & k \neq i \\ \sigma^2 & k = i \end{cases}$$

Therefore,

$$E\{ |A(n)|^2 \} = \sum_{k=0}^{N-1} E\{ X(k)\, X(k) \}\, W_N^{(k-k)n}$$

$$= \sum_{k=0}^{N-1} \sigma^2$$

$$= N\sigma^2$$

which is independent of n. Thus, on the average the periodogram is constant for each frequency value, and the process can be considered a discrete White noise process.

We now consider a single-frequency tone, which for simplicity will be taken as an exact submultiple of the sampling frequency f_s:

$$x(t) = A \sin (2\pi f t),$$

sampled at an interval $\Delta t = 1/f_s$, where

$$f = p \frac{f_s}{N} = p \frac{1}{N\Delta t}$$

and p and N are integers. A sample of x(t) at $t = k\Delta t$ is therefore written as

$$x(k) = A \sin \left(2\pi\, p \frac{f_s}{N} k\Delta t\right)$$

$$= A \sin \left(2\pi \frac{pk}{N}\right) .$$

The n^{th} discrete Fourier coefficient is given by

$$A(n) = \sum_{k=0}^{N-1} x(k)\, W_N^{nk}$$

$$= \sum_{k=0}^{N-1} A \sin \left(2\pi \frac{pk}{N}\right) \left(e^{-2\pi j/N}\right)^{nk}$$

$$= \frac{A}{2j} \sum_{k=0}^{N-1} e^{j2\pi(p-n)k/N} \quad \leftarrow = 0 \text{ for } p \neq n$$

$$- \frac{A}{2j} \sum_{k=0}^{N-1} e^{-j2\pi(p+n)k/N} \quad \leftarrow = 0 \text{ for } p \neq -n \text{ i.e., } p \neq N-n$$

Therefore, $A(n) = \frac{AN}{2j}$ for $n = p$ or $n + N - p$, so that

$$|A(n)|^2 = \frac{A^2N^2}{4}$$

It is of interest to compare the sine wave power with the average random noise power:

$$S = \frac{\text{sine wave } |A(n)|^2}{\text{random noise } E\{|A(n)|^2\}} = 10 \log_{10} \frac{\frac{A^2N^2}{4}}{N\sigma^2}$$

$$= 10 \log_{10} \frac{A^2N}{4\sigma^2}$$

This expression is seen to be dependent on N, the number of points in the discrete Fourier transform. Decreasing N by factor of two results in a 3 dB signal-to-noise degradation. This observation is confirmed using the simulated data, as seen in Figure E.7 and tabulated in Table E 1. Keep in mind, however, that the sine wave analysis assumes an exact submultiple of f_s, which does not take spreading into account when an intermediate frequency is used.

These calculations can also be used to calibrate the "spectrum analyzers" so that an absolute power reference is obtained. In conjunction with a knowledge of the system gains preceding the A/D converter, the cross section of prominent targets can be calculated.

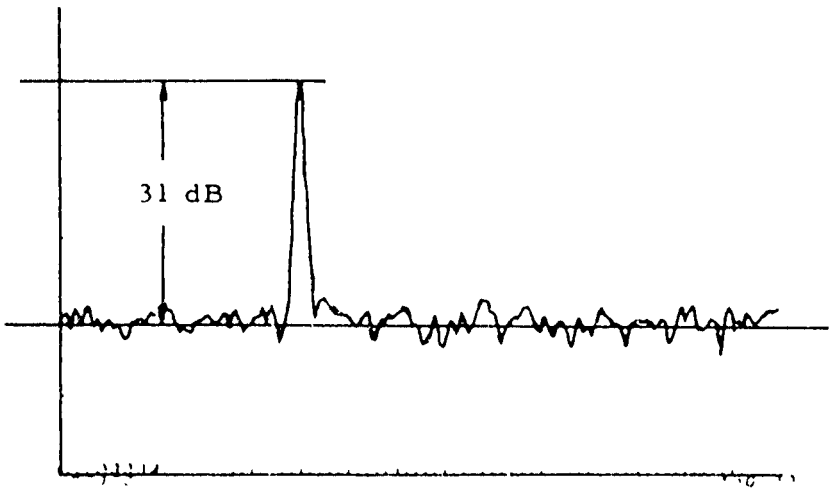

N = 512

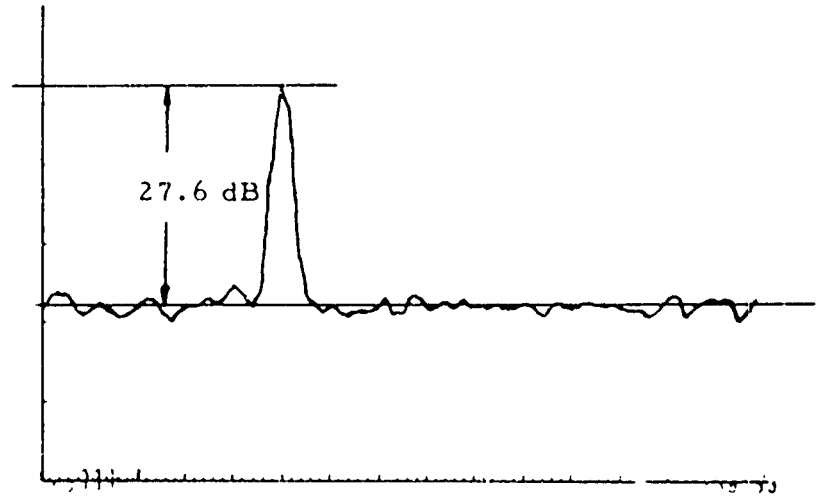

N = 256

50 Hz sine wave imbedded in
Gaussian random noise

Sine wave amplitude = A = 2047

Mean value of the noise = 0

Variance of the noise = $\sigma^2 \cong 54.46$ dB

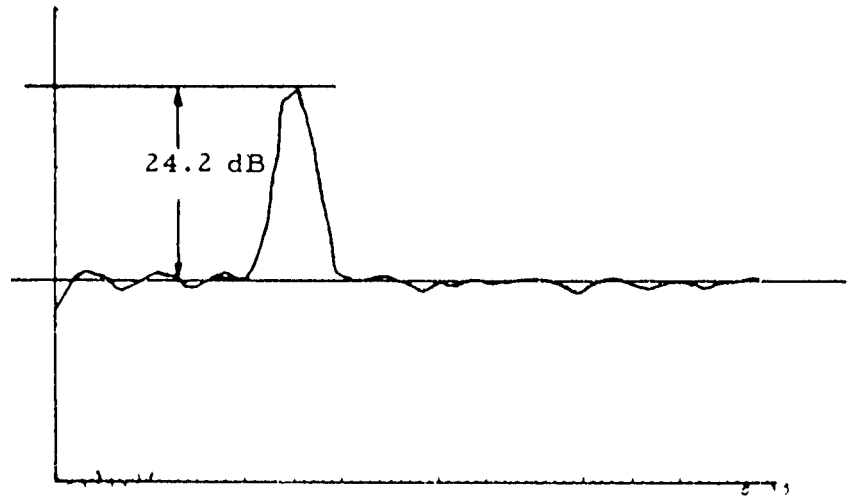

N = 128

Figure E.7. Dependence of Signal-to-Noise Ratio on the Extent of the Discrete Fourier Transform

TABLE E.1

SIGNAL-TO-NOISE RATIOS

$10 \log_{10} A^2 = 66.2$ dB

$10 \log_{10} \sigma^2 = 54.5$ dB

N	Calculated S	Observed in Figure E.5
512	32.7	3i
256	29.7	27.6
128	26.7	24.2